MAGNETOTELLURIC STUDIES IN GEOTHERMAL AREAS OF GREECE AND KENYA

DIMITRIOS GALANOPOULOS

DOCTOR OF PHILOSOPHY

UNIVERSITY OF EDINBURGH

1989

ABSTRACT

The magnetotelluric (MT) technique in the frequency range 10^{+2}-10^{-4} Hz was applied to determine the electrical structure of the geothermal fields of Milos, Greece and Olkaria, Kenya.

Data from 67 stations (37 on Milos and 30 in Olkaria) were processed using standard tensorial techniques and the data were found to be nearly one dimensional (1-D) for the frequency range 10^{+2}-10^{-1} Hz. Several 1-D modelling techniques were applied to the processed data sets. Among the various techniques, the Parker-Whaler D^{+} inversion was studied in detail. It was found that the latter is not only a necessary and sufficient condition for a 1-D solution but its delta functions have a physical meaning and correspond to real electrical boundaries. Subsequent two dimensional (2-D) finite difference modelling revealed some deeper electrical features.

On Milos the uppermost 600-800 m of the crust have very low resistivities (0.3-4 Ohm.m). This was explained by the presence of alteration clay minerals. The deeper structure was more resistive (>10 Ohm.m) mainly because of the non-volcanic origin of the rock formations present. The derived 1-D and 2-D electrical models are in agreement with the existing geothermal model (Fytikas et al., 1989).

In the uppermost 3 km below Olkaria a 3 Ohm.m conductor correlates with a graben infill of pyroclastic origin and is associated with the Olkaria West potential field. The 50 Ohm.m structure below central Olkaria correlates with a zone of cold water in flow. This feature seems to extend below Longonot in the East and to depths of 8 km. The 10 Ohm.m resistivity at depths > 8-10 km was interpreted as due to the thinning of the crust and the partial melting in the upper mantle beneath the rift floor.

ΜΗΝΙΝ ΑΕΙΔΕ ΘΕΑ ΠΗΛΙΑΔΩ ΑΧΙΛΗΟΣ
ΟΥΛΟΜΕΝΗΝ Η ΜΥΡΙ ΑΧΑΙΟΙΣ ΑΛΓΕ ΕΘΗΚΕΝ
ΠΟΛΛΑΣ ΔΙΦΘΙΜΟΥΣ ΨΥΧΑΣ ΑΙΔΙ ΠΡΟΙΑΨΕΝ
ΗΡΩΩΝ ΑΥΤΟΥΣ ΔΕ ΕΛΩΡΙΑ ΤΕΥΧΕ ΚΥΝΕΣΣΙΝ
ΟΙΩΝΟΙΣΙ ΤΕ ΔΑΙΤΑ ΔΙΟΣ Δ ΕΤΕΛΕΙΕΤΟ ΒΟΥΛΗ
ΕΞ ΟΥ ΔΗ ΤΑ ΠΡΩΤΑ ΔΙΑΣΤΗΤΗΝ ΕΡΙΣΑΝΤΕ
ΑΤΡΕΙΔΗΣ ΤΕ ΑΝΑΞ ΑΝΔΡΩΝ ΚΑΙ ΔΙΟΣ
ΑΧΙΛΛΕΥΣ

ΟΜΗΡΟΥ ΙΛΙΑΣ

... to the Greeks

ACKNOWLEDGEMENTS

I gratefully acknowledge the help and direction given to me by my two supervisors Dr Rosemary Hutton and Mr Graham Dawes. Dr Rosemary Hutton has not only given me the opportunity to participate in the two intensive magnetotelluric projects on Milos, Greece and Olkaria, Kenya but also provided me with every means the chance to complete this thesis. I am deeply indebted to her and her family for the kindness and hospitality shown me during my stay in Edinburgh. I would like to express my sincere thanks to Mr Graham Dawes for the field preparation of the two projects in Greece and Kenya, and for valuable guidance and help during the fieldwork, data analysis and modelling. My special thanks to him for many long discussions about the magnetotelluric method and computer programming.

I am thankful to the Department of Geology and Geophysics and in particular to Professor Ken Creer for providing facilities for my research. I would like to express my special thanks to him and his wife Mrs Zoe Creer for the hospitality they have extended to me during my studies in Edinburgh.

I would like to thank Dr Bruce Hobbs and Dr Roger Hipkin for advice and help with geophysical problems and computer programming. I am grateful to Dr Gillian Pickup for her friendship and valuable help during the Milos and Olkaria projects. I gratefully acknowledge her patience when commenting on parts of this thesis. My thanks must also go to Mr M. Valiant for the preparation of the Olkaria fieldwork.

I wish to thank all of my Milos project colleagues for help and advice given to me during this work. I am pleased to extend my sincere thanks to Professor Peter Weidelt for his advice and suggestions on many theoretical problems. I thank Mr Hans-Martin

Maürer, Mrs Christina Drews, Mr Oliver Ritter and Mrs Patricia Ritter for the useful discussions I had with them and for their hospitality during my visit to Germany.

I wish to extend my sincere thanks to Dr Michalis Fytikas and Dr Dinos Thanassoulas for their advice and help on the Milos project. I am grateful to Dr Erricos Tzanis for his valuable help during the early stages of my studies, for providing various computer software and for his friendship. I thank Dr Tugrul Genc for providing his gravity modelling package.

I would like to mention my colleagues Mr Tony Morris for his friendship and help on various problems and Mr Phil Jones and Mr Ronnie Parr for their suggestions on various aspects of this work.

My warm thanks go to Mr Martin Mwangi for his friendship, help and advice during and after the Olkaria project.

I thank all the participants of the Milos and Olkaria fieldwork, especially Mr Steven Onacha. I would also like to thank my former supervisor in the University of Leeds Dr Kathy Whaler for encouraging me to start these studies.

Financial support for this work was provided by a University of Edinburgh studentship during the first sixteen months and an E.E.C sectoral grant for the following two years. I express my deep gratitude to these bodies.

CONTENTS

LIST OF FIGURES

LIST OF TABLES

CHAPTER 1

INTRODUCTION

1.1. The objectives of this study.

In the present thesis the contribution of the magnetotelluric method to geothermal exploration is discussed through the results of magnetotelluric surveys on Milos island, Greece and in Olkaria, Kenya respectively. The aims of the two surveys were the determination of the electrical structures beneath the geothermal fields of Milos and Olkaria, and a comparison of their results in the interpretation of the electrical models.

Prior to the discussion of the surveys in chapters 3-7 the significance of the electrical resistivity and the importance of the magnetotelluric method in geothermal exploration are considered in the following sections of this chapter and theoretical aspects in chapter 2.

1.2. The significance of electrical resistivity.

In the magnetotelluric method the natural electromagnetic fields of the earth are used in order to determine its electrical structure. The relation between the oscillating electric and magnetic fields is given by the ratio of their complex representations. This is known as the electrical impedance Z which has units of Ohms. Its reciprocal Y is called the electrical admittance with units of Siemens (Schelkunoff, 1943). More practical quantities are the electrical resistivity ρ and its reciprocal, the electrical conductivity σ with

units of Ohm.m and S/m respectively. In the magnetotelluric method the former is given in terms of the electrical impedance Z. In particular, Cagniard (1953) by studying the diffusion of the electromagnetic waves within a homogeneous half space of resistivity ρ, showed that $\rho=1/w\mu|Z|^2$, with a constant phase of 45° between the electric and magnetic field.

Electric currents may be propagated in rocks and minerals in three ways : electronic, electrolytic and dielectric conduction (Telford et al., 1981).

The first type is the normal ohmic current flow in materials containing free electrons, such as metals. In this case the electrical resistivity ρ is defined by the following equation :

$$\rho = \frac{R\,A}{L} \qquad (1.1)$$

L and A are the length and the cross-section of a cylindrical solid having resistance R. Where A is in m^2, L in m and R in Ohms.

Most rocks are porous and the pores are filled with fluids, mainly water. Therefore rocks are electrolytic conductors and conduction is of the second type. In an electrolyte the current is carried by ions at a comparatively slow rate. The electrical resistivity varies with the volume and arrangement of the pores and even more with the resistivity and amount of contained water. According to an empirical formula due to Archie (1942) the electrical resistivity of a porous rock is given as follows :

$$\rho = a\phi^{-m}s^{-n}\rho_w \qquad (1.2)$$

where ϕ is the fractional pore volume (porosity), s is the fraction of the pores containing water, ρ_w is the resistivity of water, $n\approx2$,

a,m are constants with $0.5 \leq a \leq 2.5$ and $1.3 \leq m \leq 2.5$.

Semiconduction takes place in poor conductors or insulators which have very few carriers or none at all.

The magnetotelluric method is sensitive to the detection of good conductors and therefore plays an important role in geothermal exploration. The electrical resistivity of fluids and rocks in geothermal regions depends on several physical parameters (Berktold, 1983) such as :

(i). The concentration of ions (amount of salt per unit solvent, degree of dissociation).

(ii). The interaction between ions in the solution.

(iii). The charge number of the ions (kind of substance).

(iv). The mobility of the ions in the solution.

(v). The density, viscosity, dielectric constant, pressure and temperature of the fluid.

The density, viscosity and dielectric constant of water decrease with increasing temperature. The decrease of viscosity results in an increase in the mobility of the ions and therefore a decrease in resistivity. The decrease in density and dielectric constant has the opposite effect of an increase in resistivity. For temperatures below 300-400°C the temperature dependence of resistivity is mainly determined by the viscosity and therefore the resistivity decreases considerably with increasing temperature (Fig.1.1, page 26). For temperatures above 300-400°C the effects of decreasing density and

dielectric constant predominate resulting in a increase in resistivity (Fig.1.1). The temperature dependence for water saturated samples is governed by an exponential law :

$$\rho = \rho_o \exp(+\frac{E_o}{KT}) \quad (1.3)$$

where E_o is activation energy, K is Boltzmann's constant and T is absolute temperature. E_o for water is about 0.2 eV and for the rocks given as examples below is 0.16-0.19 eV (Volarovich and Parkhomenko, 1976).

The electrical resistivity of moisture-containing rocks as a function of pressure and temperature has been investigated by several authors (Brace, 1971 ; Hermance, 1973 ; Shankland and Waff, 1974 ; Hermance and Grillot, 1974 ; Volarovich and Parkhomenko, 1976 ; Duba, 1976 ; Rai and Manghnani, 1981 ; Olhoeft, 1981). Fig.1.1, page 26, (Olhoeft, 1981) shows how the electrical resistivity of a granite varies with the pressure, temperature and the water content.

The electrical resistivity of a rock depends not only on the matrix permeability due to the pore space but also on the permeability due to fractures, fissures and joints. The latter is much higher in fractures than in the permeable porous channels within the rock matrix (Berktold, 1983).

The electrical resistivity of rocks varies also with the rock type. Examples demonstrating the resistivity variation with the pressure, temperature and salinity for various rock types such as, sedimentary and crystalline rocks are discussed below.

All the examples refer to the temperature range 0-400°C which is representative of geothermal fields.

1.2.(i). Sedimentary rocks.

Sedimentary rocks such as sandstones, limestones and clays can occupy the upper part of the earth's crust to a depth up to 10 km. A characteristic of sedimentary rocks is that they contain a significant amount of interstitial moisture. The latter is determined by the porosity ratio k. Porosity is higher for clays, between 20-50% while rather smaller (5-20%) for sandstones and (1.5-15%) for limestones (Volarovich and Parkhomenko, 1976).

In the present section most of the discussion is devoted to clays and clay minerals for the reasons presented below.

The ultimate solid product of weathering is the material called soil and chief among the constituents of most soils are the clay minerals.

The fact that clay particles have the ability to adsorb water and organic materials makes them plastic and good electrolytes which are ready to exchange ions with water and other liquids. In addition clays show very low vertical permeability.

The clay minerals are formed by alteration of aluminum silicates, both in weathering and in low-temperature (< 300-400°C) hydrothermal processes. Kaolinite forms at temperatures under about 300°C, muscovite appears at higher temperatures. Montmorillonite is favoured by oxides or chlorides of sodium and the alkaline earth metals (Krauskopf, 1979).

Typical resistivity values for water or saline water saturated clays are between 1-100 Ohm.m (Volarovich and Parkhomenko, 1976). These authors provide a diagram of the variation of $\rho_n/\rho_n(20°C)$ with

temperature, for clays saturated by 2N NaCl solution, which is reproduced here as Fig.1.3 (page 26).

1.2.(ii). Crystalline rocks.

The most widespread crystalline rocks in the Earth's crust are the igneous such as, granites, gabbro, diabases, andesites, diorites as well as metamorphic rocks like gneisses, amphibolites, slates and crystalline limestones. The porosity of these rocks lies in the range 0.01-3%, much less than that of the sedimentary rocks.

Despite the fact that the porosity of these rocks is low, interstitial solutions have a considerable effect on their electrical resistivity.

The electrical properties of metamorphic and igneous rocks in the earth's crust are subject to pressures and temperatures. Fig.1.4a-c illustrate the electrical resistivity variation of various metamorphic and igneous rocks with pressure, temperature and salinity respectively as presented by Volarovich and Parkhomenko (1976).

1.3. Geothermal Models.

Fytikas (1977) and Berktold (1983) based on Goguel's (1953) pioneering work provide the following simplistic model for a typical geothermal field. The model is illustrated in Fig.1.5 (page 31).

In terms of plate tectonics, geothermal regions occur mainly at or near divergent and convergent plate boundaries (spreading ridges and subduction zones), at intraplate rifts (continental rifts and

thermal anomalies (hot spots)). Plate movement may be accompanied by magma intrusions and volcanism. A hot magma chamber which is located at a relatively shallow depth within the Earth's crust provides the heat source of the geothermal field.

In these areas heat is not transfered only by conduction but also by vertical mass transfer. Since at shallow depths the rock permeability is higher, then meteoric fluids can penetrate to greater depths and reach the hot rocks. There, they are heated, become lighter and then ascend to the surface of the Earth while new cooler masses of fluids take their place. This fluid circulation system permits heat transfer from great depths to the surface of the Earth.

The fluids which circulate within the crust, consist mainly of meteoric or sea-water and only a small percentage has magmatic origin (Goguel, 1953). Marinelli (1963) agrees with these ideas by pointing out that the permeability of rocks decreases with the depth and therefore water is of magmatic origin near the magmatic chamber.

The necessary conditions which should be satisfied in the region of a typical geothermal field were specified by Goguel as follows.

(i). A heat source must be located at 3-10 km depth.

(ii). There must be a sequence of highly fractured rocks, sometimes metamorphics, in order to allow the fluid circulation and heat conduction.

(iii). Above or within this rock sequence, at 0.3-2 km depth, there must be a permeable layer. The latter is known as the geothermal reservoir.

(iv). For an ideal geothermal model there must be always an impermeable layer to cover the reservoir and serve as a cap rock.

Fig.1.1. Electrical resistivity (Ohm.m) variation with temperature (°C), pressure (dashed lines, Kb) and water content for granite (After Olhoeft, 1981).

Fig.1.2. Effect of temperature (°C) and pressure (Kb) on the electrical resistivity (Ohm.m) of 0.01 demal KCl solution (After Berktold, 1983).

Fig.1.3. Temperature (°C) induced relative changes of the specific electrical resistivity of sedimentary rocks saturated by 2N NaCl solution. 1 - limestone ; 2 - clay (After Volarovich and Parkhomenko, 1976).

Fig.1.4. Dependence of the electrical resistivity (Ohm.m) on pressure, temperature and NaCl solution for various crystalline rocks (After Volarovich and Parkhomenko, 1976).

a. Dependence on pressure (Kb). 1 - rhyolite tuff ; 2, 5, 6 - gabbro ; 3 - diabase ; 4 - peridotite.

b. Dependence on temperature (°C). 1 - gabbro ; 2, 3 - granites ; 4 - syenite.

c. Dependence on NaCl solution (%). 1 - albitophyre with solution concentration c=3g/l ; 2 - basalt of c=3g/l ; 3, 4, 5 - gneiss with c=0, 10, 20 g/l NaCl respectively.

Fig.1.1

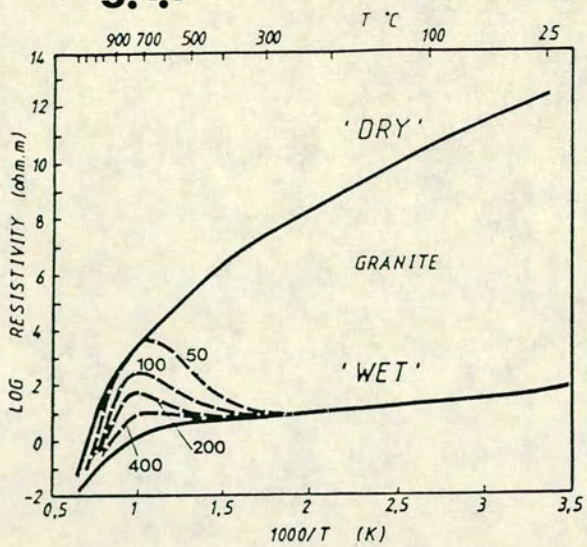

Fig.1.2

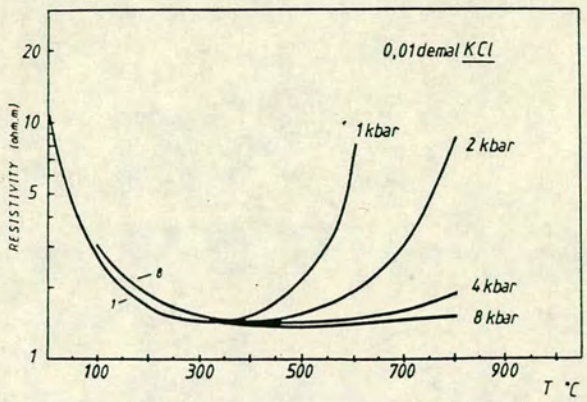

Fig.1.3

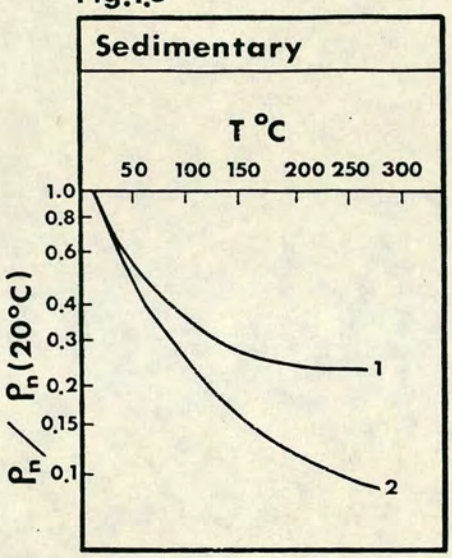

Fig.1.4a

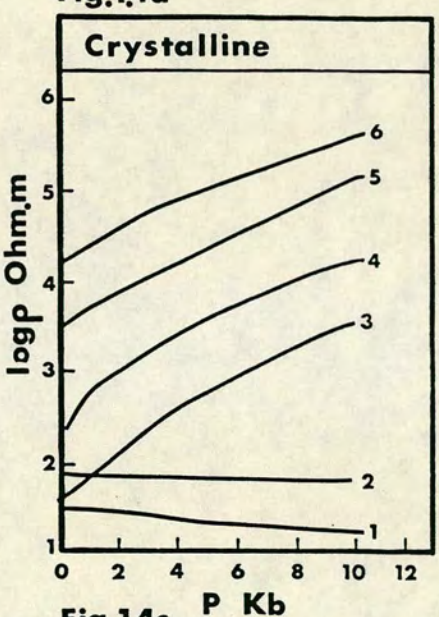

Fig.1.4b

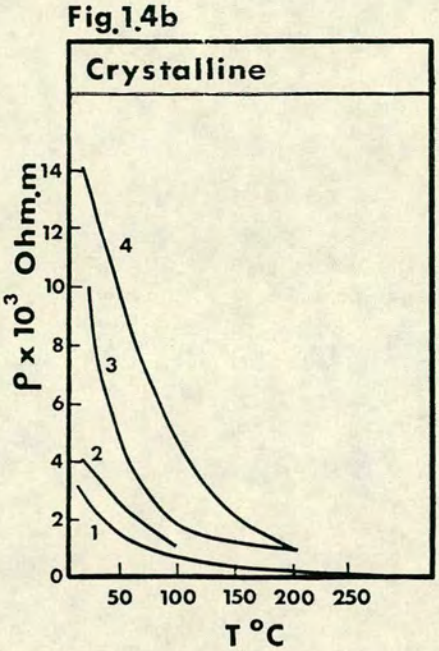

Fig.1.4c

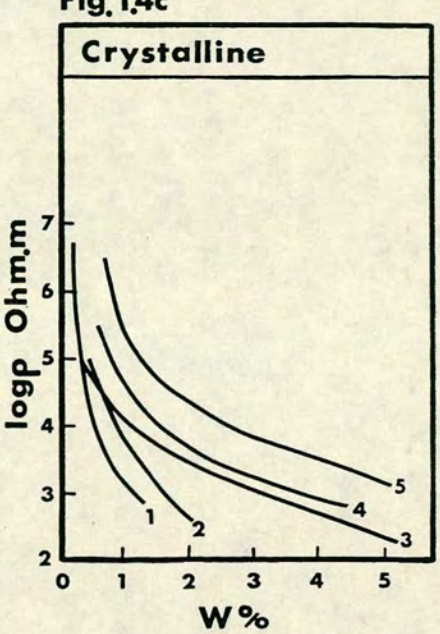

1.4. The outline of this thesis.

Some theoretical aspects of the magnetotelluric method are discused in chapter 2. Particular attention is paid to studying the diffusion of electromagnetic fields within the earth. Comments on some previous and recent work associated with the analogies between seismic methods and the magnetotelluric method on the basis of electromagnetic wave propagation are given and arguments presented to show that much of this research requires re-examination.

Studying the one dimensional inversion magnetotelluric problem, it is shown that an alternative idea can be the determination of the Earth's " electromagnetic energy spectrum " for which the Parker-Whaler D^+ algorithm is employed.

Chapters 3-5 refer to an electromagnetic induction study on Milos island, Greece which displays a high thermal anomaly. This intensive broadband (10^{+2}-10^{-4} Hz) magnetotelluric survey was part of a multinational project which involved several geophysical methods and which was sponsored by the Commission of the European Communities. The geological history and tectonics of the Aegean and Milos are described in brief in chapter 3, the results of several geophysical surveys undertaken in the Aegean and on Milos, during the last two decades being summarized in the same chapter. The magnetotelluric data analysis and modelling are described in chapter 4. In chapter 5 and Appendix I (Hutton et al., 1989) the resulting magnetotelluric models and other induction parameters such as the Parkinson induction arrows are interpreted with respect to the regional and local geology

and tectonics. Results from other previous and recent geophysical surveys were combined with the magnetotelluric models of the present study to prepare an integrated geophysical model below Milos.

Chapters 6 and 7 deal with the magnetotelluric survey in Olkaria, Kenya. The geology and tectonics of the region with the results of the previous geophysical studies are described in chapter 6. The data analysis and modelling are fully described with examples in the report submitted to KPC by Hutton et al. (1989) and attached in the present work as Appendix II. Chapter 7 deals with the dimensionality tests applied to the magnetotelluric data and some limited two dimensional modelling studies. The results from this study are finally discussed in the same chapter.

The present study ends with chapter 8 in which the main conclusions from this work are given in brief. Special attention is paid to the combined interpretation of the results from both the magnetotelluric case studies in Greece and Kenya in terms of the electrical properties of rocks and the general properties of geothermal systems.

CHAPTER 2

THE MAGNETOTELLURIC METHOD

2.1. Introduction.

A great deal of our knowledge about the physical world is a result of either direct sensory experience or the study of experiments whose subjects are non perceptive.

Examples of the former refer to our ability to give answers concerning various parameters or the behaviour of objects encountered in our daily experience. The latter relate to sub-microscopic phenomena, geophysical and astrophysical research or medical imaging.

Phenomena inaccessible to our perception share a common feature. In each case a source emits particles or wave energy which propagate and interact with the environment they encounter and finally are detected at receivers. The receivers can record characteristics of the particles or the wave energy. These characteristics can be used to reveal the nature of the source or the environment experienced by the emitted probe.

In geophysics there are phenomena where a natural or artificial source emits wave energy which propagates within the Earth and then is recorded at our receivers. Such phenomena are the acoustic and electromagnetic wave propagation within the Earth. The characteristics of the recorded waves enable us to determine the structure of the Earth.

The following discussion is restricted to the second category of waves and particularily to the natural electromagnetic waves relating

to the magnetotelluric fields in the period range 10^{-2} secs to 10^{+4} secs.

2.2. Magnetotelluric fields : Source mechanism .

The magnetotelluric fields arise from a variety of causes. The amplitude of the magnetic variations shows a minimum for 1 Hz (Fig.2.1). Therefore this frequency is important in that it distinguishes two kinds of activity with relative sources above 1 Hz and below 1 Hz (Patra and Mallick, 1981 ; Rokityanski, 1982).

2.2.(i). Sources above 1 Hz .

The magnetotelluric fields above 1 Hz originate from meteorological activity. This meteorological component consists of fields from lightning associated with thunderstorms. The signals created from lightning strokes are known as " sferics " . The " sferics " attain their peaks in the early afternoon. They propagate around the world trapped in the wave guide formed between the ionosphere and the earth's surface. In the day time the wave guide width is 60 km and increases at 90 km during the night time. Places with high thundershower activity are located in the equatorial regions.

2.2.(ii). Sources below 1 Hz .

The complex interaction between the terrestrial magnetic field

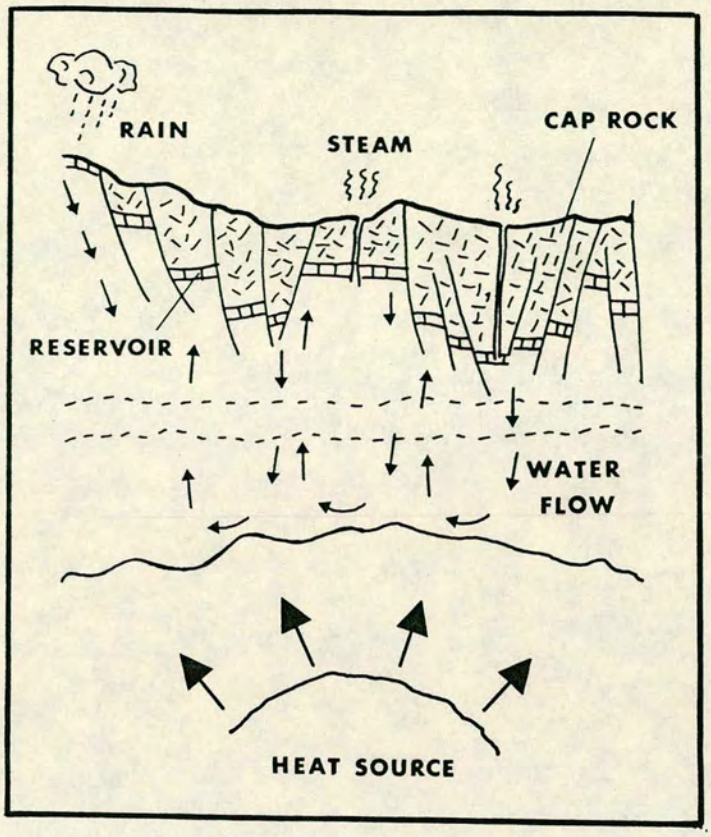

Fig.1.5. A prototype geothermal model (After Fytikas, 1977).

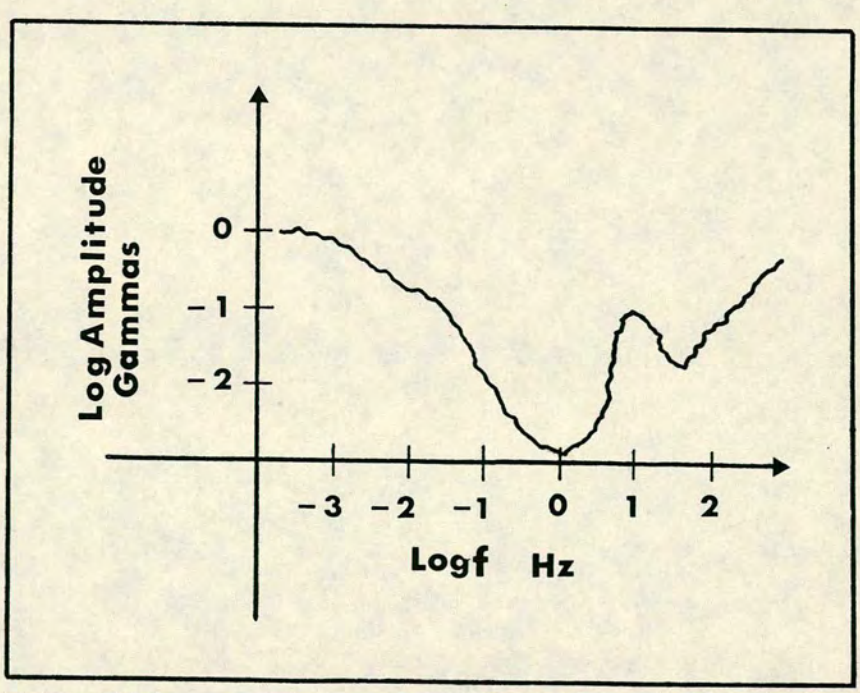

Fig.2.1. Amplitude of magnetic variations (in gammas) versus frequency (Hz) (After Patra and Mallick, 1981).

and the flow of plasma from the sun is the main cause of the natural electromagnetic fields below 1 Hz. The magnetic field which arises in the interior of the earth is not important in the magnetotelluric method because it varies slowly with time. This field has been found to have a boundary called the " magnetopause " which is the outer boundary of the earth's magnetosphere.

When ionized particles moving outward from the sun encounter the earth's magnetic field this causes rapid distortions in the earth's magnetosphere. The ionized particles are protons and electrons and are known as the " solar wind ". When the electrons and protons encounter the terrestrial magnetic field, they are deflected in opposite directions and thus an electric field occurs.

When sunspots occur the solar wind is enhanced and magnetic storms are observed. The solar wind is also enhanced by smaller masses of plasma which activate substorm phenomena. At altitudes of 80-160 km the Earth's atmosphere is strongly ionized. The motion of charged particles in this zone which is known as " ionosphere " is associated with the induction of current. The interaction of magnetic and inertial forces gives rise to " Magnetohydrodynamic " waves. Magnetic effects due to these waves are the micropulsations which are the main source of the natural electromagnetic waves below 1 Hz.

Micropulsations are classified as Regular P_c, Irregular P_i and Pearls (amplitude modulated). The Regular pulsations are subdivided to P_{c1} , P_{c2} ,P_{c3}, P_{c4} , P_{c5} , with period range 0.2 secs to 600 secs. Irregular pulsations are subdivided to P_{i1} , P_{i2} with period range 1 sec to 150 secs. Pearls have a period range 0.3 secs to 3 secs. Magnetotelluric fields due to " magnetic bays " and diurnal

effects have a period range starting from 600 secs extending up to few hours (Patra and Mallick, 1981).

2.3. Electromagnetic induction in the earth : Diffusion or Wave equation ?

In the magnetotelluric method the natural electromagnetic fields of the earth are used in order to determine its electrical structure.

The basic assumption of the method is the existence of plane electromagnetic waves incident on a plane earth surface (Cagniard, 1953). In the early days some researchers (Wait, 1954 ; Price, 1962) argued about this plane wave assumption of the source field. Cagniard's ideas were defended by Madden and Nelson (1964) and are generally accepted. For most studies, Srivastava (1965) found that the spherical shape of the earth can not influence the magnetotelluric interpretation.

In the discussion of the basic MT theory which follows, I assume plane harmonic (e^{+iwt}, w=radian frequency in s^{-1}) electromagnetic waves impinging on the Earth, the latter approximated by a homogeneous, isotropic, conductive half space.

Maxwell's general electromagnetic equations hold and have the following form in three dimensions (r=r(x,y,z)) :

The time dependent equations :

$$\nabla \times \mathbf{E}(\mathbf{r},t) = -\mu \frac{\partial \mathbf{H}(\mathbf{r},t)}{\partial t} \quad (2.1) \qquad \nabla \times \mathbf{H}(\mathbf{r},t) = \mathbf{J}(\mathbf{r},t) + \varepsilon \frac{\partial \mathbf{E}(\mathbf{r},t)}{\partial t} \quad (2.2)$$

where **E** , **H** , **J** are the electric field, magnetic field and the conduction current density respectively.

Since plane harmonic electromagnetic waves have been assumed i.e

$E(r,t)=E(r)e^{+iwt}$, $H(r,t)=H(r)e^{+iwt}$ and $J(r,t)=\sigma E(r,t)$ then eqs. 2.1 and 2.2 reduce to the following :

The time independent equations :

$$\nabla xE(r)=-iw\mu H(r) \quad (2.3) \qquad \nabla xH(r)=J(r)+iw\varepsilon E(r) \quad (2.4)$$

The constants μ and ε are the magnetic permeability and the dielectric constant of the medium. The term $J(r)$ relates to conduction currents and the term $\varepsilon E(r)$ to displacement currents.

In good conductors, conduction currents prevail and the term $J(r)$ is dominant. In perfect dielectrics displacement currents dominate and only the term $\varepsilon E(r)$ exists. In ordinary dielectrics, both kinds of current exist but the term $\varepsilon E(r)$ predominates (Schelkunoff, 1943).

The " Q " of a medium is defined as the ratio of the displacement current density to the conduction current density :

$$Q=\frac{w\varepsilon E}{\sigma E}=\frac{w\varepsilon}{\sigma}=\frac{2\pi\rho 10^{-9}}{36\pi T}\approx\frac{\rho 10^{-10}}{2T}\ \frac{Ohm.m}{sec} \quad (2.5)$$

(Schelkunoff, 1943 ; Cevallos, 1986).

In the magnetotelluric method the period range normally used is 10^{-4} to 10^{+4} secs. The values of resistivity of rocks are in the range 0.1 to 10000 Ohm.m. The " Q " for these ranges is very small because $w\varepsilon<<\sigma$. Thus the term $\varepsilon E(r)$ can be neglected. This is the quasi-stationary field case.

In the Earth, variations in resistivity occur but the magnetic permeability is considered to be everywhere the vacuum permeability μ_o .

Neglecting the displacement currents and assuming $\mu=\mu_o$ Maxwell's equations 2.3, 2.4 are reduced to the following:

The time independent equations :

$$\nabla \times \mathbf{E}(\mathbf{r}) = -i\omega\mu_0 \mathbf{H}(\mathbf{r}) \quad (2.6)$$

$$\nabla \times \mathbf{H}(\mathbf{r}) = \mathbf{J}(\mathbf{r}) \quad (2.7)$$

In these representations taking the cross product $\nabla \times \mathbf{E}$ and considering the relations $\nabla \times \nabla \times \mathbf{E} = \nabla(\nabla . \mathbf{E}) - \nabla^2 \mathbf{E}$ and $\mathbf{J} = \sigma \mathbf{E}$ the following equation is derived :

$$\nabla^2 \mathbf{E}(\mathbf{r}) + \nabla(\nabla\sigma(\mathbf{r})\mathbf{E}(\mathbf{r})/\sigma(\mathbf{r})) = i\omega\mu_0\sigma(\mathbf{r})\mathbf{E}(\mathbf{r}) \quad (2.8)$$

The time independent homogeneous diffusion equation

This expression is a second order differential equation describing a diffusion process for **E** (Arfken, 1985 ; Kong, 1986) and therefore the electromagnetic induction in the Earth is a diffusion process.

2.4. The determination of the Magnetotelluric Earth Response Functions (MERF) in the time and frequency domain.

In the magnetotelluric method the natural electric field **E** and magnetic field **H** are measured in two orthogonal directions, frequently N-S and E-W. The conventional coordinate system is x-positive North, y-positive East, z-positive downwards. The electric field **E** is measured in mV/km and the magnetic field **H** * in nT. The relationship between the two oscillating fields **E** and **H** is given by the ratio Z of their complex representations. This was defined in section 1.2 as the electrical impedance. The relations which hold between two orthogonal components of **E** and **H** are the following :

Time domain : $E(t) = Z(t) * H(t)$ (2.9)

Frequency domain : $E(w) = Z(w)H(w)$ (2.10)

where * denotes convolution.

* Note : Although **H** is usually the symbol for magnetic field strength, it is conventionally used in MT to denote the magnetic induction (unit nT).

Equations 2.9 and 2.10 imply that Z(t) or Z(w) is the response function of the " Earth Filter " in the time or the frequency domain respectively. The input signals H(t) and H(w) and the output signals E(t) and E(w) are the measured signals for **E** and **H** on the surface of the earth. E(t) and H(t) are Fourier transformed to E(w) and H(w) respectively and the opposite is valid for E(w) and H(w). In order to determine Z(t) and Z(w) the following techniques are applied in the time and frequency domain respectively.

2.4.(i). The time domain interpretation.

Estimation of the transfer function Z in the time domain is not commonly used. Several researchers (e.g. Kunetz) during the last 15 years have shown that the time domain estimation of Z provides more accurate results. Kunetz (1972) devoted much discussion to the time domain estimation of Z . A summary of his procedure follows.

The electric field **E** and the magnetic **H** are connected through the relation 2.9 where E, Z, H are functions of time and * indicates convolution process. **E** and **H** are measured along two orthogonal directions. Consequently :

$$E_x(t)=Z_{xx}*H_x(t)+Z_{xy}(t)*H_y(t) \qquad (2.11)$$

$$E_y(t)=Z_{yx}*H_x(t)+Z_{yy}(t)*H_y(t) \qquad (2.12)$$

Equations 2.11 and 2.12 imply that we are dealing with a double deconvolution problem since the electrical conductivity of the Earth varies two dimensionally.

Consider now a plane stratified earth of n layers with thicknesses $d_1, d_2, d_3, \ldots, d_n=\infty$ and conductivities $\sigma_1, \sigma_2, \sigma_3, \ldots, \sigma_n$.

For a one dimensional earth the function U(t) is defined by :

$$E(t)=U(t)*H'(t) \quad (2.13)$$

where H'(t) is the first derivative of H(t) with respect to time . H'(t) is the Fourier transform of -iwH(w). H is known to satisfy the equation :

$$E(w)=Z(w)H(w) \quad (2.14)$$

Therefore $U(w)=-\frac{Z(w)}{iw}$, is the Fourier transform of U(t) .

The Wiener-Levinson algorithm is finally used to compute U(t) in 2.13 from a system of n equations with n unknowns.

2.4.(ii). The frequency domain interpretation.

The frequency domain estimation of the electrical impedance Z is the most common computational procedure. The relation 2.10 for an Earth with conductivity varying in three dimensions i.e. $\sigma=\sigma(x,y,z)$ results in the following matrix equation:

$$\begin{vmatrix} E_x \\ E_y \\ E_z \end{vmatrix} = \begin{vmatrix} Z_{xx} Z_{xy} Z_{xz} \\ Z_{yx} Z_{yy} Z_{yz} \\ Z_{zx} Z_{zy} Z_{zz} \end{vmatrix} \begin{vmatrix} H_x \\ H_y \\ H_z \end{vmatrix} \quad (2.15)$$

Indices x,y,z relate to the two horizontal and the vertical components of the electric field E and the magnetic field H respectively. In order to compute the 3x3 impedance tensor, the two fields have to be measured in all directions. Practical problems arise in measuring the vertical component of the electric field Ez although in a few field studies it has been recorded (Bahr, 1983). However, since Ez is not normally measured, 2.15 invokes substitution of the 3x3 impedance matrix by a 2x2 matrix where only the x and y contributions are considered (see section 4.3.(ii), eq.4.3).

A frequency domain analysis procedure developed by Rooney (1977) and improved computationally by Dawes (1984) is presented in detail in chapter 4. Through this procedure the impedance tensor elements are determined for the upward and downward biased case (Sims et al., 1971). In the first case noise is assumed to be present only in the two magnetic channels while in the second case noise is assumed to be present only in the two electric channels. An example of the estimation of the off-diagonal tensor element Z_{xy} is given below for the two cases of biasing.

Electric component noise free - Upward bias.

$$Z_{xy}=\frac{(H_xE_x^*)(E_xE_y^*)-(H_xE_y^*)(E_xE_x^*)}{(H_xE_x^*)(H_yE_y^*)-(H_xE_y^*)(H_yE_x^*)} \qquad (2.16)$$

$$Z_{xy}=\frac{(H_xE_x^*)(E_xH_x^*)-(H_xH_x^*)(E_xE_x^*)}{(H_xE_x^*)(H_yH_x^*)-(H_xH_x^*)(H_yE_x^*)} \qquad (2.17)$$

Magnetic component noise free - Downward bias.

$$Z_{xy}=\frac{(H_xE_y^*)(E_xH_y^*)-(H_xH_y^*)(E_xE_y^*)}{(H_xE_y^*)(H_yH_y^*)-(H_xH_y^*)(H_yE_y^*)} \qquad (2.18)$$

$$Z_{xy}=\frac{(H_xH_x^*)(E_xH_y^*)-(H_xH_y^*)(E_xH_x^*)}{(H_xH_x^*)(H_yH_y^*)-(H_xH_y^*)(H_yH_x^*)} \qquad (2.19)$$

where * denotes conjugates and $(A_iB_j^*)$ represents auto-power spectra if A=B and i=j or cross-power spectra if $A\neq B$ and i=j or $i\neq j$. The impedance tensor elements $Z_{xx}, Z_{xy}, Z_{yx}, Z_{yy}$ for each frequency for each kind of biasing are computed by using similar expressions to 2.16-2.19 and finally averaged for the whole number of accepted windows assuming a lognormal distribution.

Accepted windows should satisfy specific preset criteria, such

as, a minimum power threshold, a minimum coherence and a minimum number of frequencies accepted per window.

2.5. The analytical properties of the MERF c(w) for the one dimensional earth.

I assume plane harmonic electromagnetic waves (e^{+iwt}) impinging on a plane Earth where $\sigma=\sigma(z)$ with the depth $z>0$ downwards. The diffusion equation for the Transverse Electric (TE) mode using equation 2.8 is :

$$\frac{\partial^2}{\partial z^2}E(z,w)-iw\mu_o\sigma(z)E(z,w)=0 \qquad (2.20)$$

The transfer function c(w) has been defined as the " modified impedance ". Schmucker and Weidelt (1975) determine c(w) as:

$$c(w)=-\frac{f(0,w)}{f'(0,w)} \qquad (2.21)$$

where f(0,w) is the TE mode potential satisfying the above diffusion equation. They have shown that :

$$c(w)=\frac{1}{iw\mu_o}\frac{E(z,w)}{H(z,w)} \qquad (2.22)$$

The transfer function c(w) has the dimension of length, therefore its real part defined by Schmucker (1970) as the " centre of gravity " of the in-phase induced current system can be used as a kind of a " skin depth ". Let $c=g-ih$ or $c=|c|e^{-i\phi}$; then $g\geq 0$, $h\geq 0$ or $0\leq\phi\leq\pi/2$ where g,h,ϕ are the real, imaginary parts of c and its argument respectively. The limiting values of c for $w\to 0$ and $w\to\infty$ are :

$$c(w)=\begin{cases}\dfrac{1}{k}\tanh(kH) & w\to 0\\[2ex] \dfrac{1}{\sqrt{iw\mu_o\sigma(0)}} & w\to\infty\end{cases} \qquad (2.23)$$

where H is the depth of a possible perfect conductor and $k=\sqrt{iw\mu_o\sigma(z)}$ and k is in km^{-1}. The relation of c to the Cagniard's apparent resistivity is $\rho=w\mu_o|c(w)|^2$. The analytical properties of c have been studied by Weidelt (1972) and Yee and Paulson (1988) for the special S^+ class of conductivity models (Parker, 1980 ; Yee and Paulson, 1988) for the interval $[0,z_B]$ where z_B is the depth to a perfect conductor.

The transfer function c(w) is shown to be zero-free and analytic in the whole w-plane except on the positive imaginary axis. Here it has an infinite series of interlacing simple poles and zeros or a finite number of poles and two branch points (Fig.2.2a, page 46) according to whether the integral :

$$\lim_{z\to z_B}\int_0^z \sqrt{\sigma(t)}\,dt \qquad (2.24)$$

converges or not. When the integral converges, c(w) is a meromorphic function with simple poles at $w=iK_n$ and permits by the Mittag-Leffler theorem an expansion in terms of partial fractions (Weidelt, 1972) given by the following expression :

$$c(w)=\int_0^\infty \frac{\alpha(K)\,dK}{K+iw} \qquad (2.25)$$

where $\alpha(K)$ is a non-decreasing function which includes both the discrete and the continuous part of the spectrum and is known as the

" spectral function ". Equation 2.25 provides the basis for a study for the solution of the one dimensional magnetotelluric problem.

2.6. A seismic analogue for the magnetotelluric sounding method : Realistic or not ?

The application of geometrical optics and image theory to the magnetotelluric sounding method is controversial.

Yost (1952) and Orsinger and Van Nostrad (1954) with their " image theory " were the first to consider the " reflection of electromagnetic waves " in the Earth.

During the last 20 years several authors approached the electromagnetic induction problem in the Earth using geometrical optics.

In the earlier papers (Chauveau, 1967 ; Kunetz, 1972 ; Szaraniec, 1975) the authors concentrated on finding analogies of the magnetotelluric with the seismic methods. In Chauveau's (1967) study Maxwell equations for the magnetotelluric fields have the time dependent form as given in 2.1 and 2.2. He shows that the electric field **E** and the magnetic field **H** satisfy the second order differential equations :

$$\nabla^2 \mathbf{E}(\mathbf{r},t) = \mu\left(\sigma \frac{\partial \mathbf{E}(\mathbf{r},t)}{\partial t} + \varepsilon \frac{\partial^2 \mathbf{E}(\mathbf{r},t)}{\partial t^2}\right) \qquad (2.26)$$

$$\nabla^2 \mathbf{H}(\mathbf{r},t) = \mu\left(\sigma \frac{\partial \mathbf{H}(\mathbf{r},t)}{\partial t} + \varepsilon \frac{\partial^2 \mathbf{H}(\mathbf{r},t)}{\partial t^2}\right) \qquad (2.27)$$

These are known wave equations for **E** and **H** and have a similar form to the wave equation :

$$\nabla^2 U(r,t) = \frac{1}{v^2} \frac{\partial^2 U(r,t)}{\partial t^2} \qquad (2.28)$$

which is satisfied by acoustic waves, where U(r,t) is the elastic displacement and v is the acoustic wave velocity. In 2.28 there is no damping factor given by the first derivative of U with respect to t as in eqs.2.26 and 2.27 where there are first derivatives of **E** and **H** with respect to t.

In this representation Chauveau assumes electric displacement currents to be present. As in seismics, computation of reflection and transmission coefficients is involved. At a later stage, he is required to neglect the displacement currents to satisfy the diffusion character of the electromagnetic induction in the Earth. A subsequent work applying the geometrical optics to the magnetotelluric sounding method is based on such an approach. Kunetz (1972) in addition introduces time domain processing to estimate the transfer functions. His ideas are influenced by the deconvolution techniques applied in seismics. Szaraniec (1975) introduces equal time homogeneous layers while simultaneously Lowenthal (1975) and Shoham and Lowenthal (1975) develop their equal penetration depth discretizable models.

Recently Lee et al. (1987) and Levy et al. (1988) apply purely seismic reflection techniques to solve the magnetotelluric inversion problem for the one and two dimensional cases respectively. Their computations involve the principles of two-way travel time and reflection coefficients.

While they borrowed ideas from seismics another group of authors has treated the problem as a diffusion process with almost no raypath theory involved. Parker (1980) and Parker and Whaler (1981) with

their H^+ inversion scheme introduced Goupillaud equal penetration time models. Engelhard (1982) used the raypath theory but tried to overcome the ambiguity by converting the diffusion equation to a wave equation. Zhdanov and Frenkel (1983a ; 1983b) and Zhdanov and Frenkel (1984) introduced the " electromagnetic field migration ", the equivalent to the seismic migration. They used the Stratton-Chu integral equations in " reverse time " for observed electromagnetic fields in the quasi-stationary range. Very recently Tzanis (1987) made an attempt to relate Parker's delta functions to electromagnetic reflectors. His work is covered theoretically by Szaraniec's (1975) and Goupillaud's (1961) ideas.

2.7. Two analogues for the one dimensional magnetotelluric problem.

Physical phenomena in our world quite often share common features. This most of the times is steering to common tactics for solving the imposed problem. Two physical phenomena, serve as analogues for electromagnetic induction within the Earth. These are the free particle motion as a quantum physics analogue and the beads on a vibrating string as a mechanical equivalent.

2.7.(i). A quantum physics analogue.

The quantum physics problem of particle motion in the presence of potential V(x) is considered. The time independent Schrödinger equation describing the particle motion in one dimension is :

$$\frac{\partial^2}{\partial x^2}\Phi(x)+\frac{2m}{h^2}(E-V(x))\Phi(x)=0 \quad (2.29)$$

where m is the mass of the particle, h is the modified Planck's constant, $\Phi(x)$ is the usual wave function, E and V(x) are its total energy in the state considered and the potential energy respectively. In the case of free particle motion V(x)=0.

The Green's function expansion for the equivalent eigenvalue problem (Economou, 1979) is :

$$G(x,x')=\frac{2m}{h^2}\int_{-\infty}^{+\infty}\frac{\Phi(x)\Phi^*(x')}{z-E_n}dx \quad (2.30)$$

where * denotes conjugate for Φ. As is known from quantum physics equation 2.30 implies that G(x,x') has a set of simple poles at the positions of its discrete eigenvalues E_n. These poles are on the real axis E of the complex z-plane (Fig.2.2b) and define the discrete energy spectrum of the particle, i.e its eigenstates. The continuous energy spectrum corresponds to a branch cut. The physical meaning of the discrete spectrum is that the free particle is moving at energy levels indicated by the spectrum.

2.7.(ii). The beads on a vibrating string problem.

Consider now a set of N beads with different masses m_k, k=1,..,N distributed along a weightless vibrating string fixed at its right extremity (Barcilon, 1975). If l_k is the distance between the k and the k+1 masses, the total length of the string is taken to be unity $\Sigma_k l_k=1$ (See Fig.2.3a). The response of the system $\frac{u_o}{\theta_o}$ is a rational function of u and θ therefore permitting the following

Fig.2.2. A quantum physics analogue for the magnetotelluric problem.

a. The magnetotelluric problem : The transfer function c(w) is meromorphic when the integral of 2.24 converges. It has a series of poles $K=iw_n$ on the positive imaginary axis of the the complex w-plane.

b. Free particle motion : The Green's function G(x,x') has a set of simple poles on the real axis of the complex z-plane and a branch cut.

Fig.2.3. The beads on a vibrating string problem and their energy spectrum.

a. N beads of different masses m_k, k=1,...,N (on this illustration N=9) on a weightless vibrating string of total length $\Sigma_k l_k=1$. u_k and Θ are the time reduced displacement of the n=0 bead and the angle of n=0 segment of the string from the equilibrium position. The discrete energy spectrum of the system is provided exactly below this diagram in a delta function sense. Note that the energy levels are dependent on the masses of the vibrating beads.

b. The same problem where now the fifth-eighth beads have the same mass. The discrete energy spectrum is provided below this diagram in a delta function sense. Beads of the same mass m_k correspond now to delta functions representing the same energy level.

Fig.2.4. A two layer synthetic model. The model resistivity and phase responses are shown with dashed lines. The D^+ delta function model and the corresponding resistivity and phase responses are shown with continuous lines.

Fig.2.2

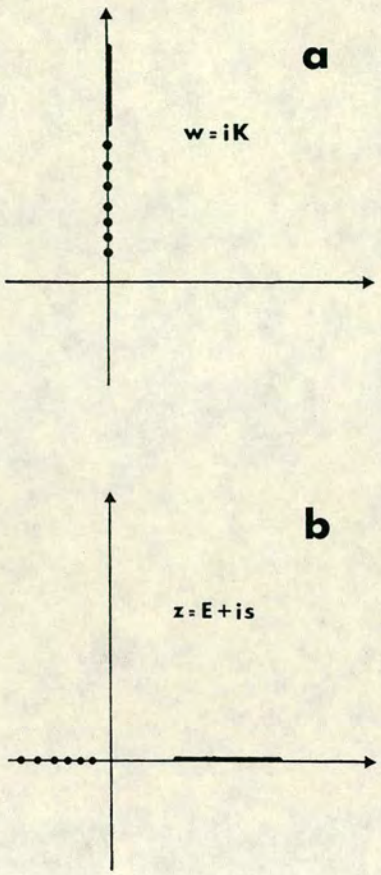

Fig.2.3

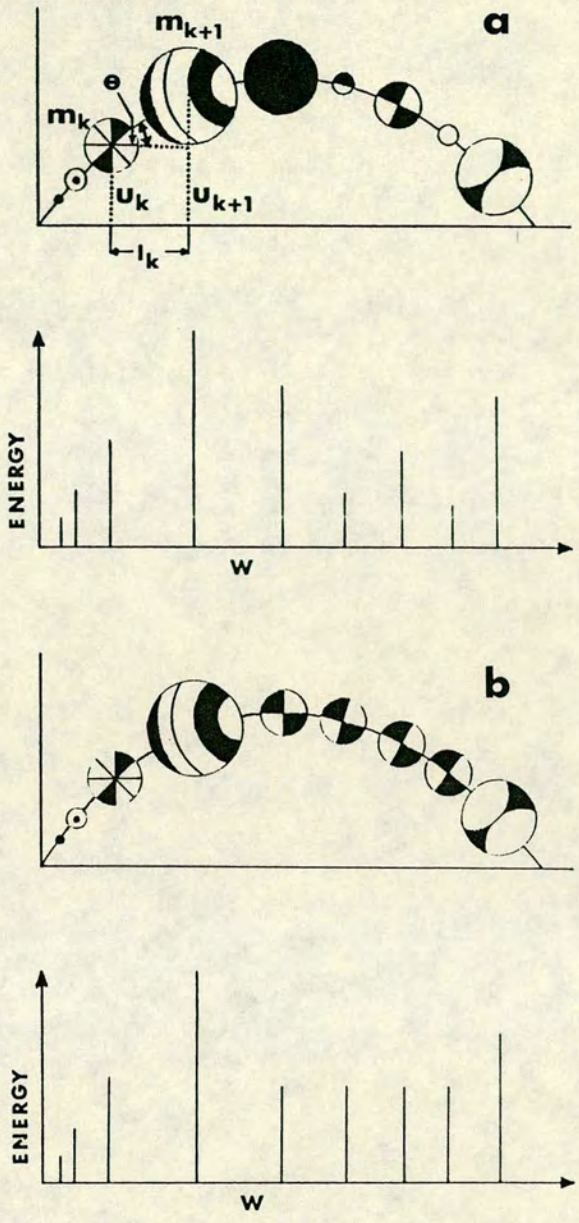

Fig.2.4

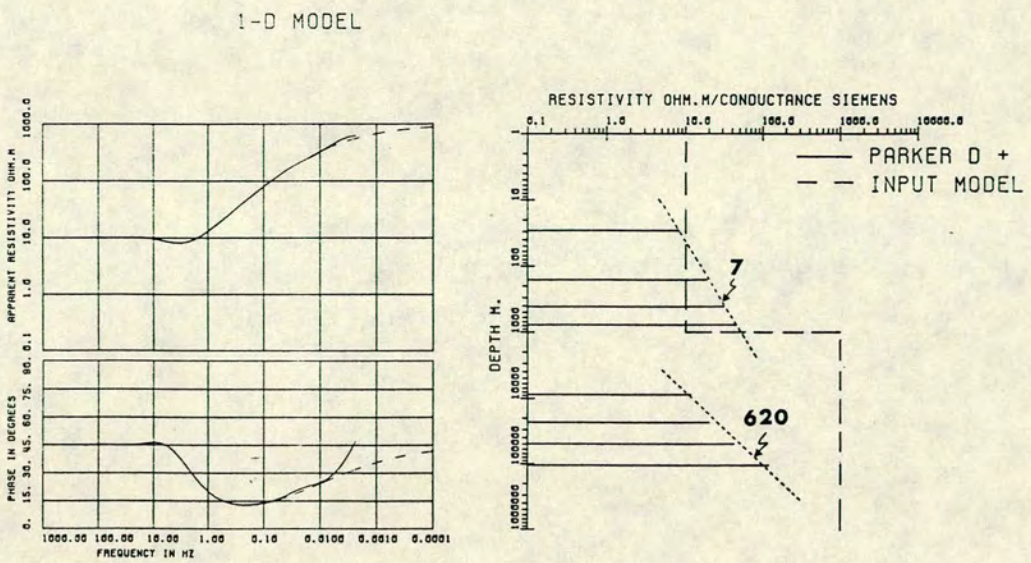

continued fraction for N beads (Wall, 1948) :

$$-\frac{u_o}{\theta_o} = l_o + \cfrac{1}{-m_1 w^2 + \cfrac{1}{l_1 + \cfrac{1}{-m_2 w^2 + \ldots + \cfrac{1}{l_N}}}} \qquad (2.31)$$

u_o, θ_o are the time reduced displacement of the n=0 bead and the angle of the n=0 segment of the string from the equilibrium position. Knowing the natural frequencies w of the system and the response $-\frac{u_o}{\theta_o}$, the masses and the distances l_k can be determined. The discrete energy spectrum of the system is shown in Fig.2.3a as Energy versus angular frequency w in a delta function sense. It can be noticed that the energy levels are dependent on the masses of the vibrating beads.

2.8. The spectral function and the " electromagnetic energy spectrum " of the earth.

I recall the case where plane harmonic electromagnetic waves are impinging on a plane earth surface. The Earth is considered to be one dimensional under the same conditions as in section 2.5. The diffusion equation 2.20, for the TE mode is similar to equation 2.29 (when V(x)=0) which describes free particle motion in quantum physics. The difference occurs in the factors $2mE/h^2$ and $-iw\mu_o\sigma(z)$ which are obviously associated with the two different physical phenomena. The eigenvalue problem for 2.20 is given by the following expression :

$$\frac{1}{\mu_o \sigma(z)} \frac{\partial^2}{\partial z^2} u_n(z) = -K_n u_n(z) \qquad (2.32)$$

where $K_n = iw_n$. The variables u_n, K_n are the eigenfunctions and eigenvalues for 2.32. The boundary conditions for 2.32 are $u_n'(0) = u_n(z_B) = 0$ where z_B is the depth to a perfect conductor with which the model terminates (Parker and Whaler, 1981). The set of functions $\{u_n\}$ can be considered as in the free particle problem, orthonormal i.e :

$$\int_{-\infty}^{+\infty} u_n(z) u^*_m(z) dz = \delta_{nm} \quad / \quad \delta_{nm} = 1, \ 0 \text{ for } n=m, \ n \neq m \qquad (2.33)$$

The completeness of the set is expressed by the following relation :

$$\sum_n u_n(z) u^*_n(z') = \delta(z-z') \qquad (2.34)$$

If $G(z,z')$ is the Green's function corresponding to the differential operator $\frac{1}{\mu_o \sigma(z)} \frac{\partial^2}{\partial z^2}$, then $G(z,z')$ is defined as the response of the point source expressed by the delta function $\delta(z-z')$. $G(z,z')$ satisfies the inhomogeneous form :

$$\left(\frac{1}{\mu_o \sigma(z)} \frac{\partial^2}{\partial z^2} - iw \right) G(z,z') = \delta(z-z') \qquad (2.35)$$

In particular the difference of the two physical phenomena is expressed mathematically by the kind of poles of $G(z,z')$ or $G(x,x')$. In the electromagnetic induction problem u_n can be expanded in the form :

$$G(z,z') = -\frac{1}{\mu_o \sigma(z')} \int_{-\infty}^{+\infty} \frac{u_n(z)\, u^*(z')}{K+iw}\, dz \qquad (2.36)$$

with G(z,z') satisfying 2.35. The poles of G(z,z') lie on the positive imaginary axis of the complex w-plane (K=iw). Parker (1980) has proved that c(w)=-G(z,z') and consequently :

$$c(w) = \frac{1}{\mu_o \sigma(0)} \int_{0}^{z_B} \frac{|u_n(z)|^2}{K+iw}\, dz \qquad (2.37) \text{ where } |u_n(z)|^2 = u_n(z)\, u^*{}_n(z')$$

In the magnetotelluric method measurements are taken for discrete frequencies and therefore 2.25 and 2.37 are reduced to :

$$c(w) = \sum_n \frac{\alpha_n}{K_n+iw} \qquad \alpha_n > 0,\ K_n > 0 \qquad (2.38)$$

$$c(w) = \frac{1}{\mu_o \sigma(0)} \sum_n \frac{|u_n(0)|^2}{K_n+iw} \qquad (2.39)$$

From 2.38 and 2.39, it is obvious that $\alpha_n = \frac{1}{\mu_o \sigma(z)} |u_n(z)|^2$, $z \to 0$. In 2.38 residues α_n of c(w) correspond to the poles K_n of c(w) which are the eigenvalues of 2.32. In 2.39 the quantity $|u_n(z)|^2$ relates to the density of states of the system i.e the eigenstates.

In the case of a multi-layered Earth with n layers of thicknesses h_1, h_2,..., h_n and conductivities σ_1, σ_2,..., σ_n respectively, the eigenstates of the system relate to the free decay modes of the electromagnetic waves. The current flow for TE-decays occurs in horizontal planes within the n conductive layers. The factor iw_n in the denominators of 2.38 and 2.39 expresses energy dissipation at the points given by the poles of c(w). The energy dissipation is dependent on conductivity changes.

Therefore conductivity inferences in the Earth can be made by finding the poles and the residues of c(w), i.e the " electromagnetic energy spectrum " of the Earth. The Parker-Whaler D^+ inversion is one known algorithm with which these parameters can be estimated. The derived discrete spectrum of a(K) is converted to a conductance-depth delta function model.

The delta functions in the Parker D^+ algorithm represent conductances in Siemens. Generally conductance $\tau(h)$ is a function of bounded variation. Parker (1980) introduced the Banach space NBV[0,h] for τ. Every $\tau \varepsilon$ NBV[0,h] and $\tau(h)$ is the integrated conductivity within [0,h] i.e :

$$\tau(h)=\int_0^h \sigma(t)dt \qquad (2.40)$$

Conductance is a piece-wise continuous function. The points of its discontinuity correspond to delta functions in conductivity.

Since $\sigma > 0$ then S^+ is a positive cone in S (Parker, 1980) and all delta function models belong to the normed vector space D^+ which is a subspace of S^+. Because c(w) is a rational function of E and H then c(w) in eq. 2.25 can be expanded in the following continued fraction :

$$c(w)=h_0+\cfrac{1}{i w\mu_0\tau_1+\cfrac{1}{h_1+\cfrac{1}{i w\mu_0\tau_2+\cfrac{1}{\ldots+\cfrac{1}{h_N}}}}} \qquad (2.41)$$

where generally $\tau_n=\sigma_n h_{n-1}$. As an example if τ_2 is the conductance which corresponds to the second delta function of a D^+ model then this is the integrated conductivity σ_2 for the separation h_1 from the delta function above.

2.9. Numerical examples with synthetic data.

Some thoughts on the one dimensional magnetotelluric problem were given in the previous section of this chapter, the main subject of the discussions being the Parker-Whaler D^+ algorithm (1981). The D^+ algorithm was first introduced as a necessary and sufficient condition for solution of the one dimensional inverse magnetotelluric problem (Parker, 1980 ; Parker and Whaler, 1981 ; Parker, 1983). Since then, many authors and researchers have used and still use this algorithm for this purpose (Jady et al., 1983 ; Jady and Patterson, 1983 ; Oldenburg et al., 1984). In their interpretation the attention is necessarily paid to the significance of the X^2 misfit, and the obtained delta function model is only accepted as an extreme of all the acceptable models. In the present study attempts are made to give some physical meaning to the delta functions.

Some theoretical ideas concerning the question of the physical meaning of the D^+ delta functions were described in 2.8. It was concluded that the subject needs further theoretical examination. At the moment the ideas that the D^+ delta functions could be related to conductivity changes are speculative only . However some results of computations with synthetic and real magnetotelluric data are now presented for discussion.

EX BIBL. UNIV. EDINBURGH

2.9.1. Resolving a 1000 Ohm.m half space.

The test of the resolving power of the D^+ algorithm was initiated by applying it to a simple two layer Earth model. In particular, the example of one layer overlying a resistive half-space, was studied.

Fig.2.4 (page 46) shows a two layer synthetic model (dashed line) and its resistivity and phase responses. The top layer has resistivity of 10 Ohm.m and the underlying half space 1000 Ohm.m. The 10-1000 Ohm.m resistivity contrast is located at 1000 m depth. The best fit D^+ model (solid line) is shown on the same figure.

Forty frequencies were used in the computations and the calculated X^2 misfit was found to be 49.4 for an expected value of 80 ($x^2=2N$ where $N=40$). Based on observations associated with real data, a 10 % of the real part of c(w) was adopted as an error value per frequency.

The D^+ model consists of eight delta functions. The fourth delta function is the only one which is located at 770 m, a depth comparable to the 1000 m depth resistivity contrast of 10-1000 Ohm.m. The eighth delta functions can be grouped into two sets, each giving a different slope, calculated by dividing the delta function separations by the relative conductances, the derived slopes having units of resistivity. The first group consists of the first four delta functions with an average slope (resistivity) of 7 Ohm.m and the second group of four delta functions with an average slope (resistivity) of 620 Ohm.m (Fig.2.4, page 46). Efforts to assign a physical meaning to the D^+ delta functions, lead to the possible assumption that, they could correspond each to a resistivity contrast. This is not always the case. The delta functions in this

experiment as already shown, are grouped into two sets. The first set of 7 Ohm.m slope corresponds to the first 10 Ohm.m layer of the synthetic input model and the second set of 620 Ohm.m slope corresponds to the input half space of 1000 Ohm.m. Several attempts were made to give an explanation to this inconsistency. The most comprenhensive results are discussed in the next paragraph.

2.9.2. Simulating a granitic intrusion.

Fig.2.5 (page 56) shows a synthetic one dimensional earth model with five layers of different electrical properties, overlying a conductive half-space. The model simulates a hypothetical granitic intrusion. The top 100 m consist of slates and grits overlying a layer dominated by slates, with thickness 400 m. The granite is wet in its top 1.5 km and rather dry from 2-10 km. The underlying structure represents a more conductive middle and lower crust extending to an even more conductive upper mantle.

Resistivity and phase data due to this structure are shown in Fig.2.5 (solid line). The smooth synthetic data were perturbed to simulate artificial or instrumental random noise (Fig.2.5, solid bars). The noise was introduced by adding to the smooth data random numbers obeying a normal distribution. Error bars have been taken to be 20 % and 10 % of the actual resistivity and phase values respectively. The latter was not an arbitrary choice but results from real data observations. The D^+ algorithm was tested for both smooth and noisy data successively.

2.9.2.(i). Test 1 : D^+ models for the unperturbed data.

Table 2.1 shows the modified impedance data c(w) for 38 frequencies taken from the smooth data set. Error bars indicate 10 % of the real part of c(w). Fig.2.6 (page 56) shows the D^+ model, the input model and their corresponding resistivity and phase responses. The continuous solid line relates to the D^+ model while the dashed one, indicates the input model. The delta function separations above each delta function were divided by the relative conductances, assuming that resistivity within the same layer is uniform.

The result was a resitivity-depth output model. Model parameters, for the input, D^+ and the output resistivity-depth models respectively are shown in Table 2.2 (page 57) for comparison. The 1.4 calculated misfit reflects the 10% error bars of the real part of c(w). However it does not have any particular meaning for the exact data of this experiment.

The D^+ model consists of nine delta functions. The first two delta functions seem to give comparable structure with the input. The third and fourth delta functions appear to relate to the same layer with resistivity about 4000 Ohm.m. The 2000 Ohm.m to 10000 Ohm.m contrast is not detected. Delta functions, fifth up to eighth clearly relate to the 500 Ohm.m layer of the input model. It was noticed that these delta functions were located at such depths with such conductance values so as to keep the electrical properties of this layer the same throughout this depth range.

The beads on a vibrating string problem is being used here to simulate the discussed magnetotelluric problem. Fig.2.3a (page 46) illustrates beads of different masses on a vibrating string with

TABLE 2.1

The unperturbed data for the model of Fig.2.5

No	w in sec^{-1}	c(w) in m		error δc(w)
		Real	Imaginary	
1	0.047	56000.0	-22730.0	5611.0
2	0.062	53050.0	-20390.0	5305.0
3	0.083	50290.0	-18490.0	5029.0
4	0.112	47770.0	-17010.0	4777.0
5	0.149	45410.0	-15910.0	4541.0
6	0.199	43140.0	-15150.0	4314.0
7	0.265	40880.0	-14710.0	4088.0
8	0.353	38560.0	-14530.0	3856.0
9	0.471	36090.0	-14520.0	3609.0
10	0.628	33430.0	-14570.0	3343.0
11	0.834	30580.0	-14540.0	3058.0
12	1.117	27620.0	-14280.0	2762.0
13	1.490	24710.0	-13740.0	2471.0
14	1.987	22030.0	-12940.0	2203.0
15	2.650	19680.0	-12030.0	1968.0
16	3.533	17680.0	-11170.0	1768.0
17	4.712	15920.0	-10500.0	1592.0
18	6.283	14240.0	-10050.0	1424.0
19	8.379	12500.0	-9734.0	1250.0
20	11.170	10670.0	-9431.0	1067.0
21	14.900	8760.0	-8999.0	876.0
22	19.870	6892.0	-8355.0	689.2
23	26.500	5192.0	-7489.0	519.2
24	35.330	3771.0	-6465.0	377.1
25	47.120	2679.0	-5390.0	267.9
26	62.830	1899.0	-4369.0	189.9
27	83.790	1372.0	-3471.0	137.2
28	111.700	1029.0	-2726.0	102.9
29	149.000	806.9	-2131.0	80.7
30	198.000	659.7	-1669.0	66.0
31	265.000	555.6	-1316.0	55.6
32	353.000	475.1	-1047.0	47.5
33	471.200	408.0	-840.2	40.8
34	628.300	349.0	-679.3	34.9
35	837.900	299.2	-552.2	29.9
36	1117.000	254.8	-450.5	25.5
37	1490.000	216.6	-368.0	21.7
38	1987.000	184.7	-300.5	18.5

No=Number

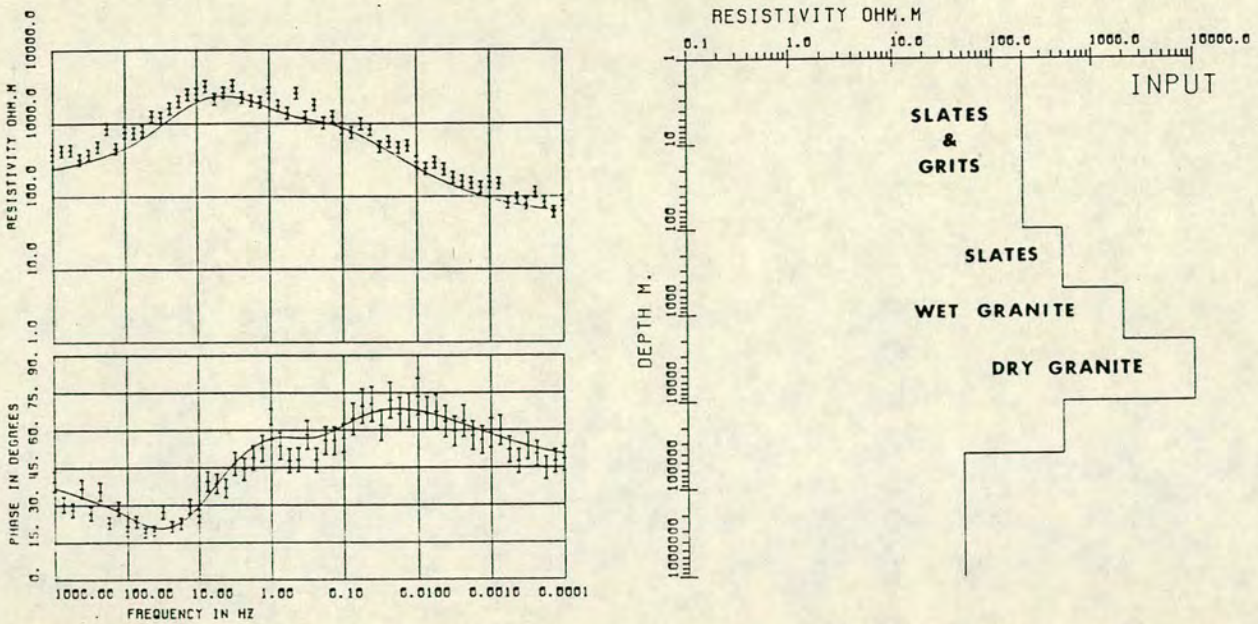

Fig.2.5. Simulating a granitic intrusion. A synthetic model with five layers. Noise was introduced to the smooth data by adding random numbers obeying a normal distribution. The model resistivity and phase responses are illustrated with continuous lines (unperturbed data) and solid error bars (perturbed data) respectively.

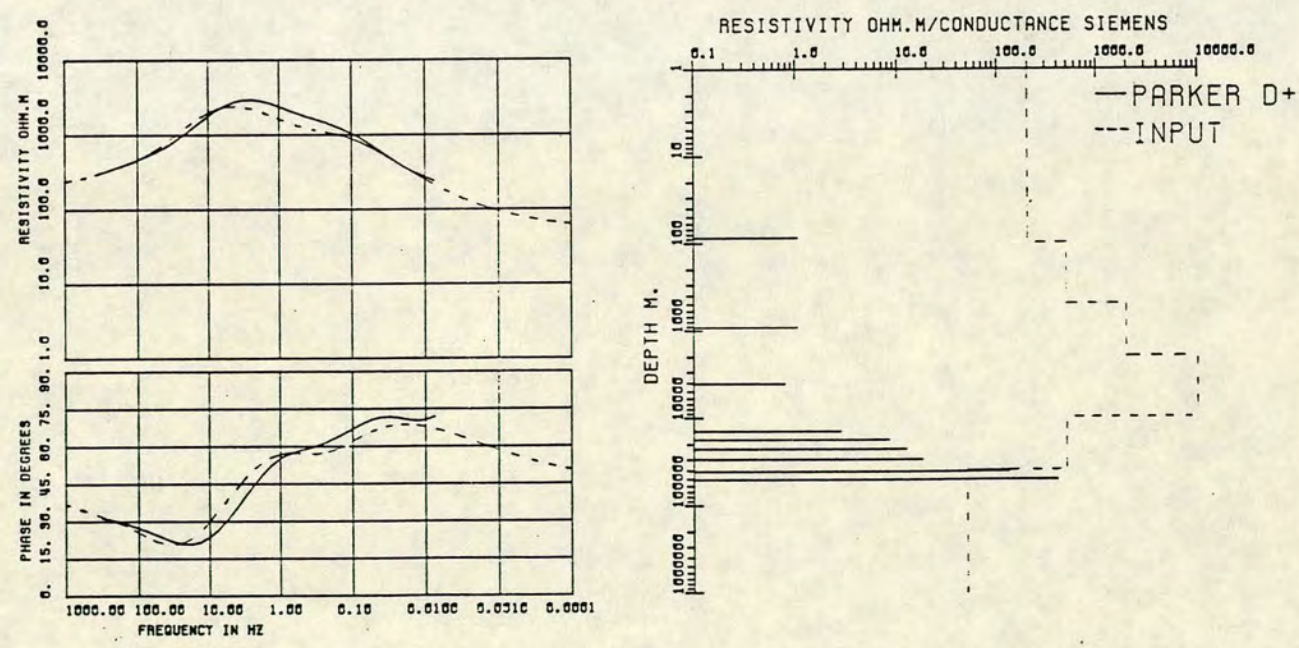

Fig.2.6. The input five layer model and the derived Parker-Whaler D+ model for the unperturbed data set of Fig.2.5. The corresponding resistivity and phase responses are shown with dashed and continuous lines respectively.

their respective energy spectrum.

Fig.2.3b (page 46) illustrates the same beads but now the fifth, sixth, seventh and eighth bead counted from the left have the same masses. The result is that the four peaks, fifth to eighth from the left to the right represent the same energy levels at about the same frequency range of their spectrum. The distance between these four equivalent energy peaks can vary with the distance between the corresponding beads. If their distance is small the peaks can hardly

TABLE 2.2

Model parameters for the D⁺ model of Fig.2.6

	Input		Parker-Whaler D⁺			
No	Resistivity (Ohm.m)	Depth (m)	Conductance (Siemens)	Depth (m)	Resistivity (Ohm.m)	Depth (m)
1	200.0	100.0	1.05	87.0	83.0	87.0
2	500.0	500.0	1.04	922.0	801.0	922.0
3	2000.0	2000.0	0.77	4078.0	4000.0	14230.0
4	10000.0	10000.0	2.72	14230.0	400.0	41147.0
5	500.0	40000.0	8.2	17790.0	25.0	∞
6	50.0	∞	12.2	22743.0		
7			17.8	29890.0		
8			128.3	41147.0		
9			401.6	50992.0		
			Perfect Conductor			
			$x^2=1.4$			

No=Number

be distinguished and rather give one peak. When their distances increase the peaks separate. The last example can easily simulate the previous case of the four delta functions which as was shown provide the same information which is comparable with the properties of the fifth layer of the input model which has a thickness of 30 km. The last delta function gives information for the conductive half space.

2.9.2.(ii). Test 2 : D^+ models for the perturbed data.

Table 2.3 shows the modified impedance data for 40 frequencies taken from the perturbed data set of Fig.2.5 (page 56). Errors are 10 % of the real part of c(w). It was found that there is no model to fit this data set. The computed x^2 was found to be 105.3 for an expected of 80.

Fourteen data points had high misfits and were the main contributors to the large total misfit. The former are the most noisy data points and were finally discarded. Fig.2.7 (page 60) shows resistivity and phase data for the 40 frequencies in comparison with the unperturbed responses of the input model. Error bars represent 20 % and 10 % of resistivity and phase values respectively, as this was discussed above.

The discarded 14 data points are marked with solid boxes and their listed values are indicated with asterisks in Table 2.3.

When the 14 bad data points were removed an acceptable D^+ model was obtained for the remaining 26 frequencies. The x^2 misfit was reduced to 28.8 nearly half of the expected value 52. Fig.2.8 (page 60) illustrates the best fitting D^+ model with its resistivity and

TABLE 2.3

The perturbed data for the model of Fig.2.5

No	w in sec^{-1}	c(w) in m		error δc(w)	
		Real	Imaginary		
1	0.014	74160.0	-36920.0	7416.0	
2	0.019	65370.0	-38690.0	6537.0	
3	0.026	66990.0	-33620.0	6699.0	
4	0.035	66760.0	-27960.0	6676.0	
5	0.047	52180.0	-22610.0	5218.0	
6	0.062	52450.0	-15650.0	5245.0	
7	0.083	56780.0	-23010.0	5678.0	
8	0.112	47200.0	-20630.0	4720.0	
9	0.149	46540.0	-15240.0	4654.0	
10	0.199	34410.0	-18410.0	3441.0	*
11	0.265	41930.0	-14940.0	4193.0	
12	0.353	39540.0	-14760.0	3954.0	
13	0.471	28700.0	-13770.0	2870.0	
14	0.628	24540.0	-16110.0	2454.0	
15	0.834	25330.0	-17290.0	2533.0	
16	1.117	19890.0	-13530.0	1989.0	
17	1.490	20530.0	-18520.0	2053.0	*
18	1.987	16760.0	-10430.0	1676.0	*
19	2.650	18500.0	-16620.0	1850.0	*
20	3.533	11630.0	-10600.0	1163.0	*
21	4.712	12310.0	-9077.0	1231.0	
22	6.283	14410.0	-7567.0	1441.0	*
23	8.379	9656.0	-7366.0	965.6	
24	11.170	8107.0	-7091.0	810.7	
25	14.900	6853.0	-7019.0	685.3	
26	19.870	7422.0	-7040.0	742.2	
27	26.500	4740.0	-6365.0	474.0	*
28	35.330	3874.0	-4860.0	387.4	*
29	47.120	4188.0	-5102.0	418.8	
30	62.830	2186.0	-4561.0	218.6	*
31	83.790	2139.0	-3789.0	213.9	
32	111.700	1291.0	-3115.0	129.1	
33	149.000	951.2	-2438.0	95.1	
34	198.700	896.0	-1742.0	89.6	*
35	265.000	579.0	-1626.0	57.9	*
36	353.300	379.8	-1119.0	38.0	*
37	471.200	392.5	-915.9	39.5	
38	628.000	292.3	-825.8	29.2	*
39	837.900	279.2	-513.1	27.9	*
40	1117.000	268.1	-639.2	26.8	*

No=Number

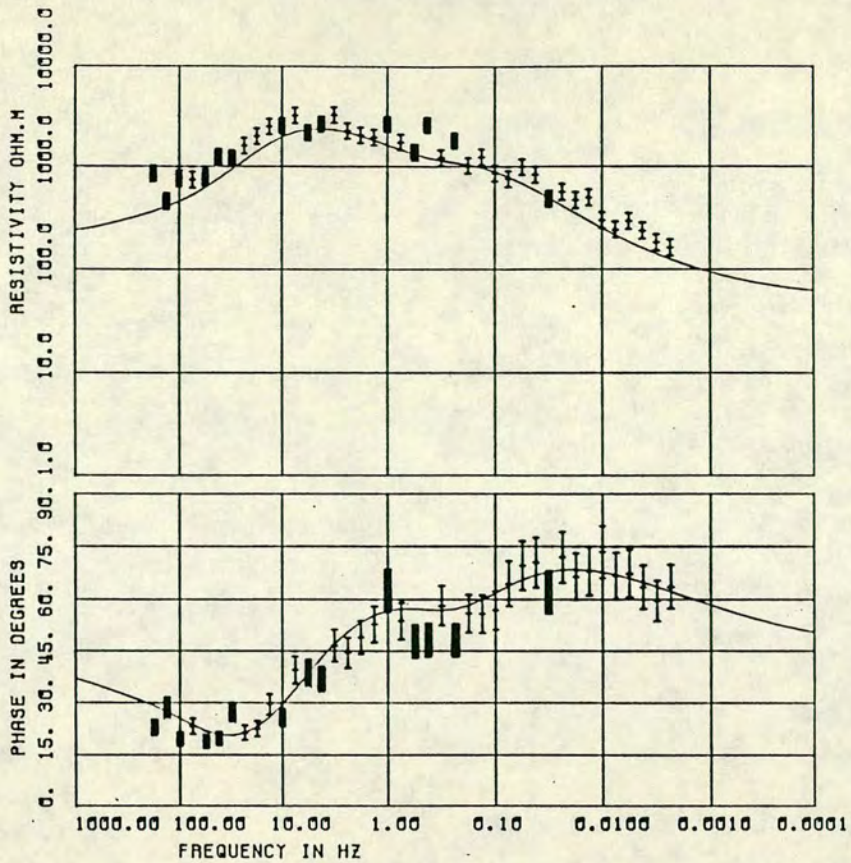

Fig.2.7. The unperturbed (continuous line) and the perturbed (error bars) resistivity and phase responses for the five layer model of Fig.2.5. Solid black bars indicate 14 data points which were discarded in order to obtain a D^+ delta function model.

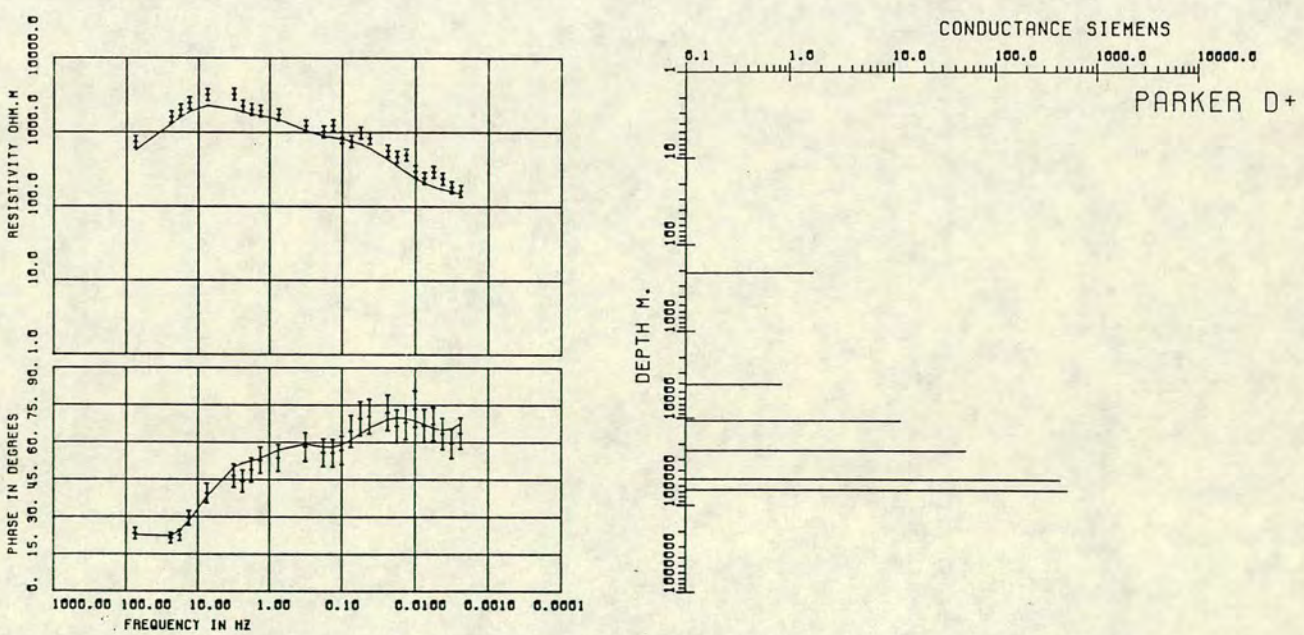

Fig.2.8. The best fit Parker-Whaler D^+ model for the perturbed data set of Fig.2.7 (error bars). The 14 discarded points were not included. The model resistivity and phase responses are represented with solid lines.

phase response in comparison with the input responses of the perturbed 26 frequencies. Model parameters for the input, D^+ and the output resistivity-depth models respectively are shown in Table 2.4.

The D^+ model involves six delta functions. The first delta function relates to with the first two layers of the input model. The next two delta functions are associated with the granite and the boundary at 10.8 km coincides with the 1000 Ohm.m to 500 Ohm.m contrasts at 10 km in the input model. The fourth delta function relates to the fifth layer and the last two delta functions to the relatively conductive half space of 50 Ohm.m of the input model respectively. The D^+ algorithm has been applied as a data quality criterion but did not recover exactly the true structure.

TABLE 2.4

Model parameters for the D^+ model of Fig.2.8

	Input		**Parker-Whaler D^+**			
No	Resistivity (Ohm.m)	Depth (m)	Conductance (Siemens)	Depth (m)	Resistivity (Ohm.m)	Depth (m)
1	200.0	100.0	1.67	213.0	127.0	213.0
2	500.0	500.0	0.85	4090.0	2700.0	10800.0
3	2000.0	2000.0	11.70	10800.0	257.0	23780.0
4	10000.0	10000.0	50.50	23780.0	45.0	∞
	500.0	40000.0	435.00	50393.0		
6	50.0	∞	512.0	66828.0		
			Perfect Conductor			
			x^2=105.3			

No=Number

2.10. Numerical examples with real field data.

The practical aspects of the D^+ algorithm were tested with real field data collected at the geothermal fields of Milos island, Greece and Olkaria, Kenya. Sixty seven soundings were conducted in total at both studies. Nineteen soundings were broadband, in the frequency range 10^{+2}-10^{-4} Hz, while the majority of the magnetotelluric measurements was undertaken in the frequency range 10^{+2}-10^{-2} Hz. The two case studies are fully described in chapters 3-5 and 6-7 respectively.

Only two data sets from a corresponding number of sites, are shown as examples to demonstrate the resolving power of the Parker-Whaler D^+ algorithm. These are, site 631 on Milos island and site 927 in Olkaria. This choice was based on the fact that both the sites are located very close to two boreholes - site 631 within 150-200 m from well M1 and site 927 within 1000 m from well OW701 respectively. The models will be discussed with respect to the borehole stratigraphy and relative temperature profiles in chapters 5 and 7 respectively.

In this section the resulting D^+ models are compared with the electrical models derived by using three other inversion techniques. These were the Fischer et al. (1981), Dawes (Sule, 1985) and the Jupp-Vozoff (1975) methods respectively. The four electrical models are discussed in terms of their misfit to the observed apparent resistivity and phase data. The Jupp-Vozoff method was used only for 631. All the calculations were carried out for the invariant electrical impedance $Z_{inv}=(Z_{xx}Z_{yy}-Z_{xy}Z_{yx})^{½}$.

Site 631 on Milos island

Modified impedances c(w) (Parker-Whaler D^+) and apparent resistivities and phases (Dawes and Fischer) for 47 frequencies were modelled. Only the 27 higher frequencies were used by the Jupp-Vozoff method since at that time of modelling only these data were available.

Fig.2.9a shows four electrical models derived by using the methods named above. The models are represented with columns and the figures in the columns are resistivities in Ohm.m. On the left side of the column which corresponds to the D^+ model, the illustrated figures are conductances in S. The resistivity-depth model equivalent to the D^+ model was obtained by following the procedures described in sections 2.9.1 and 2.9.2.

A list of the model parameters with the relative misfits for each method are provided in Table 2.5. The fit of the models to the observed responses is illustrated in Fig.2.10a. The model resistivity and phase responses have been calculated by using the relative formulae given by Keller and Frischknecht (1966).

TABLE 2.5

Model Misfit for site 631 on Milos

Jupp-Vozoff	Dawes	Fischer	Parker-Whaler D^+
Data corresponding to			
27 frequencies		47 frequencies	
Resistivity Mean % error 11.5	Sum of weighted squared diff. 0.170	$\varepsilon_o/\varepsilon_\phi/\varepsilon$ 0.1,0.7,0.5	Calculated x^2=25.9 Expected x^2=94
Phase Mean % error 10.0		$\varepsilon_{on}, \varepsilon_{\phi n}, \varepsilon_n$ 0.009,0.5,0.4	

Fig.2.9. Comparison of the Parker-Whaler D^+ models for two sites on Milos and Olkaria respectively with the electrical models derived by using three other methods. These were the Dawes (Sule, 1985), Fischer et al. (1981) and the Jupp and Vozoff (1975) methods respectively. The models are illustrated with columns. The figures on the columns are resistivites in Ohm.m. On the right side of the D^+ model the given figures are conductances in S.

a. Site 631 on Milos, Greece.

b. Site 927 in Olkaria, Kenya.

Fig.2.10. Comparison of the fit of the models illustrated in Fig.2.9 to the observed resistivity and phase responses. The model responses are illustrated with solid, dashed or dotted lines of various thicknesses.

a. Site 631 on Milos, Greece.

b. Site 927 in Olkaria, Kenya.

Fig. 2.9

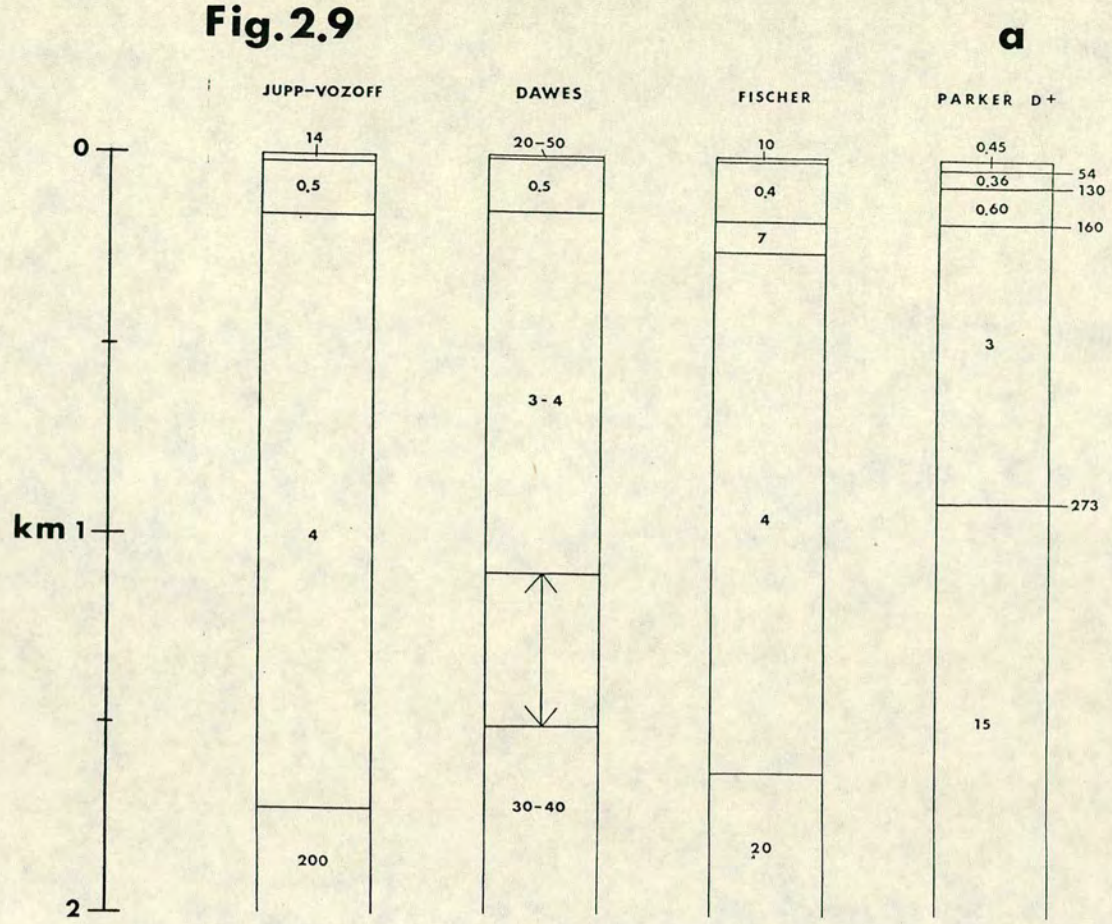
a
JUPP–VOZOFF
DAWES
FISCHER
PARKER D+
0
km 1
2
14
0,5
4
200
20–50
0,5
3 - 4
30–40
10
0,4
7
4
20
0,45
54
0,36
130
0,60
160
3
273
15

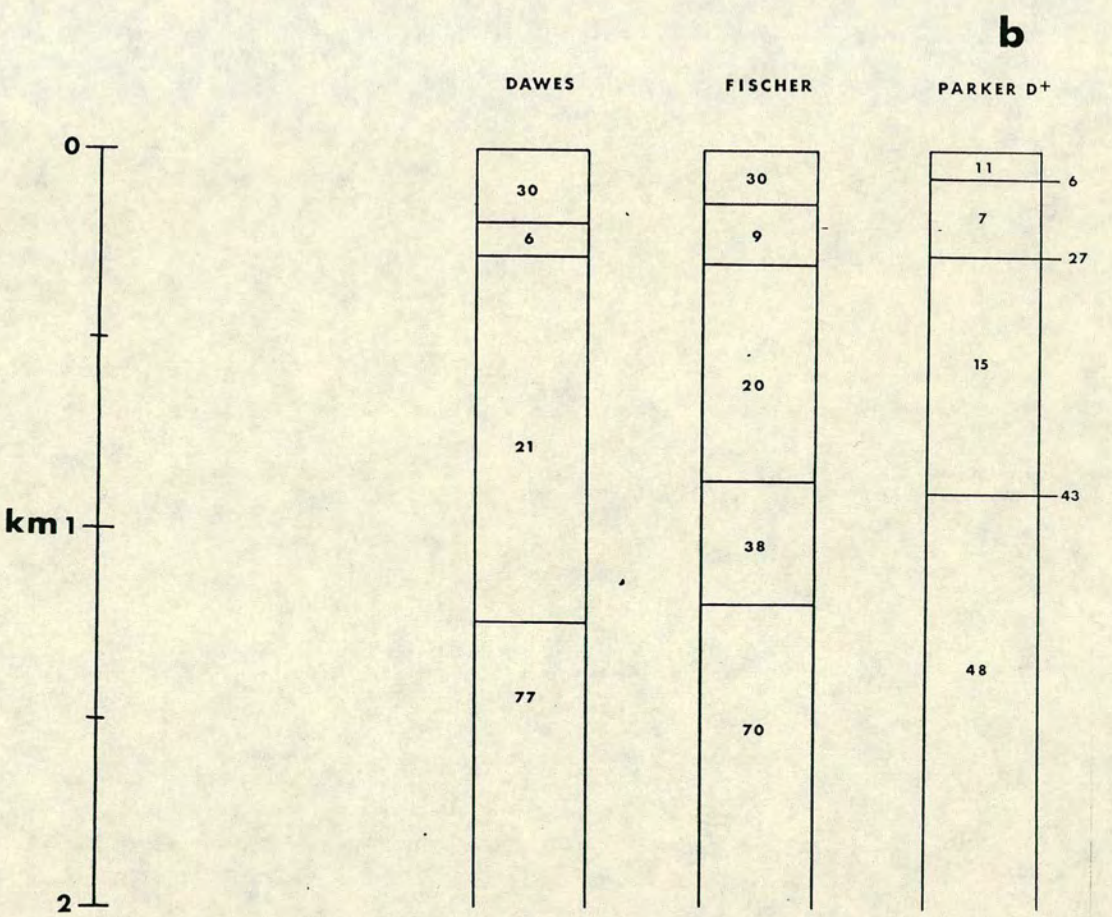
b
DAWES
FISCHER
PARKER D+
0
km 1
2
30
6
21
77
30
9
20
38
70
11
6
7
27
15
43
48

Fig. 2.10

1-D MODEL 631

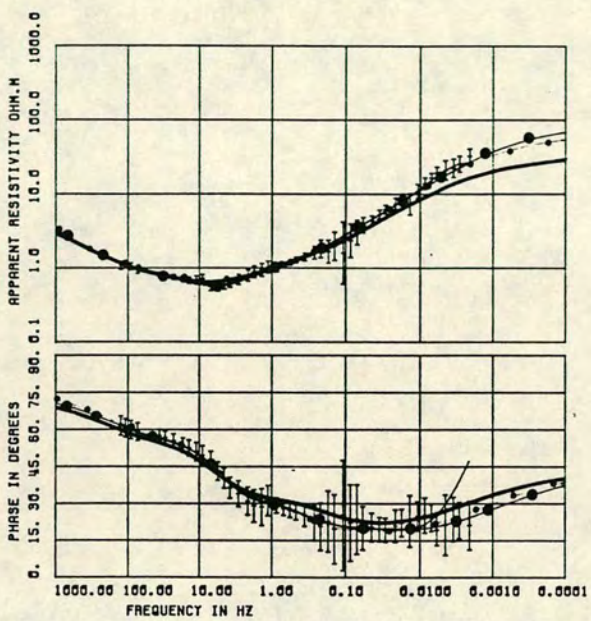

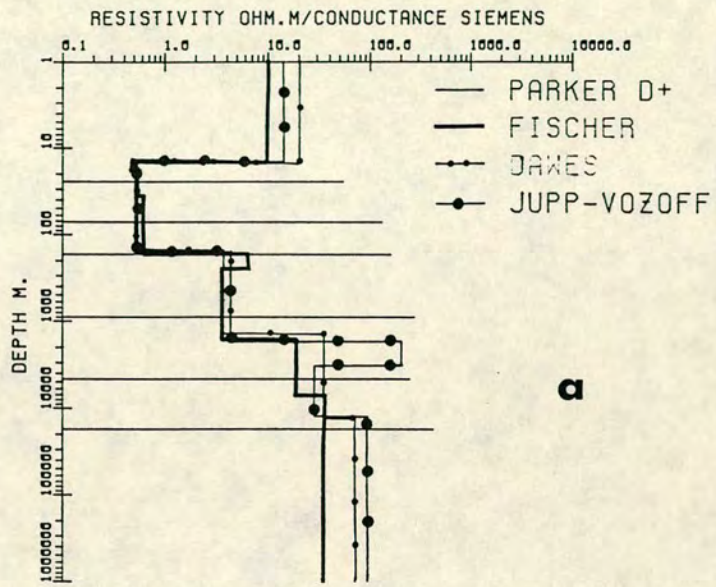

1-D MODEL 927

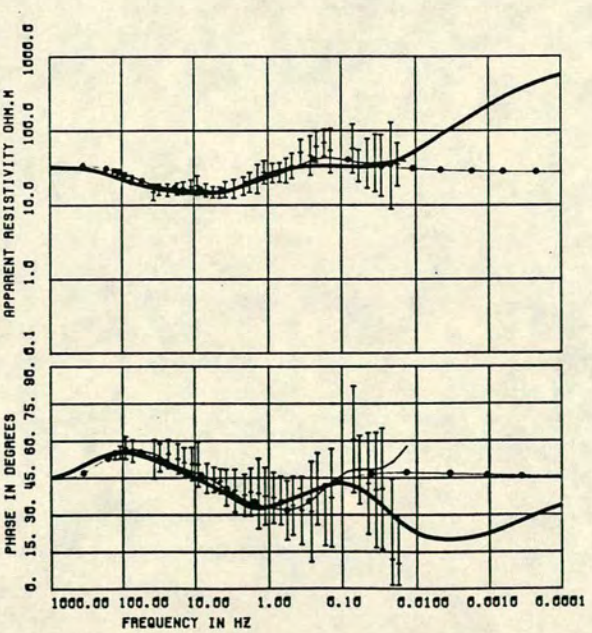

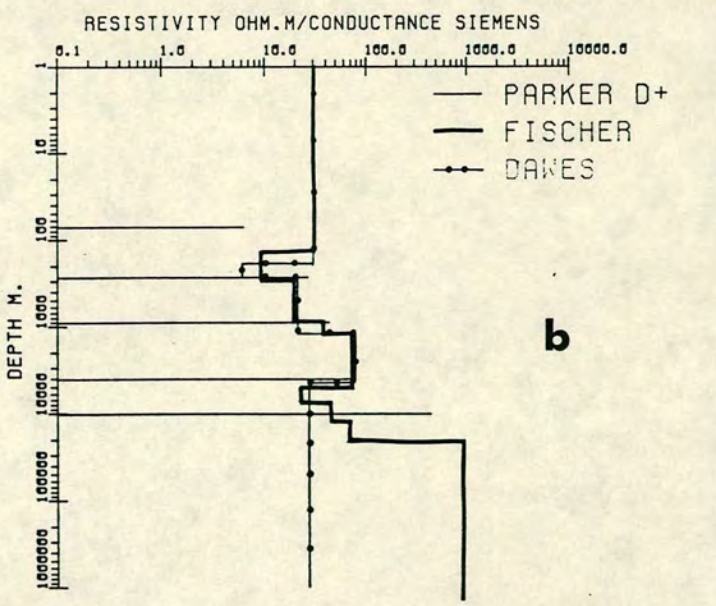

All the models provide a very good fit to the observed magnetotelluric data and compatible electrical structure. The Parker-Whaler D^+ model provides a delta function at about 900 m depth which correlates with an electrical boundary provided by the Dawes method at about 1000 m. The significance of this boundary is discussed in section 5.4.

Site 927 in Olkaria.

Similar procedures were followed for site 927 in Olkaria where the magnetotelluric data for 38 frequencies were modelled by using the Parker-Whaler D^+, Dawes and Fischer methods.

The derived models are represented again with columns and the given figures are resistivities and conductances in Ohm.m and S respectively as in Fig.2.9b (page 65).

The model parameters and the corresponding misfit values are listed in Table 2.6. Fig.2.10b illustrate the three models and their fit to the observed magnetotelluric responses.

Again all the models show good fit to the observed data and in general provide compatible electrical structure.

TABLE 2.6

Model Misfit for site 927 in Olkaria

Dawes	Fischer	Parker-Whaler D^+
Data corresponding to		
38 frequencies		
Sum of weighted squared diff. 0.228	$\varepsilon_o/\varepsilon_\phi/\varepsilon$ 0.07,0.9,0.6	Calculated x^2=10.7 Expected x^2=76
	$\varepsilon_{on}, \varepsilon_{\phi n}, \varepsilon_n$ 0.001,0.5,0.4	

CHAPTER 3

THE MILOS CASE STUDY : GEOLOGY AND GEOPHYSICS

3.1. Introduction.

Milos island is located on the southwestern end of the South Aegean Volcanic Arc. The distensional tectonics of the area due to the subduction of the African plate under the so-called " Aegea " microplate facilitated magma ascension and volcanism. Milos is volcanic itself and shows a high thermal anomaly. The Milos geothermal field is among the most interesting ones in the south Aegean. During the last two decades various geophysical surveys, mainly involving gravity and D.C resistivity measurements, were carried out to assess the geothermal resources of the island. The small dimensions of Milos and the actual limitations of these two methods could not provide adequate information about the geothermal reservoir and the deeper crustal structure below the island. This was the objective of a recent collaborative magnetotelluric survey involving 4 European institutions and sponsored by the Commission of the European Communities. The University of Edinburgh was one of these institutions and the author among the several participants in the fieldwork procedures and a main contributor in the data analysis and modelling.

The present chapter is concerned with the background geology and tectonics of the Hellenic Volcanic Arc and Milos. A summary of all the previous geophysical studies in the south Aegean and Milos is given as well. This chapter ends with a brief description of the

present geothermal model of the island.

3.2. Milos island : Its geographical location.

Milos is the largest island of the so-called Milos archipelago which also includes the smaller islands, Kimolos, Polyegos and Antimilos. The Milos archipelago is part of the Cyclades group of islands of the SW Aegean, Greece. Milos is located on the South Aegean Active Arc within the geographic latitudes 36° 35'N - 36° 50'N and the geographic longitudes 24° 15'E-24° 35'E (See Figs.3.1a-b). The island has an area of 150 km² and it can be divided into two parts - the Western and the Eastern - with respect to its major geomorphological features. The former is mountainous with steep gradients dominated by the highest peak of Profitis Ilias (750 m). The latter has generally milder topography and its major feature is the flat area of Zephyria (Fig.3.1c).

3.3. The geotectonic evolution of the Southern Aegean Active Arc.

The present geotectonic location of Greece at the boundary of the collision of the Eurasian and the African plates can generally be considered similar to that of the past. At that time, various tectonic processes were taking place in the wider area covered by the Tethys sea at the boundaries of the two tectonic plates known as Laurasia and Gondwana. The Balkans belong to Neo-Europa, which was formed by sedimentation over the Alpine geosyncline and on the Alpine orogeny. The latter which started during the Triassic, continued during the Mesozoic and Cenozoic and ended with the closure of the

Fig.3.1. Milos island : Geographic location.

a. Map of the Aegean Sea. Big black arrow - relative motion Africa-" Aegea "; Small white arrows - Average extensional directions during the Pliocene; Small black arrows - Average extensional directions during the Pleistocene.

b. The Milos archipelago.

c. Topographic map of Milos. The solid lines illustrate elevation contours in m (contour interval 100 m).

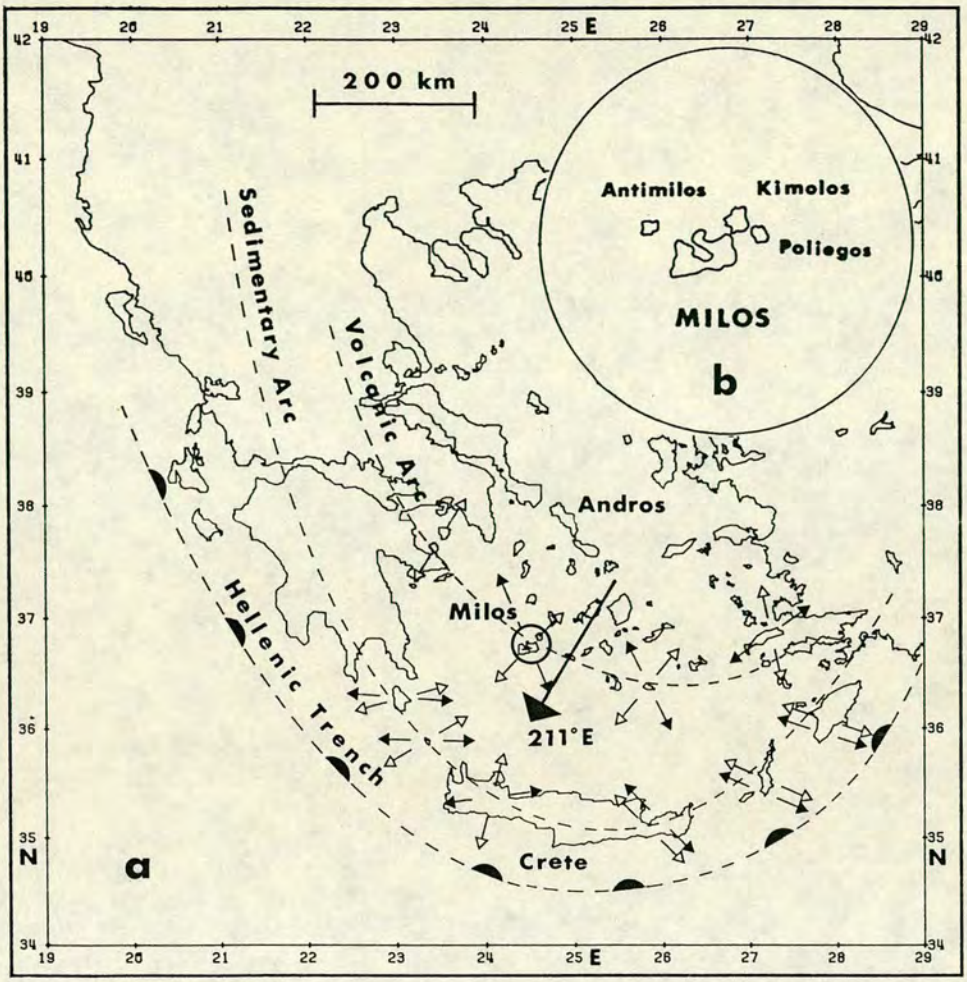

Fig.3.1

MILOS

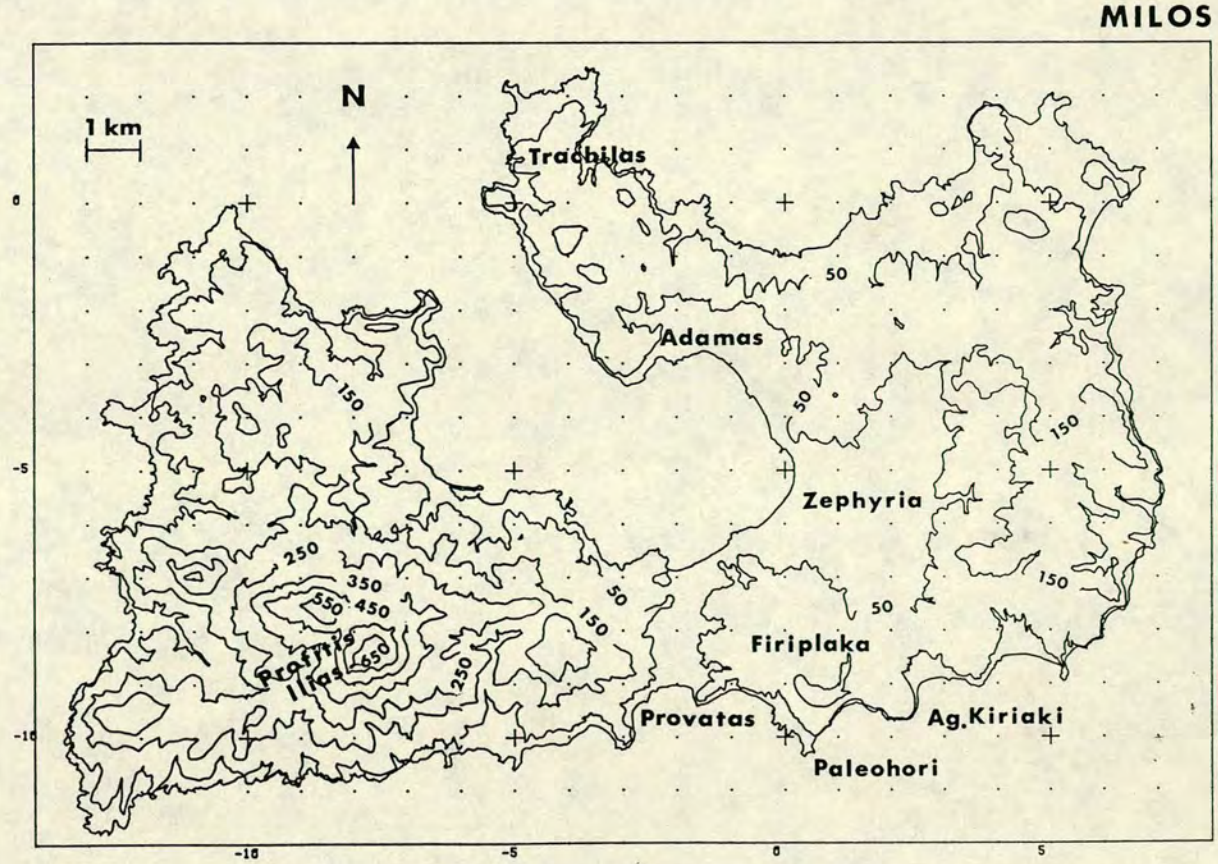

c

Tethys (Mountrakis, 1985).

The collision between the African and Eurasian plates is the dominant process in the Eastern Mediterranean during the last 70 m.y. (Papazachos and Comninakis, 1971). After the main Tertiary phase of this continental collision, along the contact of the two plates, an important lithospheric fragmentation episode occurred. The latter resulted in the formation of several microplates in the Eastern Mediterranean region (Fytikas et al., 1984). From Middle-Upper Miocene time, up to present, the African plate was subducted under the so-called " Aegea " microplate (McKenzie, 1978). Three important points of this widely accepted model can be recognized - (a) The rapid extension which is taking place in the northern and eastern parts of the Aegean, (b) the thinning of the Aegean crust which can account for the observed high heat flow, (c) the direction of the relative " Aegea "-Africa motion (Fig.3.1a) which was found to be 211° E. The age of the sinking slab has been estimated to be 13.5 m.y. (Le Pichon and Angelier, 1979), its thickness 90 km and its mean dipping angle about 35° (Papazachos and Comninakis, 1971). Aerial photographs, orbital imagery and Sea-Beam data studied by Angelier et al. (1982) lead to several conclusions for the geometry of fault systems and the extensional processes taking place in the Southern Aegean Active Arc. Angelier et al. (1982) grouped the mechanisms of extension in this area into two categories. The first one of Pliocene or early Quaternary age (Fig.3.1a, white arrows) and the second one of Middle-Upper Pleistocene or Holocene age (Fig.3.1a, black arrows).

An alternative geotectonic model for the Aegean region was presented by Makris (1976). Makris (1976) explained the

deformation of the region, as the surface expression of a large plume of hot upper mantle material which extends to the base of the lithosphere and has been mobilized through compressional processes that forced the lithosphere to sink into the asthenosphere.

The volcanic activity started in the Aegean during the Oligocene, is still taking place and it has built up the South Aegean Volcanic Arc. The erupted products are mainly of calc-alkaline chemical character (Fytikas, 1989).

The general features of the subduction taking place in the Aegean can be summarized as shown in Fig.3.1a . There is a frontal compressional region which extends along 1500 km and is distinguished by a deep trench (4000 m), the so called Hellenic Trench. Behind and parallel to this region, the Greek mountain range, Crete and the Dodekanese islands form the Sedimentary Arc. The South Aegean Volcanic Arc is located at a distance of about 120 km from the sedimentary arc. Behind the Volcanic Arc there are major subsided basins.

3.4. The elementary geology and tectonic regime of Milos.

Milos island belongs to the Attiko-cycladic mass (Mountrakis, 1985) and is volcanic with long-lasting volcanism (3.5-0.08 m.y). The calc-alkaline eruptive products vary in composition from basaltic andesites to the more dominant rhyolites (Fytikas, 1989).

Milos was clearly affected by the two extensional phases proposed by Angelier et al. (1982). During the Pliocene the direction of extension in Milos was NE-SW (Fig.3.1a, white arrows) while during

the Middle-Upper Pleistocene there was a change of strike to NW-SE (Fig.3.1a, black arrows). The latter seems to be the dominant direction, since faulting is more prominent in the NE-SW, or N-S directions. Along these directions tectonic horsts and grabens are observed (Fig.3.2a, page 76). The Pliocene NE-SW distensional processes are probably responsible for the major NW-SE faults which are still active and formed the Milos bay. Combination of the two fault systems resulted in volcanism, which is finally the cause of the high thermal anomaly observed on Milos (Fytikas, 1989).

Geological mapping (Fytikas, 1989) and stratigraphic data from five deep boreholes (Vichos et al., 1986) suggest the following structure for Milos (Figs.3.2b-c, page 76) - (a) A prevolcanic crystalline metamorphic basement of Alpine age (probably Cretaceous) underlying a Neogene sequence of Upper Miocene - Lower Pliocene clastic deposits and marly limestones - (b) Various volcanic products of the successive volcanic activities (Middle - Upper Pliocene up to Recent times), various lahars, pyroclastics and recent deposits overlying the Neogene sediments.

These geological formations can be described as follows :

Metamorphic basement

The Mesozoic metamorphic basement outcrops only in a small area in the southeastern part of the island. The basement consists of weakly metamorphosed rocks with greenschist facies (33.2 m.y), while blueschist facies (64.2 m.y) are rare. The dominant rocks are schists composed of quartz, muscovite and chlorite with gradual transition to quartzites and calcischists. Serpentinites and intercalated marble lenses which are present in the neighbouring non-volcanic Cycladic islands, are absent on Milos.

Fig.3.2. Tectonics and Geology of Milos.

a. Structural sketch map of Milos (After Fytikas et al., 1986).

b. Geological sketch map of Milos (After Fytikas et al., 1986).

c. Boreholes MZ1, MA1, M1, M2, M3 : Lithological sequence and temperature profiles (After Fytikas, 1989).

Fig.3.3. An integrated geophysical model for the Aegean crust and upper mantle.

a. A schematic model for the subduction along a N-S profile (Andros-Crete).

b. An integrated model for the crust and upper mantle below Milos inferred from Makris (1977) integrated model along the Mykonos-Crete profile. Plain numbers indicate p-wave velocities in km/s; Underlined numbers indicate density in g/cm^3.

Fig. 3.2a

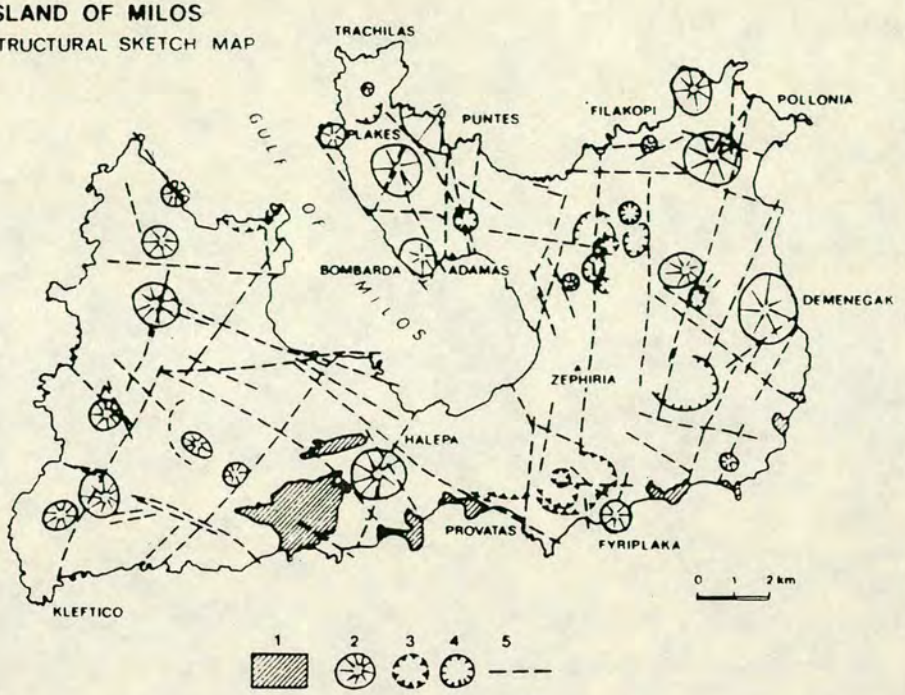

Structural sketch map of the island of Milos. 1 = Pre-volcanic basement; 2 = lava domes; 3 = Fyriplaka and Trachilas volcanic craters; 4 = phreatic craters; 5 = structural trends.

Fig. 3.2b

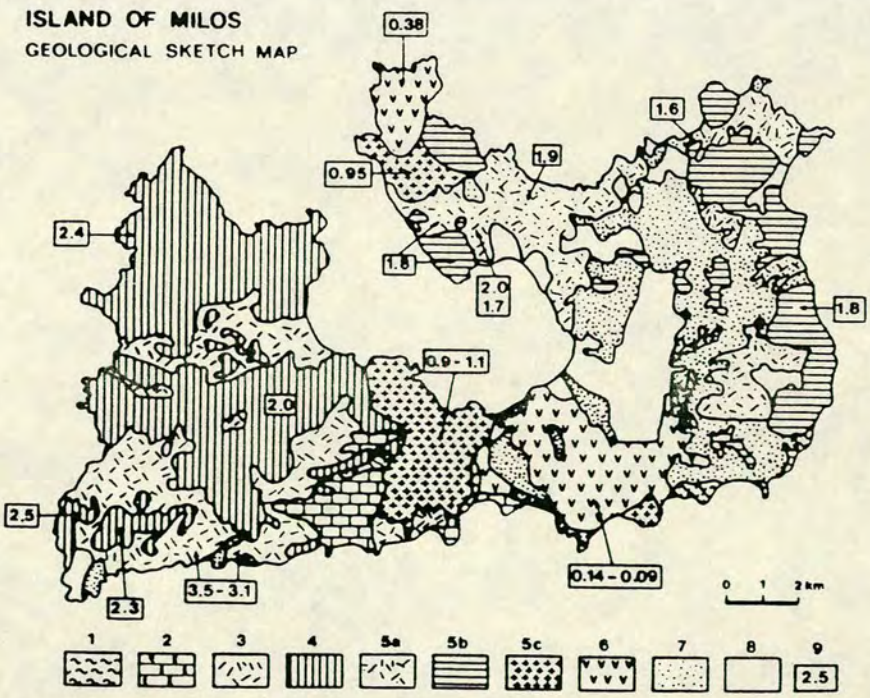

Geological sketch map of the Island of Milos. *1* = Metamorphic basement; *2* = Neogene sediments; *3* = basal pyroclastic series (Middle—Upper Pliocene); *4* = complex of domes and lava flows (Upper Pliocene); *5* = Lower Pleistocene volcanics: pyroclastic series (a), lava domes (b) and Halepa and Plakes domes (c); *6* = rhyolitic complexes of Fyriplaka and Trachilas (Upper Peistocene); *7* = products of phreatic activity; *8* = Quaternary sediments; *9* = radiometric ages integrated with selected data from Angelier et al. (1977), Bigazzi and Radi (1981) and Fytikas et al. (1976).

Fig. 3.2c

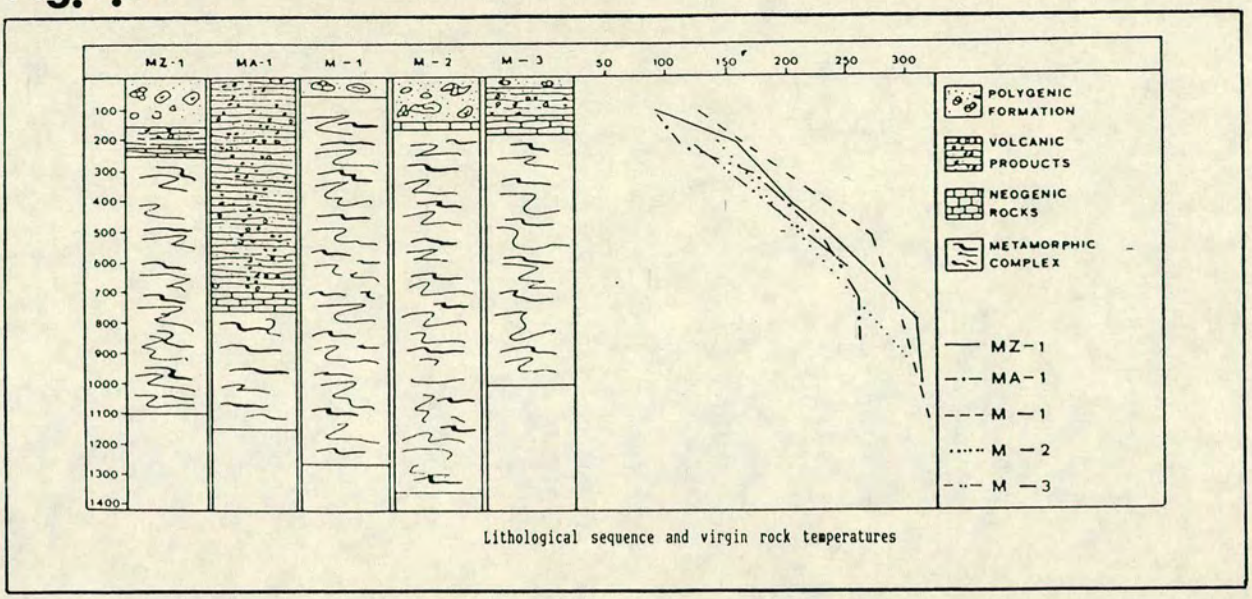

Lithological sequence and virgin rock temperatures

Fig. 3.3

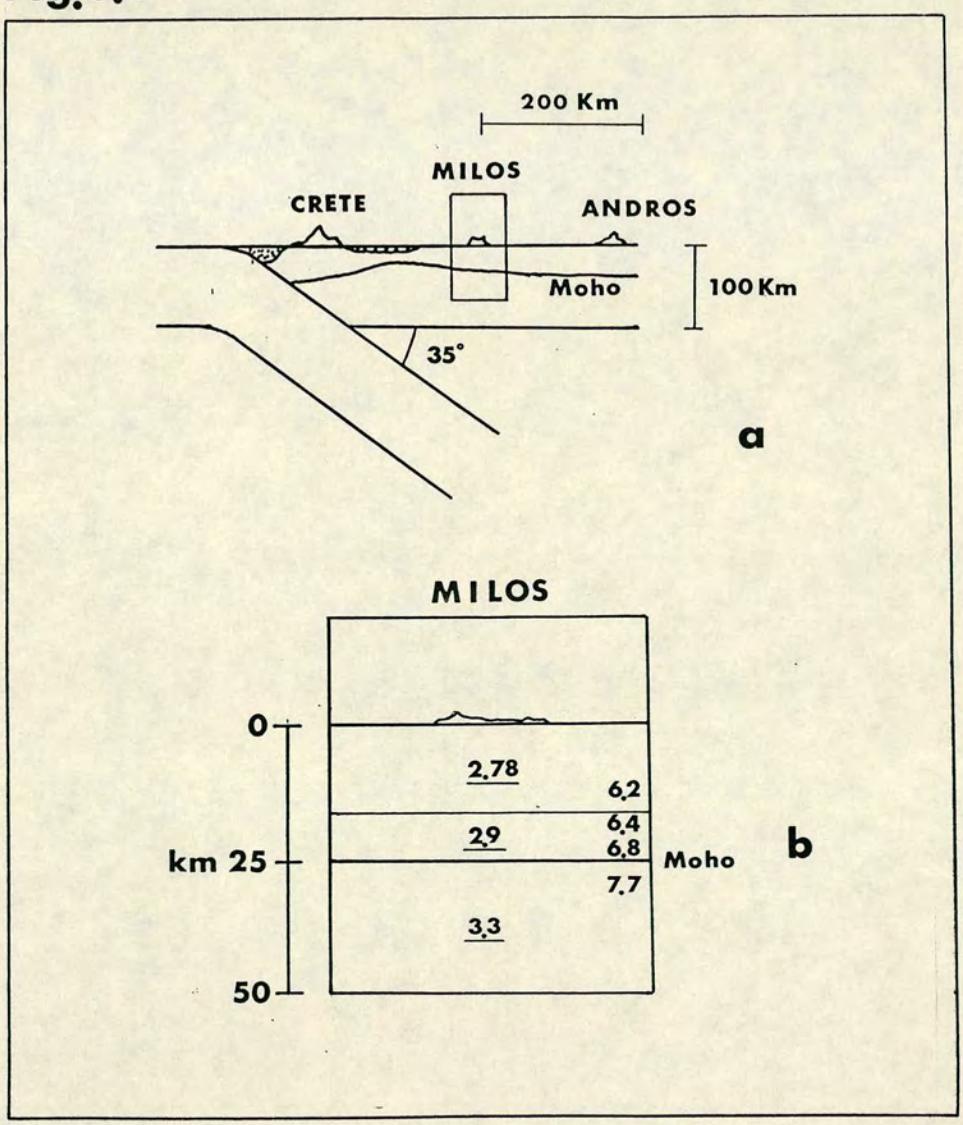

Neogene series

The transgressive sedimentary Neogene series are mainly encountered in the southern part of Milos. However a smaller outcrop of modest thickness was found in the central-eastern part of the island at boreholes M1, M2 and M3. The Neogene series are not continuous on Milos and it is believed that the area was partially transgressed. They consist of marly or pure limestones, marls, conglomerates, sandstones and clays.

Volcanics

The distensional tectonic processes which were initiated with the subduction in the Middle Miocene, enabled the resulting andesitic magmas to rise and create near surface chambers. Stratigraphic, palaeontological and geochronological data imply a separation of volcanism into several phases.

The first eruptive phase took place during the Middle - Upper Pliocene (3.5 m.y). The products were submarine pyroclastics and are present in the southern part of Milos. A subaerial effusive phase followed, with domes and andesitic - dacitic lava flows of Upper Pliocene age, which affected the western part of Milos. At the end of Upper Pliocene and the beginning of the Lower Pleistocene submarine pyroclastic activity occurred and it was followed (Upper Pleistocene) with the extrusion of subaerial acid lava domes in the southern and northern middle part of the island. During the Pleistocene strong phreatic activity occurred in the central - eastern part of the island. The recent volcanic activity is associated with the Upper Pleistocene rhyolitic volcanic centres of Trachilas (0.38 m.y) in the north and Fyriplakas (0.14-0.08 m.y) in the south.

Recent Deposits

The young non-volacanic deposits on Milos are mainly alluvial, or non-cemented beach deposits, older fluvial-torrential deposits, and layered well - cemented porous tuffs of reworked fine material.

3.5. Geophysical investigations in the South Aegean Active Arc.

During the last three decades much effort was made by several researchers to reveal the deep structure of the Aegean area. The most recent ideas concerning the geotectonic evolution of the Hellenides have been described in the previous section. These ideas were based on geological, petrological and mainly the geophysical data which are presented below. It is worth mentioning that the existing geophysical models for this region were derived from gravity and magnetic surveys, deep seismic soundings and the study of earthquakes. Deep electrical studies were missing and only the present work on Milos and two other recent surveys of Kos and Nisyros (Lagios and Dawes, 1989) provide some preliminary information for the electrical structure of the top 20 km along the South Aegean Active Arc. Although existing ideas for the plate tectonics in the Aegean are widely accepted, some deep electrical model across the Arc could offer better imaging of the subduction and its implications.

The pioneering geophysical investigations were undertaken in the 1950's. Harrison (1955) published the Airy-Heiskanen isostatic gravity anomalies observed in the Aegean. A magnetic field intensity survey by the U.S Naval Oceanographic Office followed during 1957.

The observed anomalies were interpreted much later by Vogt and Higgs (1969). Systematic studies of deep earthquakes in the Aegean were initiated during the 1950's (Galanopoulos, 1953) and were continued by several authors, (McKenzie, 1972, 1978 ; Papazachos and Comninakis, 1971 ; Papazachos, 1977 ; Makris, 1977 ; Makropoulos and Burton, 1984).

Makris (1977) compiled the gravity map of Greece using his own data and the results of Morelli et al. (1975) and others. Makris (1977, 1978) finally proposed a regional geophysical model for the area as the result of all the existing geophysical information during that time. A preliminary heat flow map of Greece was prepared by Fytikas and Kolios (1979). Reviews of the past geophysical work were undertaken by Giese and Nicolich (1982), Horvarth and Berckhemer (1982) but no additional geophysical information was provided. Very recently, Kissel and Laj (1988) presented paleomagnetic results obtained in the last 5-6 years from Tertiary formations in the Aegean.

The summarized results of all the geophysical exploration undertaken, could be grouped according to the method applied as following.

The Aegean Sea is characterized by positive Bouguer anomalies. A maximum of + 175 mgals is observed at the central trough of the Cretan Sea, while behind the arc there are anomalies of about + 50 mgals (Makris, 1977). The positive anomalies at the Cretan Sea have been interpreted by Papazachos and Comninakis (1971) to be caused by conditions of the matter that lies deeper inside the upper mantle and not only by the shallower features of the mantle. In general, the magnetic anomalies observed in the Aegean Sea are not strong (Vogt

and Higgs, 1969). Some of the strongest anomalies are observed along the volcanic arc and in the Cretan trough. Papazachos and Comninakis (1971) suggested that these anomalies are due to magnetized rocks which have been intruded by volcanism. Horvath and Berckhemer (1982) made similar comments and pointed out that sea floor spreading does not exist, since there is no regular pattern to justify it. A more detailed picture for the structure of the crust and upper-most mantle was revealed from the integrated geophysical model of Makris (1977, 1978). It was found that the Aegean Sea is underlain by a predominantly sialic crust of variable thickness. In the central Aegean the crustal thickness varies from 32 km beneath Evia to 28 km beneath the Cyclades islands. Under the centre of the Cretan Sea the crust was found to be only 20 km thick. A P-wave velocity of 6 km/s is typical for the sialic basement while an increase of 6.2 to 6.8 km/s is observed in the lower crust. The upper mantle below the Aegean has velocities of 7.6-7.8 km/s and low density of 3.3 g/cm^3. A schematic model for the subduction and an integrated geophysical model for the crust and upper mantle below Milos, inferred from Makris' (1977) integrated model along the Mykonos-Crete profile, are given in Figs.3.3a-b (page 77).

The Gutenberg-Richter b values computed by Papazachos and Comninakis (1971) were found to be 0.94 for shallow earthquakes and 0.54 for the deep earthquakes. The first value of 0.94 suggests an aseismic zone in the uppermost part of the mantle under the Aegean. The pattern of the parameter b along the central-eastern volcanic arc was recently confirmed by Tsapanos et al. (1989).

The paleomagnetic results of Kissel and Laj (1988) suggest two

phases of rotation in the Aegean, one during the Middle Miocene at the two terminations of the arc, (clockwise in the west and anti-clockwise in the east), the other one, 5 m.y ago which affected only the northwestern part of Greece.

3.6. Geophysical investigations on the Milos island.

Several geophysical surveys were conducted on Milos during the last two decades associated with the mineral and geothermal interest of the island.

The first geophysical work on Milos was a small scale gravity survey along small profiles carried out by Papanicolaou (1958) for purely mineral exploration. A complete gravity exploration was undertaken by I.G.M.E (Thanassoulas, 1983). The gravity data were analysed and modelled by Tsokas (1985). The microseismic activity on Milos was studied for the first time by Drakopoulos and Delibasis (1973). Seismic refraction or reflection studies on Milos are absent, while some results from seismic reflection profiles are available northwest, south and east of Milos island (Jongsma et al., 1977). Many D.C electrical soundings have been conducted on the island since the early 70's. Voutetakis (1972) from I.G.M.E was the first, while larger scale investigations were made by C.G.G, Duprat (1973).

The main geophysical results for the Milos island and its high enthalpy geothermal field could be summarized as below.

The Gutenberg-Richter b values were found to be 0.94 for the shallow earthquakes (Papazachos and Comninakis, 1971) while Drakopoulos and Delibasis by studying a swarm of micro-earthquakes

gave a value of 1.22. Tsapanos et al. (1989) computed for the same area b values for the shallow earthquakes of about 0.95. These values determine intermediate conditions between those of tectonic and volcanic earthquakes.

The aim of the D.C resistivity studies carried out by Voutetakis (1972), Duprat (1973) and Tsokas (1985) was the determination of the non-volcanic basement and the location of the main fractured zones on the island. Very low resistivities were observed only in Zephyria (< 0.5 Ohm.m) and Adamas (< 2 Ohm.m). The latter are regions which show high temperature gradient (> 6°/10 m) . The non-volcanic basement was found relatively resistive of 40-50 Ohm.m. The basement was located at shallow depths (100 - 200 m) south from Zephyria and seems that it dips to the north (600 - 800 m). The very low resistivities of Zephyria and Adamas were attributed by Duprat (1973) not only to the presence of sea-water but also to the special thermal conditions and the presence of hydrothermal altered rocks and young volcanic formations (Tsokas, 1985). Tsokas (1985) presented resistivity contour maps for AB/2=100, 250, 500, 1000 m. The contour maps confirm the pattern adopted by Duprat (1973) while some NW-SE, N-S, NE-SW and E-W trends are observed, which are compatible with the main faulting on the island. Since the depth of penetration was not more than 1000 m the possibility of detecting the geothermal reservoir was limited. From five deep boreholes it was shown (Fytikas, 1977 ; Vichos et., 1986) that the geothermal fluids prefer to circulate within the metamorphic basement at depths greater than 800 m.

The residual Bouguer anomaly map of Milos was interpreted by

Tsokas (1985) assuming a density of 2.0 g/cm³ for the surface formations and 2.5 g/cm³ for the metamorphic basement. The observed NW-SE and N-S gravity trends are related to the main fault systems in Milos. Additionally Tsokas (1985) tried to explain the gravity low observed in the Milos gulf, on the regional gravity anomaly map as the expression of the possible presence of a caldera. Such gravity lows are common in calc-alkaline volcanic centres in the world (Brown et al., 1987). Surface temperature gradient measurements were undertaken by Fytikas (1977) at a number of shallow boreholes (≈ 80 m deep). The surface temperature gradient map with the structural zones is reproduced in Fig.3.4 (page 89).

3.7. The Milos geothermal field.

Fytikas (1977 ; 1989) has studied thoroughly the Milos geothermal field. The main characteristics of the Milos geothermal field are summarized in the following paragraphs.

The consequences of magma ascension and volcanism in Milos are associated with several superficial and underground thermal manifestations.

The superficial thermal activities concern fumaroles, hot springs, hot grounds, submarine gas escapes and hydrothermal alteration of the superficial rocks. They are mainly located in the central and eastern part of the island and sometimes in the sea-floor. The maximum measured temperature of the fumaroles is 101°C, while in regions of high surface temperature it is 100°C. The hot springs are usually found on the coast line with maximum temperature 70°C. The most important hydrothermal alteration is the

transformation of all volcanics (mainly pryroclastics) into clay minerals. Depending on the local conditions (rock type, pH, composition and temperature of the hydrothermal fluids) this transformation is associated even with ' bentonitization ' in the deeper ' hot ' environments or ' kaolinization ' in the shallower ones (Fytikas, 1989).

The underground thermal activities are related to the circulation of hot fluids through the fractured rocks. While a good aquifer might be expected to occur within the Neogene sedimentary series, from five deep boreholes (Fig.3.2c, page 76) it was found that these formations have small thickness and the geothermal fluids were encountered only at an average depth of 900 m, within the Mesozoic metamorphic basement. They consist of hot water near the boiling state and rich in NaCl (10%) under low pressure. The presence of the hot fluids is concurrent with an increase of the temperature up to 320°C and the first appearance of epidote. The latter is a mineral with properties of a high temperature natural geothermometer.

The main thermal anomaly of Milos is located at the central-southern part of Zephyria plain and is bounded by the 8°C/10 m isoline of Fig.3.4. Two other high thermal anomaly areas are observed (Fig.3.4), one in Adamas (> 7°C/10 m) and the other one in Rivari (Western Milos (> 4°C/10 m)).

CHAPTER 4

THE MILOS CASE STUDY : THE MAGNETOTELLURIC SURVEY.

4.1. Introduction.

A broadband magnetotelluric survey was undertaken by the University of Edinburgh on Milos, Greece, as part of a collaborative electromagnetic study of the geothermal field of the island. The aim of the investigations was the determination of the electrical structure at great depths where other electrical methods were unable to penetrate. In addition it was hoped that the magnetotelluric results could provide new evidence for the local and regional tectonics of the area.

The fieldwork team was led by G.Dawes and the author was one of the field participants in the field and a main contributor during the data analysis and modelling.

The present chapter contains discussion of, (a) the data processing, (b) the computation of the magnetotelluric transfer functions and other induction parameters, (c) the computation of several dimensionality parameters and (d) the one and two dimensional modelling procedures.

Examples of the results of the above procedures are provided and the chapter ends with presentation of the one and two dimensional electrical models derived for the Milos geothermal field.

4.2. Sites occupied and field measurements.

The field measurements on Milos island were carried out within the time period 17/9/86-4/11/86. Thirty seven SPAM (AMT) soundings in the range 10^{-2}-10^{+2} secs were conducted along 4 approximately linear traverses (Figs.4.1). Three of these had an E-W direction crossing the eastern part of the island with an average station spacing 500 m. The fourth traverse had a NW-SE direction crossing the western part of the island with an average station spacing of 1000 m. Twelve long period magnetotelluric (LMT) soundings (period range 10-10^{+4} secs) were also undertaken with up to 5 stations operating simultaneously. In general their locations were identical or close to AMT sites. The coordinates of the AMT and LMT stations are listed on Table 4.1 (page 90). Identification numbers of the AMT, AMT-LMT or LMT stations are illustrated in Fig.4.1.

The NERC SPAM Mk II developed by Edinburgh University (Dawes, 1981) was used for the higher frequency (AMT) measurements. A three component fluxgate magnetometer (EDA) a telluric pre-amplifier-filter box (Dawes, 1986) and the NERC Geologger system (Valiant, 1977) were used for the long period (LMT) measurements.

Magnetic components were measured in the N-S and E-W and vertical for LMT, directions. Electric components were measured in the N-S and E-W directions. Cross-shapped or L-shapped electrode configurations were used for the majority of the AMT measurements and L-shaped electrode layout for the LMT soundings. Electrode spacings of roughly 100 m were used for both period ranges. Only a few LMT sites had electrode spacings less than 100 m.

Fig.3.4. Temperature gradient and structural map of Milos. Contour interval 1°C/10 m. Faults are illustrated with thick solid lines (After Fytikas, 1977).

Fig.4.1. Magnetotelluric stations on Milos island. Solid triangles - AMT site locations (frequency range : 10^{2}-10^{-2} Hz); solid circles - AMT-LMT site locations (frequency range : 10^{2}-10^{-4} Hz); solid squares - LMT site locations (frequency range 10^{-1}-10^{-4} Hz); open squares - borehole locations; solid lines - magnetotelluric Profiles P1, P2, P3, P4 and SS'.

Fig.3.4

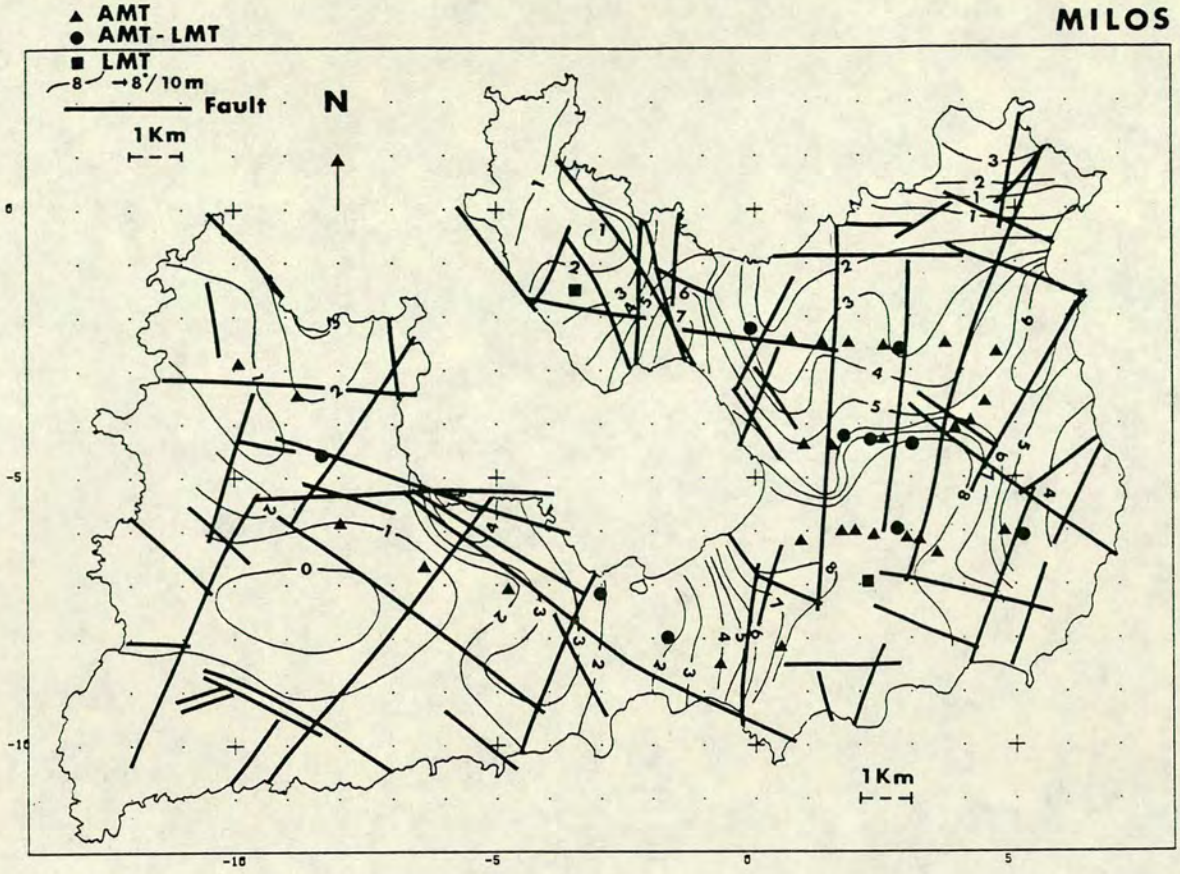
AMT
AMT - LMT
LMT
8
8°/10m
Fault
1Km
N
MILOS
1Km

Fig.4.1

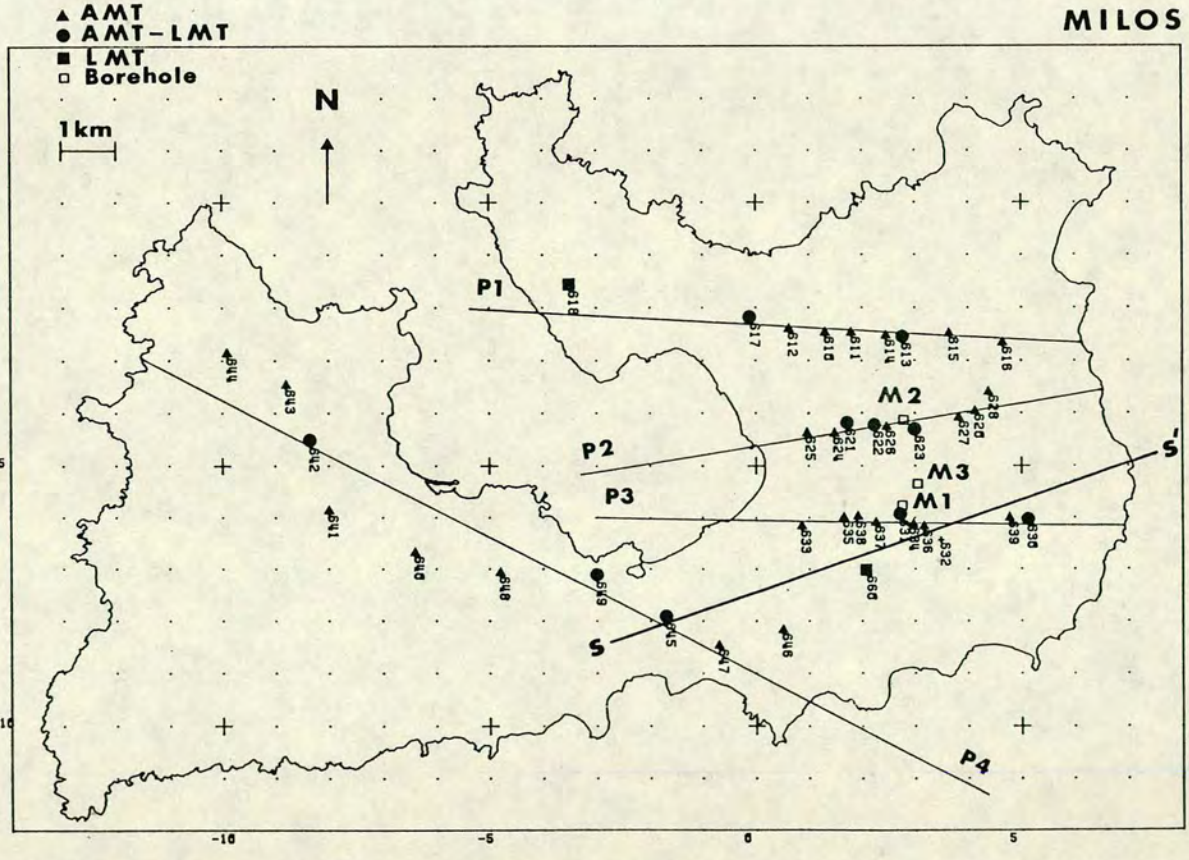
AMT
AMT - LMT
LMT
Borehole
1km
N
MILOS
P1
P2
P3
P4
M1
M2
M3
S
S'

TABLE 4.1

Magnetotelluric stations on Milos : coordinates

No	Site	Elevation m	X km	Y km	No	Site	Elevation m	X km	Y km
1	640	210	-6.40	-6.70	21	621	015	+1.70	-4.25
2	641	150	-8.00	-5.90	22	622	010	+2.23	-4.30
3	642	190	-8.35	-4.60	23	623	030	+3.01	-4.39
4	643	225	-8.80	-3.50	24	624	035	+1.47	-4.42
5	644	125	-9.90	-2.90	25	625	050	+0.95	-4.40
6	645	040	-1.70	-8.00	26	626	015	+2.46	-4.29
7	646	110	+0.50	-8.20	27	627	125	+3.84	-4.11
8	647	090	-0.70	-8.50	28	628	125	+4.40	-3.62
9	648	170	-4.80	-7.10	29	630	210	+5.12	-6.11
10	649	030	-3.00	-7.20	30	631	030	+2.72	-6.00
11	610	060	+1.30	-2.50	31	632	120	+3.49	-6.45
12	611	060	+1.80	-2.50	32	633	005	+0.86	-6.20
13	612	060	+0.62	-2.42	33	634	050	+2.90	-6.15
14	613	110	+2.76	-2.62	34	635	005	+1.65	-6.02
15	614	110	+2.45	-2.56	35	636	140	+3.15	-6.20
16	615	125	+3.65	-2.51	36	637	015	+2.25	-6.12
17	616	115	+4.65	-2.70	37	638	010	+1.89	-6.03
18	617	060	-0.09	-2.24	38	639	210	+4.77	-6.03
19	618	050	-3.50	-1.63	39	660	005	+2.10	-7.10
20	620	105	+4.13	-3.98					

No=Number

X=E-W local grid

Y=N-S local grid

For the AMT range, time series windows of 256 digitized samples were recorded for the H_x, H_y, H_z, E_x, E_y components. Windows satisfying specific preset criteria were written to data cartridges. The preset conditions were :

(i). Signal coherence.

(ii). Power (signal amplitude).

(iii). Minimum number of frequencies accepted per window..

Recorded windows were classified into 4 frequency bands according to the window frequency content. The sampling rate was dependent on the SPAM Mk II sub-band frequency range. For the LMT range the 5 components H_x, H_y, H_z, E_x, E_y were recorded digitally on magnetic tapes with pre-fixed sampling rate of 10 secs. The fieldwork procedure described by Dawes (1985) and Galanopoulos (1986) was followed for the AMT soundings and where appropriate also for the LMT soundings. All equipment was calibrated before the fieldwork procedures with the exception of the CM11E induction coils. The latter require calibration procedures not yet available in the U.K. Despite that the coil responses were checked in the laboratory by G.Dawes and M.Valiant.

4.3. Processing of the magnetotelluric data.

AMT time series windows were selected automatically in the field as previously described (Dawes, 1985 ; Galanopoulos, 1986). LMT time series windows (256 digitized samples) were selected visually under preset criteria similar to those for the AMT windows using a DEC LSI 11/73 computer system. The selected windows were classified into two additional frequency bands according to their frequency

content. All data were reprocessed (Figs.4.2a-c) on the University of Edinburgh main frame computer system using classical tensorial procedures with various criteria being applied to reduce the effects of noise biasing. These procedures are described briefly below.

4.3.(i). Estimation of the impedance tensor elements.

The data were reprocessed in the frequency domain using the analysis program written by Rooney (1977) amd improved in its logistics and computational efficiency by Dawes (1984). In particular, special care was taken by the author for the upward and downward biasing of the impedance tensor elements by random noise on the electric and magnetic components respectively (Sims et al., 1971). The tensor elements were determined for the upward and downward biased case and a weighted average of these two was adopted for the final impedance tensor estimation.

The standard window analysis at the reprocessing stage was the following :

(i). Time series were scaled by using the recording gains.

(ii). Signals were detrended and tapered by using a least squares method (Bendat and Piersol, 1971) and a cosine bell window (Harris, 1978) respectively.

(ii). The data were Fast Fourier transformed (FFT).

(iv). A power threshold of 0.0003 was used and the auto- and cross-power spectral estimates were calculated and band averaged over 8

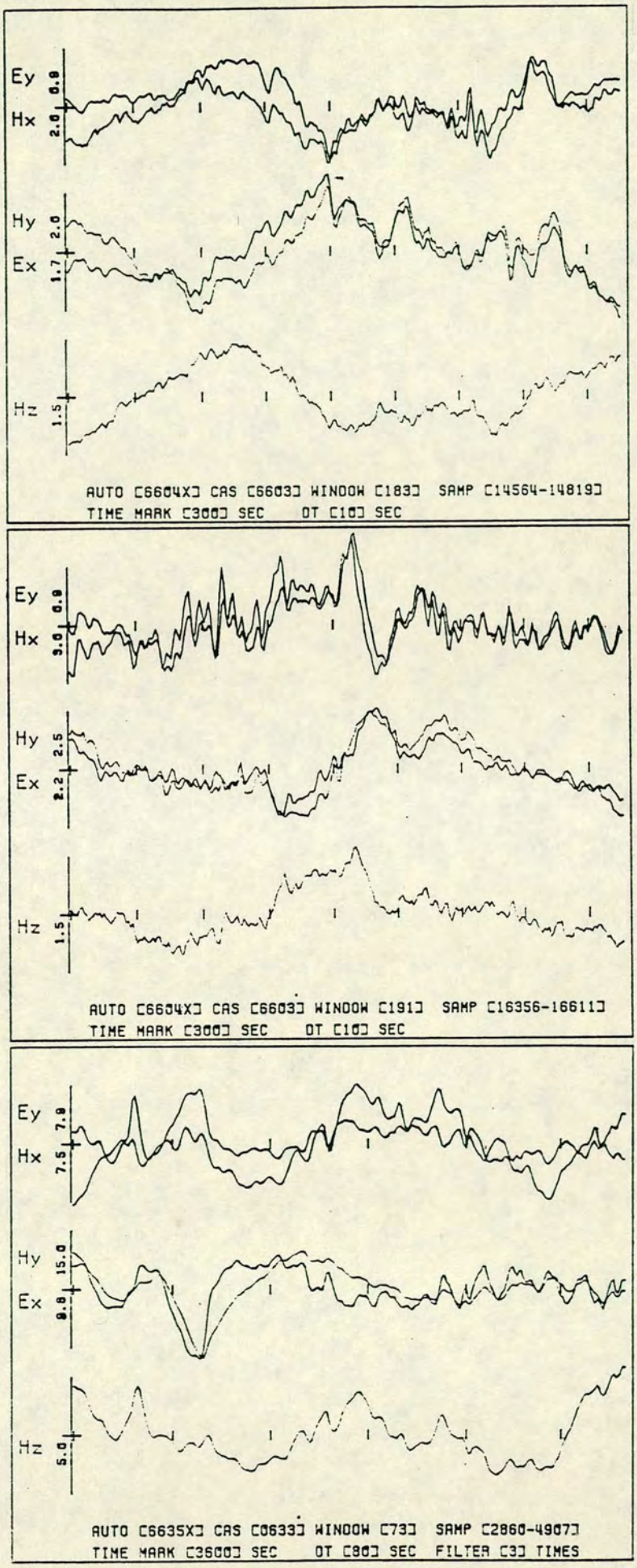

Fig.4.2. Examples of time series windows.

a. Band 4 (10^{+2}-10^{+3} secs)

b. Band 4 (10^{+2}-10^{+3} secs)

c. Band 5 (10^{+3}-10^{+4} secs)

neighbouring frequencies to reduce the variance of the estimates.

(v). Tensor elements were determined for the upward and downward biased case (Sims et al., 1971). An example of the computation of the off diagonal tensor elements Z_{xy} was given in section 2.4.(ii).

(vi). Multiple predicted coherencies were computed for overcoming the bias of responses by noise on the electric components (Kao and Rankin, 1977). Minimum multiple predicted coherency was set up to 0.8. The applied formula is given below for E_x :

$$\mathrm{coh}(\hat{E}_x, E_x) = \frac{|(\hat{E}_x E_x^*)|}{((\hat{E}_x \hat{E}_x^*)(E_x E_x^*))^{1/2}} \qquad (4.1)$$

where * denotes conjugate and ^ denotes the predicted values of E_x.

The impedance tensor elements $Z_{xx}, Z_{xy}, Z_{yx}, Z_{yy}$ for each frequency for each kind of biasing were averaged for the whole number of accepted windows assuming a log-normal distribution. Accepted windows were required to satisfy the minimum power, minimum coherence and minimum number of frequencies, criteria. Two other conditions were imposed, concerning the sign and outlier rejection criteria. It was required each frequency set to possess a preferred sign of the off diagonal elements of the impedance tensor. All estimates lying outside +2.2 standard deviations from the mean value were rejected. A new mean and a new standard deviation were calculated for each biased case as described in section 2.4.(ii). A weighted average of the upward and downward averages was computed using the following equation (example is given for the Z_{xy} tensor element) :

$$Z_{xy(weighted)} = \left(\frac{Z_{xy(up)}}{SZ_{xy(up)}} + \frac{Z_{xy(down)}}{SZ_{xy(down)}}\right) \Big/ \left(\frac{1}{SZ_{xy(up)}} + \frac{1}{SZ_{xy(down)}}\right) \quad (4.2)$$

where $Z_{xy(up)}$, $Z_{xy(down)}$ and $SZ_{xy(up)}$, $SZ_{xy(down)}$ are the xy impedance tensor elements with their squared errors for the up- and down-ward biased case respectively.

4.3.(ii). Rotation of the impedance tensor.

For two dimensional geoelectric structures the electrical resistivity o varies with the depth z and along one of the two horizontal measuring directions x,y. Usually these latter directions do not coincide with the two principal directions which are parallel and normal to the electrical strike. Along the principal directions the electric and magnetic fields decouple to their Transverse Electric or E-Polarization (TE or E-Pol) and Transverse Magnetic or H-Polarization (TM or H-Pol) modes.

In order to shift from the measuring directions to the principal ones and estimate the impedance tensor elements along these new directions, the impedance tensor is rotated in the x-y plane. For this purpose there are graphical and computational methods. Swift (1967), Word et al. (1970) employed computational methods. They tried to minimize the diagonal elements or maximize the off diagonal elements. Word et al. (1970) rotated the impedance 2x2 tensor :

$$Z = \begin{vmatrix} Z_{xx} & Z_{xy} \\ Z_{yx} & Z_{yy} \end{vmatrix} \quad (4.3)$$

geometrically through an angle θ. In matrix notation the rotation is

expressed by the following formula :

$$Z' = R\ Z\ R^{-1} \qquad (4.4)$$

where R equals :

$$R = \begin{vmatrix} \cos\theta & \sin\theta \\ -\sin\theta & \cos\theta \end{vmatrix} \qquad (4.5)$$

The rotation is clockwise with respect to a positive north and a positive east. The rotated tensor is denoted by Z'. In the present work the electrical strike direction is determined by using Swift's (1967) formula which maximizes the off diagonal elements i.e $|Z'_{xy}|^2+|Z'_{yx}|^2$ where Z'_{xy}, Z'_{yx} denote rotated tensor elements. This angle is calculated by using the following equations :

$$\theta_o = 1/4 \arctan \frac{(Z_{xx}-Z_{yy})(Z_{xy}+Z_{yx})^*+(Z_{xx}-Z_{yy})^*(Z_{xy}+Z_{yx})}{|Z_{xx}-Z_{yy}|^2 - |Z_{xy}+Z_{yx}|^2} \qquad (4.6)$$

where * denotes conjugate. The impedance tensor Z of 4.3 is rotated through the computed angle θ_o using equations 4.4, 4.5 for $\theta=\theta_o$. Specifically the matrix equation 4.4 can be seperated into 4 equations (4.7a,b,c and d) which can be solved for the rotated tensor elements $Z_{xx}, Z_{xy}, Z_{yx}, Z_{yy}$ as follows :

$$Z'_{xx}=1/2\{Z_{xx}+Z_{yy}+(Z_{xx}-Z_{yy})\cos2\theta+(Z_{xy}+Z_{yx})\sin2\theta\} \qquad (4.7a)$$

$$Z'_{xy}=1/2\{Z_{xy}-Z_{yx}+(Z_{xy}+Z_{yx})\cos2\theta-(Z_{xx}-Z_{yy})\sin2\theta\} \qquad (4.7b)$$

$$Z'_{yx}=1/2\{-Z_{xy}+Z_{yx}+(Z_{xy}+Z_{yx})\cos2\theta-(Z_{xx}-z_{yy})\sin2\theta\} \qquad (4.7c)$$

$$Z'_{yy}=1/2\{Z_{xx}+Z_{yy}-(Z_{xx}-Z_{yy})\cos2\theta-(Z_{xy}+Z_{yx})\sin2\theta\} \qquad (4.7d)$$

The new, rotated impedance tensor is :

$$Z' = \begin{vmatrix} Z'_{xx} & Z'_{xy} \\ Z'_{yx} & Z'_{yx} \end{vmatrix} \qquad (4.8)$$

4.3.(iii). Computation of the apparent resistivity and phase responses.

In the present study apparent resistivities and phases were computed for two different rotation angles using the weighted mean of the upward and downward tensor elements. The rotation angles were those, corresponding to (a) the measuring directions, (b) the principal directions. Apparent resistivities and phases were also computed for the invariant quantity :

$$Z_{inv}=(Z_{xx}Z_{yy}-Z_{xy}Z_{yx})^{1/2} \quad (4.9)$$

(Tichonov and Berdichevsky, 1966 ; Ranganayaki, 1984).

The standard formulae for computing the apparent resistivities ρ and phase ϕ, were used :

$$\rho_{ij}=\frac{\mu_o}{w}\left|\frac{E_i}{H_j}\right|^2=2T\times10^{-7}\left|\frac{E_i}{H_j}\right|^2=0.2T\left|\frac{\bar{E}_i}{\bar{H}_j}\right|^2=0.2T|Z_{ij}|^2 \quad (4.10)$$

$$\phi_{ij}=\arctan(\mathrm{Real}(Z_{ij})/\mathrm{Imag}(Z_{ij})) \quad (4.11)$$

where $\mathrm{Real}(Z_{ij})$, $\mathrm{Imag}(Z_{ij})$ denote the real and imaginary parts of the Z_{ij} * tensor elements with i,j=x,y. Equations 4.10 and 4.11 are valid for all kind of rotations and the invariant of eq.4.9 (where $Z_{ij}=Z_{inv}$). Typical examples of the magnetotelluric data acquired on Milos are given in Fig.4.3a-d, Fig.4.4a-d and Fig.4.5a-d which illustrate the frequency variation of - the apparent resistivity and phase responses along the measuring and principal directions - coherence and number of estimates - azimuth of the major apparent resistivities for the AMT-LMT stations 617, 621 and the AMT station 626 respectively (see Fig.4.1 (page 89) for their location).

* Note : $Z_{ij}=\frac{\bar{E}_i}{\bar{H}_j}$ where $\bar{E}_i$ is in mV/km and $\bar{H}_j$ in nT (see also Note on page 35).

Fig.4.3. The magnetotelluric data at site 617.

a. Frequency variation of the unrotated magnetotelluric responses.

b. Frequency variation of coherence and number of estimates.

c. Frequency variation of the rotated magnetotelluric responses.

d. Frequency variation of the azimuth of the major apparent resistivities.

Fig.4.4. The magnetotelluric data at site 621.

a. Frequency variation of the unrotated magnetotelluric responses.

b. Frequency variation of coherence and number of estimates.

c. Frequency variation of the rotated magnetotelluric responses.

d. Frequency variation of the azimuth of the major apparent resistivities.

Fig.4.5. The magnetotelluric data at site 626.

a. Frequency variation of the unrotated magnetotelluric responses.

b. Frequency variation of coherence and number of estimates.

c. Frequency variation of the rotated magnetotelluric responses.

d. Frequency variation of the azimuth of the major apparent resistivities.

Fig.4.3

617

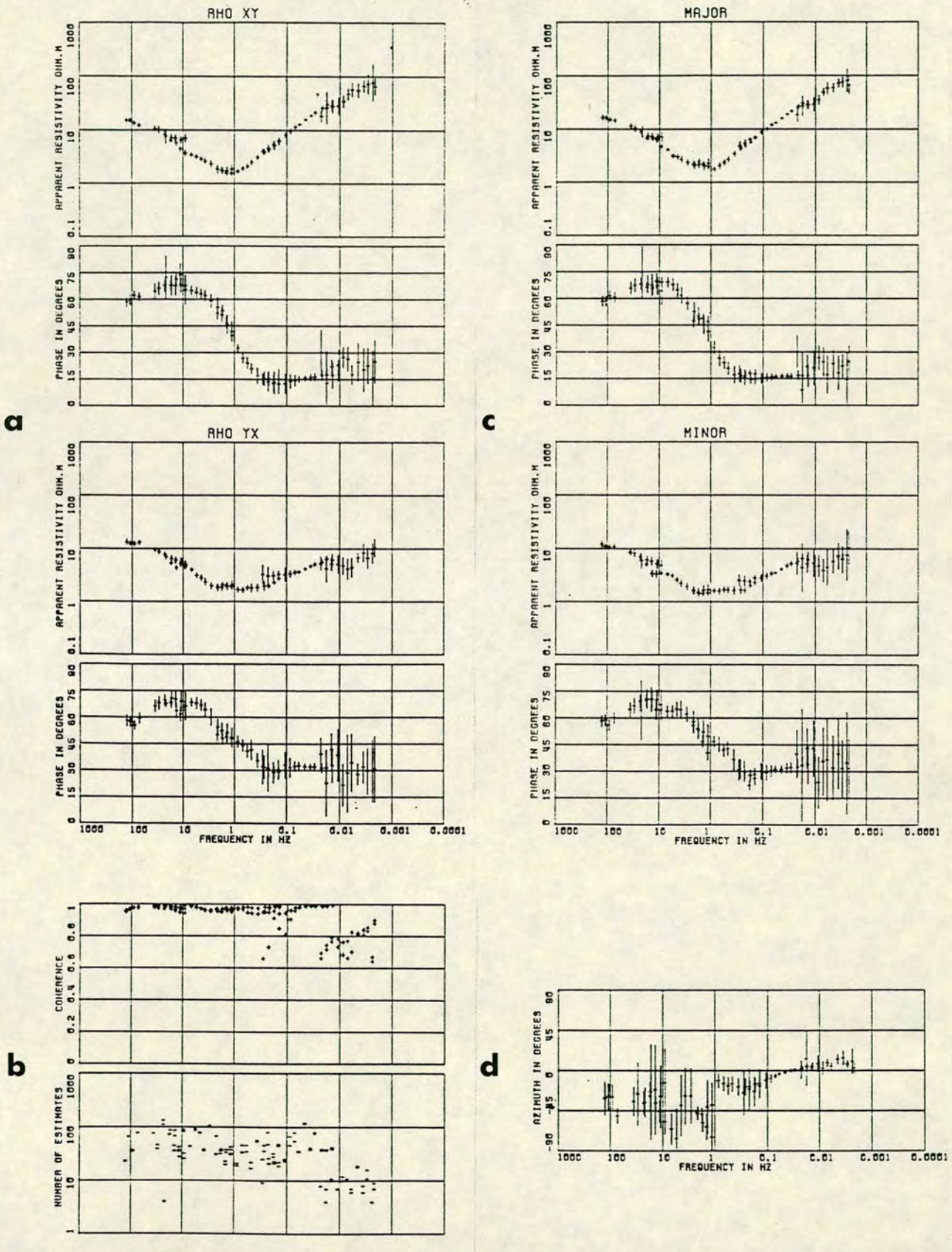
a
RHO XY
APPARENT RESISTIVITY OHM.M
1000
100
10
1
0.1
PHASE IN DEGREES
90
75
60
45
30
15
0
c
MAJOR
APPARENT RESISTIVITY OHM.M
PHASE IN DEGREES
RHO YX
APPARENT RESISTIVITY OHM.M
PHASE IN DEGREES
MINOR
APPARENT RESISTIVITY OHM.M
PHASE IN DEGREES
1000
100
10
1
0.1
0.01
0.001
0.0001
FREQUENCY IN HZ
b
COHERENCE
1
0.8
0.6
0.4
0.2
0
NUMBER OF ESTIMATES
1000
100
10
1
d
AZIMUTH IN DEGREES
90
45
0
-45
-90

Fig.4.4

621

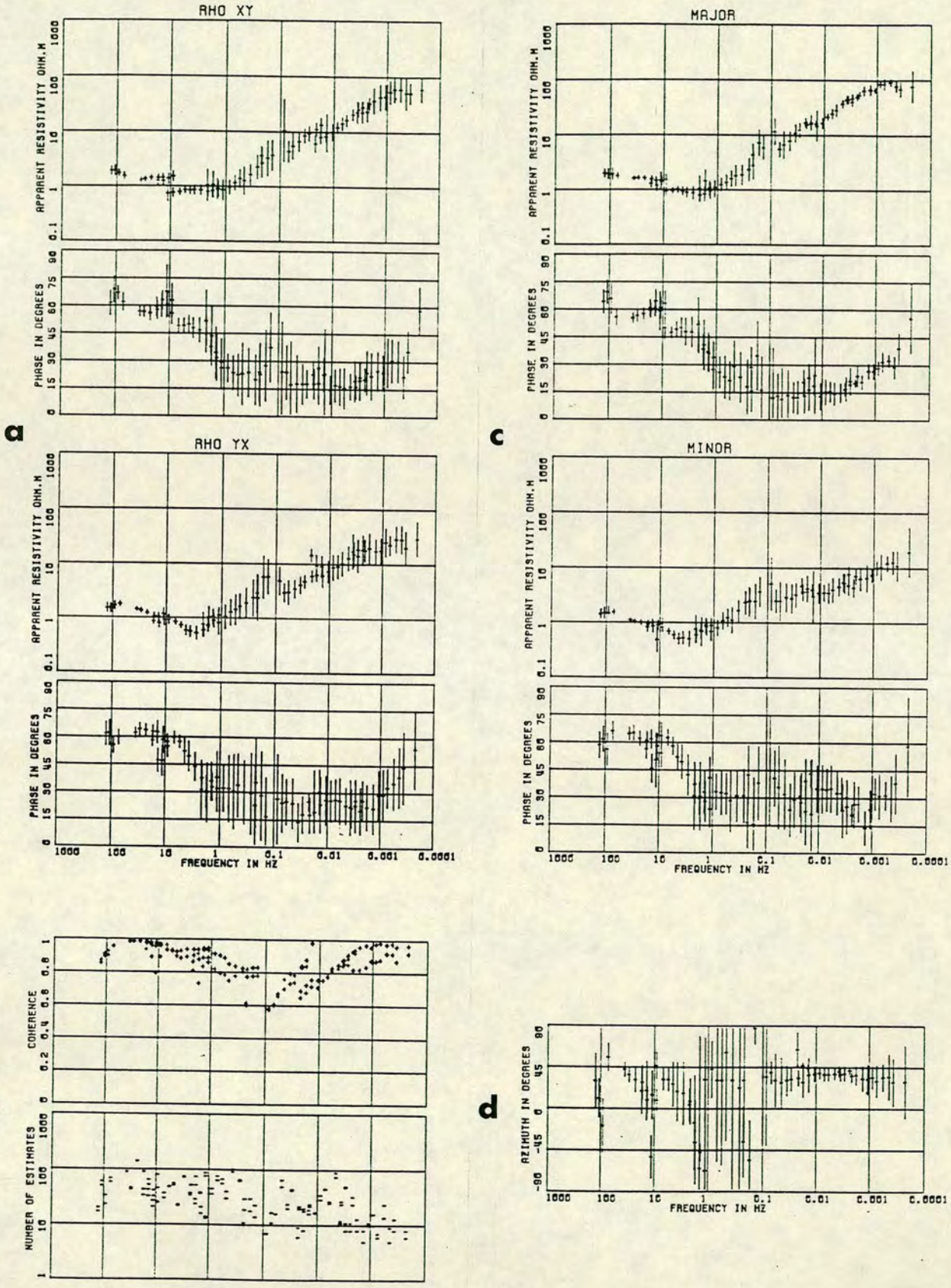
a
RHO XY
APPARENT RESISTIVITY OHM.M
1000
100
10
1
0.1
PHASE IN DEGREES
90
75
60
45
30
15
0
RHO YX
APPARENT RESISTIVITY OHM.M
PHASE IN DEGREES
1000
100
10
1
0.1
0.01
0.001
0.0001
FREQUENCY IN HZ
b
COHERENCE
1
0.8
0.6
0.4
0.2
0
NUMBER OF ESTIMATES
1000
100
10
1
c
MAJOR
APPARENT RESISTIVITY OHM.M
PHASE IN DEGREES
MINOR
APPARENT RESISTIVITY OHM.M
PHASE IN DEGREES
FREQUENCY IN HZ
d
AZIMUTH IN DEGREES
90
45
0
-45
-90

Fig.4.5 626

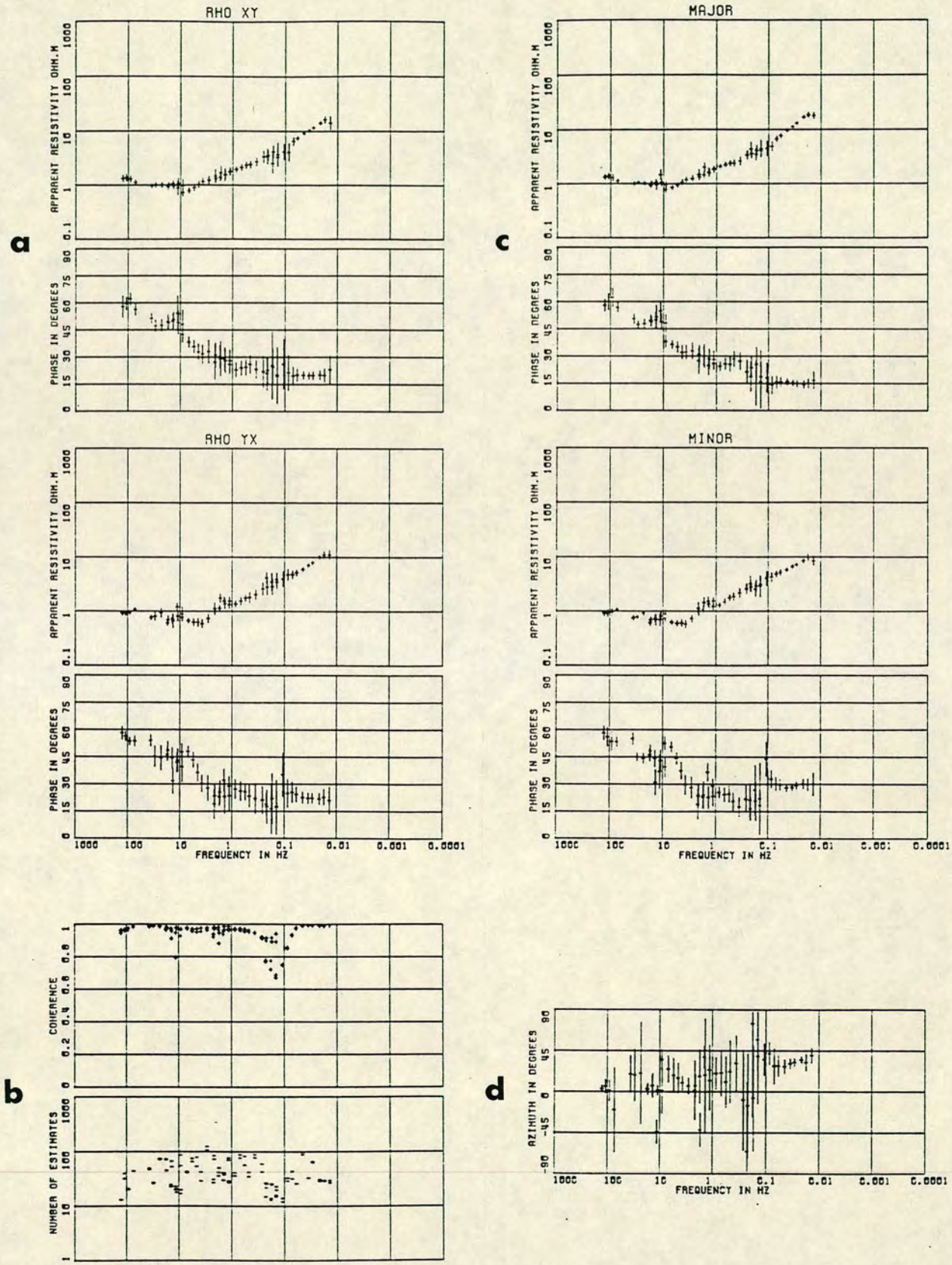
a
RHO XY
APPARENT RESISTIVITY OHM.M
1000
100
10
1
0.1
PHASE IN DEGREES
90
75
60
45
30
15
0
RHO YX
APPARENT RESISTIVITY OHM.M
PHASE IN DEGREES
1000
100
10
1
0.1
0.01
0.001
0.0001
FREQUENCY IN HZ
c
MAJOR
APPARENT RESISTIVITY OHM.M
PHASE IN DEGREES
MINOR
APPARENT RESISTIVITY OHM.M
PHASE IN DEGREES
FREQUENCY IN HZ
b
COHERENCE
1
0.8
0.6
0.4
0.2
0
NUMBER OF ESTIMATES
1000
100
10
1
d
AZIMUTH IN DEGREES
90
45
0
-45
-90
FREQUENCY IN HZ

4.3.(iv). Computation of the Parkinson Induction Arrows.

Measurements of the vertical magnetic field variations in the period range $10-10^{+4}$ secs enabled computations of the Parkinson induction arrows (1962) for this period range to be made. The vertical magnetic field H_z can be related to the other two horizontal components H_x and H_y. The relation takes the form :

$$H_z = AH_x + BH_y \quad (4.12)$$

where A and B are the geomagnetic transfer functions which can be calculated by using the same auto- and cross-power spectal estimates which were used for the impedance tensor elements above. The A and B are complex with $A=A_r+A_i$ and $B=B_r+B_i$. Subscripts r,i refer to real and imaginary parts. The induction arrows are defined by the following equations :

$$|K| = (A_k^2 + B_k^2)^{\frac{1}{2}} \quad (4.13)$$

$$\phi_k = \arctan(B_k / A_k) \quad (4.14)$$

where $|K|=|R|, |I|$ which denote the magnitudes of the real and imaginary parts of the induction arrows and k=r,i which denote as before the real and imaginary parts of the transfer functions A and B. ϕ_r and ϕ_i are the azimuths of the real and imaginary parts of the induction arrows.

The magnetic field vector lies in a preferred plane which is defined by eq.4.12. Parkinson (1962) introduced an arrow defined by eqs.4.13 and 4.14 but reversed in direction (now referred to as the Parkinson arrow) the real part of which points towards current concentrations *. Large real and smaller imaginary parts

* Note : When measurements are taken near the sea and if the conductivity of the earth is much smaller than that one of the sea-water, then considerable distortion of the Parkinson induction arrows is expected (Coast effect).

617

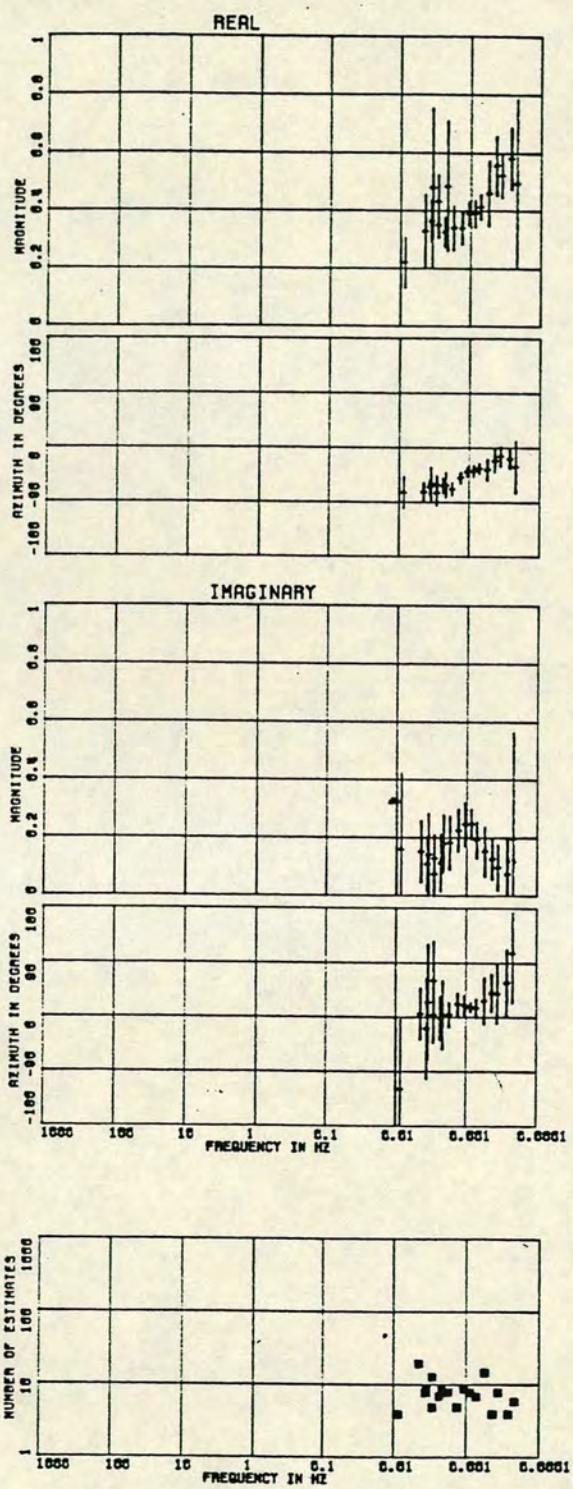

Fig.4.6. Parkinson induction arrows for site 617.

621

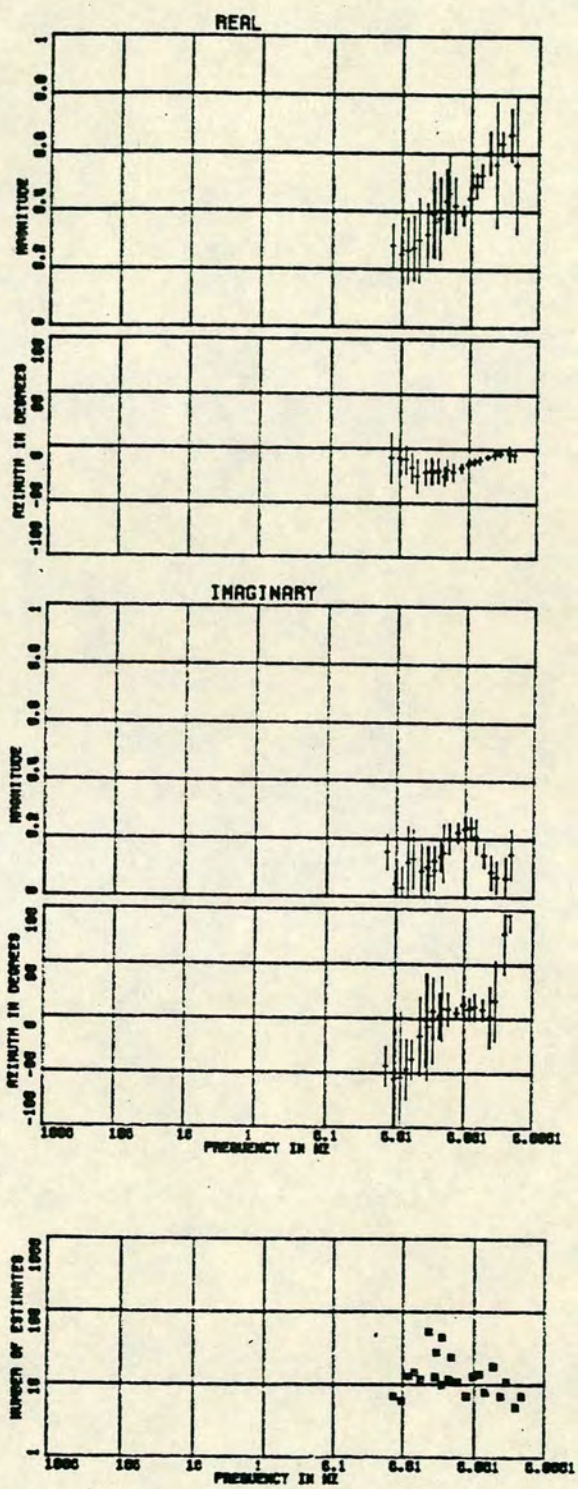

Fig.4.7. Parkinson induction arrows for site 621.

of the induction arrows are usually associated with deep conductive bodies while larger imaginary parts imply shallow conductive bodies. Fig.4.6 and Fig.4.7 (page 103) show examples of the Parkinson arrows computed at the site locations 617 and 621 respectively.

4.4. Computation of the rotation angles.

Examples of the data rotated to the principal directions were given in Figs.4.3c, 4.4c and 4.5c for sites 617, 621, 626 respectively. The frequency variation of the azimuth of the major axis of the impedance ellipses is illustrated in Figs.4.3d, 4.4d and 4.5d. The same procedure was repeated for each station. Therefore it was finally possible to obtain a picture of the magnetotelluric azimuth distribution with frequency at each station over the study area. The axes of the rotated impedance ellipses are presented in Figs.4.8a-d for a set of period (frequency) ranges, 10^{-1}-1, 10-50, 100-500, 500-5000 secs, respectively. The lengths of the axes are proportional to the square root of the major and minor resistivities.

It is observed that at the lowest period range (10^{-1}-1 secs) the axes of the magnetotelluric ellipses are small and of equal lengths for the majority of the stations. Within the longer period ranges (10-5000 secs), the axes of the magnetotelluric ellipses become gradually larger and are unequal in lengths. The major axis is about two or three times longer than the minor. At most of the sites both the axes are oriented in two perpendicular directions, NW-SE and NE-SW respectively. The principal NW-SE and NE-SW directions are approximately 20°W and 70°E respectively. The major axes within the inner part of Zephyria graben are striking NW-SE, while outside the

Fig.4.8. Azimuths of the major and minor axes of the magnetotelluric impedance ellipses.

a. Period range : 0.1-1 secs.

b. Period range : 10-50 secs.

c. Period range : 100-500 secs.

d. Period range ; 500-5000 secs.

Fig.4.8

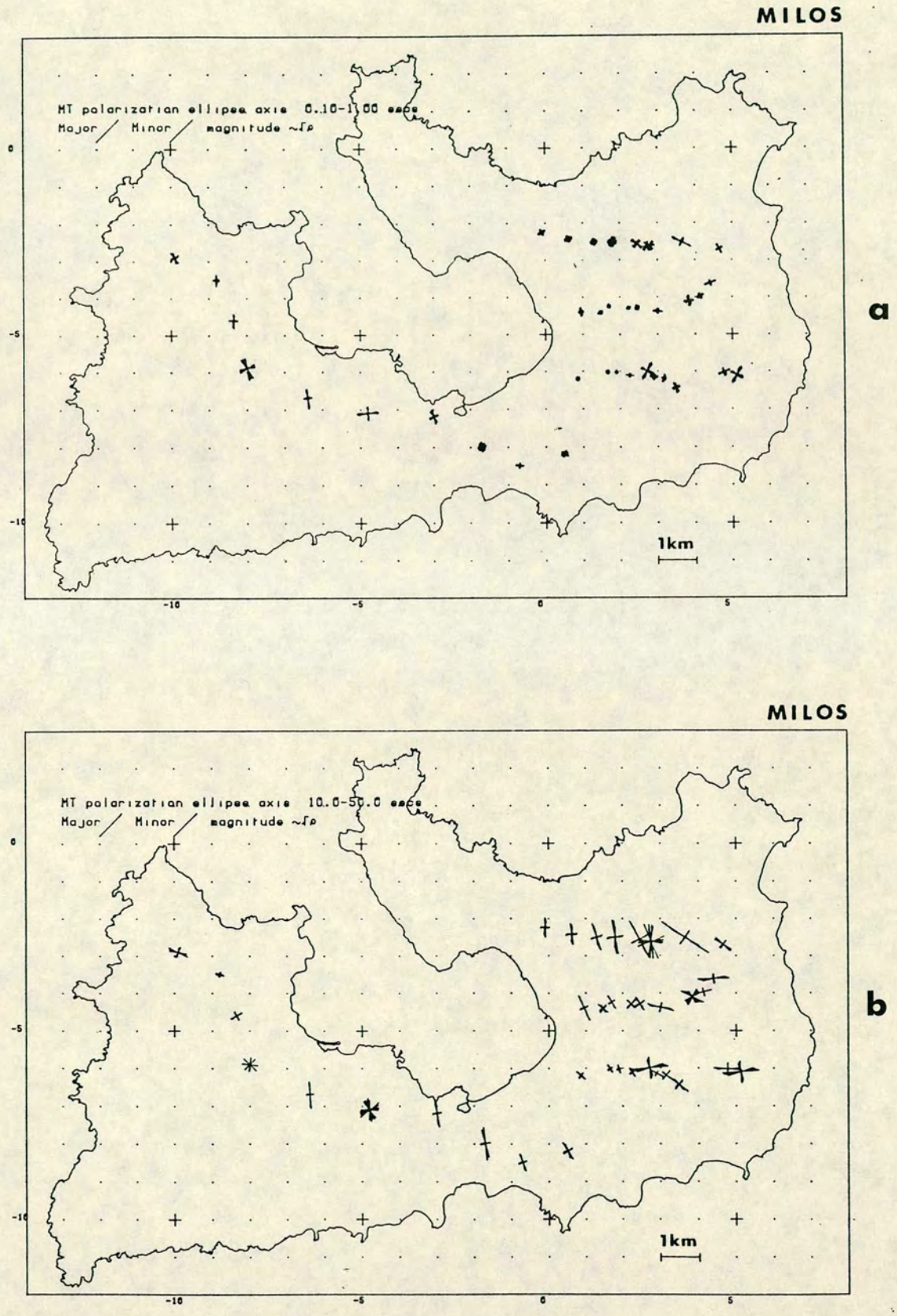
MILOS
MT polarization ellipse axis 0.10-1.00 sec
Major / Minor / magnitude ~ρ
1km
a
MILOS
MT polarization ellipse axis 10.0-50.0 sec
Major / Minor / magnitude ~ρ
1km
b

Fig.4.8

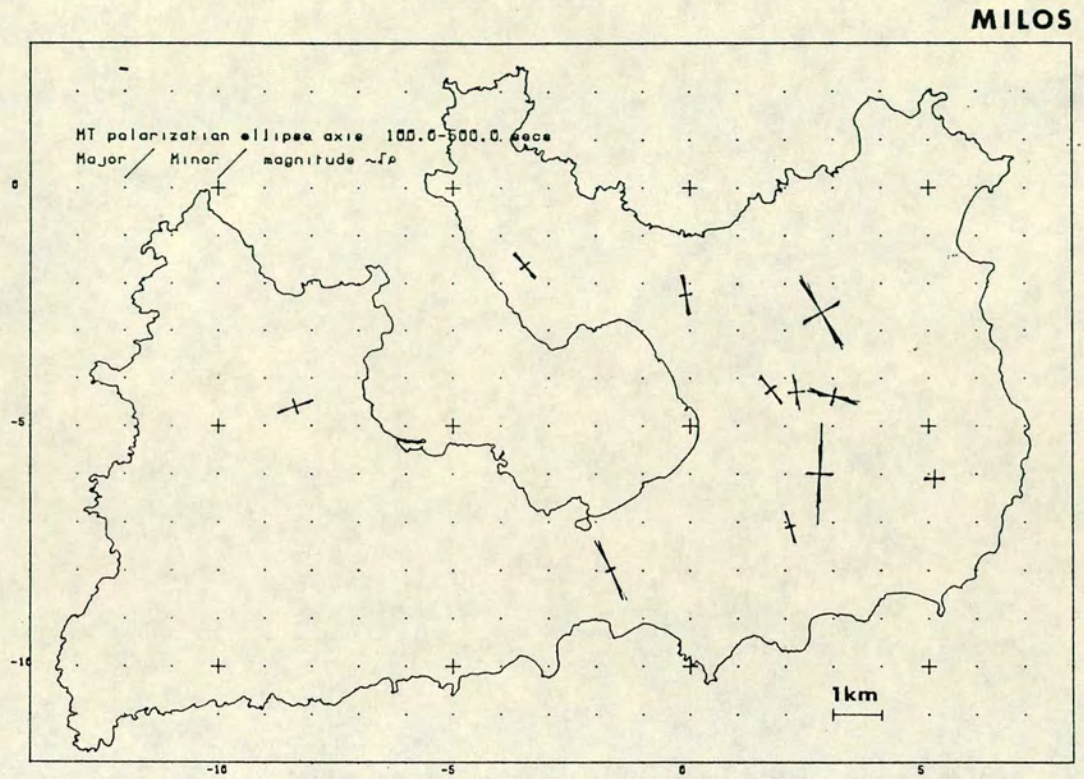
MILOS
MT polarization ellipse axis 100.0-500.0 sec
Major / Minor magnitude ~ρ
1km
0
-5
-10
-10
-5
0
5

c

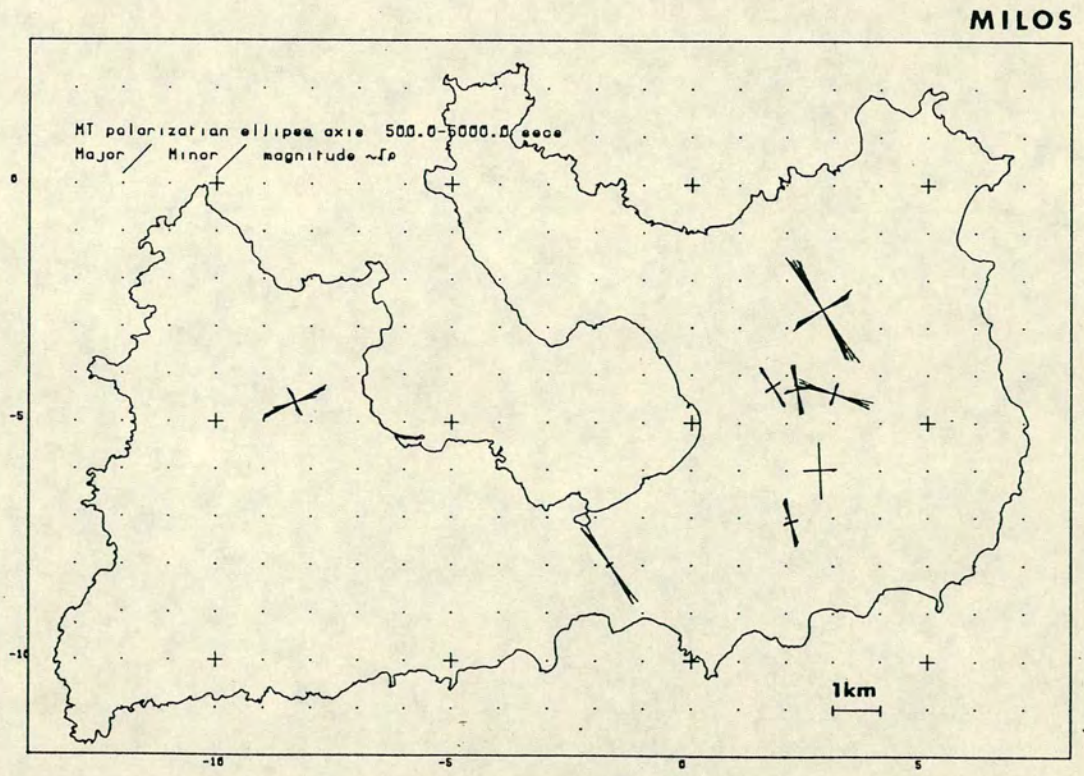
MILOS
MT polarization ellipse axis 500.0-5000.0 sec
Major / Minor magnitude ~ρ
1km
0
-5
-10
-10
-5
0
5

d

graben they tend to be in the NE-SW direction.

4.5. A dimensionality test for the magnetotelluric data.

Several dimensionality parameters were computed at a premodelling stage. These were the skew, eccentricity in the principal directions and the four Kao and Orr indices. An additional test involving application of the nine inequality constraints of Weidelt was also undertaken.

The derivation of the first six parameters is based on the horizontal rotation properties of the 2x2 impedance tensor matrix Z of equation 4.3 through an angle θ. If θ_o is the angle which determines the principal directions, the parameter combinations $(Z_{xx}+Z_{yy})/2$ and $(Z_{xy}-Z_{yx})/2$ are independent of θ_o and correspond to the centres of the rotation ellipses in the complex plane (Z_{ij} with i,j=x,y imply unrotated impedance tensor elements). The parameter combinations $(Z'_{xx}(\theta_o)-Z'_{yy}(\theta_o))/2$ and $(Z'_{xy}(\theta_o)+Z'_{yx}(\theta_o))/2$ correspond to the minor and major axes of the ellipse $Z'(\theta_o)$. $Z'(\theta_o)$ denotes the 2x2 rotated impedance tensor at an angle θ_o of equation 4.3. $Z'_{ij}(\theta_o)$ are the rotated impedance tensor elements at an angle θ_o with i,j=x,y.

The computation of the above six parameters is based on the following quantities defined by Kao and Orr (1982) :

$$Z_1=(Z_{xy}-Z_{yx})/2 \quad (4.15)$$

$$Z_2=(Z_{xx}+Z_{yy})/2 \quad (4.16)$$

$$M_1=(Z'_{xy}(\theta_o)+Z'_{yx}(\theta_o))/2 \quad (4.17)$$

$$M_2=(Z'_{xx}(\theta_o)-Z'_{yy}(\theta_o))/2 \quad (4.18)$$

$$S=|Z_1|+|M_1|+(|Z_2|+|M_2|)/2 \quad (4.19)$$

The skew α, the eccentricity in the principal directions β and the Kao and Orr indices D_1, D_2, D_3, D'_3 are derived with use of 4.14-4.18 and their expressions are given by the following equations :

$$\alpha = \frac{|Z_2|}{|Z_1|} \qquad (4.20)$$

$$\beta(\theta_o) = \frac{|M_2|}{|M_1|} \qquad (4.21)$$

$$D_1 = |Z_1|/S \qquad (4.22)$$

$$D_2 = |M_1|/S \qquad (4.23)$$

$$D_3 = |Z_2|/S \qquad (4.24)$$

$$D'_3 = |M_2|/S \qquad (4.25)$$

All these dimensionality indicators are expected to vary from 0 to 1. The skew α defined by Word et al. (1971), Swift (1967) is considered to be a three-dimensional parameter. It must approach 0 for one or two dimensional structures (Reddy et al., 1977 ; Ting and Hohmann, 1981). Word et al. (1971) refer to skew as the ratio of the displacements of the centres from the origin, of the rotational ellipses for the diagonal and cross tensor impedance elements. Reddy et al. (1977) suggest that skew values greater than 0.2 imply three dimensional effects. The eccentricity $|\beta(\theta_o)|$ in the principal directions was defined by Word et al. (1971) as another three dimensional index. For one or two dimensional earth structures it is expected to be 0 and non zero for three dimensional structures (Reddy et al., 1977 ; Ting and Hohmann, 1981). Hermance (1982) believes that the utility of $|\beta(\theta_o)|$ as an unequivocal index of three dimensionality is not apparent, something which was confirmed by

Beamish (1986). Kao and Orr (1982) realising the difficulties which may arise in the interpretation of the skew and eccentricity introduced the four normalised dimensional indices given above with equations 4.22-4.25. These relate to one, two and three dimensional effects respectively.

For one dimensional structures the condition $D_1 > D_2 > D_3, D'_3$ is expected to be satisfied. D_1 and D_2 have reciprocal behaviour and large D_2, D_3 or D'_3 weights are forecasted when two or three dimensional structures are present. The above six dimensionality indices do not give an absolute measure of the dimensionality of the earth but when they are interpreted altogether they can provide a reliable measure of the contribution of the different structural components of the earth. Weidelt (1972 ; 1986) and Yee and Paulson (1988) studied the one dimensionality problem more strictly by looking at the properties of the MERF c(w).

The analytical properties of the MERF c(w) follow the general theory of second order linear differential equations. A brief review for these properties has been given in 2.5. Weidelt introduced 22 inequality constraints which are sufficient conditions to be upheld by one dimensional data. The first nine of these inequalities are considered to be a satisfactory measure for the existence or not of one dimensional solution. These nine inequality constraints are the following, when $c(w)=g(w)-ih(w)$, where $g(w), h(w)$ are the real and imaginary parts of c(w) :

$$g \geq 0 \quad (4.26) \qquad h \geq 0 \quad (4.27)$$

$$Dg \leq 0 \quad (4.28)$$

$$0 \leq -D|c| \leq |c| \quad (4.29)$$

$|Dc| \leq h$ (4.30) $|c+Dc| \leq g$ (4.31)

$|D^2c| \leq h$ (4.32) $|c+2Dc+D^2| \leq g$ (4.33)

The differential operator D is defined as D=wd/dw=d/d(logw). The derivatives of c can be computed using the derivative of a Langrangian interpolation polynomial of degree 2, relevant to three neighbouring values of g and h on a logarithmic period scale.

The numerical procedure of estimating the first two derivatives of the response function c(w) may be unstable when the data tested are noisy. For good data sets the procedure is expected to be stable. Each inequality constraint is tested for each frequency w through the whole w range in use and the measure of satisfaction is expressed as a percentage. When the first four inequalities are satisfied, one dimensionality can be accepted.

Weidelt (1986) and Yee and Paulson (1988) generalized the previous nine inequality constraints to a set of two conditions which are necessary and sufficient to warrant the existence of a one dimensional conductivity model.

Every magnetotelluric data set was tested dimensionally. The six parameters α, $\beta(\theta_o)$, D_1, D_2, D_3 and D'_3 were computed for every frequency. In addition the first nine inequality constraints of Weidelt have been applied. Results are discussed in detail for three representative sites, 617, 621 and 626. The apparent resistivity and phase data along the measuring and principal directions for these sites are shown as examples in Figs.4.3a,c ,4.4a,c and 4.5a,c respectively.

From visual inspection of the raw curves the following conclusions are derived. In 617 the raw curves are isotropic in the range 10^{+2}-1 Hz and then become anisotropic at the lower frequencies,

by up to one decade of Ohm.m for the apparent resistivity and 15° for the phase . The magnetotelluric apparent resistivity and phase responses in site location 621 show the same degree of anisotropy as in site 617. In 626 the raw curves are fairly isotropic through the whole frequency range. Figs.4.9, 4.10 and 4.11 illustrate α, $|\beta(\theta_o)|$, D_1, D_2, D_3, D'_3 for these sites.

Skew α at all sites in the range 10^{+2}-10^{-1} Hz is very low, less than 0.1-0.2. In the lower frequency range 10^{-1}-10^{-3} Hz, the skew increases up to 0.25. The Kao and Orr indices at all sites obey the one dimensional condition $D_1 > D_2 > D_3, D'_3$. Indices D_3, D'_3 approach zero. However sites 617 and 621 show two dimensional features since index D_2 is quite high with a maximum of 0.4 at the lower frequencies. The eccentricity $|\beta(\theta_o)|$ at 617 and 621 in the frequency range 10^{+2}-10^{-1} Hz has non-zero and rather scattered values. At longer periods 10^{-1}-10^{-4} Hz it tends gradually towards zero values while D_2 increases. At 626 the eccentricity has non-zero values through the whole period range and D_2, D_3 and D'_3 weights get very low values. At both sites 617 and 621, the index D_1 decreases (down to 0.5) with decreasing frequency, while at site 626 D_1 varies only between 1.0 and 0.8.

The nine inequality constraints of Weidelt are upheld with percentages of 89.4%, 81.4% and 85% for 617, 621 and 626 respectively. It can be noted that the conditions were not satisfied for frequencies less than 0.2 Hz. The general conclusions from the dimensionality test for all sites are the following :

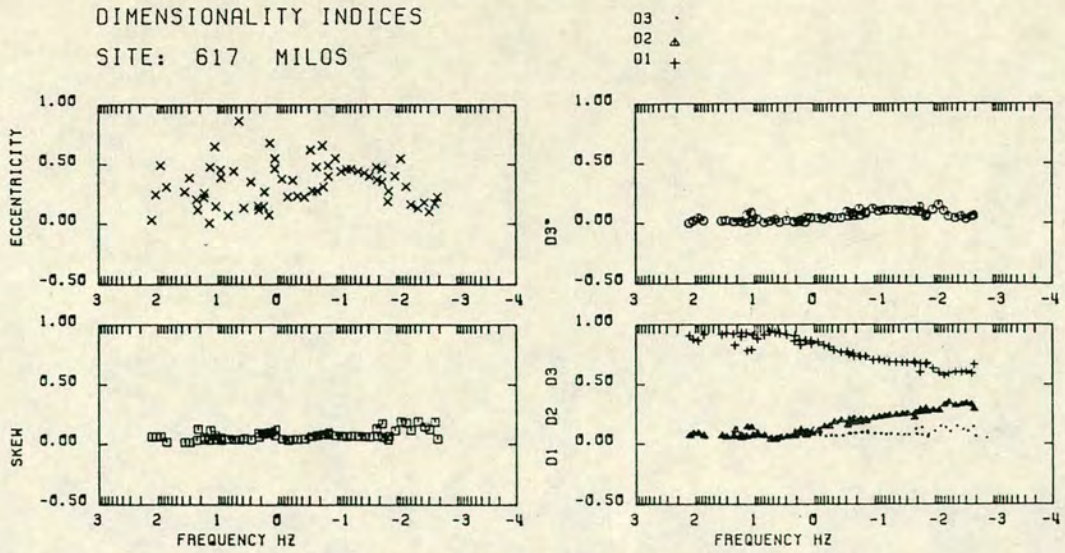

Fig.4.9. Dimensionality indices for site 617.

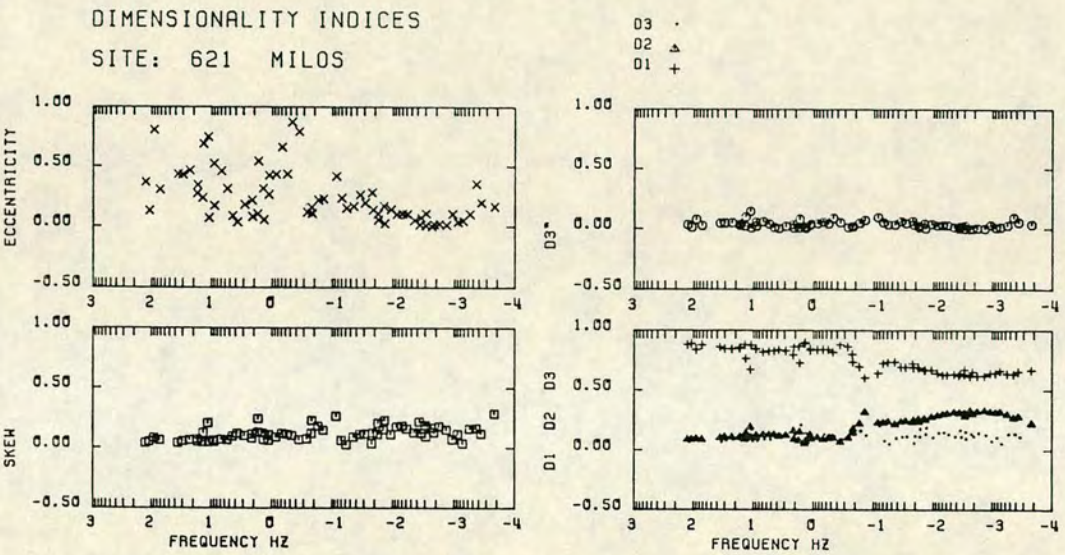

Fig.4.10. Dimensionality indices for site 621.

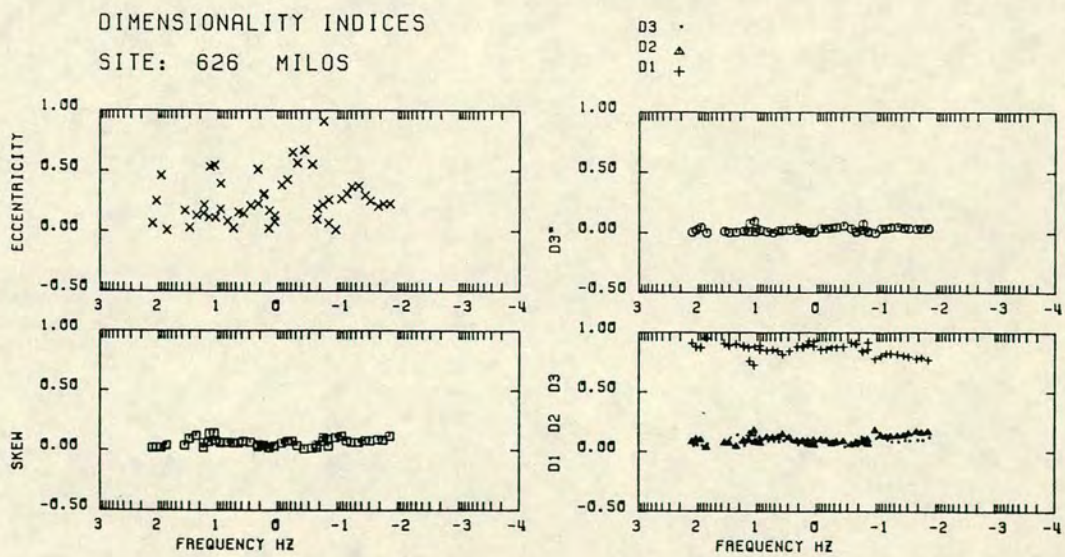

Fig.4.11. Dimensionality indices for site 626.

(i). Skew α varies from values of 0.0 to 0.2.

(ii). The eccentricity $|\beta(\theta_0)|$ is not a reliable three dimensional index since it shows non-zero values even for nearly one dimensional data.

(iii). The Kao and Orr indices vary as follows :

$0.5 < D_1 < 1.0$, $0.0 < D_2 < 0.5$, $0.0 < D_3, D'_3 < 0.2$.

(iv). Since D_3 and D'_3 are negligible it is not surprising that D_1 and D_2 show a reciprocal behaviour and generally the one dimensional relation $D_1 > D_2 > D_3, D'_3$ is valid at all the magnetotelluric stations.

(v). The nine inequality constraints of Weidelt are satisfied with total percentage greater than 60 %.

(vi). The electrical model of the Milos geothermal field for the frequency range 10^{+2}-10^{-1} Hz can be very well approximated by one dimensional modelling.

4.6. Modelling the Milos geothermal field.

For the shorter period range 10^{-2}-10^{+1} secs, the magnetotelluric modelling problem for Milos can be satisfied by one dimensional solution, while two dimensional modelling is required when the longer period data are being considered.

Several one dimensional modelling techniques were applied to the apparent resistivities and phases derived from the invariant impedance of eq.4.9. in addition to the Parker-Whaler D^+ inversion procedure discussed in chapter 2, these were the Niblett-Bostick transformation (Jones, 1983), the Fischer et al. (1981)

inversion, the modified Monte Carlo modelling scheme developed by Dawes (described by Sule, 1985) and the Jupp and Vozoff (1975) least squares method.

The one dimensional models reveal satisfactorily the electrical structure for about the top 5 km of the crust. The data become more anisotropic at the longer periods with the principal directions being normally 20°W and 70°E. The former is the dominant strike of the major apparent resistivities inside the Zephyria graben and the latter the major direction outside the graben. The magnetotelluric data were modelled two dimensionally along a profile, perpendicular to the 20°W, in order to reveal the deeper electrical structure of the Milos island. A forward modelling technique developed by Brewitt-Taylor and Weaver (1976) and later highly modified by Hill (1987) was employed. The background theory is summarized later in this chapter.

4.6.(i). One dimensional modelling : Basic relations.

The Niblett-Bostick (Jones, 1983) transformation transforms the apparent resistivity and phase responses to resistivity ρ_B and depth h respectively according to :

$$\rho_B = \rho(T) \left\{ \frac{1 + m(T)}{1 - m(T)} \right\} \qquad (4.34)$$

and

$$h = \left\{ \frac{\rho(T)\, T}{2\pi\mu_o} \right\}^{\frac{1}{2}} \qquad (4.35)$$

T is the period, μ_o the vacuum permeability and m(T) is the gradient of the apparent resistivity $\rho(T)$ on a log-log scale i.e :

$$m(T) = \frac{d\log(\rho(T)}{d\log\rho g(T)} = \frac{T}{\rho(T)} \frac{d\rho(T)}{dT} \qquad (4.36)$$

μ_o the vacuum magnetic permeability.

An alternative expression for the Niblett-Bostick resistivity at depth h was given by Goldberg and Rotstein (1982) :

$$\rho_B = \rho(T) \{ \frac{\pi}{2\phi(T)} - 1 \} \qquad (4.37)$$

The last expression employs the phase $\phi(T)$ information. This expression does not need any estimation for the resistivity gradient m(T). Eqs. 4.37 and 4.35 were used in the present study.

The Fischer et al. (1981) inversion is an analytical technique. The basic idea in this method is that the resistivity and phase responses at a certain period are only affected by the structure above a certain depth. It starts with the shorter periods of the experimental data set and tries to explain the observed responses in terms of a two layer structure. This procedure then continues progressively to longer periods. The only requirement is some a priori information for the top layer resistivity. The inversion works under two constraints, only one of which is necessary at a time. The first one requires the skin depth δ_{j+1} to the j+1 layer to be greater than the double thickness of the j-th layer, h_j, thus preventing the generation of meaningless layers. The second condition requires the skin depth $\delta_\alpha(T_{j+1})$ at period T_{j+1} to be larger than the depth H_j to that layer. This second condition is well suited to high quality data since it reveals subtle structural features.

The method developed by Dawes (Sule, 1985) is a modification of Jones and Hutton (1979) Monte Carlo inversion. The scheme is

iterative and the main specifications are described by Sule (1985) with the following.

(i). Apparent resistivity and phase data are being modelled.

(ii). One of three acceptance criteria is applied in selecting the best model fit, i.e. number of data error bars crossed by the model curve or the sum of the squared differences between model and real data or the sum squared error bar weighted difference.

(iii). The number of layers to be used in the modelling is specified.

(iv). For each of the layers, starting model parameters P (depth and resistivity) are specified with upper and lower bounds (denoted as P_{min}, P_{av} and P_{max} with P_{av} as the one used in computing the model curve).

The computer programme does 100 iterations. In the first iteration, it computes

$DIF2=\log_{10}(P_{max}/P_{av})$

$DIF1=\log_{10}(P_{av}/P_{min})$

It generates 500 random models using the relationship

$P'_i=P_i 10^{ra}$

where i=1,N=number of layers; P'_i is the new parameter value and P_i its previous value; r is a member of a set of random numbers having zero mean and a standard deviation of 1; a=DIF2 if r>0 and a=DIF1 if r<0 ($|r|<1$). In the case of the depth parameter, any situation where the depth to a lower interface is less than that to the interface above is rejected. Based on the acceptance criterion, the best 20 models are selected and put in an order table, with the best one at the top. It then finds the mean and standard deviation on a log-scale, the minimum (PMN) and maximum (PMX) of each of the parameters of these 20 best models. This mean value is taken as the

new P_{av} and it then computes

$$DIFMAX=\log(P_{max}/PMX)$$

$$DIFMIN=\log(PMN/P_{min})$$

DIFMAX and DIFMIN are used in altering P_{max} and P_{min} to new values. These new values of P_{av}, P_{max} and P_{min} are used in starting the second iteration from this equation solved in terms of DIF2 and similarily for the remaining iterations. In each iteration, the order table is updated so that it always contains the best 20 models so far. At the end of the 100 iterations, the best 20 models give a range of acceptable models and hence some indication of the non-uniqueness of the technique.

The Jupp and Vozoff method (1975) is a stable least squares method requiring an initial model **x** which is being changed by $\partial\mathbf{x}$ in order to obtain better fit to the experimental data. For this purpose the functional :

$$F(x)=\{\sum_{m=1}^{M} P_m\left(\frac{u_m-f_m(x)}{u_m}\right)^2\}^{1/2}$$

is minimized iteratively. Symbols u and f correspond to the experimental and models responses. f(x) can be written as :

$$f(x+\Delta x)=f(x)+J\Delta x+R(x,\Delta x)$$

where

$$J=\begin{vmatrix} \partial f_1/\partial x_1 & \ldots & \partial f_1/\partial x_N \\ . & \ldots & . \\ \partial f_M/\partial x_1 & \ldots & \partial f_M/\partial x_N \end{vmatrix}$$

is a Jacobian matrix of the vector function f(x). The remainder $R(x+\Delta x)$ includes second and higher order derivatives and is assumed to be small. The linearization of the inverse problem by neglecting $R(x+\Delta x)$ imposes limitations on the possibility of finding remote minima of F(x).

4.6.(ii). One dimensional modelling : Results.

In general there is a good agreement between the models derived by the application of these different modelling techniques as demonstrated by Figs.2.10a (page 66) respectively. However for reasons explained in chapter 5 the Parker-Whaler D^+ and Dawes methods were used for preparation of resistivity sections and contours of conductance and depths to the top of various electrical boundaries. Niblett-Bostick transformations were also considered useful for the one dimensional modelling.

In Figs.4.12, 4.13a and 4.14 the Niblett-Bostick transformation of the invariant magnetotelluric responses is overlayed by the D^+ and Dawes models for the same data from sites 617, 621 and 626 respectively. In Figs.4.13b, 4.13c the Niblett-Bostick transformation along the two principal directions at site location 621 is also provided for comparison.

The one dimensional models collated along the Profiles 1, 2, 3, 4 of Fig.4.1 (page 89) are presented in Figs.4.15a-d and Figs.4.16a-d (pages 124-127) for the D^+ and Dawes methods respectively.

The Dawes starting models were constrained for the top 25-50 m by using existing D.C resistivity results.

The D^+ models are illustrated in terms of layer resistivities and depths which correspond to the D^+ delta function positions. The resistivities have been computed by dividing the depths by the corresponding delta function conductances as it was described in chapter 2.

Fig.4.12. Niblett-Bostick transformation of the invariant magnetotelluric responses for site 617. The D^+ and the Dawes models are superimposed for comparison.

Fig.4.13. Niblett-Bostick transformation of the invariant and major and minor magnetotelluric responses for site 621. The D^+ and the Dawes models are superimposed on the Bostick model of the invariant.

a. Models for the invariant responses.

b. Model for the major responses.

c. Model for the minor responses.

Fig.4.14. Niblett-Bostick transformation of the invariant responses for site 626. The D^+ and the Dawes models are superimposed for comparison.

Fig.4.12

1-D MODEL 617

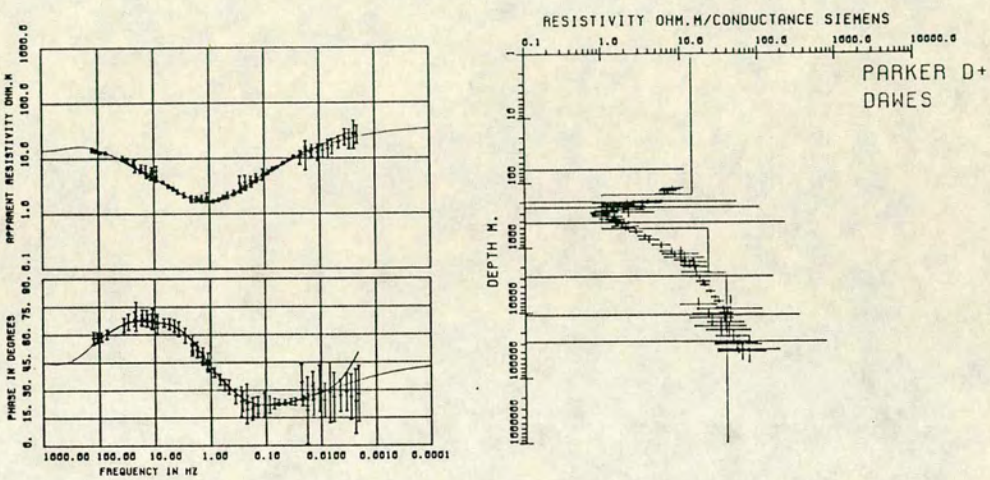

Fig.4.14

1-D MODEL 626

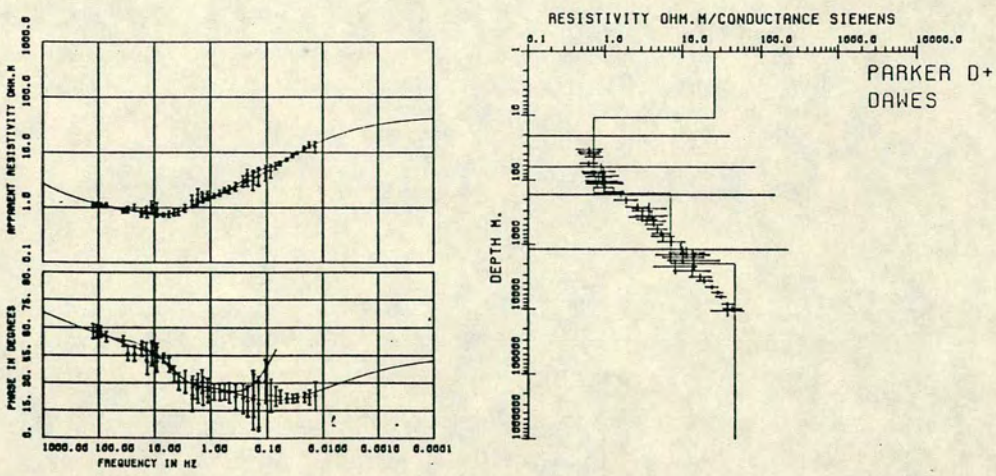

Fig.4.13

1-D MODEL 621

a

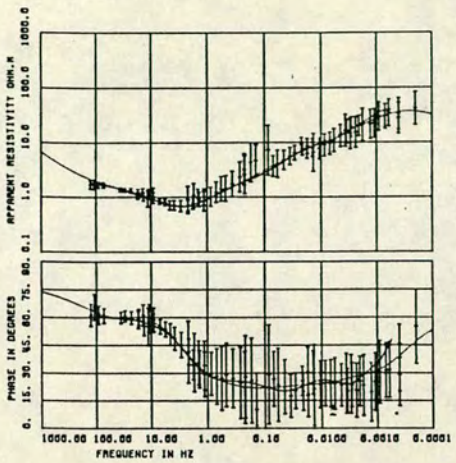

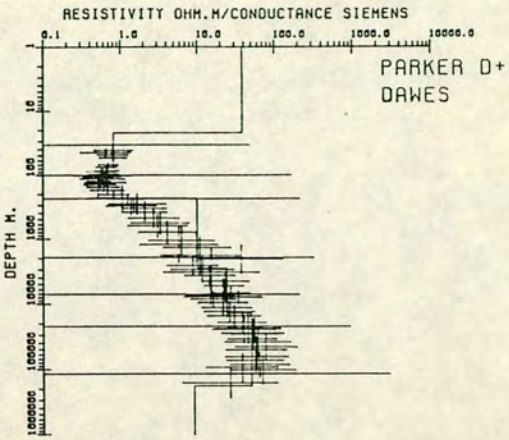

1-D MODEL 621

b

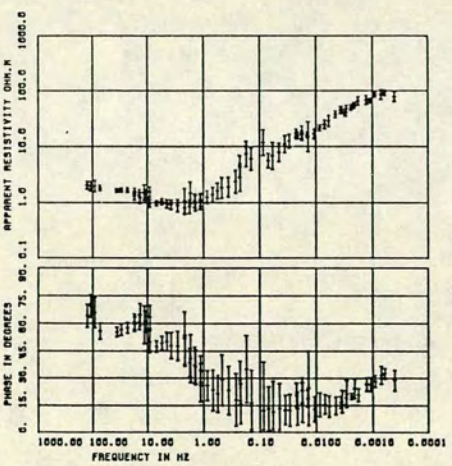

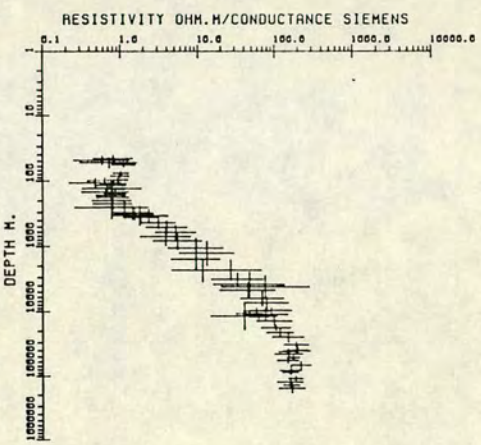

1-D MODEL 621

c

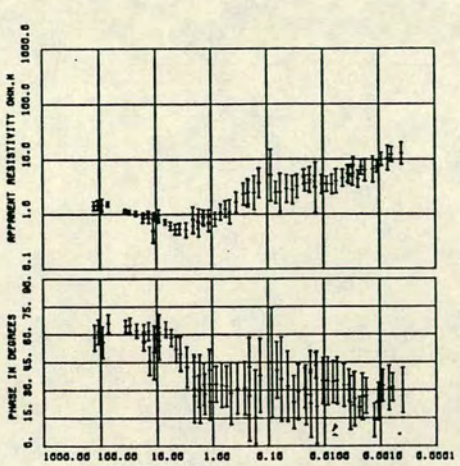

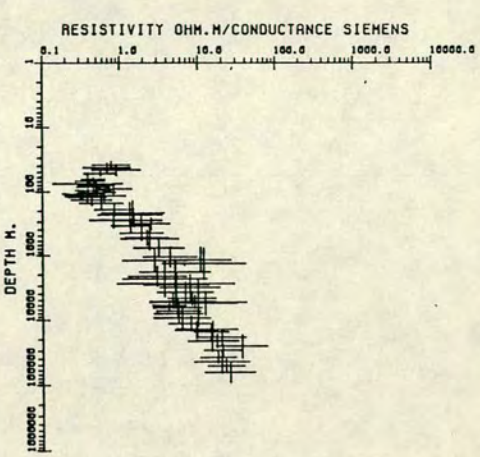

Fig.4.15. Parker-Whaler D^+ one dimensional sections along Profiles P1, P2, P3 and P4 of Fig.4.1 (apge 89).

a. Profile 1.

b. Profile 2.

c. Profile 3.

d. Profile 4.

Fig.4.16. Dawes one dimensional sections along Profiles P1, P2, P3 and P4 of Fig.4.1 (page 89).

a. Profile 1.

b. Profile 2.

c. Profile 3.

d. Profile 4.

PROFILE 1

Fig.4.15a

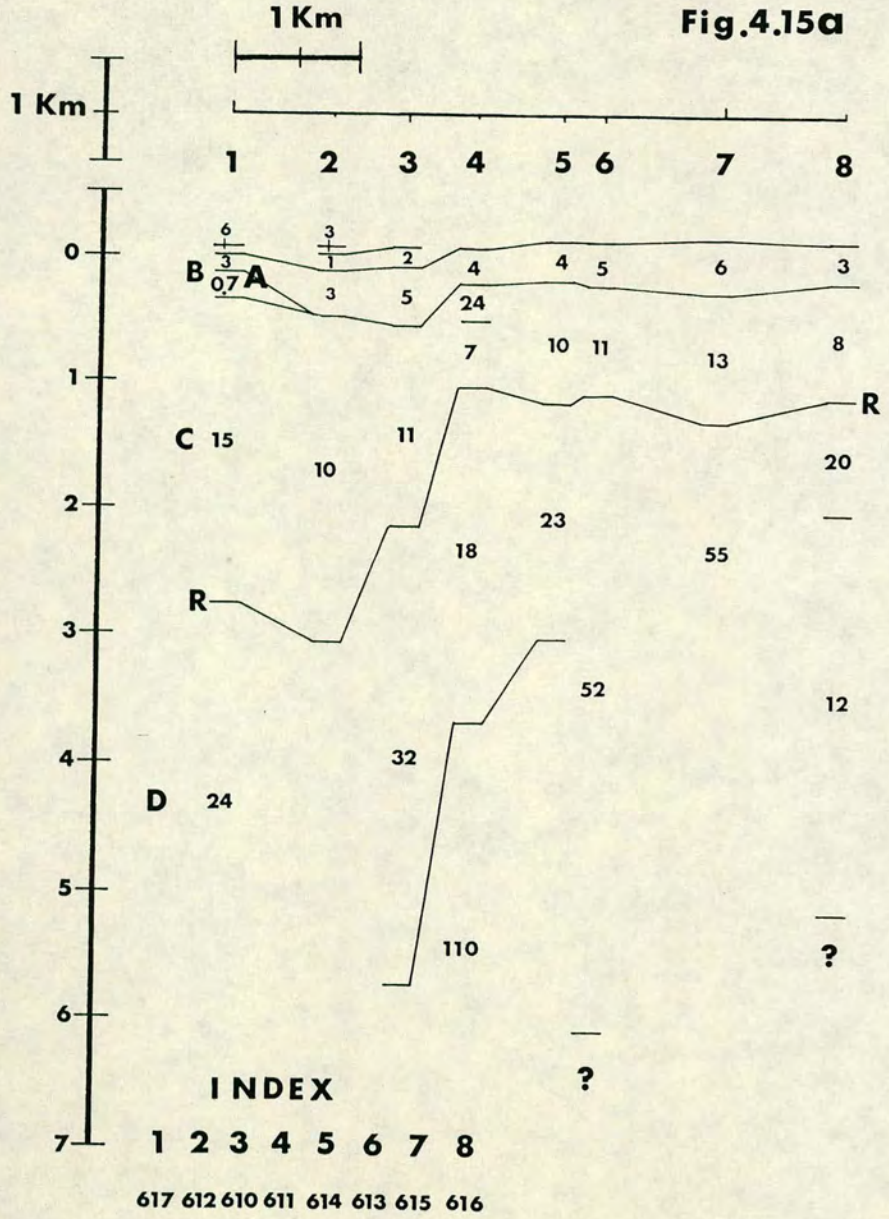

Fig.4.16a

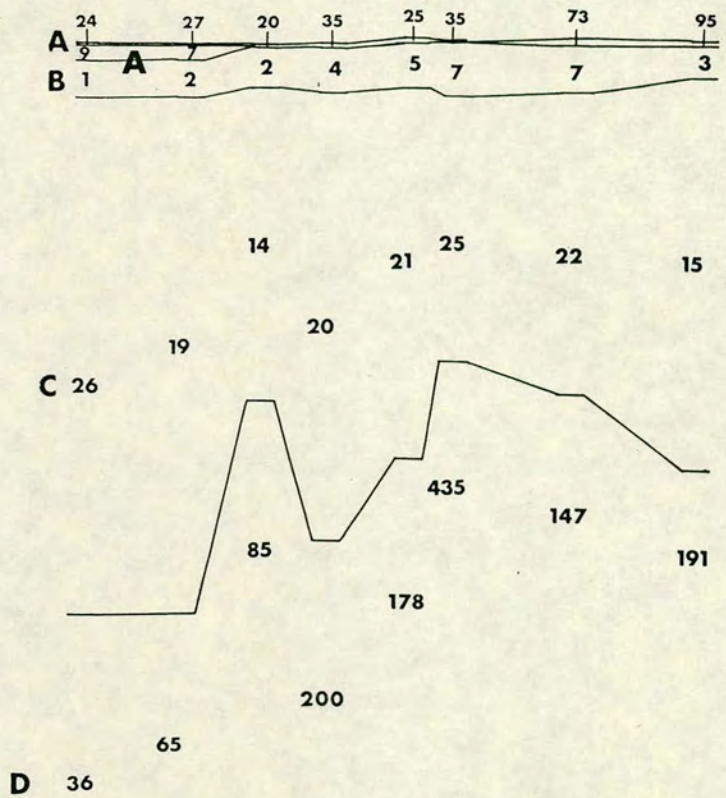

PROFILE 2

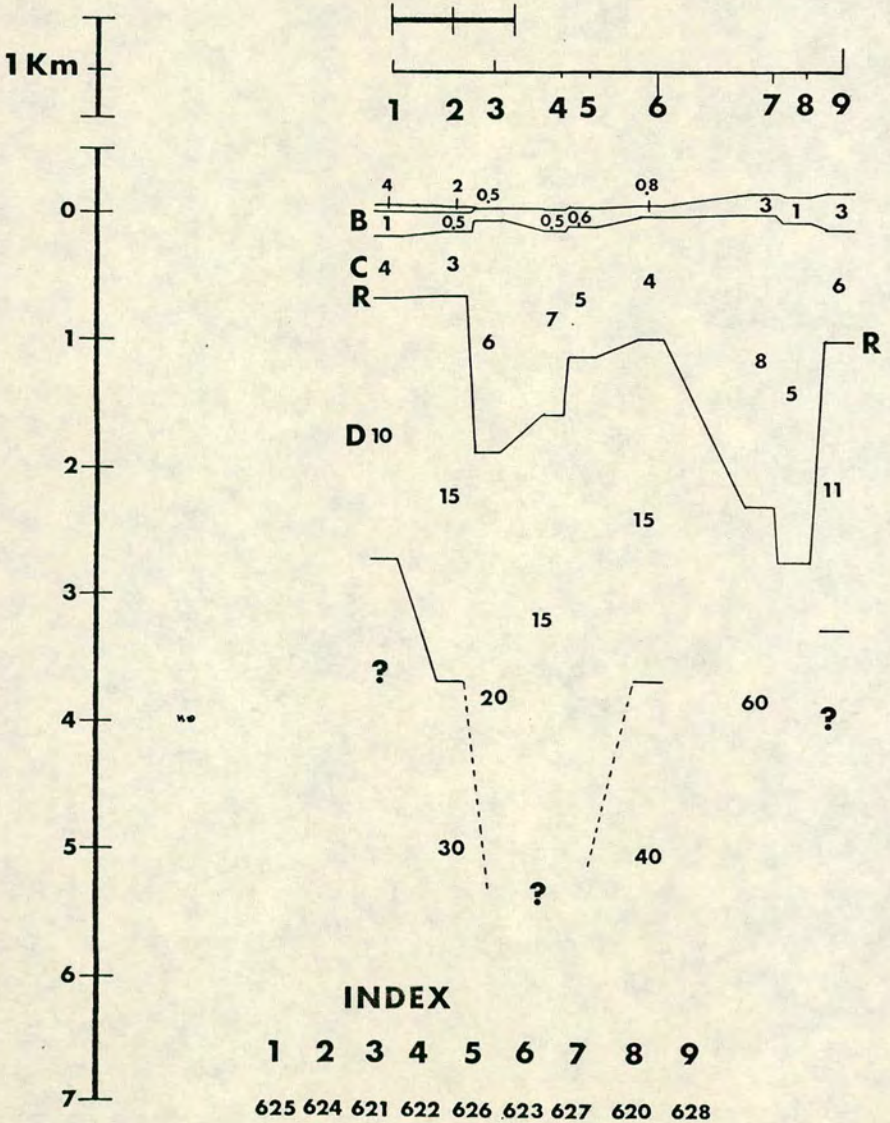

Fig.4.15b

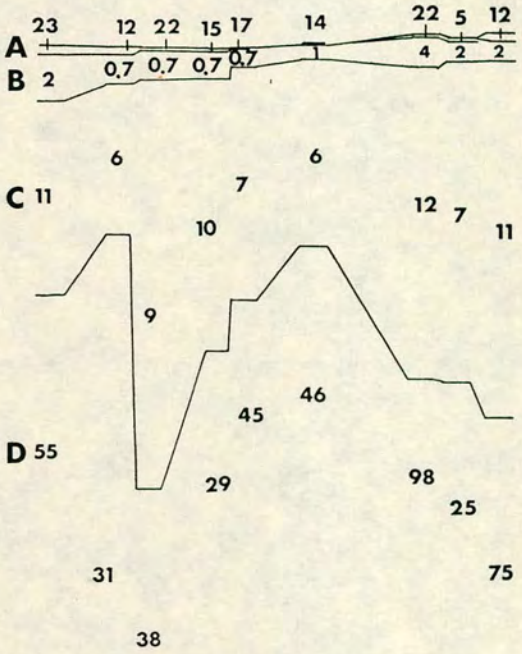

Fig.4.16b

PROFILE 3

Fig.4.15C

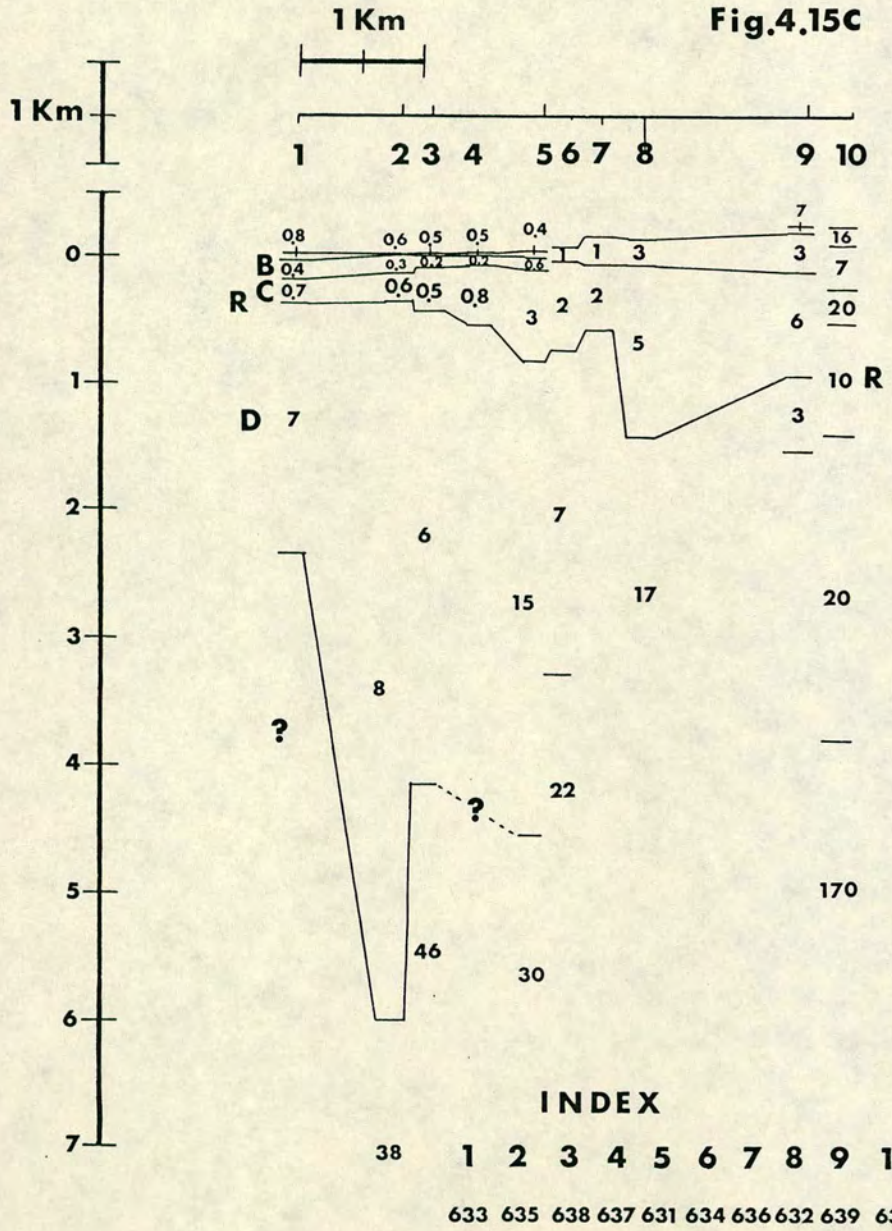

Fig.4.16C

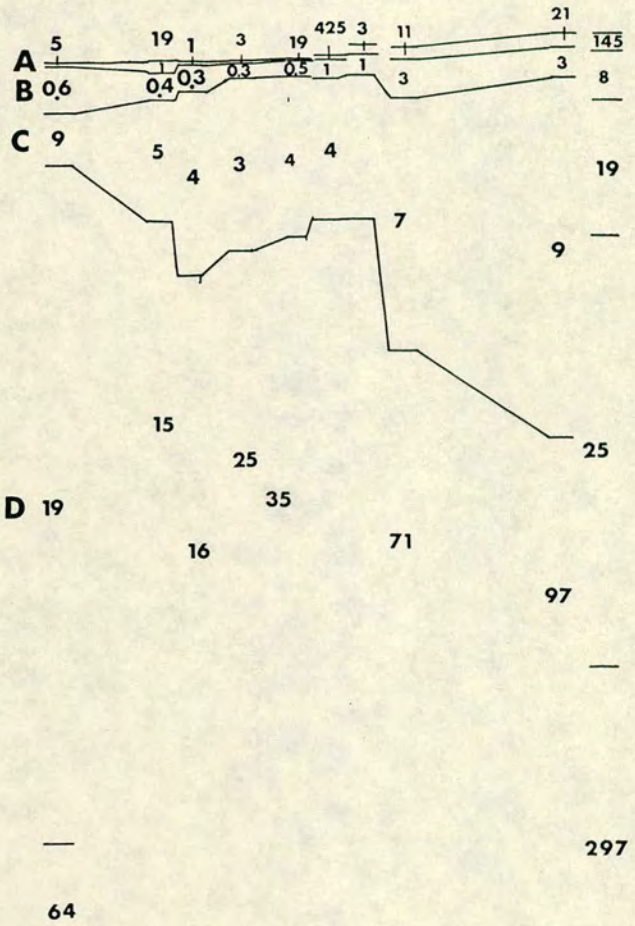

PROFILE 4

Fig.4.15d

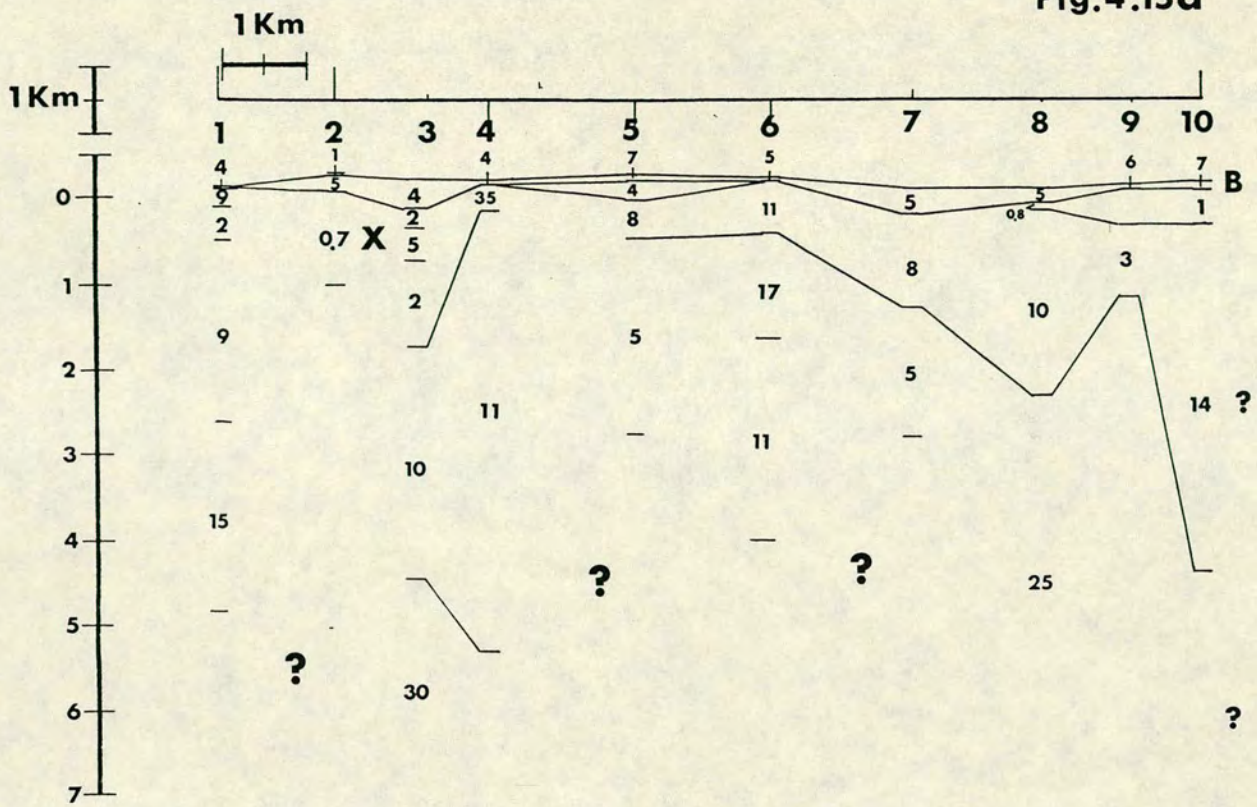

Fig.4.16d

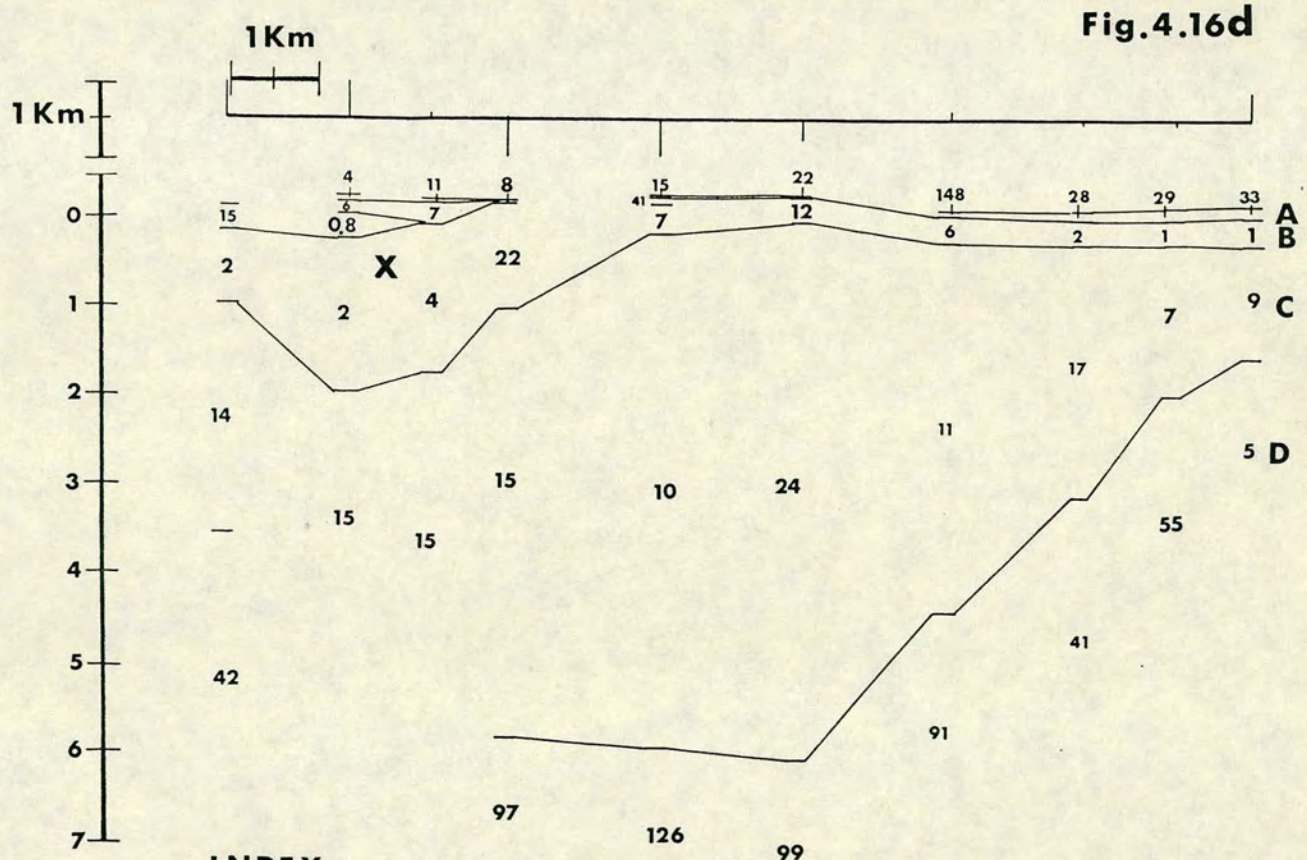

INDEX

1	2	3	4	5	6	7	8	9	10
644	643	642	641	640	648	649	645	647	646

The following summarize the electrical structure of the earth below each of the Profiles 1, 2, 3 and 4 (see Fig.4.1).

(i). The Parker-Whaler D^+ and Dawes methods provide comparable electrical structure for the upper 5 km of the crust below Milos.

(ii). For the majority of the magnetotelluric stations the one dimensional models consist of 4 layers marked as layers A, B, C and D in Figs.4.15a-d and 4.16a-d respectively.

(iii). In general layers A, B, C and D represent the depth ranges of 0-0.05, 0.05-0.5, 0.5-4 and > 4 km respectively.

(iv). Information for layer A is based on the Dawes models. This is the uppermost layer which has resistivity of about 25-100 Ohm.m below Profiles 1 and 4 and 1-25 Ohm.m below Profiles 2 and 3 respectively.

(v). Layer B is generally the most conductive below Milos with resistivity 2-12 Ohm.m below Profiles 1 and 4 and 0.2-5 Ohm.m below Profiles 2 and 3 respectively.

(vi). Layer C has resistivity of 10-20 Ohm.m below Profiles 1 and 4 and 3-10 Ohm.m below Profiles 2 and 3 respectively.

(vii). Most of the models terminate with layer D which has resistivity of 50-100 Ohm.m below profiles 1 and 4 and 15-50 Ohm.m below Profiles 2 and 3 respectively.

(viii). Apart from the main conductive zone (layer B) below Profiles 2 and 3, two smaller zones marked with A and X of about 1-2 Ohm.m are resolved below Profiles 1 and 4 respectively.

(ix). The final conclusion is that the region of Zephyria (Profiles 2 and 3) is generally more conductive than the surrounding regions to the North and West (Profiles 1 and 4).

4.6.(iii). Two dimensional modelling : Basic theory.

Undoubtedly the true electrical structure of the earth is three dimensional. This means that the electrical resistivity of the earth varies with the depth z and along the two horizontal measuring directions x,y i.e $\rho=\rho(x,y,z)$. Geological features with three dimensional signature could be, a magma chamber, a salt diapir at some depth or perhaps a more complex structure due to intense multidirectional faulting. However the three dimensional character of the earth sometimes is not so prominent especially when the dimensions of the three dimensional body are much larger than the surveyed area. The presence of some fault or a dyke with comparable dimensions with the explored region would give a clear two dimensional response. However very often as shown above, one dimensional approximations are considerably effective in modelling structures with weak two or three dimensionality.

For the case of a two dimensional structure, striking along the x axis the electrical resistivity varies along the y axis and with the depth z i.e $\rho=\rho(y,z)$. In this case the time independent Maxwell equations, 2.6, 2.7 reduce to the following six equations :

$$\frac{\partial}{\partial y}H_z - \frac{\partial}{\partial z}H_y = \sigma E_x \qquad (4.38)$$

$$\frac{\partial}{\partial z}H_x = \sigma E_y \qquad (4.39)$$

$$-\frac{\partial}{\partial y}H_x = \sigma E_z \qquad (4.40)$$

$$\frac{\partial}{\partial y}E_z - \frac{\partial}{\partial z}E_y = -i\omega\mu H_x \qquad (4.41)$$

$$\frac{\partial}{\partial z}E_x = -i\omega\mu H_y \qquad (4.42)$$

$$\frac{\partial}{\partial y}E_x = i\omega\mu H_z \qquad (4.43)$$

Equations 4.38, 4.42, 4.43 and 4.39, 4.40, 4.41 describe two distinct modes known as Transverse Electric (TE) or E-Polarization when the electric field is parallel to the strike direction and Transverse Magnetic (TM) or H-Polarization when the magnetic field is parallel to the strike direction (Schmucker and Weidelt, 1975).

Elimination of H_y and H_z from 4.38, 4.42, 4.43 and E_y, E_z from 4.39, 4.40, 4.41 leads to the time independent diffusion equations for the two dimensional problem :

$$\frac{\partial^2}{\partial y^2}E_x + \frac{\partial^2}{\partial z^2}E_x = i\omega\mu\sigma E_x \qquad (4.44) \quad \textit{TE mode}$$

$$\frac{\partial^2}{\partial y^2}H_x + \frac{\partial^2}{\partial z^2}H_x - \frac{1}{\sigma}\left(\frac{\partial H_x}{\partial y}\frac{\partial \sigma}{\partial y} + \frac{\partial H_x}{\partial z}\frac{\partial \sigma}{\partial z}\right) = i\omega\mu\sigma H_x \qquad (4.45) \quad \textit{TM mode}$$

The TE mode has no vertical electric field and any two dimensional inducing magnetic field is allowed. The TM mode has no vertical magnetic field and admits only a quasi-uniform inducing magnetic field.

In general 4.44 and 4.45 can not be solved analytically because of the difficulties encountered in applying boundary conditions to their general solution. Numerical solutions subject to boundary conditions are obtainable through mathematical procedures such as,

(a) finite difference (Jones and Price, 1970 ; Jones and Pascoe, 1971 ; Brewitt-Taylor and Weaver, 1976 ; Weaver and Brewitt-Taylor, 1978), (b) finite element (Oristaglio and Worthington, 1980 ; Wannnamaker et al., 1985 ; 1986), (c) transmission line analogy (Madden and Thompson, 1965 ; Swift, 1971) and (d) integral equation methods (Weidelt, 1975a).

A two dimensional model is usually obtained either through forward modelling procedures or direct inversion of the observed data. The former require a starting model which is then improved iteratively by minimizing the differences between the model and observed responses. Iterations are performed either automatically or manually. True inversion procedures do not require any a priori information and the model is the result of direct calculations.

In the present study the two dimensional computations were carried out by using a computer program written by Brewitt-Taylor, based on the finite difference method developed by Brewitt-Taylor and Weaver (1976). Major alterations were made to the program at a later stage by Hill (1987) to reduce the computer time to one fifth of its original value. The underlying theory of the method is described in detail by Brewitt-Taylor and Weaver (1976) and will not be reproduced in this study but rather the most essential features of the modelling procedures will be described.

4.6.(iv). Two dimensional Modelling : Model construction.

The Brewitt-Taylor and Weaver (1976) method is a forward modelling technique which requires a starting model and allows the researcher to incorporate any available a priori information in order to obtain the ultimate model which will be consistent with the observed magnetotelluric data and any of the known geophysical or geological data. Two dimensional model construction is a difficult exercise. The approach selected in this study was to test a range of models which could provide magnetotelluric responses similar to the observed ones and finally to choose the best one.

In section 4.4 the principal directions were found to be 20°W and 70°E respectively. The former was found to be the dominant direction of the major axis of the impedance ellipses within the more conductive region of Zephyria graben. Therefore this direction was adopted as the main electrical strike. The two dimensional modelling was carried out along profile SS' (Fig.4.1, page 89) which was chosen to be perpendicular to the electrical strike. All the magnetotelluric data along the Profile SS' were rotated to this direction. The one dimensional sections along profile 3 were used as a reference point to the starting model.

The region to be modelled was divided by a number of horizontal and vertical lines into a mesh of rectangular cells of variable sizes. The intersections of the horizontal and vertical lines form the nodes of the grid. The one dimensional resistivity distribution under profile SS' was used to determine the grid size. Zephyria as shown is generally conductive for the first 5-7 km. Therefore in

order to succeed with the two dimensional computations a large number of grid points was required. A grid of 50x50 points was finally used. Conductivity values are allocated by the method, to the centres of the cells, providing a smooth conductivity variation with position. By using central difference formulae, the finite difference representation of the diffusion equations 4.44, 4.45 is obtained for a smoothly varying conductivity function such that, its value at every grid point is given by a weighted mean of the assigned values at the four adjacent cells (Brewitt-Taylor and Weaver, 1976).

Devlin (1984) and Meju (1988) summarized the applied boundary conditions for the modified Brewitt-Taylor and Weaver program (Hill, 1987) as following :

(i). The conductivity is a function only of depth at infinitely large horizontal distances.

(ii). In both the modes (T.E and T.M) a constant magnetic field is assumed above the air-earth interface.

(iii). In the T.E mode a zero field value is assigned to each node at the lower boundary. The one dimensional finite difference problem is solved and field values are assigned to the nodes on the side boundaries.

(iv). At internal boundaries : The tangential components of both the fields and the normal components of the magnetic field must be continuous.

Application of the displayed boundary conditions, enables a finite difference expression for the interior points of the grid for both the TE and TM modes. In the TE mode when a solution is obtained

for the electric field, the magnetic field can be computed by use of 4.42 and 4.43. In the TM mode when 4.41 is solved for the magnetic field, equations 4.39 and 4.40 provide solutions for the electric field.

A very important matter is the grid design. There is little discussion in the literature on this subject. However there are some general rules (Wannamaker et al., 1985 ; Hill, 1987 ; Meju, 1988) for the correct distribution of the grid nodes, which were followed by the author and are summarized below :

(i). Near a boundary the element dimensions should be about one tenth of a skin depth in the medium where the element resides. At least four elements are necessary on either side of the contrast.

(ii). Far away from vertical contrasts (two or three skin depths) the size of the elements must be about one skin depth of the medium of residence.

(iii). At least three elements in the horizontal and two elements in the vertical direction are needed to define a resistivity subregion.

(iv). The vertical grid spacings can be increased logarithmically with depth since the fields decay exponentially. The same applies above the ground where only few elements are needed because of the long wavelength of the air.

(v). The grid must be extended many skin depths away at both ends in the y and z directions.

The two dimensional modelling procedures were executed for twenty periods in the range 10^{-2}-10^{+4} secs for each of the two modes, TE and TM respectively. These periods were the following : 0.01, 0.02, 0.03,

0.1, 0.2, 0.5, 1.0, 3.0, 7.0, 10.0, 30.0, 50.0, 70.0, 120.0, 170.0, 350.0, 500.0, 1000.0, 2500.0, 5000.0 secs. Each run consisted of two stages.

At the first stage the starting model was prepared, in terms of blocks of different conductivity in S/m. Computations of the appropriate skin depths and application of the mesh design rules enabled the final construction of the grid. The y and z grid points were in km. At each block apart from a conductivity value, the appropriate values for the vacuum magnetic permeability and permitivity were also assigned. The boundary conditions were finally determined for the number of grid points in use. This information was used by the data preparation program called PREP and it was assembled in a suitable form for the next stage.

At the second stage, the two dimensional forward calculations were performed by the main program called ARITHE. Resistivity and phase values at each of the y grid points on the surface of the earth were provided after each run.

The author developed two computer programs to evaluate (TWODR) and plot (TWODGP) the resistivity and phase responses as a function of frequency for each of the y grid points on the surface of the earth. Where the y grid points were common with observation points the corresponding real field data were also plotted for qualitative comparisons.

4.6.(v). Two dimensional modelling : Results.

The two dimensional forward calculations were repeated for several starting models and the distribution of the grid points was

changed where appropriate. The first starting model, based on the one dimensional section along profile SS' was finally considered inadequate for several reasons.

One of the main disadvantages was the wrong determination of the bottom half space resistivity. A 30 Ohm.m half space was initially used. The fit of the model to the observed responses was substantially improved when a half space with resistivity of 150 Ohm.m was included below the 30 Ohm.m block. Visual inspection of the model and the observed responses at the observation points directed to several other changes in the starting model. Further improvements were achieved, when the resistivity values at a number of blocks were either increased or decreased as required, when some small blocks with adjacent resistivity values were merged in order to simplify the final model. In addition, some resistivity boundaries were located more accurately. A two dimensional model was finally obtained, providing a very good fit to the observed data for both the TE and TM modes.

Figs.4.17a-b illustrate the best fit Model SS'-1 with the model and the observed resistivity and phase responses at five observation points (647, 633, 638, 632, 630) for both the TE and TM modes.

For a more qualitative interpretation the model and observed resistivity and phase responses were contoured two dimensionally along the profile SS' for the period range 10^{-2}-10^{+4} secs. Figs.4.18a-d (pages 142-143) and 4.19a-d (pages 145-146) illustrate these contours for the TE and TM modes respectively. It is interesting that in general the model responses display very similar patterns with the observed ones. It must be noticed that the model and observed TE and

TM resistivities correlate better than the relative phases. The latter can be justified by the fact that phase is not only sensitive to resistivity changes but also to noise (see Figs.4.18d, 4.19d).

Conclusions

Model SS-1' of Figs.4.17a-b provides the following electrical structure :

(i). A resistive layer is dominant at the top 25-50 m. It has a resistivity of 100 Ohm.m outside the Zephyria graben and a minimum resistivity of 10 Ohm.m in the inner part of the graben. Since a linear depth scale is used this thin layer is not illustrated in the same figure.

(ii). The upper 1000 m of the crust have low resistivities of 0.3-7 Ohm.m between 50-1000 m depths. The minimum resistivities (0.3-0.7 Ohm.m) are encountered below Zephyria. The resistivity low is bounded by relatively more resistive blocks of 1.5-6 Ohm.m in the southwest and 3-15 Ohm.m in the northeast.

(iii). Below Zephyria there is a 10 Ohm.m block, about 2-5 km wide and about 6 km thick. This block is surrounded by a relatively more resistive block of 30 Ohm.m.

(iv). At 15 km depth, the model terminates with an even more resistive half space of 150 Ohm.m.

4.6.(vi). Two dimensional modelling : Model validity.

As shown in Figs.4.17a-b and 4.18a-d, 4.19a-d the two dimensional model SS-1' displays a very good fit to the experimental

Fig.4.17. The best fit two dimensional model along Profile SS'. The figures on the model are resistivities in Ohm.m.

a. The best fit model SS'-1 and the model responses in comparison with the field data for the T.E mode.

b. The best fit model SS'-1 and the model responses in comparison with the field data for the T.M mode.

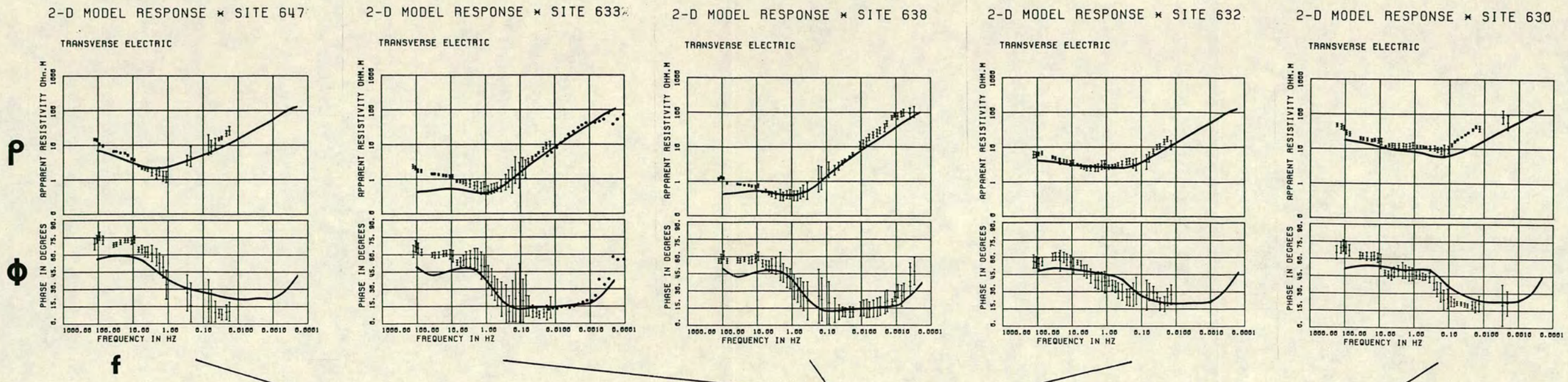
2-D MODEL RESPONSE × SITE 647
2-D MODEL RESPONSE × SITE 633
2-D MODEL RESPONSE × SITE 638
2-D MODEL RESPONSE × SITE 632
2-D MODEL RESPONSE × SITE 630
TRANSVERSE ELECTRIC
APPARENT RESISTIVITY OHM.M
PHASE IN DEGREES
FREQUENCY IN HZ
ρ
Φ
f

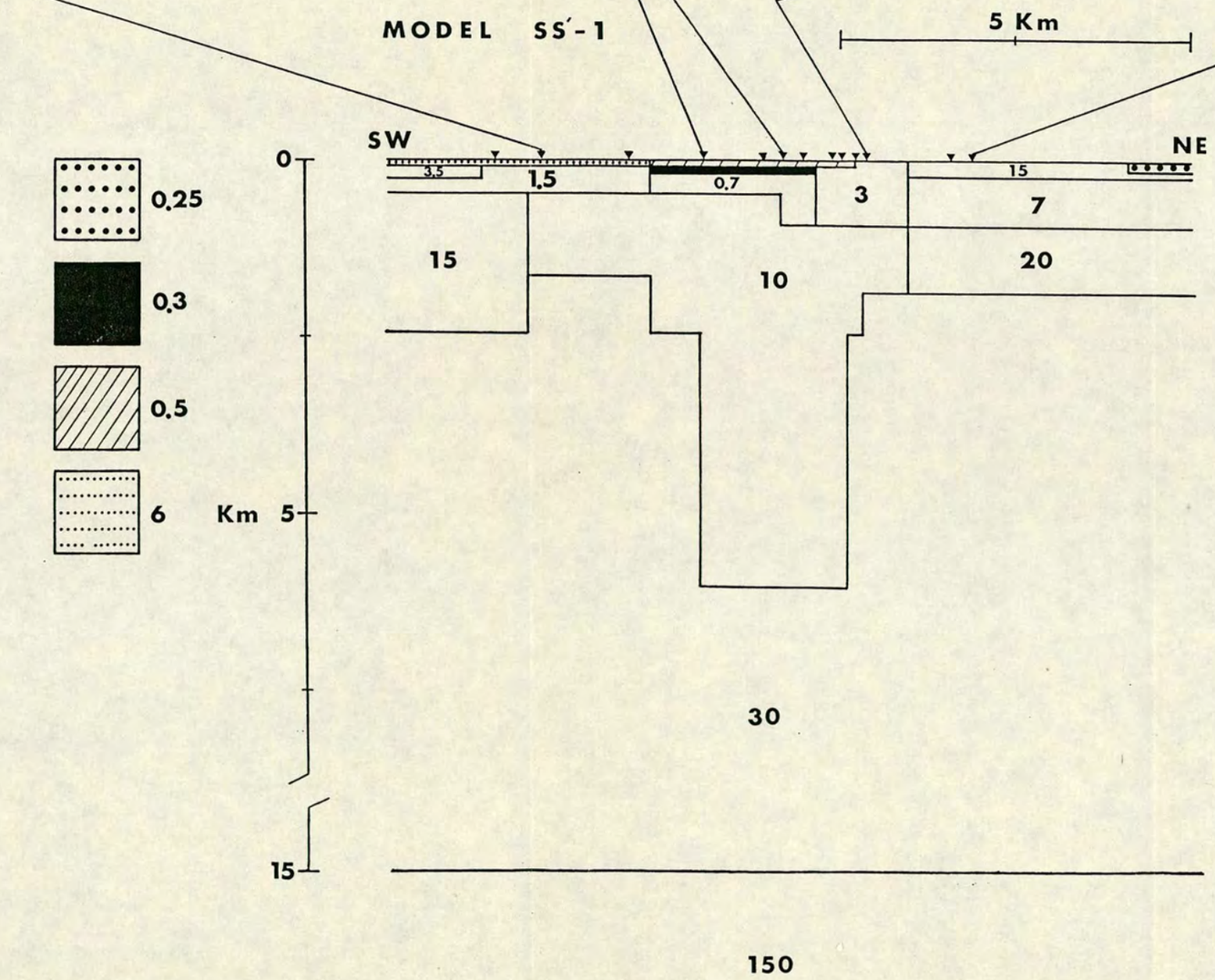
MODEL SS'-1
5 Km
SW
NE
0.25
0.3
0.5
6
Km
0
5
15
3.5
1.5
0.7
3
15
7
15
10
20
30
150

Fig.4.17a

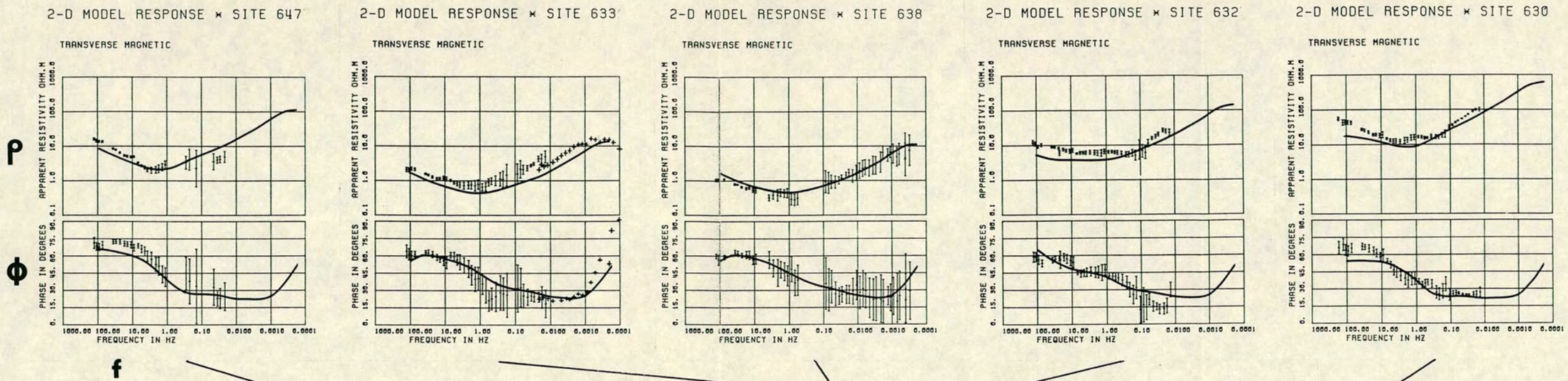
2-D MODEL RESPONSE × SITE 647
2-D MODEL RESPONSE × SITE 633
2-D MODEL RESPONSE × SITE 638
2-D MODEL RESPONSE × SITE 632
2-D MODEL RESPONSE × SITE 630
TRANSVERSE MAGNETIC
APPARENT RESISTIVITY OHM.M
PHASE IN DEGREES
FREQUENCY IN HZ
ρ
Φ
f

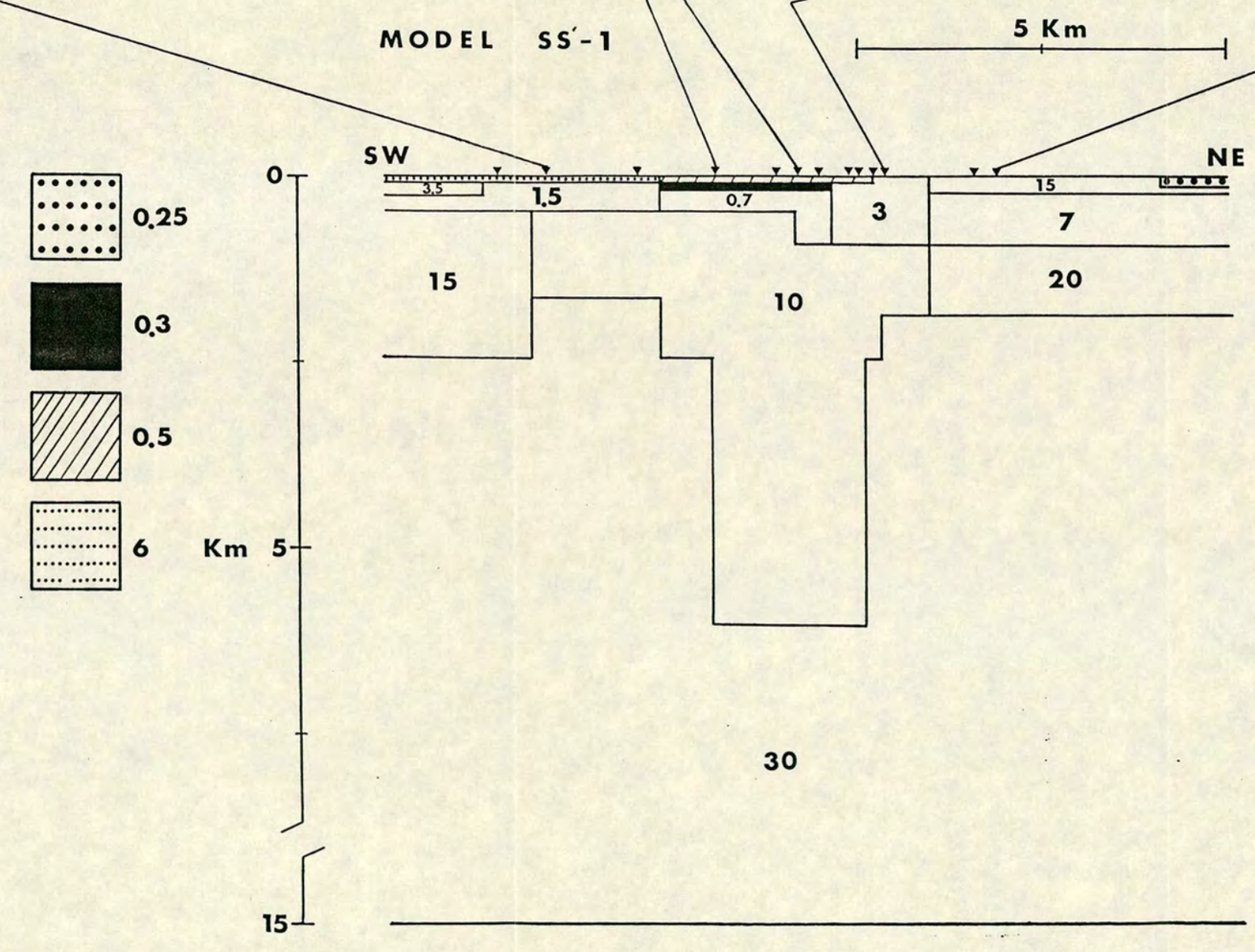
MODEL SS'-1
5 Km
SW
NE
0
0.25
0.3
0.5
6
Km
5
15
3.5
1.5
0.7
3
15
7
15
10
20
30
150

Fig.4.17b

Fig.4.18. Contours of the Model SS'-1 and observed magnetotelluric responses for the T.E mode.

a. Contour of the model resistivity.

b. Contour of the observed resistivity.

c. Contour of the model phase.

d. Contour of the observed phase.

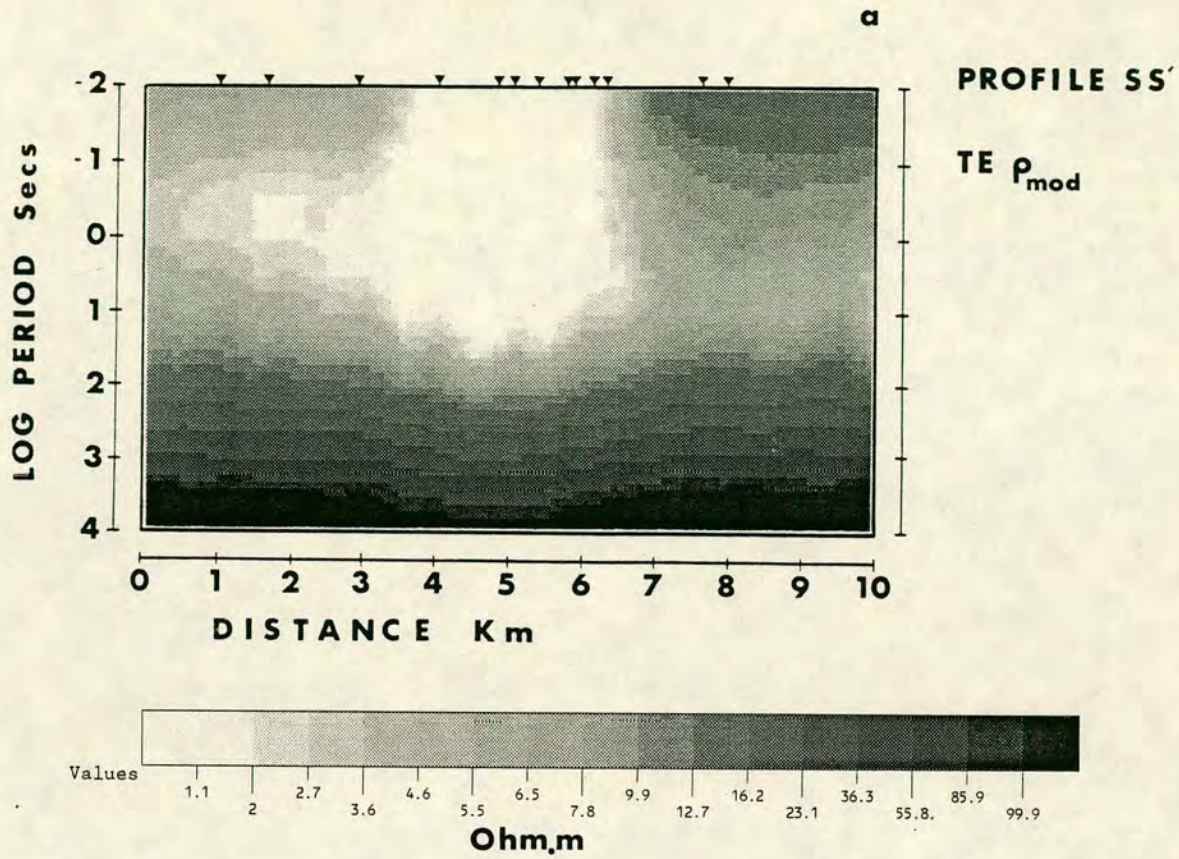
a
PROFILE SS'
TE ρ_{mod}
LOG PERIOD Secs
-2
-1
0
1
2
3
4
0 1 2 3 4 5 6 7 8 9 10
DISTANCE Km
Values
1.1 2 2.7 3.6 4.6 5.5 6.5 7.8 9.9 12.7 16.2 23.1 36.3 55.8 85.9 99.9
Ohm.m

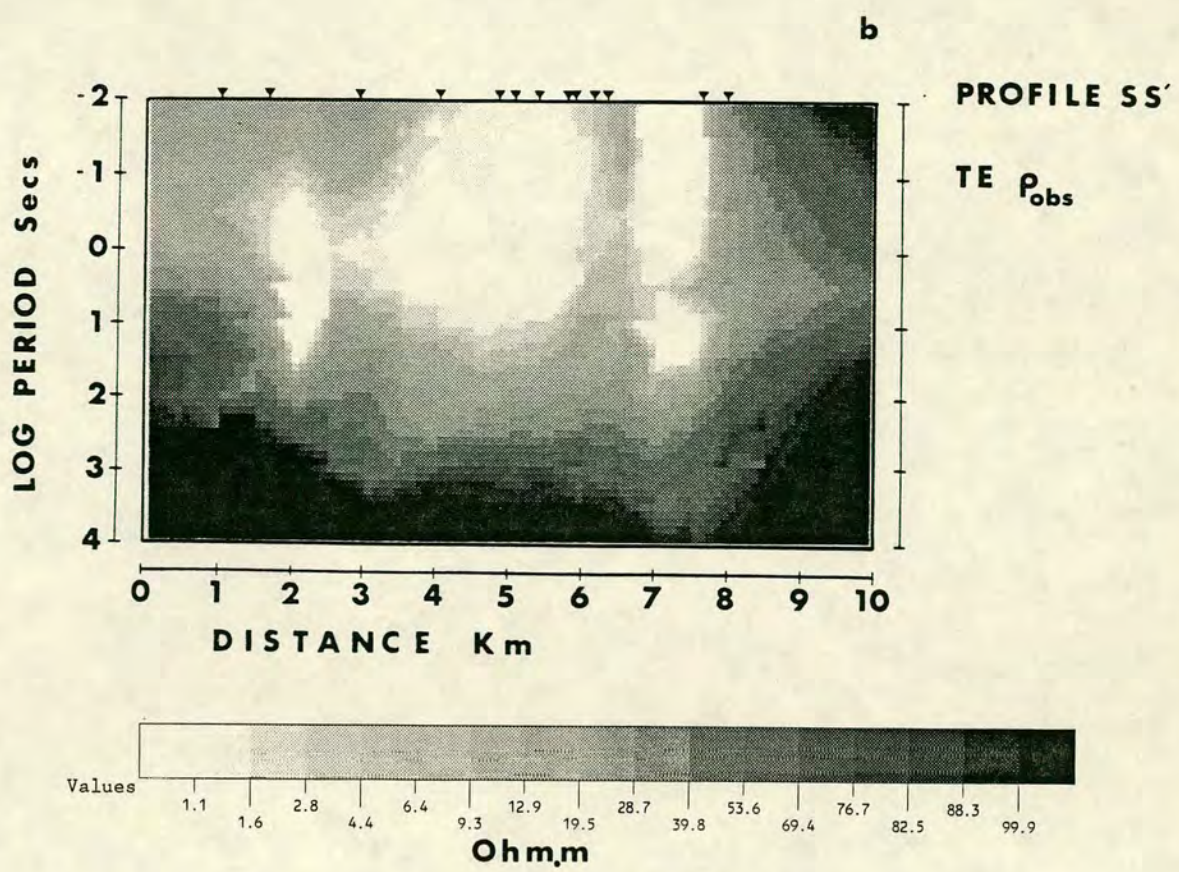
b
PROFILE SS'
TE ρ_{obs}
LOG PERIOD Secs
-2
-1
0
1
2
3
4
0 1 2 3 4 5 6 7 8 9 10
DISTANCE Km
Values
1.1 1.6 2.8 4.4 6.4 9.3 12.9 19.5 28.7 39.8 53.6 69.4 76.7 82.5 88.3 99.9
Ohm.m

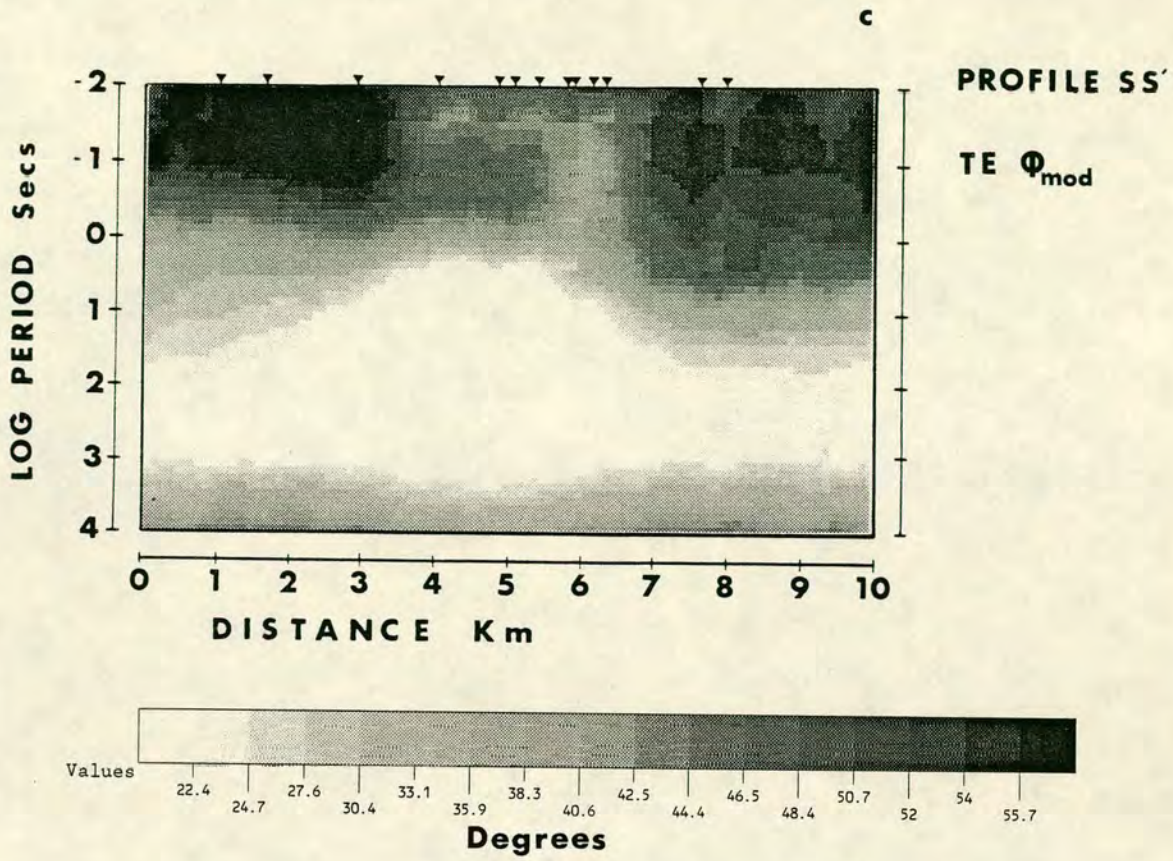
c
PROFILE SS'
TE Φ_{mod}
LOG PERIOD Secs
-2
-1
0
1
2
3
4
0 1 2 3 4 5 6 7 8 9 10
DISTANCE Km
Values
22.4 24.7 27.6 30.4 33.1 35.9 38.3 40.6 42.5 44.4 46.5 48.4 50.7 52 54 55.7
Degrees

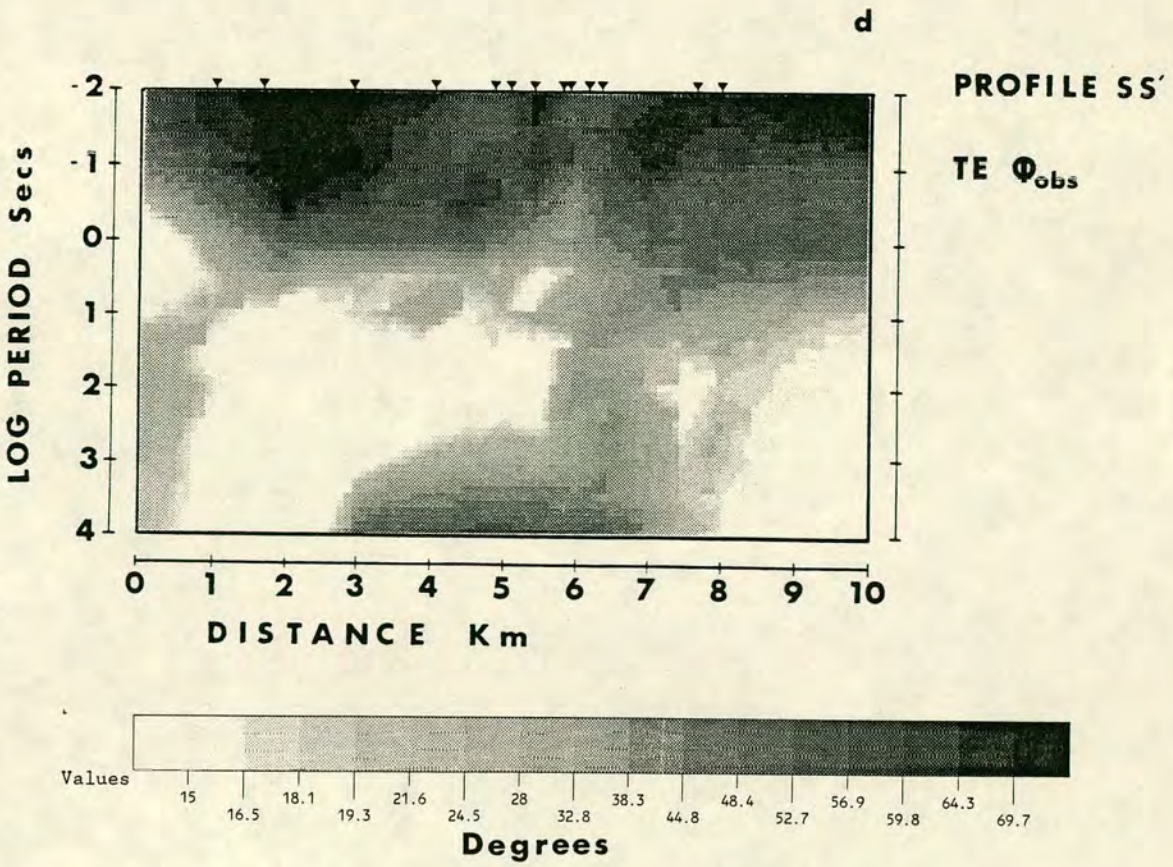
d
PROFILE SS'
TE Φ_{obs}
LOG PERIOD Secs
-2
-1
0
1
2
3
4
0 1 2 3 4 5 6 7 8 9 10
DISTANCE Km
Values
15 16.5 18.1 19.3 21.6 24.5 28 32.8 38.3 44.8 48.4 52.7 56.9 59.8 64.3 69.7
Degrees

Fig.4.19. Contours of the Model SS'-1 and observed magnetotelluric responses for the T.M mode.

a. Contour of the model resistivity.

b. Contour of the observed resistivity.

c. Contour of the model phase.

d. Contour of the observed phase.

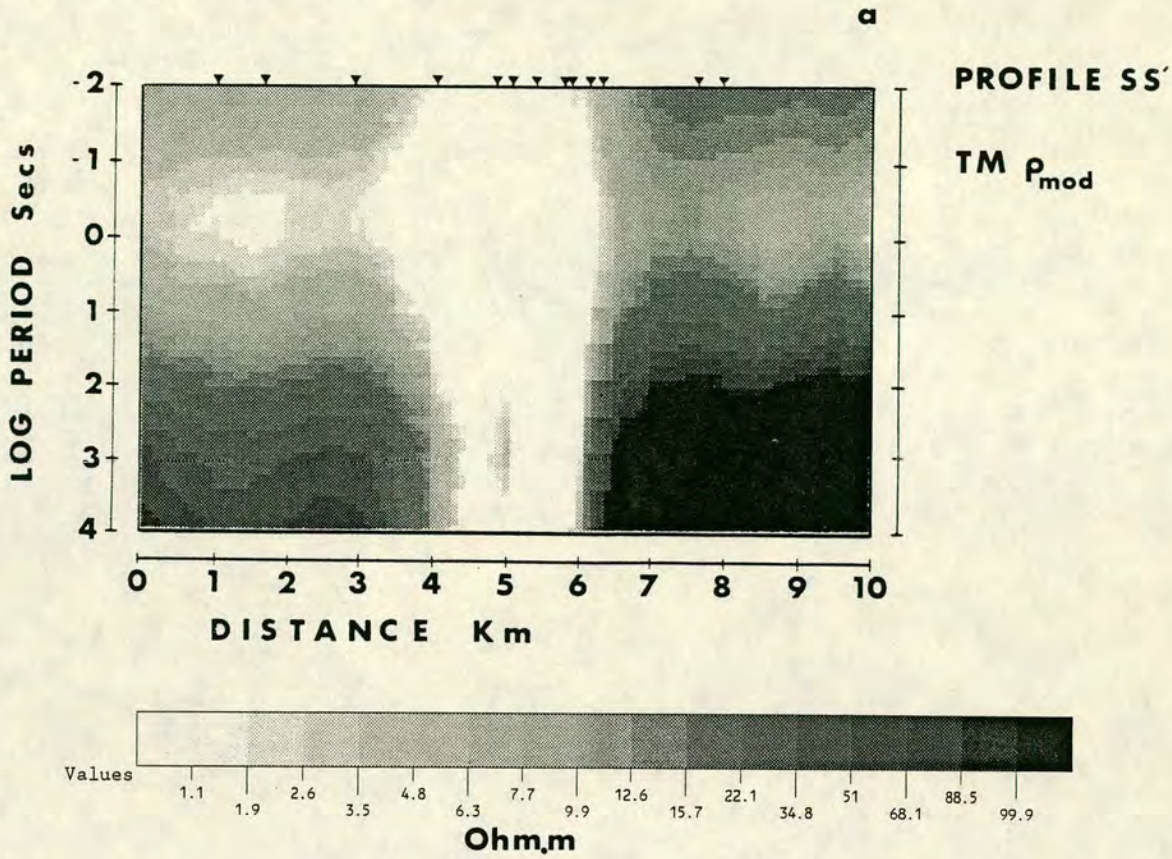
a
PROFILE SS'
TM ρ_{mod}
LOG PERIOD Secs
-2
-1
0
1
2
3
4
0 1 2 3 4 5 6 7 8 9 10
DISTANCE Km
Values
1.1 1.9 2.6 3.5 4.8 6.3 7.7 9.9 12.6 15.7 22.1 34.8 51 68.1 88.5 99.9
Ohm.m

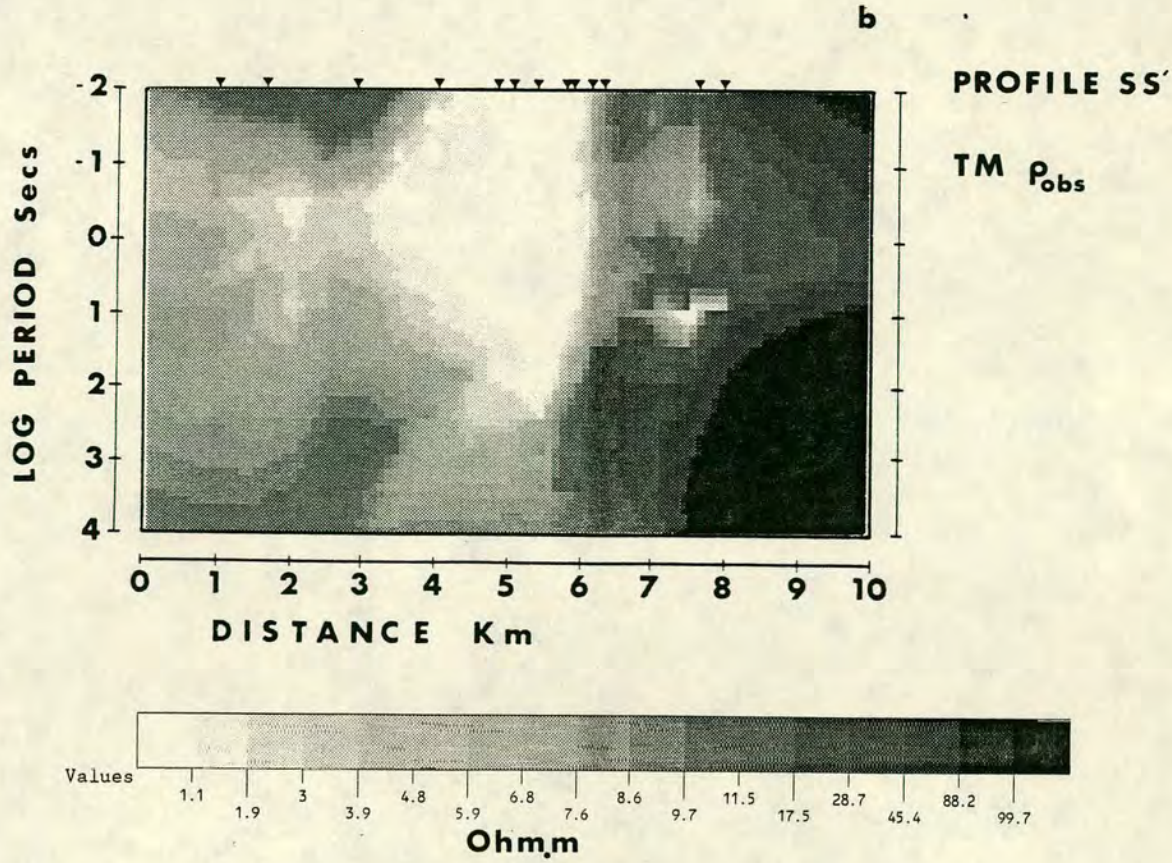
b
PROFILE SS'
TM ρ_{obs}
LOG PERIOD Secs
-2
-1
0
1
2
3
4
0 1 2 3 4 5 6 7 8 9 10
DISTANCE Km
Values
1.1 1.9 3 3.9 4.8 5.9 6.8 7.6 8.6 9.7 11.5 17.5 28.7 45.4 88.2 99.7
Ohm.m

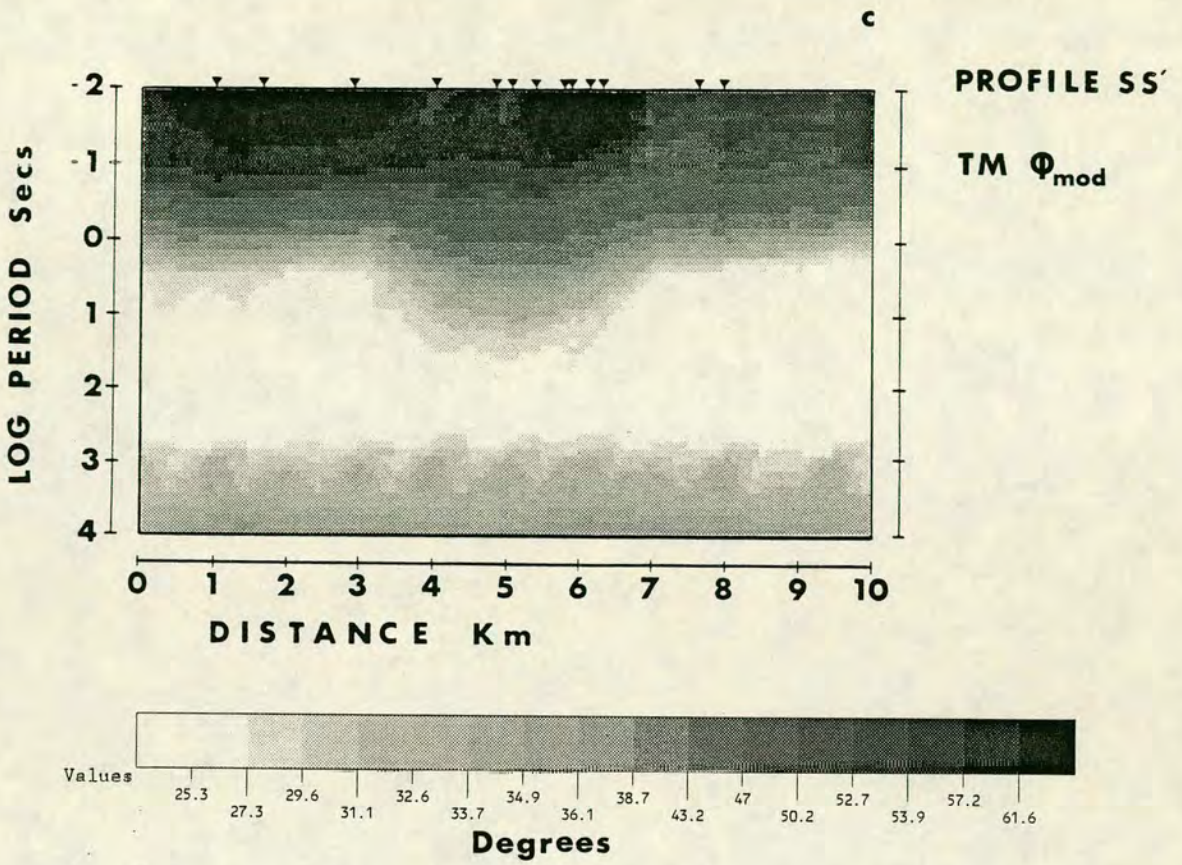
c
PROFILE SS'
TM Φ_{mod}
LOG PERIOD Secs
-2
-1
0
1
2
3
4
0 1 2 3 4 5 6 7 8 9 10
DISTANCE Km
Values
25.3 27.3 29.6 31.1 32.6 33.7 34.9 36.1 38.7 43.2 47 50.2 52.7 53.9 57.2 61.6
Degrees

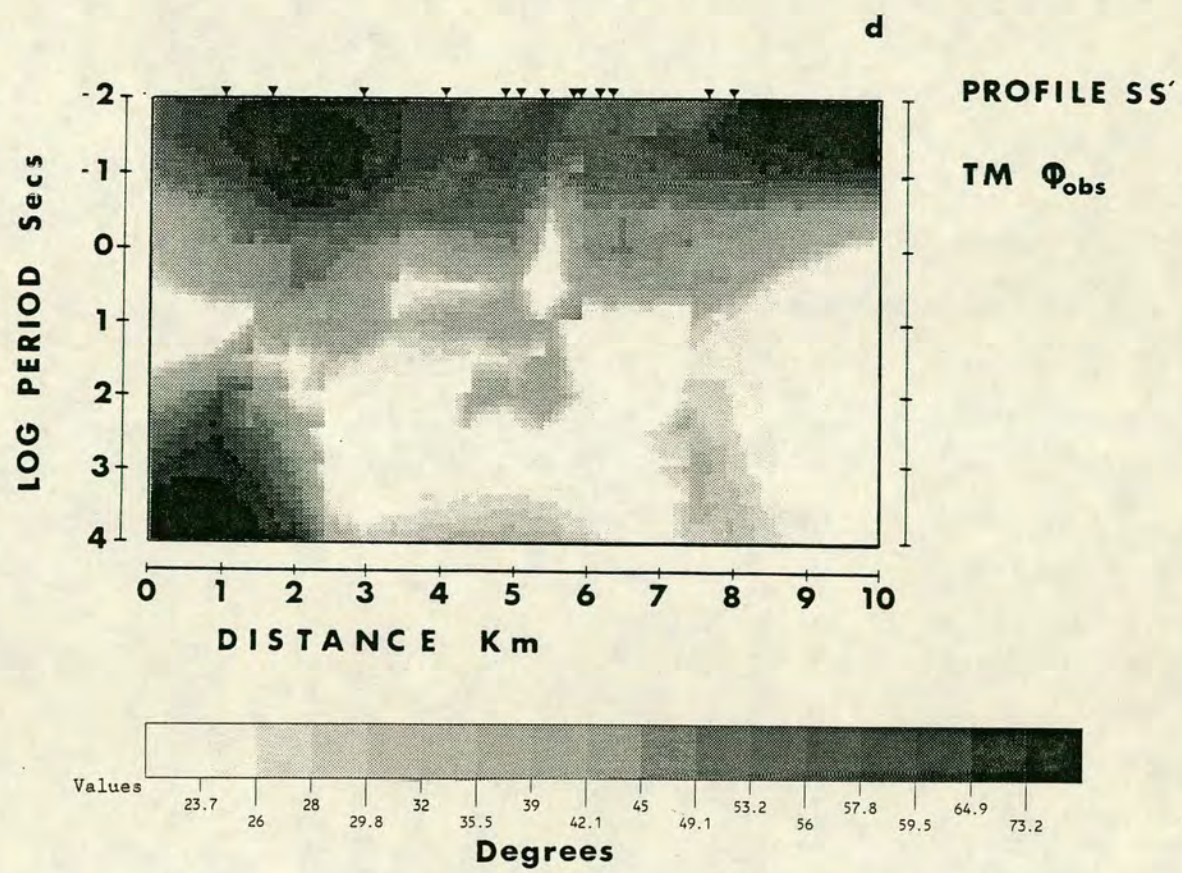
d
PROFILE SS'
TM Φ_{obs}
LOG PERIOD Secs
-2
-1
0
1
2
3
4
0 1 2 3 4 5 6 7 8 9 10
DISTANCE Km
Values
23.7 26 28 29.8 32 35.5 39 42.1 45 49.1 53.2 56 57.8 59.5 64.9 73.2
Degrees

magnetotelluric responses. The importance of the presence of several features on this model was tested by altering some of the model parameters. Two tests were carried out and the new model responses were compared with the observed ones and those corresponding to Model SS'-1. The following conclusions were extracted :

(i). The existence of a 150 Ohm.m half space located at 15 km depth seems to be one possible way to obtain a model with a good fit to the experimental data (Figs.4.17a-b, Model SS'-1). To demonstrate the above the 150 Ohm.m half space was removed and the new model was left to terminate with a 30 Ohm.m half space (Fig.4.20, Model SS'-2). The resistivity and phase responses of Model SS'-2 are compared with those of Model SS'-1 and the observed ones in Figs.4.22a-b and Figs.4.23a-b (page 150) for the site locations 638 and 631 respectively. The responses of Models SS'-1 and 2 are represented with thick and thin solid lines respectively. There is an obvious mismatch between the Model SS'-2 responses and the actual field data.

(ii). A very low resistivity value of 1 Ohm.m was assigned between 2.5-6 km depths to test the possible existence of such a conductive cube beneath the Zephyria graben (Fig.4.21, Model SS'-3). The new model responses are illustrated in Figs.4.22a-b and Figs.4.23a-b in comparison with the field data and the responses of Models SS'-1 and 2 at the same sites 638, 631. At both sites there is again a mismatch between the observed responses and the calculated ones of Model SS'-3.

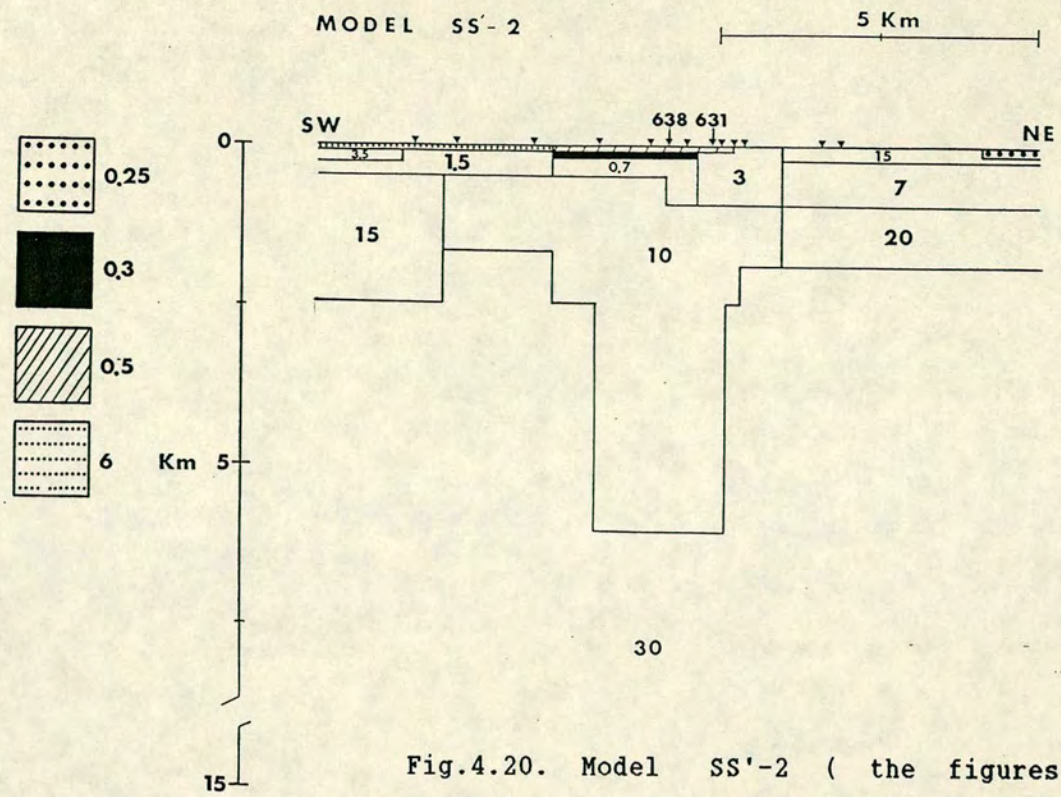

Fig.4.20. Model SS'-2 (the figures on the model are resistivities in Ohm.m).

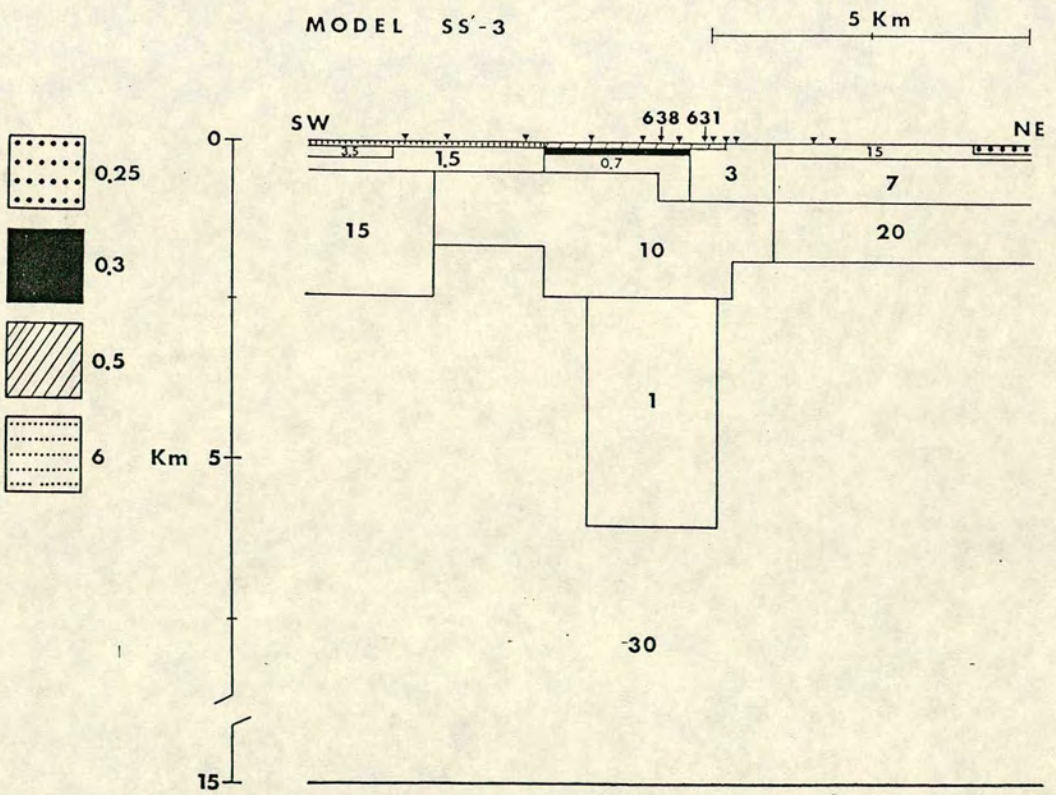

Fig.4.21. Model SS'-3 (the figures on the model are resistivities in Ohm.m).

150

Fig.4.22. Computed resistivity and phase responses for models SS'-1, -2, -3 in comparison with the field data for site 638.

a. T.E mode.

b. T.M mode.

Fig.4.23. Computed resistivity and phase responses for models SS'-1, -2, -3 in comparison with the field data for site 631.

a. T.E mode.

b. T.M mode.

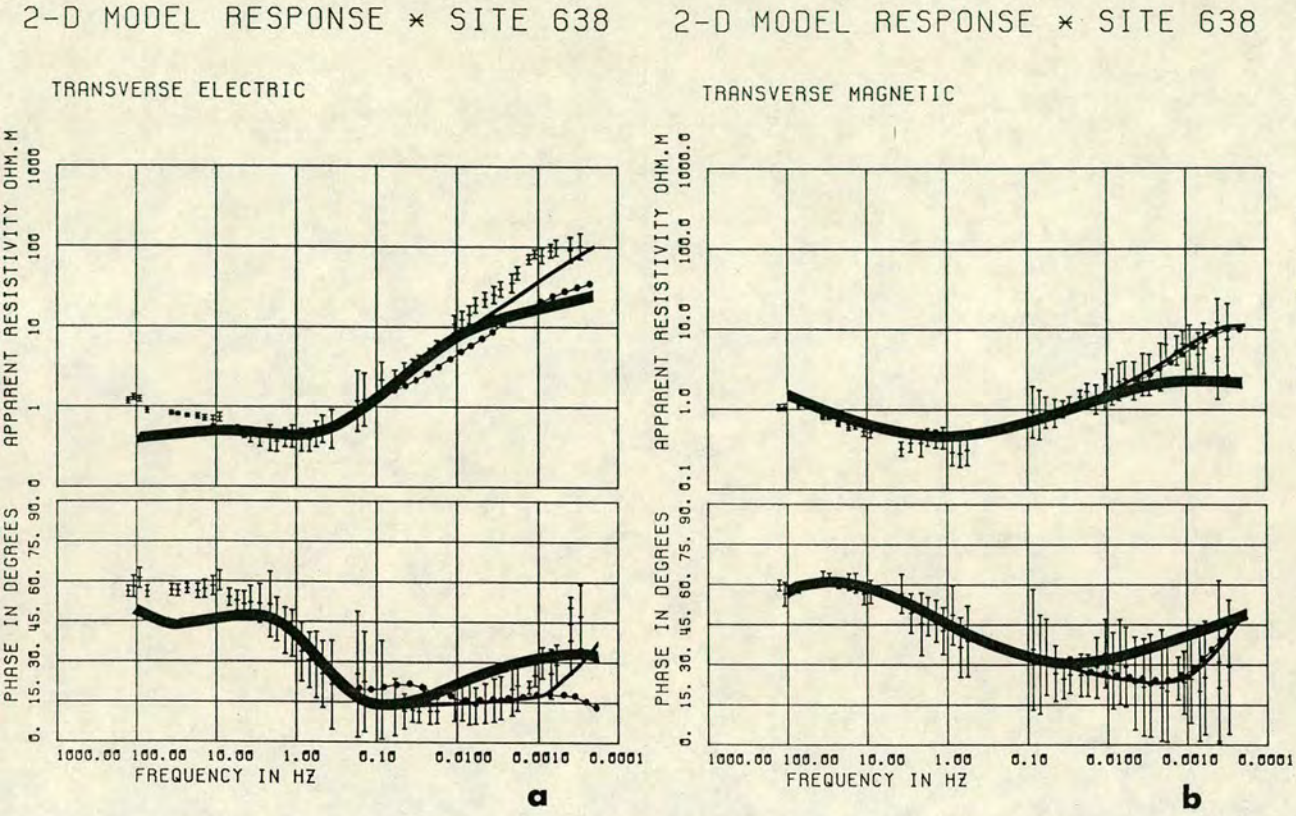

Fig.4.22

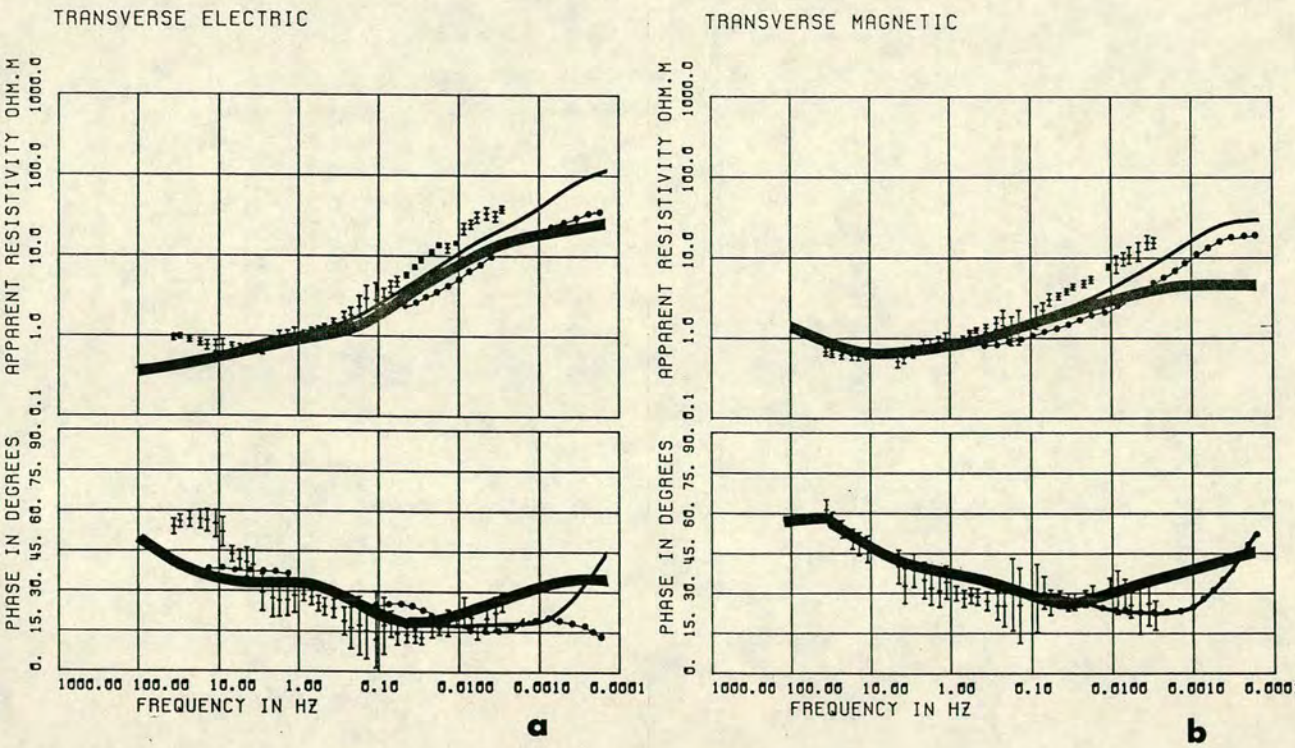

Fig.4.23

4.7. Three dimensional modelling.

Many times the magnetotelluric problem is three dimensional. In a three dimensional structure the electrical conductivity σ is a function of all coordinates x, y and z i.e. $\sigma=\sigma(x,y,z)$.

Analytical solutions to Maxwell's equations in three dimensions are difficult. The most succesful methods of solution include the finite difference methods (e.g. Jones and Pascoe, 1972 ; Jones and Vozoff, 1978), the integral equation methods (e.g. Raiche, 1974 ; Weidelt, 1975b ; Ting and Hohmann, 1981 ; Wannamaker et al., 1984), thin sheet approximations (e.g. Vasseur and Weidelt, 1977 ; Dawson and Weaver, 1979 ; Ranganayaki and Madden, 1980 ; Madden, 1980 ; Madden and Park, 1982 ; Park et al., 1983 ; Park, 1985) and hybrid techniques (e.g. Lee et al., 1981). Analogue scale modelling experiments have also been used to study three dimensional structures (e.g. Rankin et al., 1965 ; Dosso, 1966 ; 1973 ; Dosso et al., 1980). In the present work there were no three dimensional computations.

CHAPTER 5

THE MILOS CASE STUDY : DISCUSSION AND INTERPRETATION OF THE MAGNETOTELLURIC RESULTS.

5.1. Introduction.

Following the data analysis and modelling described in chapter 4 the magnetotelluric results were interpreted considering all available geological and geophysical data.

In particular the azimuths of the major axis of the impedance ellipses and the Parkinson arrows are shown to provide new information for the dominant regional and local tectonic strikes which could account for the volcanism and high thermal anomaly of the island. The final electrical model is a combination of the one and two dimensional magnetotelluric models. It correlates well with the results of other geophysical methods and provides new information for the uppermost 20 km of the crust below Milos.

5.2. Interpretation of the major and minor apparent resistivity and phase responses.

The magnetotelluric sites on Milos were clustered according to their major and minor apparent resistivity and phase responses into six clusters. It was noticed that each of these clusters is characteristic for some particular area of the island. These clusters are enclosed in solid lines on the maps of Figs.5.1a-b (pages 155-156). For convenience each cluster is named with letters or a

combination of a letter and a number.

The western part of Milos is represented by two groups, X and PI (Fig.5.1a). At the central part of eastern Milos there are two major groups Z1, Z2 (Fig.5.1b). Two other smaller clusters, A and FI are observed in the northern and southern Milos respectively (Fig.5.1a).

In both figures the solid lines on the Milos map demonstrate the major structural zones which were considered important for the understanding of the observed patterns. The major and minor responses in each of the presented examples are illustrated with thick and thin solid lines respectively.

Group Z1 is located in the main thermal anomaly of Milos, the Zephyria graben. Group Z2 consists of the majority of stations lying outside this graben. The magnetotelluric data look anisotropic at site locations 633, 638, 632, 621.

The resistive block of the mountain Profitis Ilias, PI is represented by station 641.

The remaining three families A, FI, X are very important because they represent three other conductive zones. Group A is near Adamas. The curves at sites 617, 612 show that a conductor is resolved at about 5-1 Hz. Between 617 and 612 two faults cross each other in almost perpendicular directions and could be responsible for the observed pattern.

Similar conductors are observed in the southern group FI and the northwestern group X. As in Adamas region, a pair of perpendicular faults is present near site 642 and is possibly responsible for the presence of the observed conductor at 0.1 Hz. Some results from one dimensional modelling indicate (see Appendix I, Hutton et al.,

Fig.5.1. Representative sites from the magnetotelluric survey on Milos island. Sites are clustered according to similar responses and one or more representative sites are shown for each cluster. Clusters are enclosed in solid lines and are named with letters or a letter and a number on map. The major (thick solid lines) and minor (thin solid lines) apparent resistivities and phases are plotted. Major faults are represented with thick black lines.

a. Northern (A), southern (FI) and western (X, PI) parts of Milos.

b. Eastern part of Milos (Z1, Z2).

Fig.5.1a

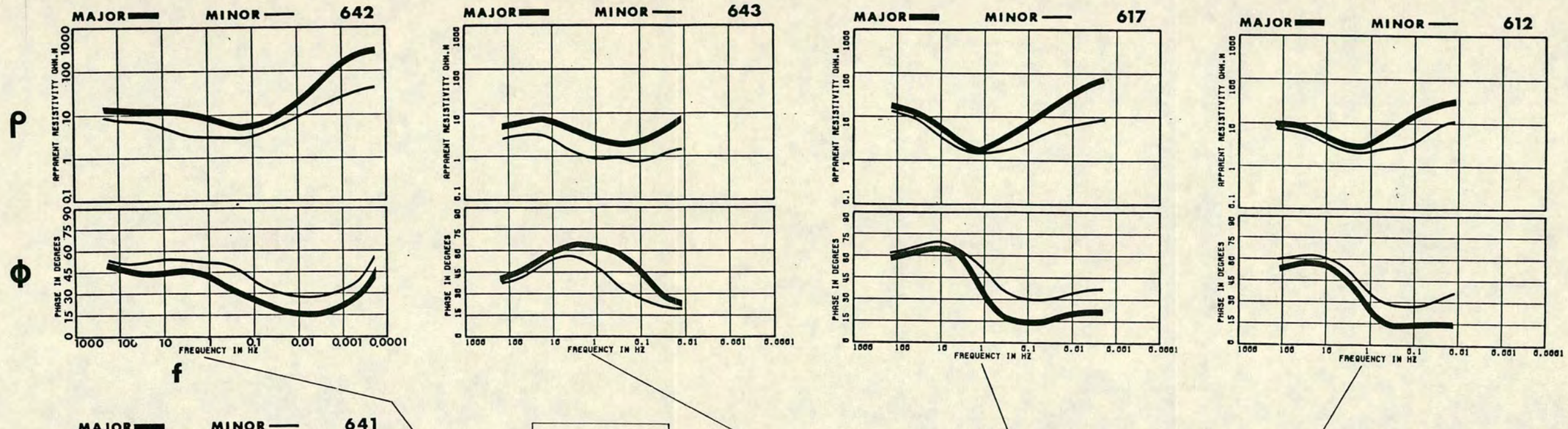
MAJOR
MINOR
642
643
617
612
641
646
APPARENT RESISTIVITY OHM.M
PHASE IN DEGREES
FREQUENCY IN HZ
ρ
Φ
f
▲ AMT
● AMT-LMT
■ LMT
MILOS
A
X
PI
FI
1km

Fig.5.1b

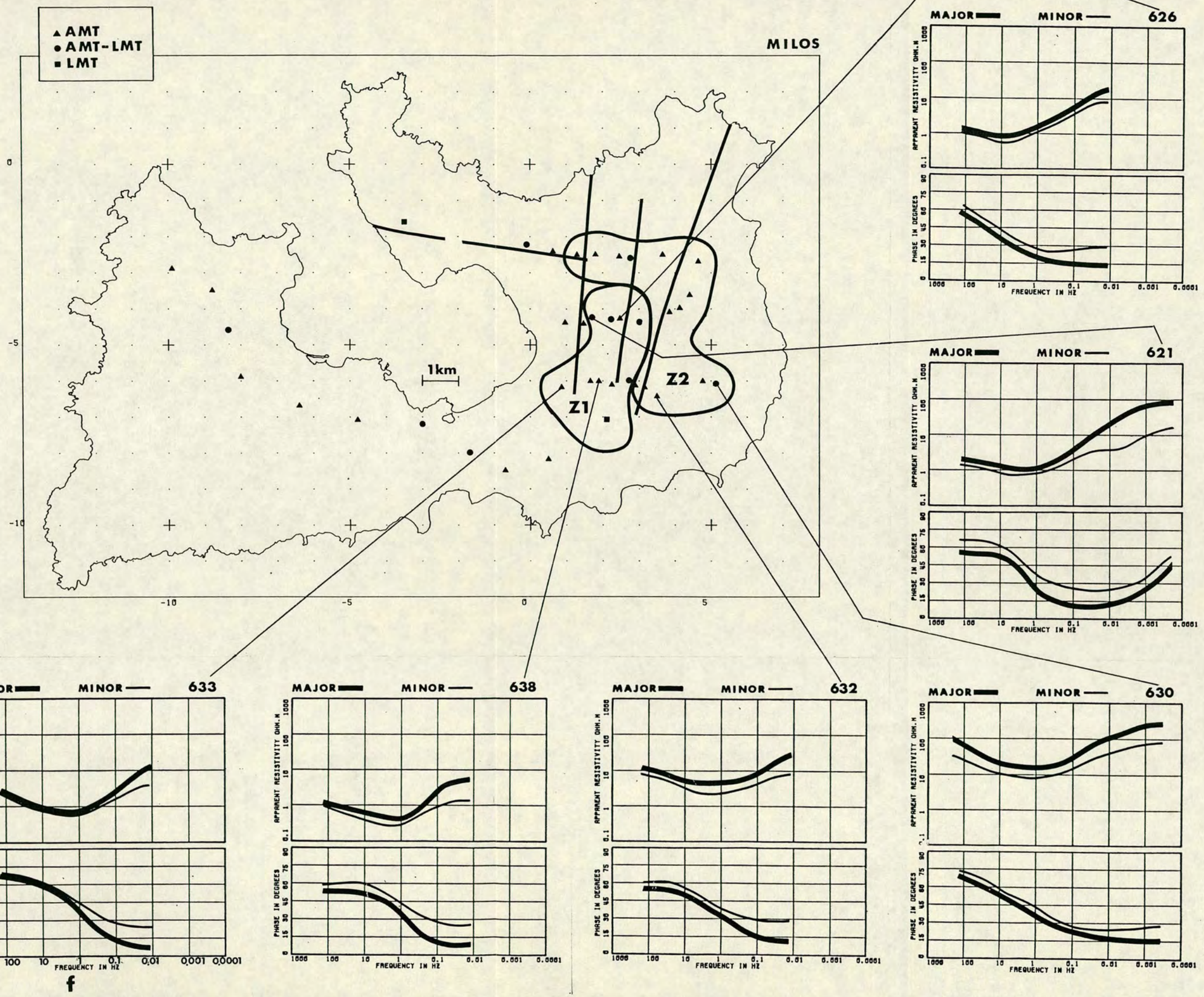
▲ AMT
● AMT-LMT
■ LMT
MILOS
1km
Z1
Z2
-10
-5
0
5
MAJOR
MINOR
626
621
633
638
632
630
APPARENT RESISTIVITY OHM.M
PHASE IN DEGREES
FREQUENCY IN HZ
ρ
Φ
f

1989) the presence of a conductor of 3 Ohm.m at 1000 m depth. Fytikas et al. (1989) have interpreted this, with the possible presence of a second smaller geothermal field.

Further discussion on the observed conductors of groups A, FI, X is presented later.

5.3. Interpretation of the Parkinson Induction Arrows.

Real and imaginary Parkinson induction arrows are presented in Figs.5.2a-c for the period ranges 50-500, 500-5000, 5000-10000 secs respectively. The real arrows terminate with an arrow head while the imaginary ones terminate with a line. The magnitudes and the azimuths of both the real and imaginary arrows represent average values over the period ranges indicated above (a scale of 0.1 per division along each arrow is provided for quantitative comparison). There was no danger of biasing, since both the magnitudes and azimuths are consistent within the stated period ranges as shown in Figs.4.6, 4.7. Induction arrows from the study of Haak et al. (1989) are also included in these figures. Only the real part of these arrows is illustrated. Since the imaginary part of the induction arrows is very small, and could not be distinguished from the real ones. The three figures show a clear change in pattern with period increasing.

The real induction arrows at the lowest period range (50-500 secs) point towards two major geological features located in the eastern part of the island. The first set of arrows point towards the southern part of Zephyria graben where the temperature gradient was found to be greater than 8°C/10m (Fytikas, 1977). The second set of induction arrows point towards the Firiplaka crater which lies

* Note : Drews et al. (1989) have found that the Coast effect on Milos is negligible, therefore this problem is not discussed here.

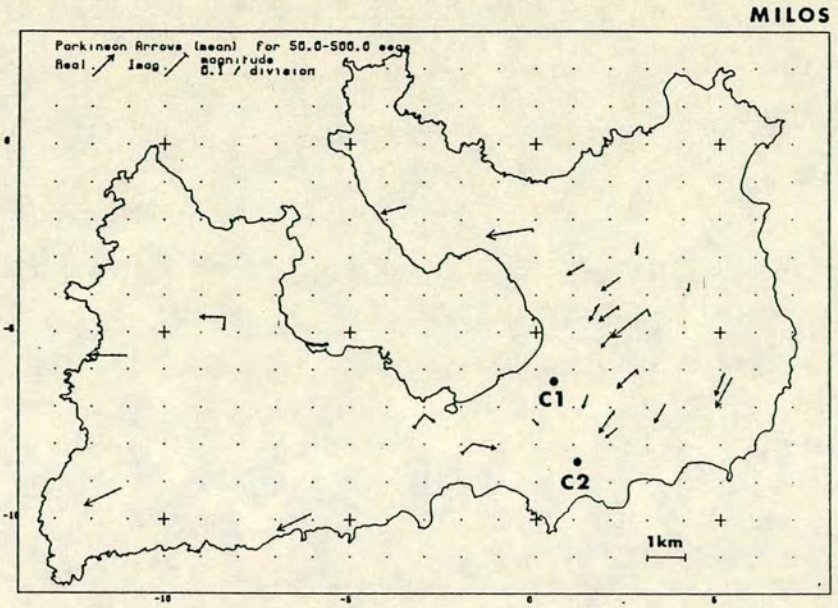

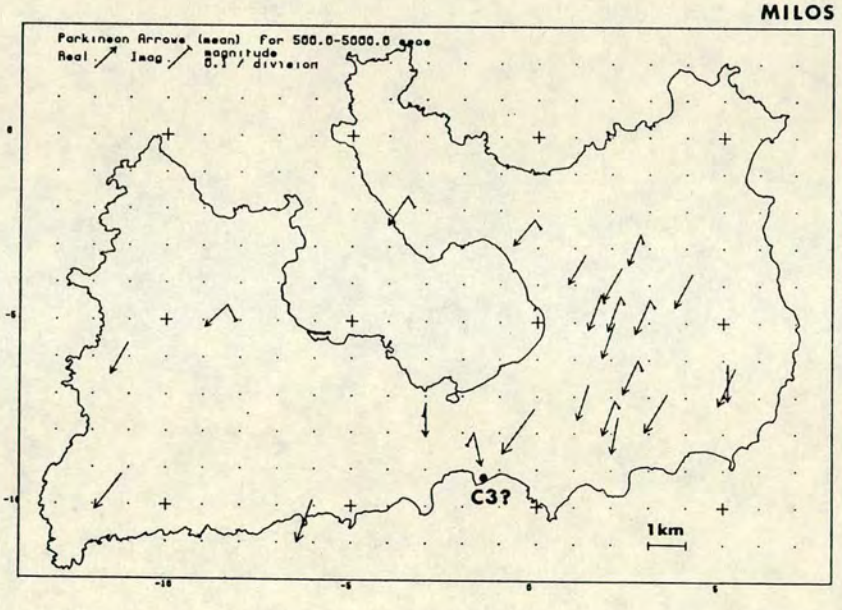

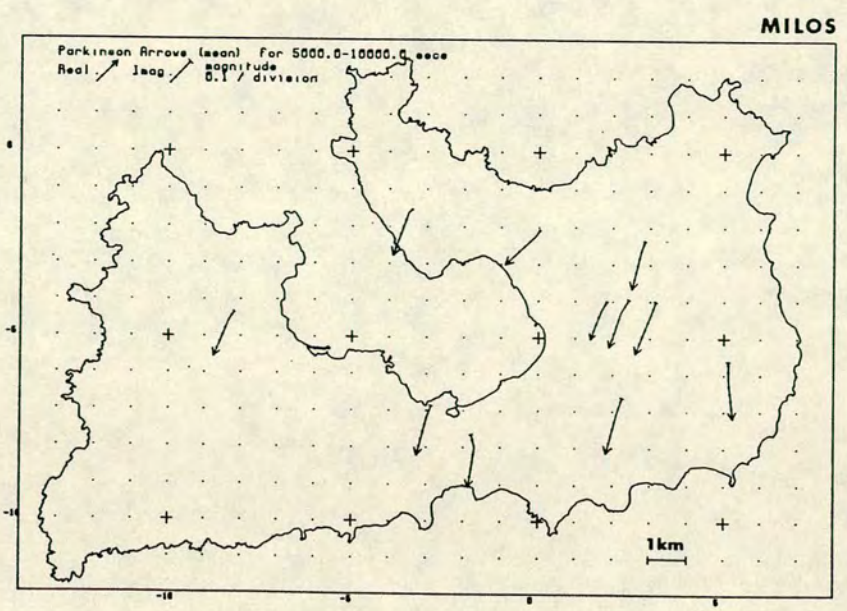

Fig.5.2. Parkinson induction arrows : Magnitudes and azimuths of the real and imaginary parts averaged over three period ranges.

Period range :

a. 50-500 secs.

b. 500-5000 secs.

c. 5000-10000 secs.

south from Zephyria. The presence of two anomalous conductivity bodies indicated as C1 and C2 in Fig.5.2a could explain the pattern discussed above. It is characteristic for this period range that the imaginary parts are very small (less than 0.1) and probably this implies that the conductors are quite shallow.

The pattern of Fig.5.2a does not hold for the two longer period ranges. In the period range 500-5000 secs (Fig.5.2b), there is a clockwise or anti-clockwise rotation of the real part of the Parkinson arrows towards a consistent direction 205°E at all stations. Their magnitudes are large (0.4-0.8) and they point to the southwest, towards a conductor which seems to be parallel to the Hellenic Arc and offshore.

Three arrows point perhaps towards a different feature. It seems that a conductive body may be present in the bay of Provatas (indicated with C3 ? in Fig.5.2b) or that these three stations are still affected by conductor C2. It should be noticed that the imaginary parts at this period range are larger (0.2-0.3) and most of them have a NW-SE direction , (about 20°W) and point to the southeast. This strike coincides with one of the principal directions of the magnetotelluric impedances.

At the longest periods, 5000-10000 secs (Fig.5.2c) the real parts of the Parkinson induction arrows remain with the same magnitude and orientation as for the period range 500-5000 secs and point towards a distant conductor as described above. In addition, these arrows which were pointing towards the possible conductor C3 ?, have now rotated clockwise towards the 205°E direction. The imaginary parts of the Parkinson induction arrows show a remarkable behaviour in this range. They also rotate towards the 205°E direction but their

heads point to the northeast instead. Their magnitudes remain with similar values as before (0.2-0.3).

5.4. Interpretation of the one dimensional magnetotelluric models.

For three sites the one dimensional models were compared with the borehole stratigraphy and temperature data, from deep wells located in the Zephyria graben (Fytikas, 1977 ; 1989 ; Vichos et al., 1986). The results of these comparisons are given below.

5.4.(i). One dimensional magnetotelluric models and local geology.

Fig.5.3 (page 162) shows the one dimensional magnetotelluric models for site 631 for comparison with the stratigraphy of the nearby (≈ 150 m) well M1 (Fig.4.1, page 89). The models were obtained by using the four inversion techniques described in section 4.6.(i).

The Jupp and Vozoff, Dawes, Fischer and the Parker-Whaler D^+ models are reproduced in columnar form with the figures in the columns being resistivities in Ohm.m. The D^+ model conductances are given on the right side of the relevant column. The Jupp and Vozoff and the Dawes methods provide a depth range for each resistivity boundary.

All the models provide comparable electrical structure and correlate well with the borehole stratigraphy. In addition the

Parker-Whaler D^+ method seems to detect the top of the deeper part of the crystalline basement where geothermal fluids have been encountered. Therefore the D^+ models for site 631 and two other sites, 623 and 303 respectively, were chosen for interpretation of the electrical resistivities. Data for site 303 were provided by the BRGM group (Beauce et al., 1989) to the author for the purpose of this study.

Figs.5.4a-c show the Parker-Whaler D^+ models for sites 631, 623 and 303 for comparison with the stratigraphy and temperature profiles of the nearby ($\approx$ 150 m) boreholes M2 and M3 respectively (see Fig.4.1). The models are presented in the same way as in Fig.5.3.

As shown in Figs.5.3 and 5.4a-c there is a good correlation between the geological and electrical boundaries. In particular :

(i). The uppermost layer of alluvium deposits relates to the relatively resistive (10-50 Ohm.m) top layer of the Jupp and Vozoff, Dawes and the Fischer models (Fig.5.3). This layer corresponds to layer A in Figs.4.15a-d and 4.16a-d.

(ii). The green lahar and various volcanic products seem to relate to the very low resistivity layer of 0.3-0.6 Ohm.m (Figs.5.3 and 5.4a-c). This layer corresponds to layer B in Figs.4.15a-d and 4.16a-d.

(iii). The upper 600-800 m of the crystalline metamorphic basement correspond to the 3-4 Ohm.m layer (Figs.5.3 and 5.4a-c). This layer is the same as that illustrated as layer C in Figs.4.15a-d and 4.16a-d (pages 124-127).

(iv). The deeper part of the crystalline basement defined in Figs.5.3 and 5.4a-c as the " geothermal reservoir " corresponds to the more resistive bottom layer with resistivity of $>$ 15

Fig.5.3. One dimensional magnetotelluric models for site 631 and geological stratigraphy of the nearby (≈ 150 m) borehole M1. Models are illustrated in columnar form and figures in the columns are resistivities in Ohm.m. Where appropriate a depth range is provided for the several electrical resistivity contrasts. The models were derived by using the Jupp and Vozoff (1975), Dawes (Sule, 1985), Fischer et al. (1981) and the Parker-Whaler D^+ (1981) inversion techniques. The D^+ conductances are also given in Siemens on the right side of the relative column.

Fig.5.4. Parker-Whaler D^+ models for sites 631, 623 and 303 in comparison with the geological and temperature data from the nearby (≈ 150) wells M1, M2 and M3. The magnetotelluric data for site 303 were offered by Beauce et al. (1989). Models are illustrated in columnar form and figures in the columns are resistivities in Ohm.m. The delta function conductances are also provided in Siemens on the right side of each column.

a. Site 631.

b. Site 623.

c. Site 303.

Fig.5.3

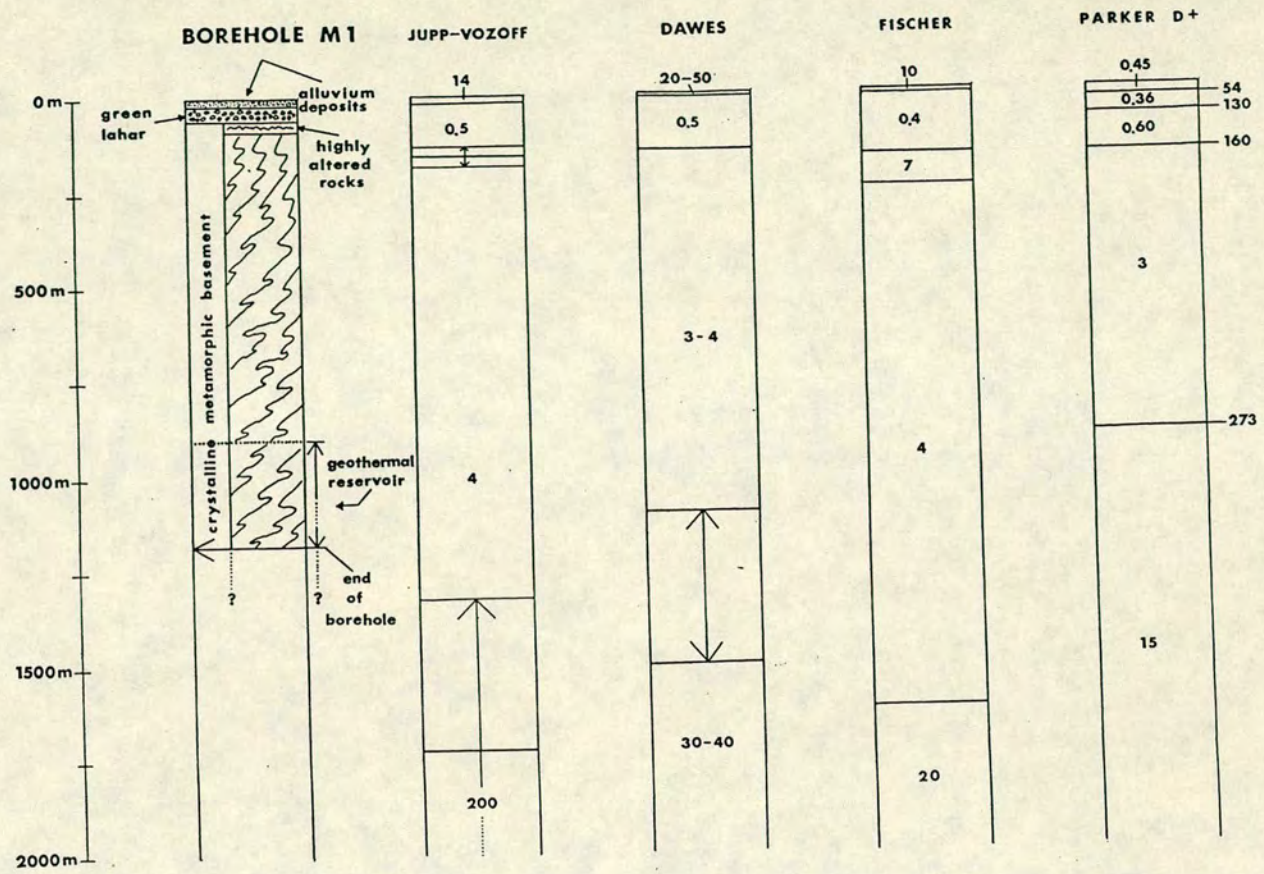

Fig.5.4a

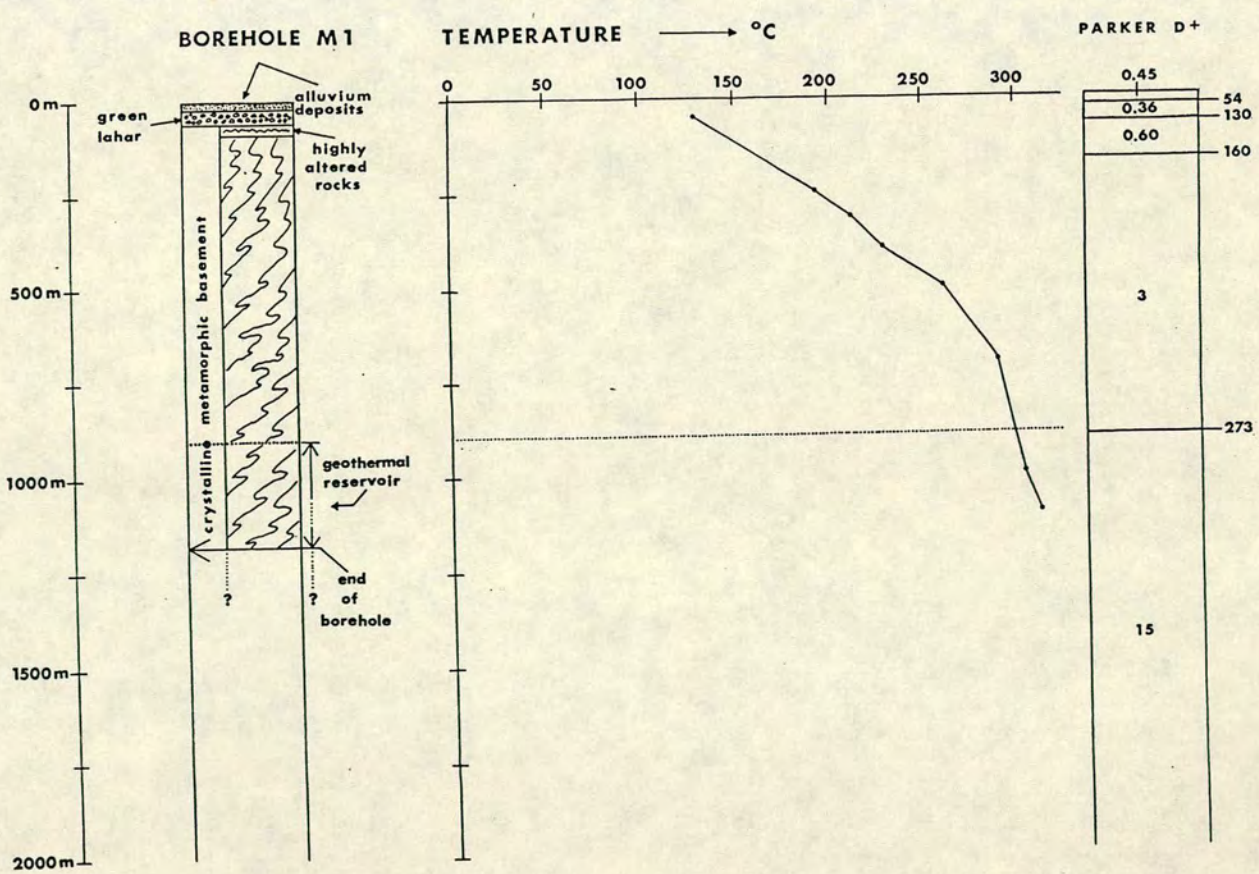

Fig. 5.4b

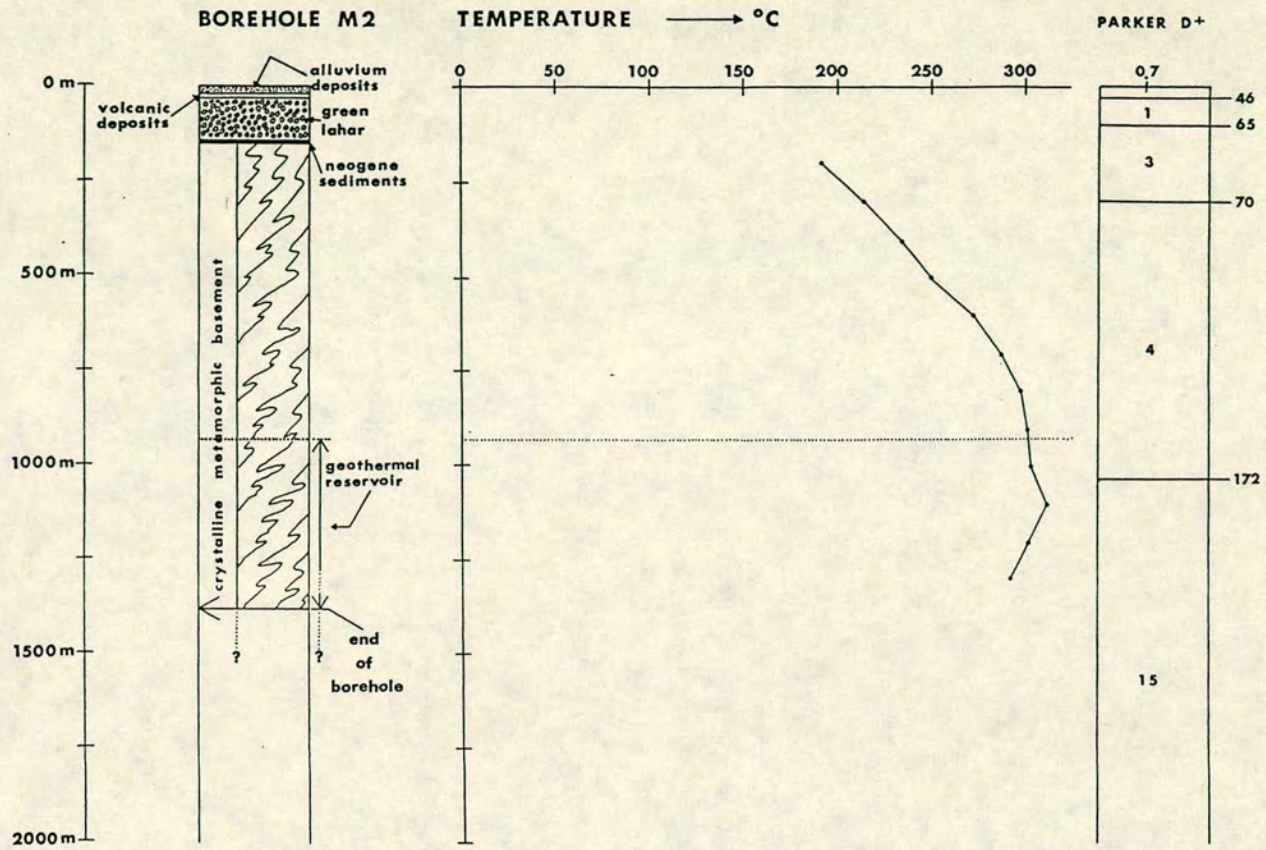

Fig. 5.4c

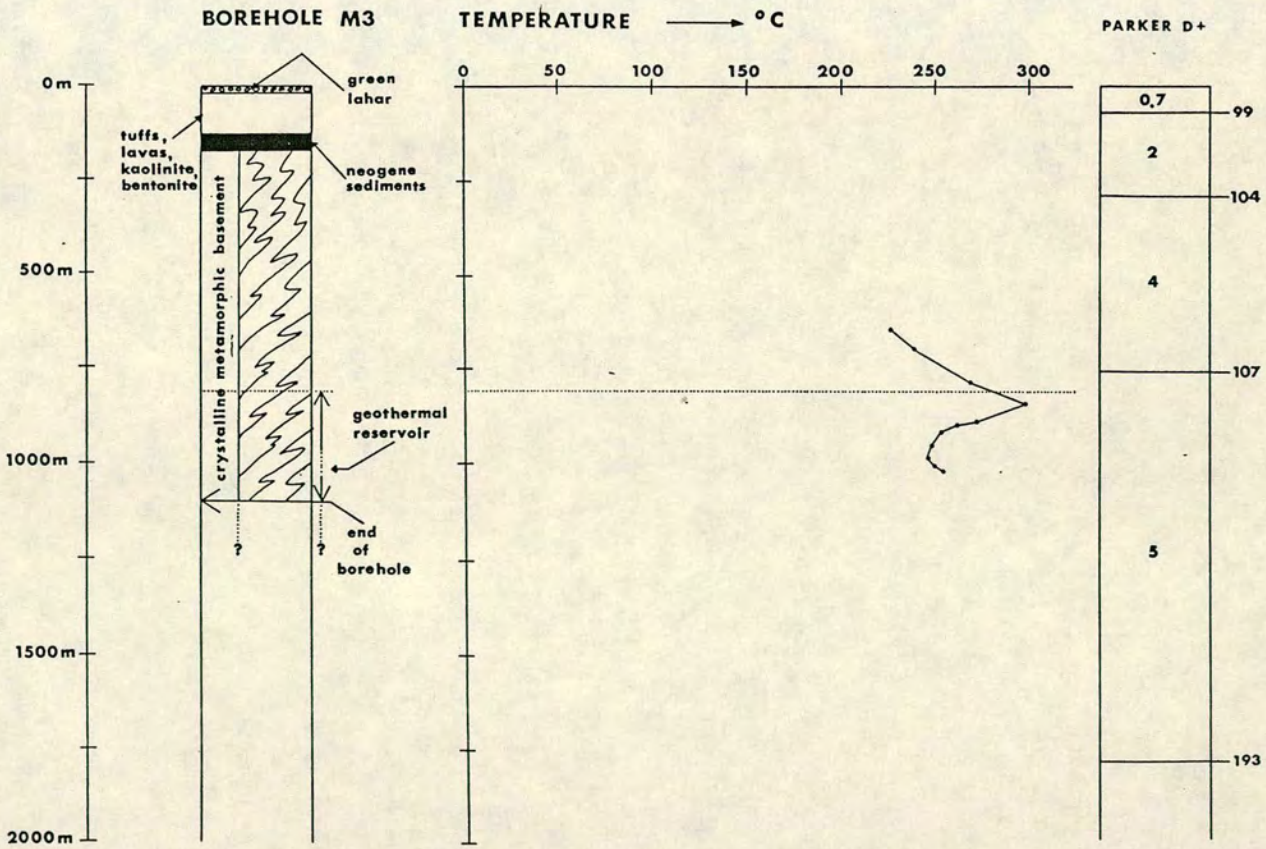

Ohm.m. This layer corresponds to the bottom layer D at most of the models in Figs.4.15a-d and 4.16a-d (pages 124-127).

5.4.(ii). One dimensional magnetotelluric models and temperature gradient.

A set of contours is illustrated in Figs.5.5a-b displaying the total conductance and depth distributions to the top of an interface marked as R, on the D^+ sections of Figs.4.15a-d. This interface was found (section 5.4.(i)) to correlate with the part of the crystalline basement where geothermal fluids have been encountered (Vichos et al., 1986).

For comparison the region of high temperature gradient is reproduced on Fig.5.5a with solid black lines. The major and minor axes of the magnetotelluric impedance ellipses for the period range 10-100 secs are also presented in Fig.5.5b. The choice of this particular period range was based on the fact that the relative skin depths correlate with the depth range of interface R.

It can be noticed that, the high conductance regions coincide approximately with areas of high surface temperature gradient and that the dominant NW-SE strike in the map of Fig.5.5b correlates with the azimuth of the major impedance axis at the majority of the observation points.

It must be remembered that this presentation is qualitative and the results must be interpreted within the limitations of the contouring program used (i.e extrapolation of conductance and depth values near the boundaries of the contoured region).

Fig.5.5. Parker-Whaler D^+ contour maps. The total conductance and the depth to an interface R (see Figs.4.15a-d) are contoured for comparison with - (a) the temperature gradient map of Milos (Fytikas, 1977) and - (b) the magnetotelluric impedance ellipses of the period range 10-100 secs.

▲ AMT STATION

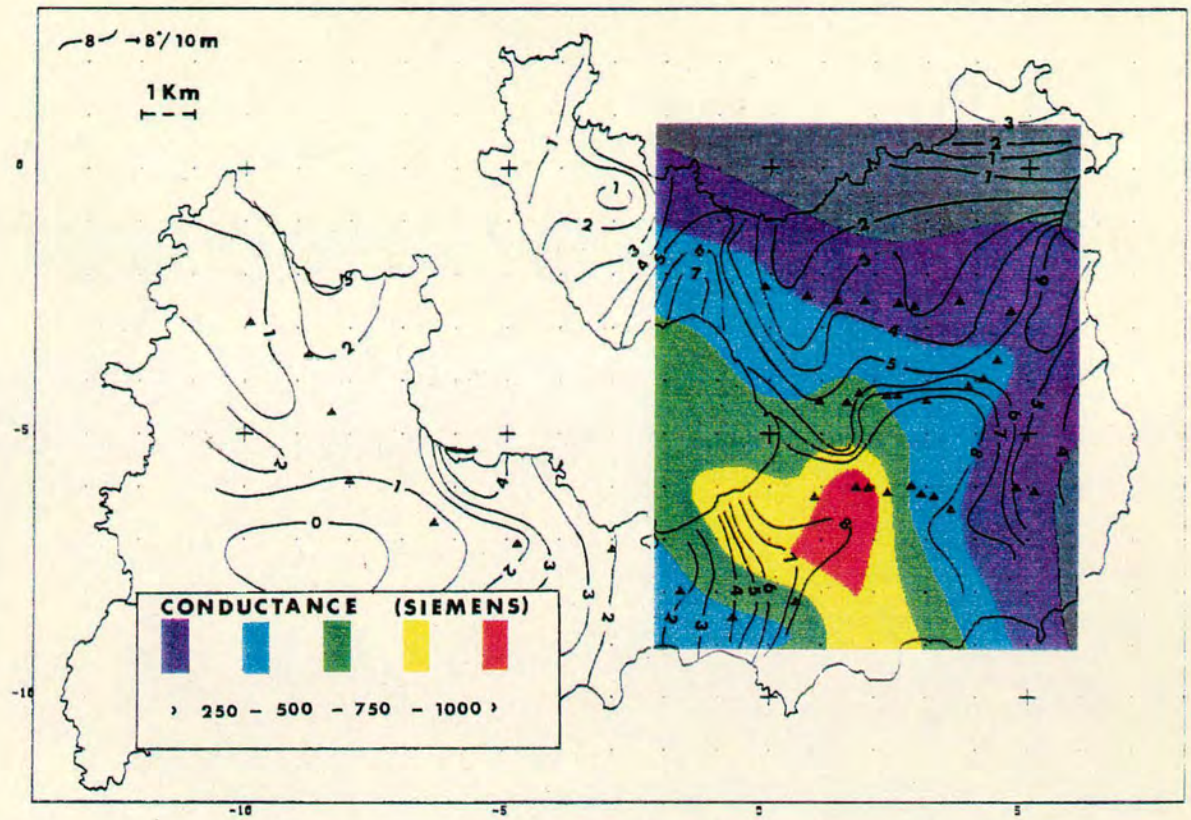
8 → 8°/10m
1Km
CONDUCTANCE (SIEMENS)
› 250 – 500 – 750 – 1000 ›

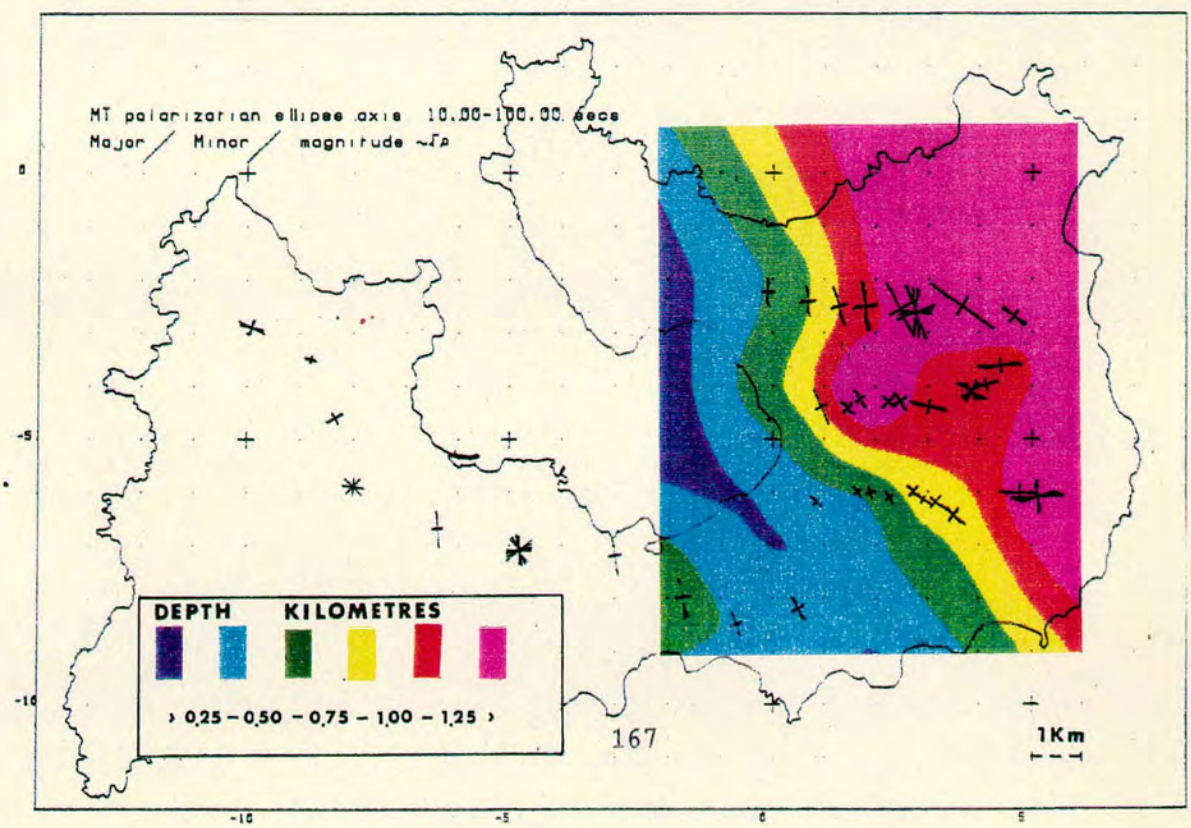
MT polarization ellipse axis 10.00-100.00 secs
Major / Minor / magnitude ~ρ
DEPTH KILOMETRES
› 0.25 – 0.50 – 0.75 – 1.00 – 1.25 ›
1Km

5.4.(iii). Interpretation of the electrical resistivities.

Although two dimensional calculations were undertaken the one dimensional models are used below for interpretation of the electrical resistivities. This choice was based on the fact that - (a) the magnetotelluric data were found nearly one dimensional for the uppermost 5 km (see section 4.5) - (b) the two dimensional calculations were limited.

The following interpretation is given of the layered resistivity models of the one dimensional magnetotelluric sections of Figs.4.15a-d and 4.16a-d (pages 124-127). The results from the borehole comparisons in sections 5.4.(i) and (ii) have been used as a reference.

The uppermost layer A has resistivities of 25-100 Ohm.m in the Western and Northern parts of Milos and 1-25 Ohm.m in the central part of eastern Milos (Zephyria). In the region of Zephyria the lower resistivities could be explained by - (a) the presence of various Quaternary alluvium deposits (see Fig.3.2b, page 76). Sedimentary rocks normally have high porosity and therefore are less resistive than any crystalline rock (see section 1.2.(i)) and - (b) the high temperature gradient ($>$ 6°C/ 10 m) (see Figs.3.4, page 88 and 5.5a, page 167).

The higher resistivities observed in the West and North are rather due to - (a) the superficial pyroclastics and Upper-Pliocene lava domes and flows (see Fig.3.2b). Igneous rocks are expected to be more resistive than the sedimentary rocks of Zephyria (see section 1.2.(i), see also Telford et al., 1981) - (b) the lower

temperature gradient (Figs.3.4 and 5.5a) in these regions.

The low resistivities of layer B - 2-12 Ohm.m in the West and North and 0.2-5 Ohm.m in Zephyria - are probably due to the low temperature (< 300-400°C) hydrothermal processes taking place in the uppermost 200 m (Fytikas, 1977 ; 1989). Kaolinite is the dominant product of these processes. This is a known clay mineral which has the ability to absorb water and exchange ions and therefore is a very good electrolyte (see section 1.2.(i)). The products of hydrothermal alteration in Zephyria have volcanic origin and are mixed with conglomerates of metamorphic rocks. This is the so-called " green lahar " formation (Fytikas, 1977 ; 1989). In the same region the temperature gradient is high (> 6°C/ 10 m) which accounts for the observed lower resistivities here than in the West and North. In addition, Kaolinite as a clay mineral is plastic and has low permeability (see section 1.2.(i)).

The significance of alteration minerals in resistivity changes has been discussed by Stanley et al. (1976) and recently by Fitterman et al. (1988) and Park and Torres-Verdin (1988). The last two studies relate to magnetotelluric measurements in the Newburry volcano (Fitterman et al., 1988) and the Long Valley Caldera (Park and Torres-Verdin, 1988). Steiner (1968) and Browne (1970) found that alteration minerals such as smectite, chlorite, calcite, illite and epidote are very common in active and fossil hydro-thermal systems.

Stanley et al. (1976) found that hydrothermally altered tuffs in Long Valley, California have resistivities of 1-10 Ohm.m. Fitterman et al. (1988) have interpreted their shallow (500-700 m) conductivity anomalies as due mainly to the presence of

alteration minerals such as smectite and partly to high-temperature pore fluids. They believe that these minerals are very conductive even though they are no longer at high temperatures. At greater depths than the smectite alteration the low resistivities have been assigned to the presence of high-temperature pore fluids.

Park and Torres-Verdin (1988) have also interpreted a low resistivity thin layer at depths of 500-700 m in terms of hydrothermal clay overlying the thermal aquifer.

Layers C and D are in general more resistive than the overlying layer B. In section 5.4.(i) it was shown that these layers seem to correspond to the Mesozoic metamorphic basement. This is made up of weakly metamorphosed rocks with mainly green-schist facies (Fytikas, 1989 ; see also section 3.4). Crystalline rocks have in general low porosity and therefore have higher resistivities than the sedimentary rocks (see section 1.2.(i)). Typical resistivity values for these rocks when they are dry and at low temperatures are about 10^{+3}-10^{+4} Ohm.m. The electrical resistivity of crystalline rocks decreases significantly when the temperature increases (Fig.1.4b, page 26).

The observed low resistivities 3-10 Ohm.m of layer C and 15-50 Ohm.m of layer D in Zephyria, can be interpreted in terms of the high temperature. In the North and West, layers C and D have resistivities of 10-20 Ohm.m and 50-100 Ohm.m respectively. These are relatively higher than those in Zephyria but this is expected since the temperature is lower. The metamorphic rocks which correspond to layer C (200-800 m) have undergone hydrothermal alteration. The products of alteration are known hydrous minerals such as pyrite, chlorite,

serpentinite, sauconite (see section 1.2.(i) ; Vichos et al., 1986) and have decreased its permeability and electrical resistivity (see section 1.2.(i)). Layers B and C together provide a good impermeable zone (" cap rock ") for the geothermal reservoir.

The fact that at the " reservoir " depths (see Figs.5.4a-c, pages 163-164) the electrical resistivity is higher (> 15 Ohm.m) can be explained by - (a) the smaller amounts of the products of hydrothermal alteration at depths greater than 800-1000 m (Vichos et al., 1986) probably increases the electrical resistivity of layer D, - (b) the sudden increase in pressure at the reservoir depths from 60 to 120 bars (Vichos et al., 1986). As shown in Fig.1.4a (page 26) electrical resistivity increases when the pressure increases, - (c) the " flashing " of the geothermal fluids at the reservoir depths. The geothermal fluids are mainly water with 10% NaCl at the boiling point which due to the low pressure and the low permeability of the overlying formations (layers B and C) are transformed into steam. Steam if dry has normally high resistivity.

5.5. Interpretation of the two dimensional magnetotelluric model.

The final two dimensional model is SS'-1 illustrated in Figs.4.17a-b (pages 139-140). Several hypotheses have been tested in section 4.6.(vi). The results of these tests imply that SS'-1 is the best fit model. However the resulting electrical structure is interpreted with care considering the non-uniqueness of the two dimensional modelling problem.

By studying the conclusions of sections 4.6.(ii) and 4.6.(v) the following deductions can be made.

The one dimensional sections of Figs.4.15c and 4.16c (page 126) and the two dimensional model SS'-1 provide similar electrical structure for the upper crust below Zephyria. It has to be remembered that the two dimensional modelling was constrained by the results of one dimensional modelling. Therefore the derived electrical resistivities can be interpreted like those from the one dimensional modelling.

The two dimensional model provides information for the deeper (> 5 km) electrical structure. Two additional features are resolved (Figs.4.17a-b) - (a) a depression of a 10 Ohm.m block below Zephyria and - (b) a resistivity contrast at 15 km depth.

Model SS'-1 is one of the many models which satisfy the magnetotelluric data along profile SS' (Fig.4.1, page 89). Therefore these features can be easily questioned. However in the next section it is shown that they can be supported by the results of other geophysical methods.

The following stand as general conclusions.

(i) The 10 Ohm.m block is equivalent to layers C and D below Zephyria (Figs.4.15c and 4.16c) and can be related to the metamorphic basement.

(ii) The underlying 30 Ohm.m and 150 Ohm.m blocks are geologically undefined.

(iii) There is no indication of the heat source of the Milos geothermal field in the electrical Model SS'-1 of Figs.4.17a-b. In their interpretation of all data resulting from the EEC program Fytikas et al. (1989) have proposed a geothermal model which may include a cooling magma chamber or many small magma

chambers which electrically seem to be undetected (Fig.5.6).

Newman et al. (1985), Wannamaker (1986) and Fitterman et al. (1988) have discussed at length the detectability of a magma chamber with the magnetotelluric method. Wannamaker (1986) argued that a silicic melt in the midcrust with 2.5 % water would have resistivity of about 4 Ohm.m. Fitterman et al. (1988) using resistivities in this range have computed several simple models to illustrate possible detection of magma with MT soundings. Their results lead to conclusions similar to those of Newmann's et al. (1985) that it is very difficult to detect a magma chamber. Such a body is usually masked by the presence of a lower crustal conductor or even a shallow conductive body such as the Newburry smectite or the alteration clays in Long Valley.

5.6. The Magnetotelluric model of the Milos island and other geophysical results.

In this section the derived magnetotelluric models are interpreted in terms of other previous or recent geophysical results.

The previous geophysical work on Milos is related mainly to the gravity and D.C resistivity measurements undertaken by IGME and interpreted by Tsokas (1985). These studies were described in section 3.6. The recent geophysical work is associated with the 3rd EEC Geothermal Programme and involves apart from the present work, passive magnetotellurics (Beauce et al., 1989 ; Haak et al., 1989), controlled source audio-magnetotellurics (Drews et al., 1989), Self Polarization (S.P) measurements (Thanassoulas, 1989) and micro-seismics (Beauce et al., 1989 ; Hirn et al., 1989 ; Ochmann et al.,

1989). A collection of papers based on these studies can be found at the special issue of Geothermics (Vol.14, 1989). However some of the most important results from these geophysical surveys are used in this section to construct an integrated geophysical model for the Milos geothermal field.

The following discussion is based on comparisons between the one and two dimensional electrical models along profiles 1, 2, 3, 4 and SS' respectively and relative seismic, gravity and D.C resistivity sections which are located in Fig.5.7.

Fig.5.8 (page 177) shows the tomographic results for the v_p/v_s ratio (Hirn et al., 1989) along Profile 4075, together with a vertical contour section of the Bostick invariant resistivities along Profile SS'. Within the top 2.5 km good correlation is observed between the low resistivity areas and areas of high v_p/v_s ratio. The latter were interpreted (Hirn et al., 1989) as liquid-filled fractured zones. The 10 Ohm.m region correlates with an area of intermediate v_p/v_s ratio. The earthquake hypocentres are located at the boundaries of this region and their mechanism was associated with temperature variations in the source region or the maximum depth of fluid penetration (Hirn et al., 1989).

Fig.5.9 (page 179) illustrates two composite geophysical sections, oriented approximately along the direction of the magnetotelluric Profile 2 (Fig.5.7). Fig.5.9 shows the gravity and D.C resistivity sections derived by Tsokas (1985) along the profiles CD and B3B4 respectively (Fig.5.7). The solid line represents the top of a basement with density of 2.5 g/cm^3 and the dotted line corresponds to top of the electrical basement. The

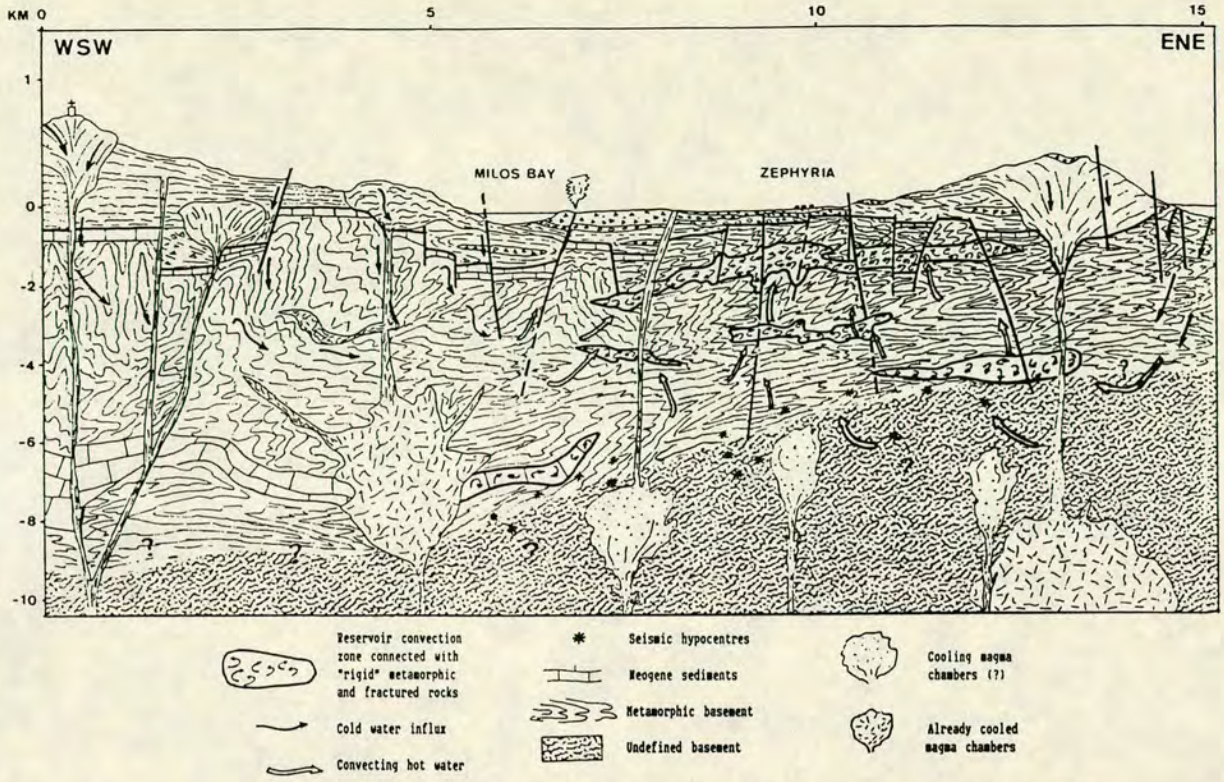

Fig.5.6. Schematic geological profile along a WSW-ENE direction on Milos (Fytikas et al., 1989).

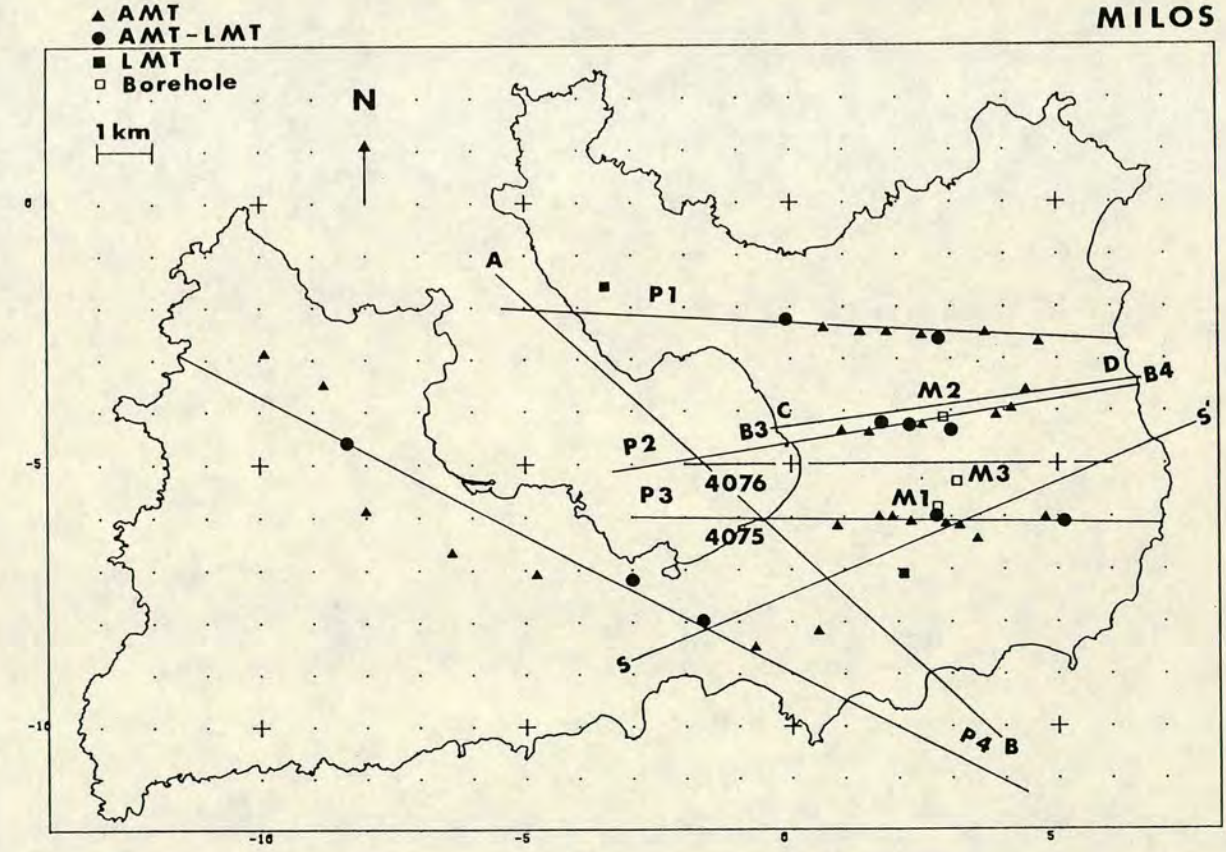

Fig.5.7. Geophysical sections on Milos island. Profiles are illustrated with solid lines. These are the four magnetotelluric Profiles 1, 2, 3 and 4 of this study, the seismic profiles 4075 by Hirn et al. (1989) and AB by Ochmann et al. (1989) and the gravity (CD) and D.C resistivity (B3B4) profiles by Tsokas (1985).

Fig.5.8. Niblett-Bostick invariant resistivity section along Profile SS' in comparison with the v_p/v_s distribution along the seismic Profile 4075 (Hirn et al., 1989) (see Fig.5.7).

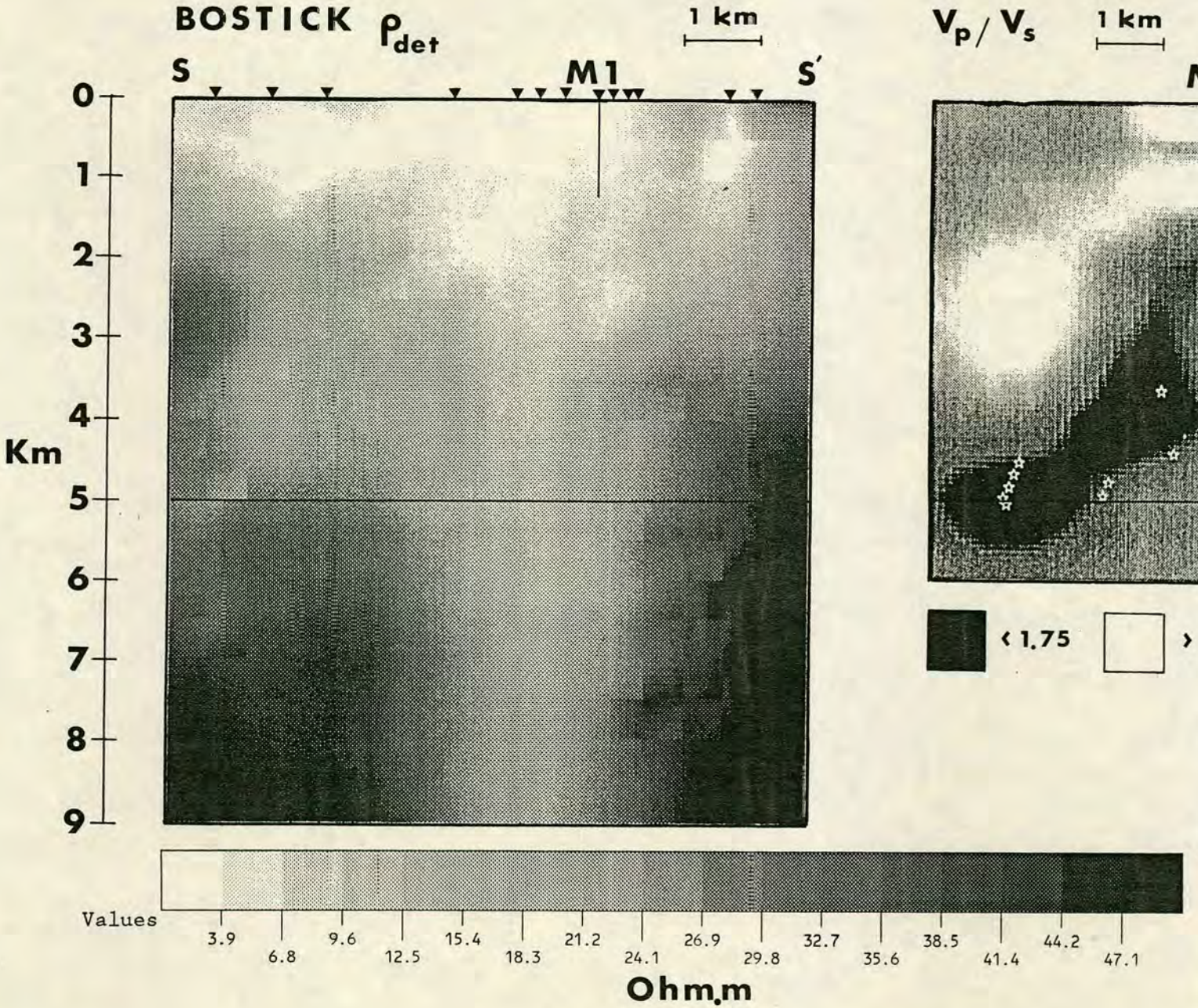
BOSTICK ρ_{det}
1 km
S
M1
S'
0
1
2
3
4
5
6
7
8
9
Km
Values
3.9
6.8
9.6
12.5
15.4
18.3
21.2
24.1
26.9
29.8
32.7
35.6
38.5
41.4
44.2
47.1
Ohm.m

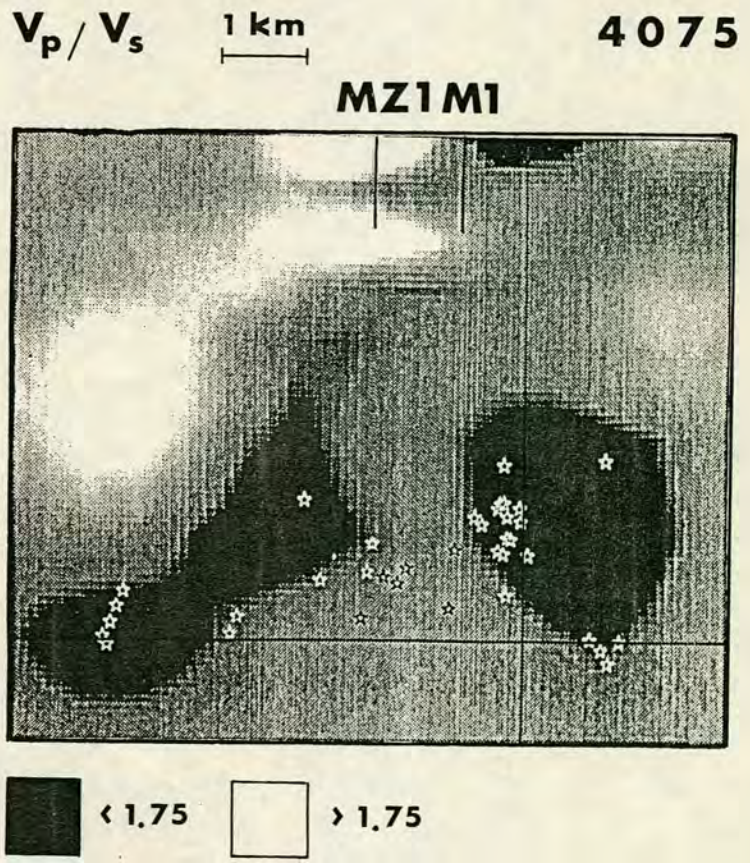
V_p / V_s
1 km
4075
MZ1M1
< 1.75
> 1.75

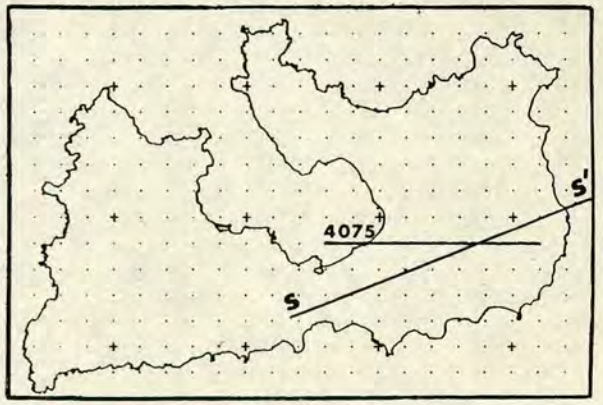
4075
S
S'

residual gravity anomaly, observed along CD is redrawn on top of this section.

An interface located at depths of about 100-500 m and interpreted by Tsokas, (1985) as the top of the crystalline metamorphic basement correlates well with the D^+ interface between layers B and C in Fig.4.15b which was also interpreted as the top of the same formation. The top layer D.C resistivities agree with those from the present magnetotelluric study while there is a disagreement for the deeper structure. The D.C resistivity method could not penetrate deeper than 1000 m and therefore the latter must be attributed to the limitations of the D.C resistivity modelling.

Fig.5.10 shows the earthquake hypocentres which are located below the Milos bay along the seismic line AB (Ochmann et al., 1989). The magnetotelluric one dimensional Dawes section of Fig.4.16d below Profile 4 was redrawn for comparison. The seismic line AB was projected on Profile 4 (see Fig.5.7). The earthquake hypocentres are dipping to the northwest and they are situated below the top of the relatively resistive electrical basement.

The use of several parameters derived from the magnetotelluric models of the present study, enabled the author to constrain the modelling of the residual Bouguer anomaly along profile SS'. The residual gravity anomaly was digitized from the residual Bouguer anomaly map compiled by Tsokas (1985) and redrawn in Fig.5.11 (page 180). Several blocks, simulating the shallower more conductive structure of Model SS' were used as an input.

The results of the gravity modelling are shown in Fig.5.12 (page 180). The two blocks with the negative density contrast of about

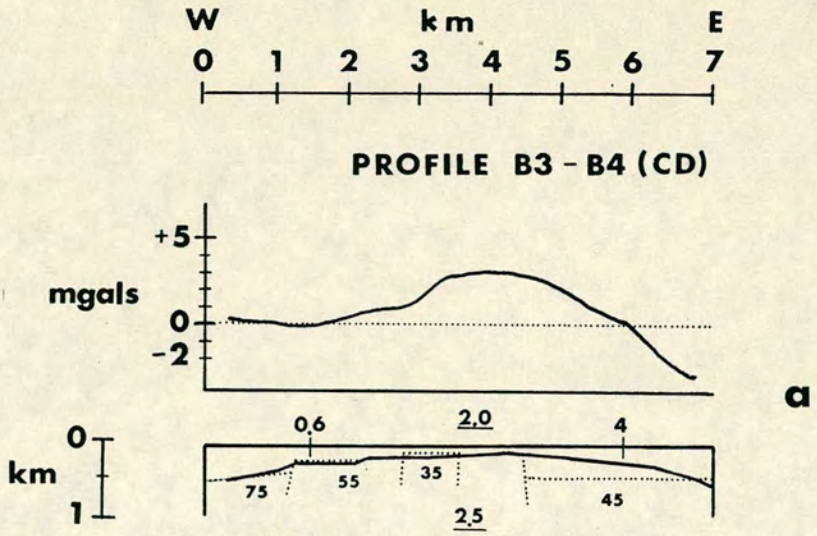

Fig.5.9. Gravity and D.C resistivity Profiles B3B4 and CD respectively (see also Fig.5.7). The residual Bouguer anomaly along profile CD is shown on top (Tsokas, 1989). Underlined figures on models indicate densities in g/cm³. Plain figures are electrical resistivities in Ohm.m.

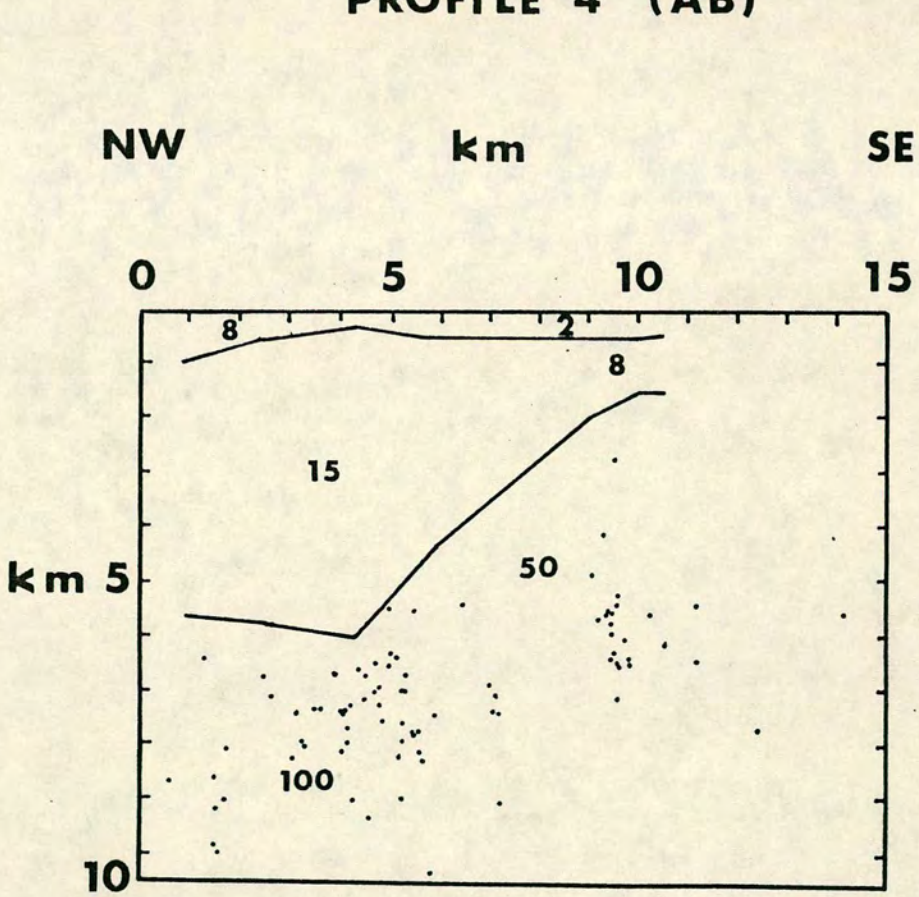

Fig.5.10. Earthquake hypocentres below the seismic line AB (Ochmann et al., 1989). The Dawes one dimensional magnetotelluric section along Profile 4 (see Fig.5.7) is shown for comparison.

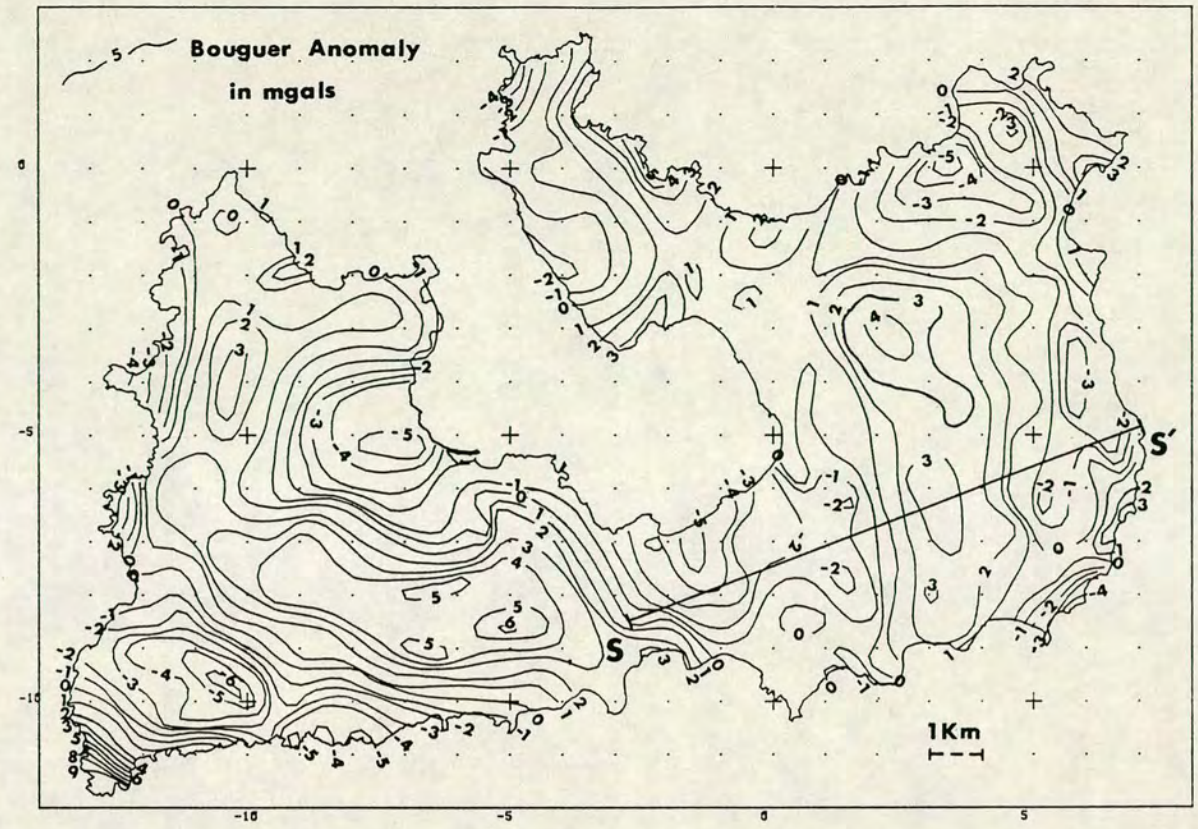

Fig.5.11. Residual Bouguer anomaly map of Milos (Tsokas, 1985).

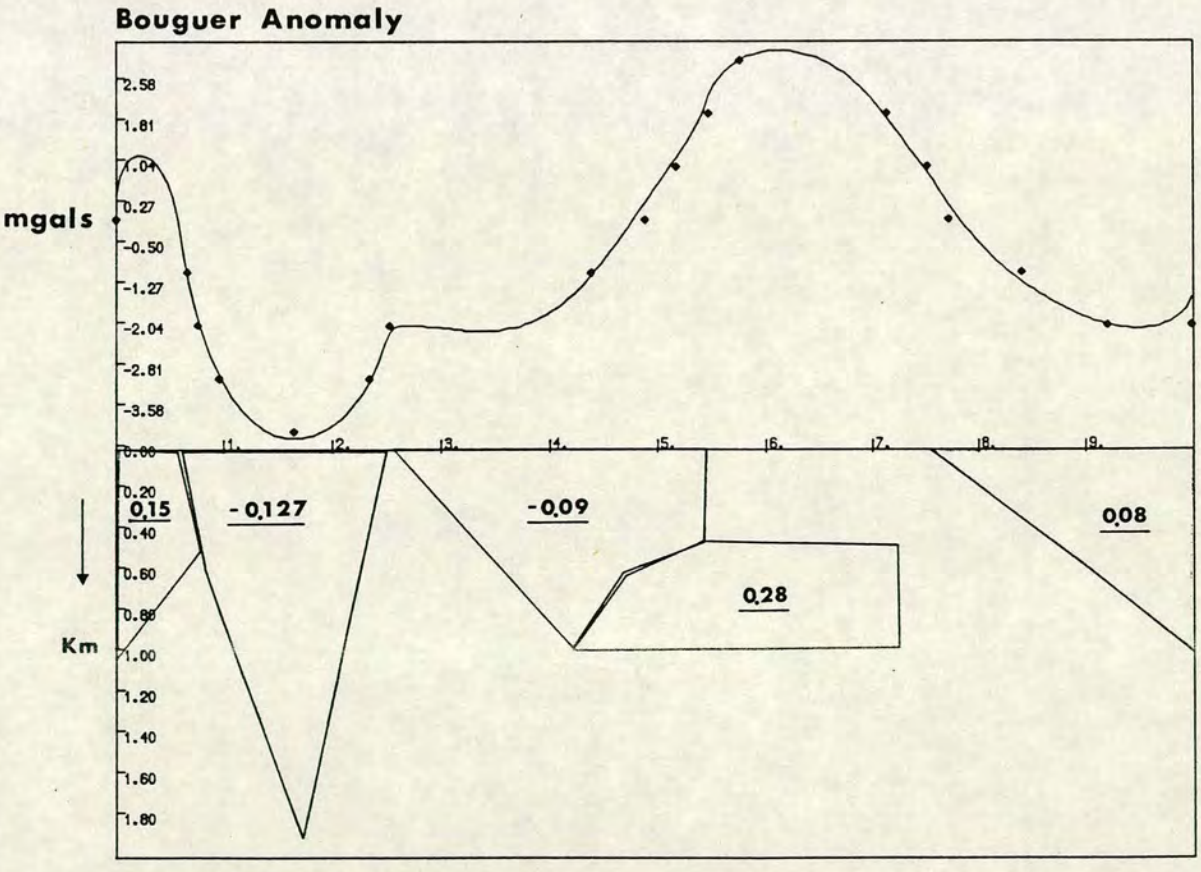

Fig.5.12. A gravity model along Profile SS'. Figures on the several blocks are density contrasts in g /cm³.

-0.1 g/cm³ below Provatas and Zephyria could correlate with the presence of sediments in the narrow zone of Provatas and with the liquid-filled fractured zone of the metamorphic basement below Zephyria (Hirn et al., 1989). According to this explanation the block with positive density contrast of 0.28 g/cm³ rather represents a less fractured basement east of Zephyria graben. These contrasts are given with respect to a density of 2.0 g/cm³ assumed for the uppermost 2 km of the crust below Milos.

However, this gravity model must be interpreted with care, taking into account , (a) that the modelled data originate from a contour map and (b) the non-uniqueness of the gravity models.

The results of the present magnetotelluric study and those from other geophysical methods, enabled the construction of an integrated geophysical model which extends below the magnetotelluric Profiles 4 and SS' (Fig.5.7) and it is shown in Fig.5.13 (page 183).

There are six dominant features on this model.

(a) The top 2 km below the Zephyria-Firiplaka region which is characterized by a low resitivity, low density and high v_p/v_s ratio, zone.

(b) The large depression of the metamorphic basement below Zephyria, which electrically is identified by a 10 Ohm.m block penetrating into the relatively more resistive (30 Ohm.m) upper crust. Seismically this feature is identified by an aseismic zone bounded by two bodies of small v_p/v_s ratio. The earthquake hypocentres are located at the boundaries of this block.

(c) The low resistivity, low density narrow zone of Provatas.

(d) The electrical boundary dipping to the northwest beneath the south and northwestern part of Milos. It is characterized by

intense seismicity (see also Appendix I, Hutton et al., 1989 ; Fytikas et al., 1989) at depths of 5-10 km.

(e) The conductive region below Xirocambos (Fig.5.1a : X).

(f) All the upper crust is characterized by low p-wave velocities, from 4.7 km/s at the top 3 km to 6.8 km/s down to a depth of 15 km. The electrical boundary of the 30 Ohm.m block with the 150 Ohm.m half-space, seems to correlate very well with a seismic refractor proposed by Makris (1977). This refractor is located at about 15-20 km depths east of Milos and north of Santorini.

5.7. The Magnetotelluric results and their tectonic implications.

In this section the magnetotelluric results are discussed in terms of regional and local tectonics. During the Pliocene, NE-SW extensional processes took place on Milos and deep normal faults were created along NW-SE directions (Angelier et al., 1982). These features were thoroughly mapped during two seismic reflection surveys undertaken by Jongsma et al. (1977) and Makris (1977). Part of this map was redrawn by the author in Fig.5.14 to illustrate the major faults in the Milos archipelago. In this figure the white arrows indicate the Pliocene extensional directions in the region.

From the study of the Parkinson induction arrows (see section 5.3) it was found that there is a preferred direction of 205°E for the longer period (500-10000 secs) arrows. This direction is represented in Fig.5.14 with a black vector which points to the southwest, towards a remote, undefined, anomalous conductivity body aligned with the arc direction. The effect of the subducting slab

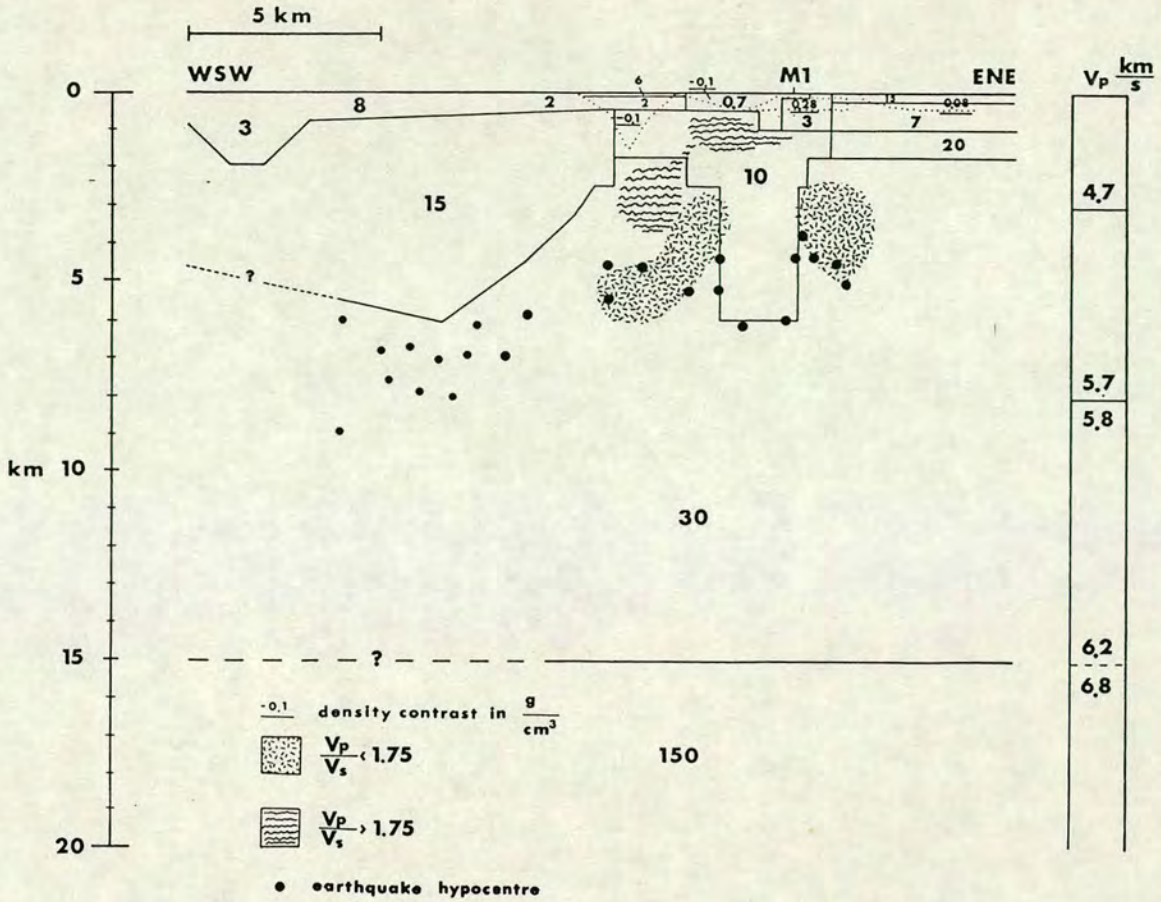

Fig.5.13. An integrated geophysical model for the Milos geothermal field. A composite section of the proposed magnetotelluric models along Profiles 4 and SS' (see Fig.5.7, 4.16d and 4.17a-b) the gravity and microseismic (Hirn et al., 1989 ; Ochmann et al., 1989). Plain figures are electrical resistivities in Ohm.m.

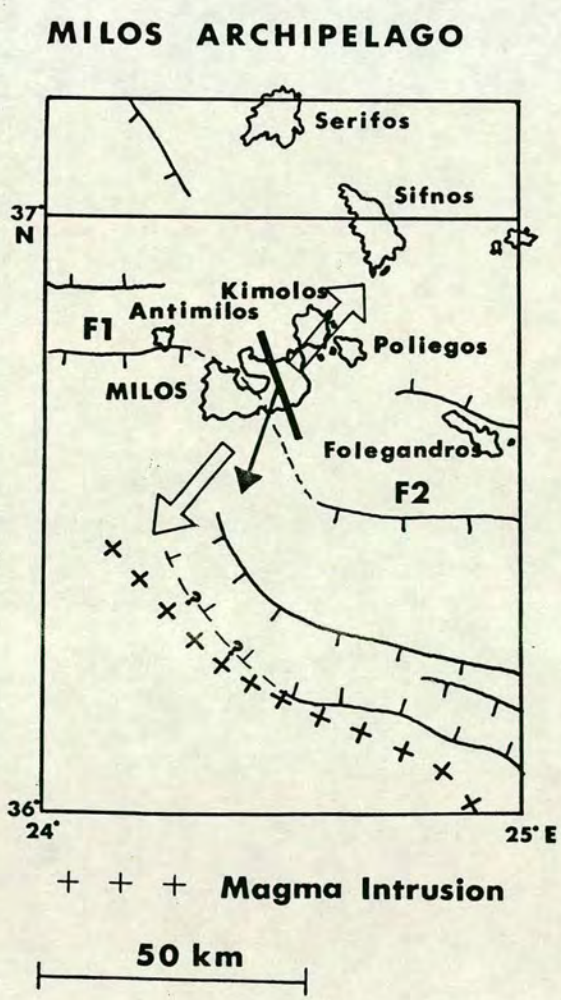

Fig.5.14. The magnetotelluric results on the Milos island and their local and regional (Milos archipelago) tectonic implications. Ticked solid lines - normal faults mapped by Jongsma et al. (1977) and Makris (1977) ; Dashed line - hypothetical fault ; Open arrows - Pliocene extensional direction on Milos ; Black arrow - average Parkinson iduction arrows for the period range 5000-10000 secs ; Thick solid line - dominant electrical strike in Zephyria graben.

seems not to be detected electrically on Milos. There are no low apparent resistivities observed within the period range 10^{+3}-10^{+4} secs (Fig.5.1a : site 642, Fig.5.1b : site 621, pages 155-156).

Alternatively, the remote conductor could be the southwestern continuation (Fig.5.14, thick dashed line) of a fault controlled elongated trough, which is observed 30 km southeastern from Milos along a WNW-ESE direction. The trough is covered with Pliocene and recent uncosolidated sediments with maximum thickness of 1-1.5 km (Jongsma et al., 1977). Those can be expected to have low resistivities of about 1-20 Ohm.m (Telford et al., 1981).

In the lowest period range, 10^{-2}-1 secs, the magnetotelluric data are very isotropic but within the longer period range of 10-5000 secs the data become anisotropic. At most of the sites the major and minor axes of the impedance ellipses are oriented along two perpendicular directions, NW-SE (20°W) and NE-SW (70°E) respectively Figs.4.8a-d). The NW-SE direction is the dominant electrical strike in the inner part of Zephyria graben, and is marked with a thick black solid line in Fig.5.14. This direction does not correlate with the N-S topographic boundaries of the Zephyria graben but with the Pliocene NW-SE oriented faults which are believed (Fytikas, 1977) to have formed Milos bay (Fig.5.14, dashed line).

Jongsma et al. (1977) assumed that the fault (or faults) which formed Milos bay is rather associated with the two major normal faults, northwestern and southeastern of Milos marked as F1 and F2 in Fig.5.14. The latter cannot be proved since there is lack of geophysical information in the area surrounding Milos at the present time.

CHAPTER 6

THE OLKARIA CASE STUDY : GEOLOGY AND GEOPHYSICS.

6.1. Introduction.

Olkaria is located at the western flank of the Gregory rift valley, south of Lake Naivasha. Since the Miocene, during the formation of the rift, the region underwent extensive volcanism and intense faulting. Volcanism and faulting are responsible for the high enthalpy geothermal field of Olkaria.

Olkaria East is currently exploited. During the last 4-5 years more than 20 productive wells supply with hot fluids and steam the Geothermal Power station of Olkaria. The current plans of the Kenyan Power Company (KPC) are associated with the geophysical mapping of the Olkaria West and North potential fields and the detection of a possible heat source. The geophysical investigations included a magnetotelluric survey which was undertaken recently by the University of Edinburgh, in collaboration with KPC. This study is described in this and the following chapters of this thesis with the background geology and geophysics of the Kenya Rift Valley and Olkaria being discussed first in brief in the following sections.

6.2. Geographic location.

Olkaria is located (Figs.6.1a-c) on the central part of the Kenyan rift valley (Gregory rift), SW of Lake Naivasha and extends

a

KENYA RIFT VALLEY

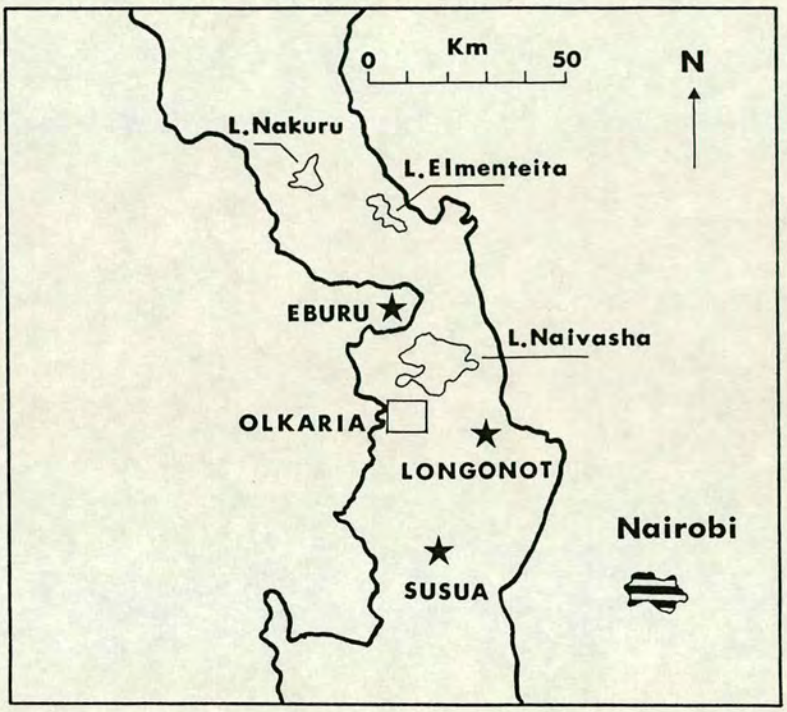

b

Fig.6.1. Olkaria : Geographic location.

a. The African Rift Valley.

b. The Kenyan Rift Valley.

c. Olkaria geothermal field (black solid lines indicate normal faults; Dashed lines indicate hypothetical extension of existing faults).

OLKARIA

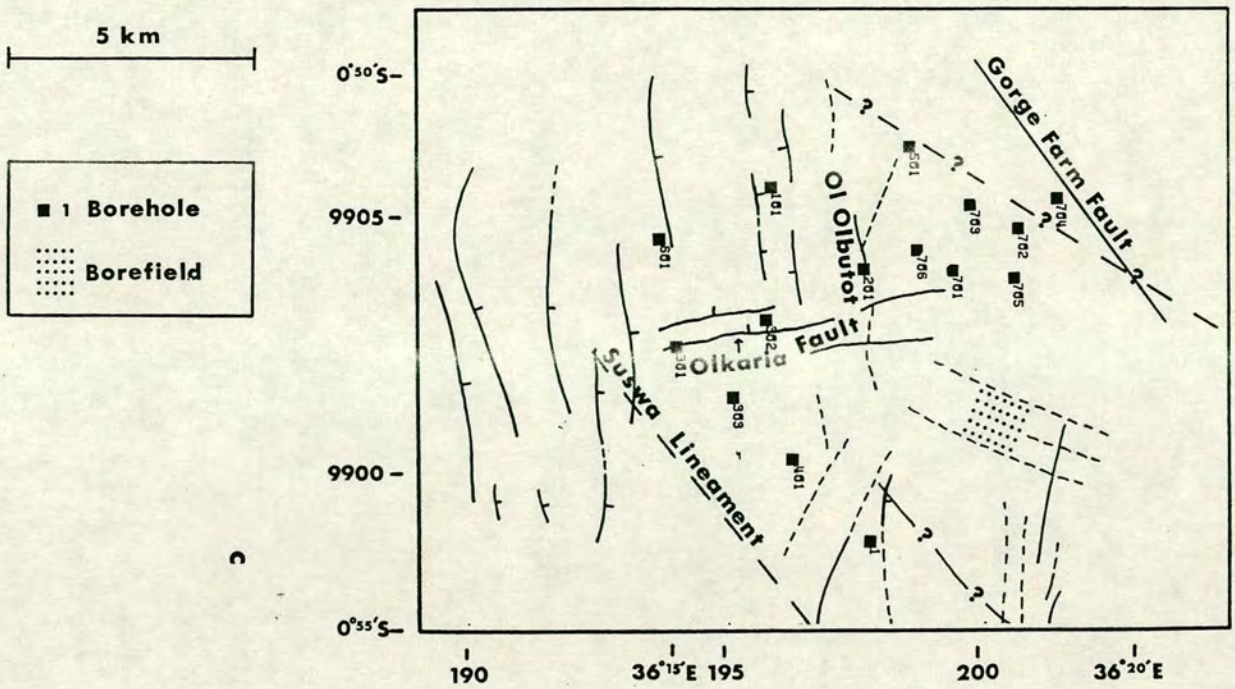

c

from 0°45'S to 0°55'S. The area is bounded by the Mau Escarpment in the West and the Nairobi-Nakuru national motorway in the East. The area of interest extends over approximately 500 km² and is situated at 1700-2300 m above the sea level. The average elevation is about 2000 m but major topographic features such as the Olkaria Peak (about 2300 m.a.s.l) and the Ol Njorowa deep gully (Hell's gate, about 1700 m.a.s.l) are present.

6.3. The geotectonic evolution of the Kenyan Rift Valley.

The Kenyan rift valley is part of the East African rift system which extends from north Tanzania through Kenya and Ethiopia to join the Red Sea and Gulf of Aden rifts at the Afar triple junction. The East African rift is considered to be a continental extension of the World rift system (Baker and Wohlenberg, 1971). In its central part the major faults define a complex graben in the central part of the rift known as the Gregory rift system which is 60-70 km wide. The graben floor is cut by many young sub-parallel faults (Baker and Wohlenberg, 1971).

A major domal uplift, the Kenya dome, is bisected by the Gregory rift (Baker and Wohlenberg, 1971 ; Maguire and Long, 1976 ; Savage and Long, 1985).

The volcanism initiated during the Miocene is of alkaline chemical character with several volcanic chains being formed along the axis of the rift and large volcanoes to the East - Mount Kenya and Kilimanjaro.

The geotectonic evolution of the Kenyan rift was subdivided into four stages by Baker and Wohlenberg (1971) which have been

described by Rooney (1977) as follows.

Lower-Upper Miocene (23-12 m.y).

The foundation of Eastern Africa is a complex of metamorphic and igneous rocks of Precambrian and Lower Paleozoic age. Rifting started in the Lower Miocene with the subsidence of the Turkana depression in northwestern Kenya and uplift of the area along the Uganda-Kenya border. The Turkana depression was partly filled by flood basalts and on the uplifted area a linear arrangement of volcanoes was formed. During the Upper Miocene volcanism shifted towards the Kenya dome. The central rift area was uplifted and was the site of immense fissure eruptions of phonolites. During this stage of the rifting there was tremendous magma production.

Lower-Middle Pliocene (10-5 m.y).

In the Lower-Middle Pliocene more than 19 volcanoes erupted along the floor or over the scarps of the future rift valley and several extensive rift faults were developed creating an asymetrical graben. The products of the eruptions were mainly basalts with minor phonolites and trachytes.

Upper Pliocene-Middle Pleistocene (5-1 m.y).

During this period there was a change of volcanism back to massive eruptions of trachytic ignimbrites along the central part of the trough in the Naivasha sector. At about the same time the last and major uplift of the marginal plateau began, accompanied by several phases of graben faulting. The latter outlined the Gregory rift, the density of faults formed at that time being about 2-3 faults per km. At the same time major volcanoes appeared to the east of the rift such as the Kenya, Kilimanjaro and Kulal.

Late Quaternary (1-0 m.y).

In the later Quaternary, trachyte, basalt-trachyte and phonolite caldera volcanoes built up axially in the floor of the inner graben, while in areas well to the east of the rift there were extensive basaltic eruptions in three main areas forming linear multicentre volcanic centres.

The central part of the Gregory rift is very important because it is the geometric centre and the zone of the highest volcanic productivity. The formation of the Gregory rift has been explained in several ways, as a result of crustal doming, crustal streching and thinning (Girdler et al., 1969) and as a zone of crustal rupture and injection of igneous rocks (McKenzie, 1970). Baker and Wohlenberg (1971) believe that the Kenya rift valley should be regarded as a typical example of the first stage of continental break up. The geological data are consistent with maximum crustal disruption and basic igneous intrusion during the Upper Miocene.

The intense faulting and volcanism along the Kenyan rift enabled the formation of several geothermal fields, one of which is the geothermal field of Olkaria.

6.4. Geology and tectonics of Olkaria.

Olkaria is one of the several volcanic centres along a N-S belt in the East African Rift Valley. This belt includes Mount Suswa to the South and the Eburru volcanic complex to the North.

Petrological data indicate that the products of the eruptions are predominantly alkali volcanics of rhyolite to trachyte composition

together with calc-alkaline basalts and rare dacites.

Volcanicity in the Rift Valley is approximately symmetrical with respect to the Rift axis. Volcanoes in areas West of the axis, such as Olkaria, were found to be about 2-7 m.y old (Girdler et al., 1969). Massive eruptions of trachytic ignimbrites in the Naivasha sector of the Rift floor occured during the late Pliocene times (Baker and Wohlenberg, 1971).

Normal faulting occurs mainly in N-S, ENE-WSW directions, but also in NW-SE directions. The N-S structures are associated with the dominant trend of the Rift-floor faulting, while the ENE-WSW trending is related to the Olkaria fault zone. The major N-S, NW-SE, ENE-WSW structures in Olkaria, are the Ol Olbutot fault, the Suswa lineament and the Olkaria fault respectively.

Surface mapping by Naylor (1972) identified the Olkaria area as the remnant of an old caldera complex, subsequently cut by north-south normal rift faulting which then provided the loci for later eruptions of rhyolitic and pumice domes and the massive flows of soda rhyolitic lavas. Later volcanic activity associated with the Olkaria volcano and the Ol Olbutot fault zone produced rhyolitic and pumiceous obsidian flows. Naylor's interpretation was not universally accepted but Virkir (1985) defended Naylor's ideas and presented a very well documented hypothesis based on the work of others. The only difference was that Virkir (1985) placed the trace of the caldera further to the west than initially anticipated by Naylor, who placed the caldera boundary along the N-S Olkaria fissure (Fig.6.1c, page 186). This ring structure was also proposed by Woodhall (1987).

Geological mapping and stratigraphic data from about 50 deep

wells (KLPC, 1986) invoke the following structure for Olkaria :

(i). The surface is covered by Quaternary pyroclastics, tuffs and volcanic ash except in erosion gullies where the predominantly alkali-rhyolites are exposed. The tuffs and pyroclastics display intense hydrothermal alteration and a wide range of textures and composition, from highly porous, scoracious basaltic tuff to chaotic moderately coarse rhyolitic lithic tuff, to indurated distinctly welded tuffs.

(ii). The superficial deposits and pyroclastics are underlain by a composite pile of subaerial volcanic lavas and associated pyroclastic rocks of rhyolitic, trachytic and basaltic compositions about 2000 m thick.

(iii). Up to the maximum drilled depth of 2600 m no common basement, intrusive rocks or any major unconformity have been identified.

The description of the various volcanic lavas encountered in Olkaria can be summarized as follows :

Rhyolites

Rhyolitic lavas, obsidian flows and intercalated rhyolitic tuffs and pyroclastics are encountered in most of the boreholes in the upper 300-500 m. Intercalated tuffs are generally poorly indurated chaotic and variably oxidized. This formation appears to be thickest in the north and northeast.

Trachytes

Trachytes are the dominant lavas throughout the thick volcanic sequence and show the most variation in thickness across the field.

Basalts

Basalts were encountered over a wide depth range in the exploration wells and show variation in thickness. In the East

Production field basalts are encountered at about 500-700 m depth while to the NW of the East field they were encountered at about 1000 m depth. To the west at the well locations OW601, OW301 (Fig.6.1c, page 186), basalts have a thickness of 700 and 300 m respectively.

6.5. Geophysical investigations in the Kenyan Rift Valley.

For more than eight decades the Kenyan rift valley has attracted the interest of Earth scientists. Most of the geophysical surveys which have been undertaken have been concerned with the understanding of the nature and mechanism of rifting.

Geophysical investigations in the Kenyan rift were initiated with the pioneering gravity work of Bullard (1936). Long wavelength negative Bouguer and isostatic anomalies were found over the Kenyan dome with narrower negative anomalies over the rifts themselves.

McCall (1967) made a gravity survey in the Gregory rift between 0.5°N and 0.5°S and found a positive Bouguer anomaly over the rift floor. The positive anomaly is superimposed on the negative one which extends over the rift shoulders. Searle (1970) found the same positive anomaly to extend over a large section of the rift and he interpreted it as resulting from an axial crustal intrusion of partially molten mantle material.

Baker and Wohlenberg (1971) derived the same conclusions from their gravity modelling results along a profile south of Menengai. The ideas they developed for an asthenosphere penetrating the lithosphere to within 20 km of the earth's surface were confirmed with the results of several seismic surveys.

Griffiths et al. (1971) with their seismic refraction experiment observed an anomalous crust limited to a narrow zone along the rift axis. For depths of 3-25 km their model consisted of a high p-wave velocity zone (6.4 km/s) in comparison with the velocity of about 5 km/s of normal continental crust. This zone was underlain by a medium with p-wave velocity of 7.5 km/s which is intermediate between that of normal crust and normal mantle. These zones correspond to the low density blocks found by Searle (1970), of 3.0 g/cm^3 and 3.2 g/cm^3 respectively.

Long et al. (1972) derived a crustal model for the region by studying local and regional earthquakes recorded at seismic stations sited west of the Gregory rift, in Kaptagat. They concluded that the anomalous zone deepens from its crustal intrusion along the rift axis, to lie beneath normal sub-Moho material on the flank. A composite model consistent with these published gravity and seismic results was given by Banks and Ottey (1974) and is redrawn in Fig.6.2 (page 196).

The low velocity, low density zone below 20 km was also confirmed by the geomagnetic deep sounding studies of Banks and Ottey (1974), Beamish (1977), Rooney and Hutton (1977), Banks and Beamish (1979). The study of Parkinson induction arrows indicated electric current concentration below and along the central part of the rift valley. Banks and Ottey (1974) derived a two dimensional conductivity model for the region constrained by the gravity and seismic results. Their model (Fig.6.3, page 196) involved a sub-rift zone of 10 Ohm.m at 20 km depth with, in addition a thick slab (100 km) of material with resistivity 20 Ohm.m at a depth of 50 km beneath the eastern flanks of the rift. The lateral extent of

the latter was several hundred kilometres. The two low resistivity regions were interpreted as zones of partial melting in the upper mantle coinciding with regions of Quaternary volcanism.

The magnetotelluric study of Rooney (1977) and Rooney and Hutton (1977) provided independent evidence for the existence of high conductivities at depths corresponding to the upper mantle below the Kenyan rift. Maximum resistivities were found to lie between 2 and 20 Ohm.m. With their two dimensional modelling studies showed that the magnetotelluric data require the presence of conductive material at a depth of less than 8 km below the rift. The great thickness of this upper crustal conductor was explained not only in terms of the conductive infill of the rift but also in terms of high temperatures and water saturation of the crust. Conductive material was also required at depths greater than 30 km but the top and the thickness of the upper mantle conductor could not be resolved because of the obscuring effect of the crustal conductor. The derived electrical models (Rooney and Hutton, 1977) are shown in Fig.6.4.

6.6. Geophysical investigations in Olkaria.

During the last two decades many geophysical investigations employing several methods such as, D.C resistivity, gravity, aeromagnetics, seismic refraction and magnetotellurics have been undertaken in the Olkaria region. Interpretation of the recent D.C resistivity and aeromagnetic results, together with a re-evaluation of already existing D.C resistivity and gravity data has provided the integrated geophysical model shown in Fig.6.5 (page 196).

Fig.6.2. An integrated geophysical model for the Kenyan Rift Valley (After Banks and Ottey, 1974).

Fig.6.3. A conductivity model for the Kenyan Rift Valley (After Banks and Ottey, 1974).

Fig.6.4. Two dimensional magnetotelluric models for the Gregory Rift Valley. Computed one and two dimensional apparent resistivity versus period curves for the three electrical models shown (After Rooney and Hutton, 1977).

Fig.6.5. An integrated geophysical model for Olkaria (After Mwangi and Bromley, 1986). The model is based on aeromagnetic and D.C resistivity data.

Fig.6.2

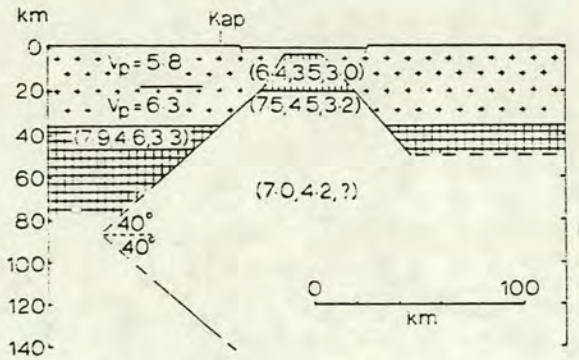

Fig.6.3

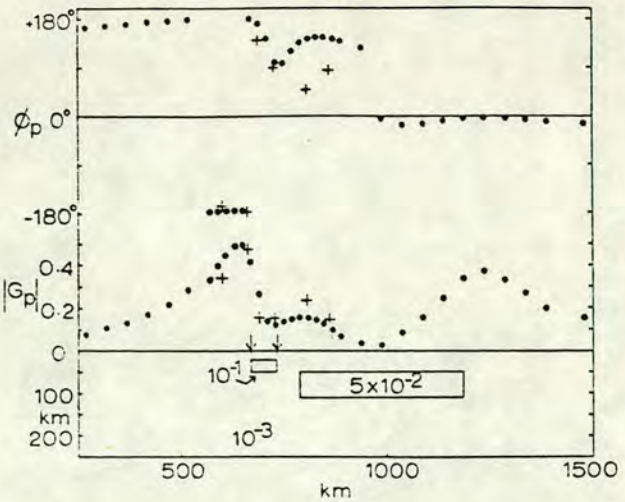

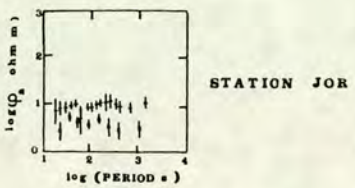

Fig.6.4

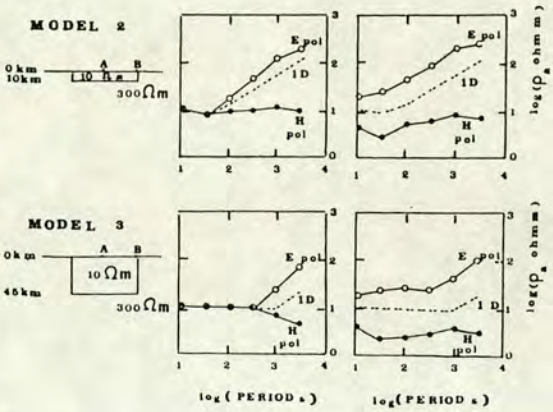

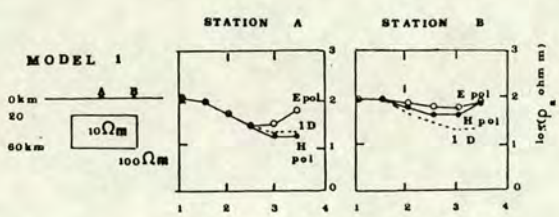

Fig.6.5

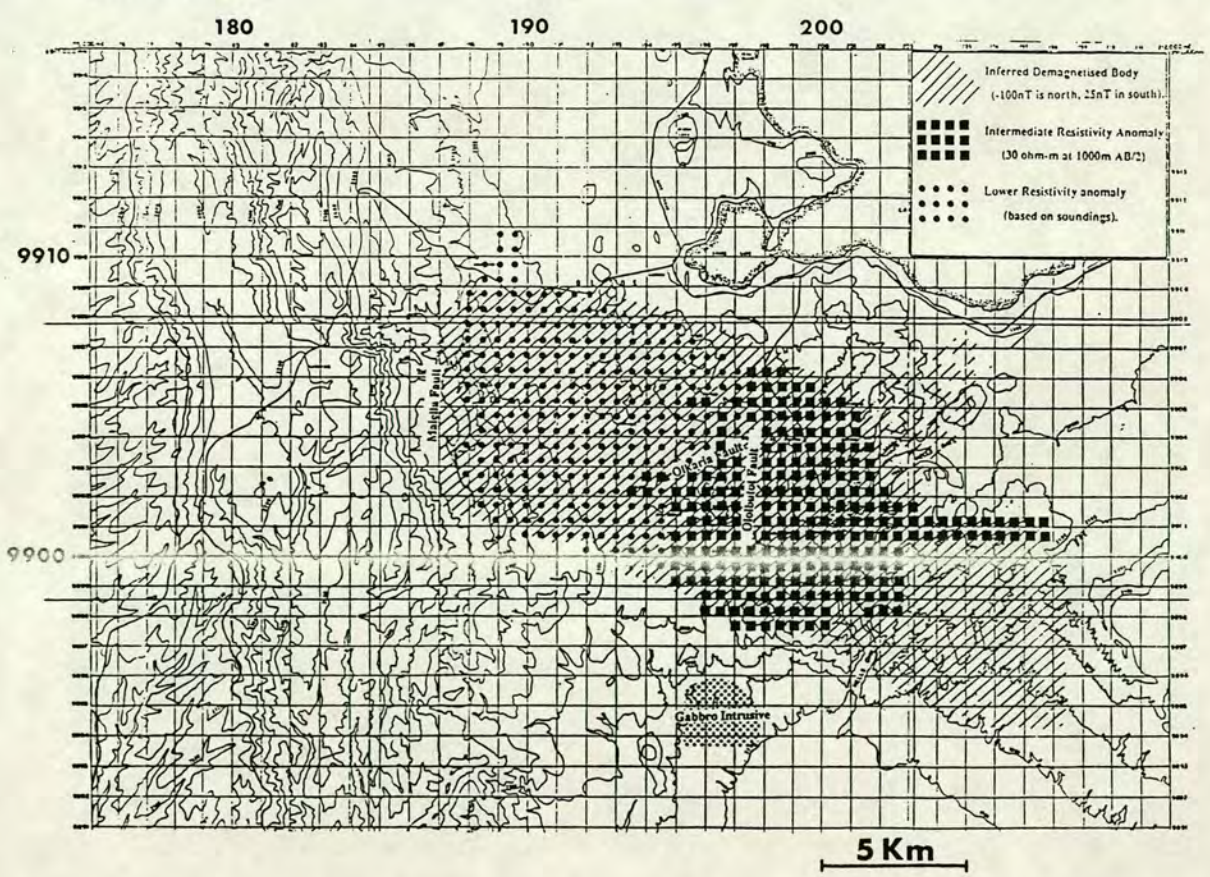

Petrographic analysis of well cores and cuttings together with the geophysical results provided a possible hydrological model for the geothermal field (Mwangi and Bromley, 1986) - Fig.15 of Appendix II.

A Roving dipole (Group Seven, 1972), a Dipole-dipole and five Schlumberger sounding surveys (Group Seven, 1972 ; Furgerson, 1972 ; Bhogal, 1980 ; Mwangi, 1983 ; Mwangi, 1986) provide the D.C resistivity data for the Olkaria region.

Resistivity modelling was based only on the five Schlumberger sounding surveys considered the most reliable and easily interpreted (Mwangi and Bromley, 1986). Most of the Sclumberger soundings investigate to a depth of 1000-1500 m which is not adequate to determine the dimensions of the Olkaria geothermal field. It defines only the shallow conductive or resistive anomalies. However resistivity contour maps for AB/2 equal to 500 m, 1000 m and 1500 m were presented. All contour maps show an extensive zone of low resistivities (< 30 Ohm.m) extending from the Suswa lineament in the west to the east and southeast of the Ol Njorowa gorge (Hell's Gate). The northern and southwestern boundaries of the low resistivity zone correlate with the boundaries of the positive magnetic anomaly observed in Olkaria.

A pilot gravity survey was carried out by Leicester University in Olkaria during 1971. The results from these investigations were supplemented by large scale gravity measurements undertaken by Swain and Khan (1977). A localized positive anomaly south of the present Power Plant was explained as a small basalt or gabbro intrusive. Weak positive anomalies are observed over Olkaria Peak and southwest of the Gorge Farm Fault correlating with the local topography. To the

west and the northwest of Olkaria, a steep negative gradient was explained as the possible expression of deep structural features associated with the rift faulting and partly reflecting a thickening, near surface impermeable layer of pyroclastics.

An aeromagnetic survey was carried out by GENZL during 1986 and interpreted by Van Dijck (1986). A broad positive magnetic anomaly trending WNW-ESE bounded by two negative anomalies to the north and south was interpreted as resulting from a demagnetized body extending almost directly below the positive anomaly. The demagnetized body could be explained either lithologically as a sequence of essentially non-magnetic trachytes, rhyolites and tuffs or geothermally from alteration of magnetite to non-magnetic pyrite and haematite or thermally if temperatures were above the Curie point of magnetite (575°C).

Recently a regional seismic refraction survey was undertaken along a N-S direction. This indicated that the deep N-S axial rift intrusive under Olkaria lies at about 6-10 km depth. The velocity structure of the overlying rocks suggests that the high formation porosity observed in the Olkaria field probably continues to depths greater than already drilled.

Electromagnetic (Group 7 Inc, 1972) and magnetotelluric measurements undertaken by GEMP cover a limited period range of 10-64 secs and therefore were inadequate for interpretation. However more recently magnetotelluric soundings have been carried out by Geotermica Italiana over an area east of Olkaria and close to Longonot volcano. The results are not yet available in the literature but the general conclusions have been provided to aid the modelling

of the University of Edinburgh Olkaria magnetotelluric study (Mwangi, 1989, private communication).

CHAPTER 7

THE OLKARIA CASE STUDY : THE MAGNETOTELLURIC SURVEY.

7.1. Introduction.

Olkaria is one of the most interesting geothermal areas in the central Kenya Rift Valley. The eastern part of the field is currently exploited and it is known as Olkaria East. The present interests of the Kenyan Power Company Ltd. (KPC) are associated with the potential exploitation of the western and northeastern parts of the field.

The upper 10 km of the crust below Olkaria had previously been mapped by several geophysical methods such as, gravity, aeromagnetics, D.C resistivity and deep seismic refraction. Temperature measurements had also been made in several deep or shallow boreholes.

Most of the methods could not reveal the deeper lithospheric structure. This was the main objective of the work described below. In particular, the University of Edinburgh in collaboration with the KPC carried out a broadband magnetotelluric survey in Olkaria where the author was one of the participants during the fieldwork, data analysis and modelling.

The present chapter deals mainly with the dimensionality tests applied to the magnetotelluric data and some limited two dimensional forward calculations concerning the deep electrical structure in the Olkaria region. A full description of the data collection and analysis procedures together with the results and interpretation of

the one dimensional modelling can be found in the report submitted to KPC by Hutton et al. (1989) attached at the back of the present work as Appendix II.

7.2. Data collection and analysis.

Between 1 February and 15 March 1989, a broadband magnetotelluric survey was undertaken in the region of Olkaria geothermal field. In particular, 30 SPAM (AMT) soundings in the range 10^{-2}-10^{+2} secs were conducted along 4 approximately linear profiles. Three of these had a NE-SW direction while the fourth one was crossing the other three in a WNW-ESE direction (see Appendix II, Fig.1c). At 9 of these sites, a broader period range was used (AMT-LMT, 10^{-2}-10^{+4} secs). Three component EDA fluxgate magnetometers were operated for recording signals in the longer period (LMT) range 10^{+2}-10^{+4} secs. A detailed description of the fieldwork procedures and the instrumentation, are given in Appendix II and the station coordinates are given in Table 7.1.

The magnetotelluric data were reprocessed on the mainframe computer system of the University of Edinburgh, using the same acceptance criteria as for the Milos study. For the LMT period range the data processing additionally included time series window selection undertaken in real time for the SPAM period range. The frequency variations of the apparent resistivity and phase responses were computed along the measuring and principal directions and the invariant (see section 4.3.(iii)). In addition the vertical magnetic field measurements enabled estimation of the real and imaginary vertical magnetic field response functions and their

azimuths. A detailed discussion on these aspects with examples is given in Appendix II.

TABLE 7.1

Magnetotelluric stations in Olkaria : coordinates

No	Site	Elevation m	National Grid X	Y	No	Site	Elevation m	National Grid X	Y
1	910	2060	197.92	9898.65	16	926	2220	201.45	9906.70
2	911	1880	202.30	9902.90	17	927	2120	198.65	9903.95
3	912	1895	203.40	9903.50	18	928	2040	202.40	9907.35
4	913	1870	201.90	9901.95	19	930	2000	195.30	9905.70
5	914	1860	201.50	9901.05	20	931	1980	197.70	9906.50
6	915	1890	200.80	9900.15	21	932	1980	196.65	9906.05
7	916	1900	200.50	9899.50	22	933	2040	193.20	9902.40
8	917	2030	195.30	9899.30	23	934	2080	193.90	9903.15
9	918	2160	196.40	9899.55	24	935	2060	192.35	9901.70
10	919	1960	199.40	9899.00	25	936	2120	191.55	9901.45
11	921	2040	194.75	9900.40	26	937	2140	190.70	9900.55
12	922	2160	197.15	9902.55	27	938	2020	194.35	9904.00
13	923	2040	193.25	9899.15	28	939	2000	194.80	9904.90
14	924	2120	200.16	9905.30	29	941	2000	199.40	9901.70
15	925	2240	201.00	9906.00	30	961	2060	191.70	9903.75

No=Number

7.3. Interpretation of the major and minor apparent resistivity and phase responses.

The magnetotelluric sites in Olkaria were clustered according to their major and minor apparent resistivity and phase responses into three clusters. These clusters are enclosed in solid lines on the maps of Figs.7.1a-b and are named O1, O2 and O3 respectively. Each cluster is represented by one or more sites. The major and minor responses in each of the presented examples are illustrated with thick and thin solid lines respectively.

Western Olkaria is represented by cluster O1. This region

includes all the magnetotelluric sites of Profile 3 and the two southwestern sites of Profile 2 (see Appendix II, Fig.1c). This region is characterized by the lowest resistivities (< 15 Ohm.m) observed in Olkaria within the frequency range of 1-0.1 Hz. The observed conductor is associated with the Olkaria West potential field (see Appendix II, section 7). Clusters O2 and O3 represent the central and eastern Olkaria. Cluster O3 includes the central sites of Profile 1 (see Appendix II, Fig.1c). Most of the magnetotelluric sites of this region show low resistivities (< 10 Ohm.m) within the higher frequency range 100-10 Hz. Cluster O3 corresponds to the currently exploited Olkaria geothermal field.

All the sites of cluster O2 have resistivities of 10-100 Ohm.m through the whole recorded frequency range. Cluster O2 includes Olkaria Peak, the Ol Olbutot fault and the region north of the Olkaria fault (Appendix II, Figs.1a-b). The higher resistivities observed in this region correlate with the proposed zone of cold water flow (KPLC, 1986 ; see also Appendix II, Fig.15).

7.4. A dimensionality test for the magnetotelluric data.

The same dimensionality parameters used in the Milos study were also applied on the magnetotelluric data collected in Olkaria. These tests were carried out at the premodelling stage to facilitate interpretation.

The relevant theory has been presented in section 4.5. Results for two of the Olkaria sites 911 and 935 are now discussed. They are typical of the results of the majority of the Olkaria sites.

Fig.7.1. Representative sites from the magnetotelluric survey in Olkaria. Sites are clustered according to similar responses and one or more representative sites are shown for each cluster. Clusters are enclosed in solid lines and are named with letters or a letter and a number on map. The major (thick solid lines) and minor (thin solid lines) apparent resistivities and phases are plotted.

a. Olkaria West (O1).

b. Central Olkaria (O2) and Olkaria East (O3).

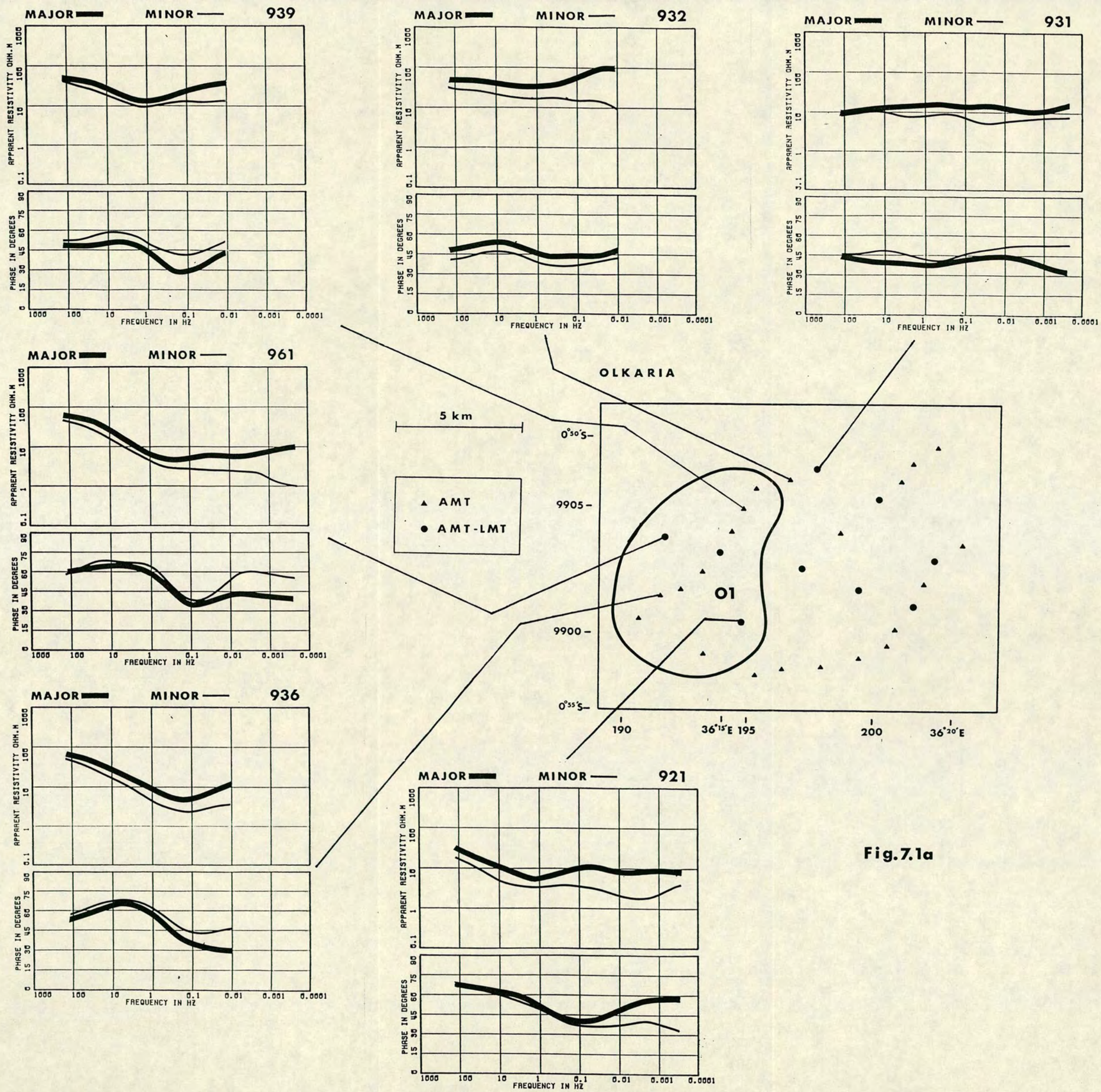
MAJOR
MINOR
939
932
931
961
936
921
APPARENT RESISTIVITY OHM.M
PHASE IN DEGREES
FREQUENCY IN HZ
OLKARIA
5 km
AMT
AMT-LMT
01
0°50'S
0°55'S
9905
9900
190
195
200
36°15'E
36°20'E

Fig.7.1a

Figs.7.2a-d and 7.3a-d show the frequency variation - of the apparent resistivity and phase responses along the measuring and principal directions - coherence and number of estimates - azimuth of the major apparent resistivities for the AMT-LMT station 911 and the AMT station 935 respectively. From visual inspection of the raw curves the following conclusions are derived. In 911 the rotated curves are nearly isotropic in the range 10^{+2}-1 Hz and then become anisotropic at the lower frequencies.

Figs.7.4, 7.5 (page 211) illustrate the 6 dimensionality indices, for sites 911 and 935 respectively. The skew α, D_3 and D_3' at both sites are very low, less than 0.2, within the range 10^{-2}-10^{+2} secs. At site 911 the same parameters show an increase with period of up to 0.3-0.5. The one dimensional condition $D_1 > D_2 > D_3$, D_3' is upheld by both the data sets while in 911 at the longer periods the drop of D_1 to lower values (0.5-0.6) is associated with a drop of D_2 to lower values of about 0.2 and the increase of D_3 up to 0.3. Eccentricity $|\beta(\Theta_0)|$ shows a uniform pattern and approaches near-zero values in 911 with the exception of some high values up to 0.6 at the longer periods. In 935 the same parameter has non-zero scattered values. The near-zero values of eccentricity have been interpreted in section 4.5 as indicative of two dimensionality. The scattered non zero values of the same parameter were explained as due to two or three dimensional effects. Fig.7.5 shows that when strong three dimensional effects are present eccentricity shows rather a uniform non-zero pattern. D_1 at both sites lies between 1.0 and 0.6 and decreases with period increasing. The nine inequality constraints of Weidelt are upheld with total percentages of 83.33% and 86.32% for

Fig.7.2. The magnetotelluric data at site 911.

a. Frequency variation of the unrotated magnetotelluric responses.

b. Frequency variation of coherence and number of estimates.

c. Frequency variation of the rotated magnetotelluric responses.

d. Frequency variation of the azimuth of the major apparent resistivities.

Fig.7.3. The magnetotelluric data at site 935.

a. Frequency variation of the unrotated magnetotelluric responses.

b. Frequency variation of coherence and number of estimates.

c. Frequency variation of the rotated magnetotelluric responses.

d. Frequency variation of the azimuth of the major apparent resistivities.

Fig.7.2

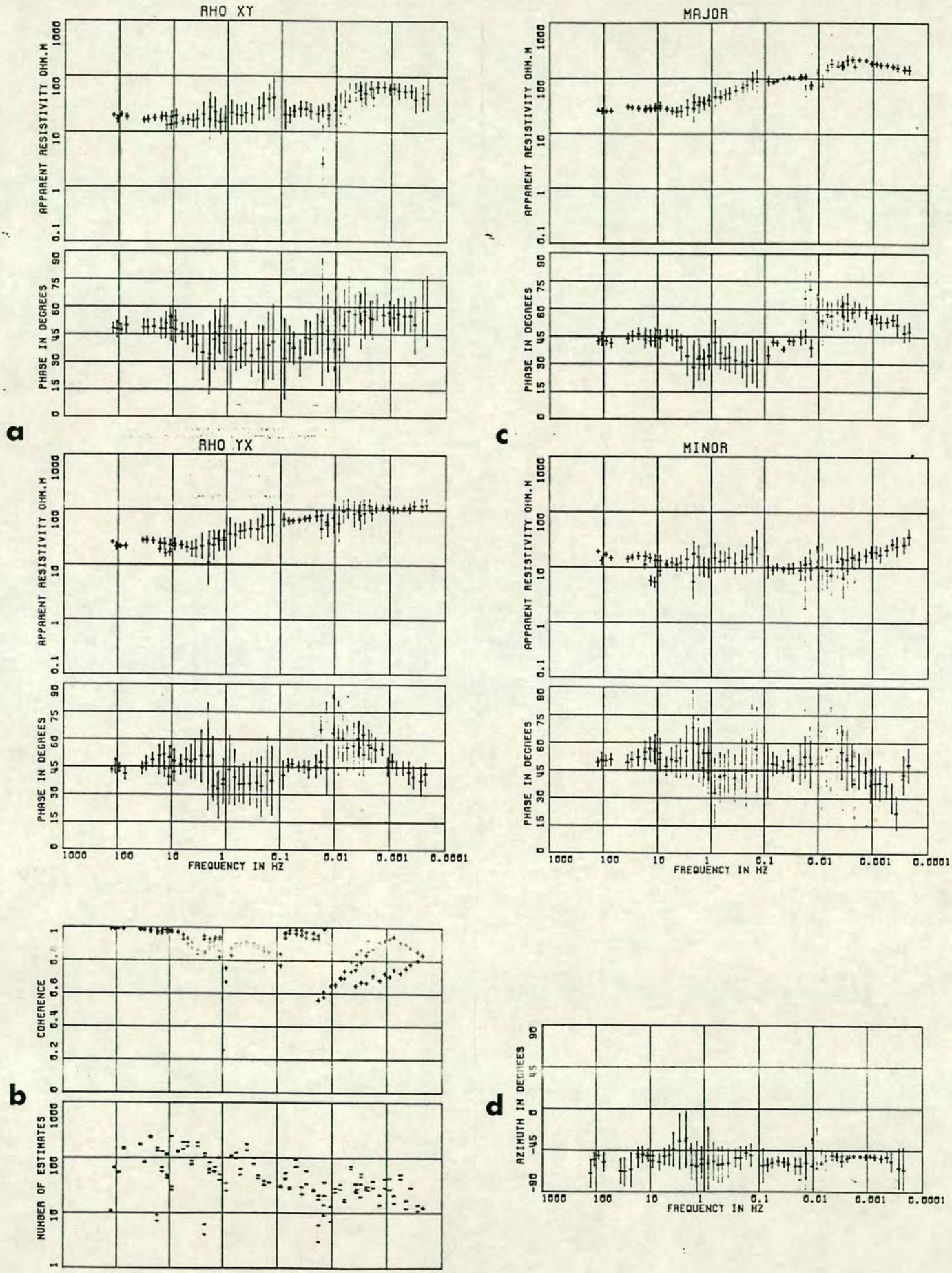
RHO XY
APPARENT RESISTIVITY OHM.M
1000
100
10
1
0.1
PHASE IN DEGREES
0
15
30
45
60
75
90
a
RHO YX
APPARENT RESISTIVITY OHM.M
PHASE IN DEGREES
1000
100
10
1
0.1
0.01
0.001
0.0001
FREQUENCY IN HZ
MAJOR
APPARENT RESISTIVITY OHM.M
PHASE IN DEGREES
c
MINOR
APPARENT RESISTIVITY OHM.M
PHASE IN DEGREES
FREQUENCY IN HZ
COHERENCE
0
0.2
0.4
0.6
0.8
1
b
NUMBER OF ESTIMATES
1000
100
10
1
AZIMUTH IN DEGREES
90
45
0
-45
-90
d
FREQUENCY IN HZ

Fig. 7.3

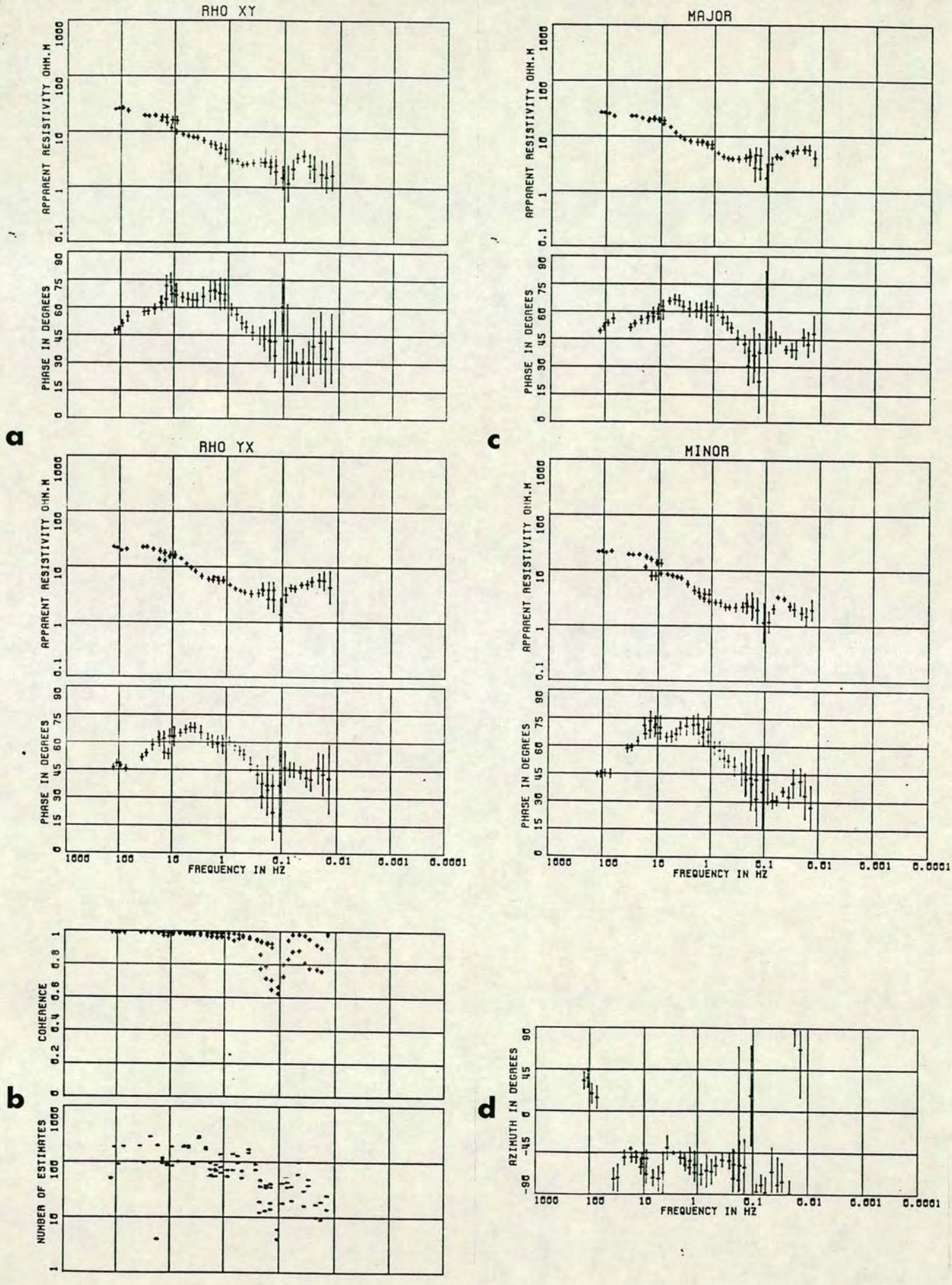
a
RHO XY
APPARENT RESISTIVITY OHM.M
1000
100
10
1
0.1
PHASE IN DEGREES
0
15
30
45
60
75
90
b
RHO YX
APPARENT RESISTIVITY OHM.M
PHASE IN DEGREES
FREQUENCY IN HZ
1000
100
10
1
0.1
0.01
0.001
0.0001
c
MAJOR
MINOR
COHERENCE
0
0.2
0.4
0.6
0.8
1
NUMBER OF ESTIMATES
1000
100
10
1
d
AZIMUTH IN DEGREES
-90
-45
0
45
90

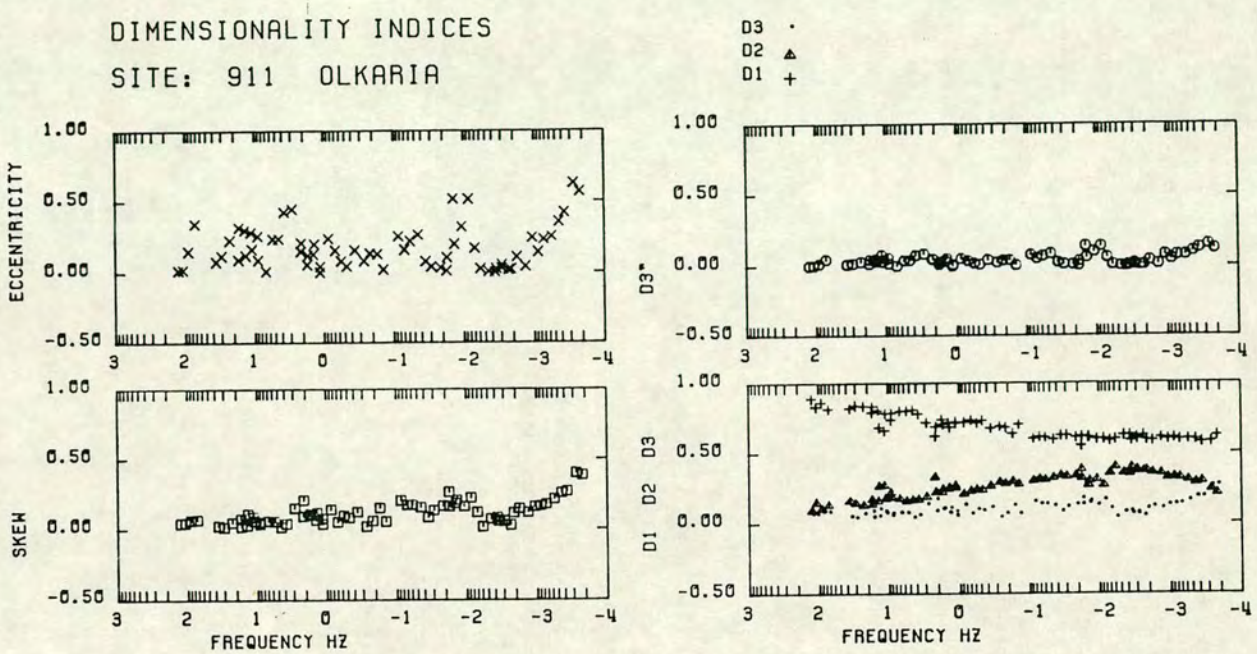

Fig.7.4. Dimensionality indices for site 911.

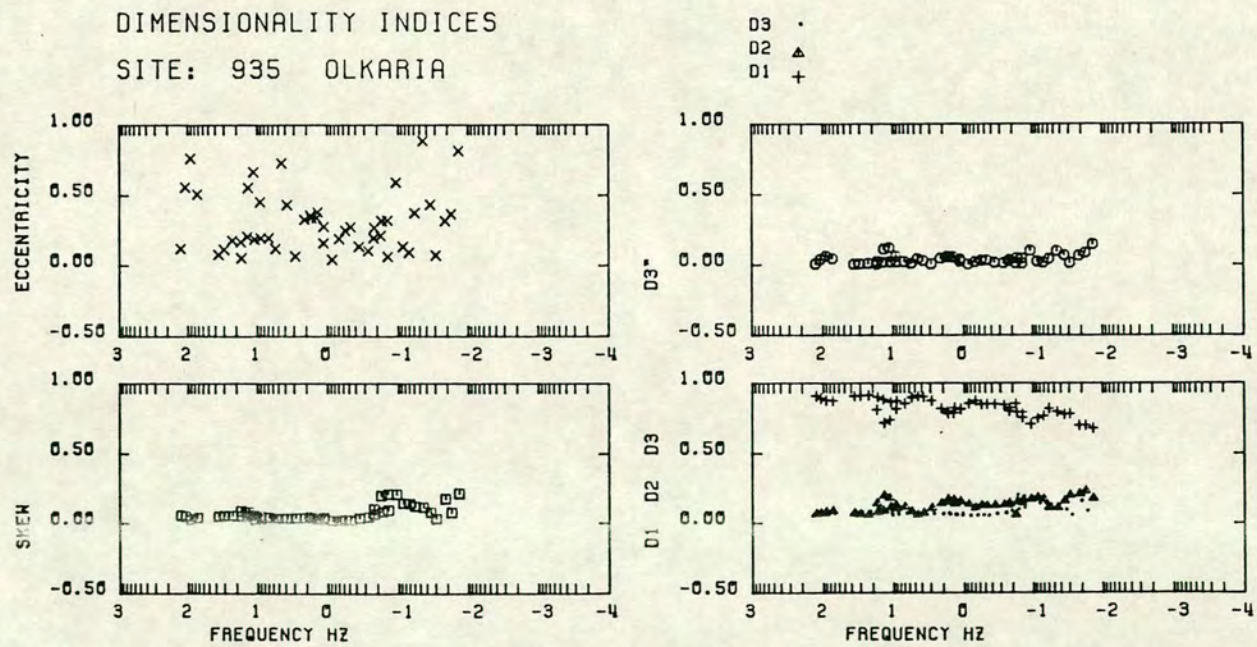

Fig.7.5. Dimensionality indices for site 935.

911 and 935 respectively.

The general conclusions from the dimensionality tests at all the observation points could be summarized as follows :

(i). Skew varies from values of 0.0 to 0.2, in general but there are sites where it displays a maximum of 0.5 at longer periods.

(ii). The eccentricity shows similar patterns to those observed in the Milos study but a uniform non-zero pattern is now observed for three dimensional structures.

(iii). The one dimensional condition $D_1 > D_2 > D_3, D_3'$ is valid at most of the sites for the higher frequencies but indices D_2, D_3 and D_3' display high values at many sites but at lower frequencies confirming the presence of two or three dimensional features.

(iv). The magnetotelluric data along profile 3 are the most isotropic.

(v). The nine inequality constraints of Weidelt are satisfied with total percentages greater than 70%.

(vi). One dimensional modelling is valid for the frequency range 10^{+2}-10^{-1} Hz but two or three dimensional modelling is required when the lower frequencies are taken into account.

7.5. One dimensional modelling.

Since most of the magnetotelluric data were found to be one dimensional for frequencies 10^{+2}-10^{-1} Hz, one dimensional modelling was undertaken as a first approach to the interpretation of the observed responses. This involved preparation of composite resistivity sections along the four profiles of the magnetotelluric

survey in Olkaria (see Appendix II, Fig.1c). Two different modelling procedures were used, the Fischer et al. (1981) algorithm which provides layered earth models and the Niblett-Bostick transformation (Jones, 1983) which provides continuous resistivity-depth profiles. The results from the one dimensional modelling are shown and discussed in Appendix II.

7.6. Two dimensional modelling.

In order to reveal the deeper electrical structure, two dimensional forward computations were carried out along a profile crossing the Kenya Rift Valley. In particular, the forward modelling calculations were associated with the construction of an electrical model reflecting the regional features of the Kenya Rift and the local electrical features of the Olkaria geothermal region.

The modified (Hill, 1987) Brewitt-Taylor and Weaver (1976) two dimensional forward modelling program was used. The relevant background theory, the model construction rules and the computer program description have already been given in sections 4.6.(iii) and 4.6.(iv). The model construction procedures, results and interpretation are discussed in the following sections.

7.6.(i). Two dimensional modelling : Model construction.

Only limited two dimensional modelling has been undertaken to date. The starting model was constrained by the results of the Niblett-Bostick contour sections along profiles 1, 2, 3, and 4 (see

Appendix II, Fig.1c). In addition the results of the magnetotelluric survey undertaken in Longonot by Geotermica Italiana (Mwangi, personal communication) were also taken into account. Due to the limited range of the tested models, the best fit model is interpreted as a preliminary two dimensional electrical model for the Kenya Rift Valley and Olkaria geothermal region.

From visual inspection of the major and minor axes of the magnetotelluric impedance ellipses (see Appendix II, Figs.7a-b) it seems that most of the major axes are oriented approximately along a NE-SW (65°E) direction. The uppermost 10 km of the crust below the central Olkaria have relatively higher resistivities (30-75 Ohm.m) than the surrounding areas (> 15 Ohm.m). It seems that the 25°W direction (normal to 65°E) is the dominant electrical strike.

The two dimensional forward modelling computations were carried out along Profile OO' (Fig.7.6) which crosses the Kenya Rift through Olkaria and along a distance of 150 km in an approximately NE-SW (65°E) direction.

The model resistivity and phase responses were compared with the magnetotelluric field data collected by, Rooney (1977), Geotermica Italiana (Mwangi, personal communication) and data from the present study in Olkaria. These data correspond to the two stations, KER, JOR of Rooney's (1977) study, stations 1 and 3 of the UN study and the stations 923, 961, 934, 922 and 927 of the present study. Stations KER and JOR are located far from Olkaria (> 50 km) and therefore their magnetotelluric responses were used only for reference. The nine observation points were projected on Profile OO' (Fig.7.6). The data of the present study were rotated by an angle of 65°E.

The starting model consisted of a conductive (10 Ohm.m) block

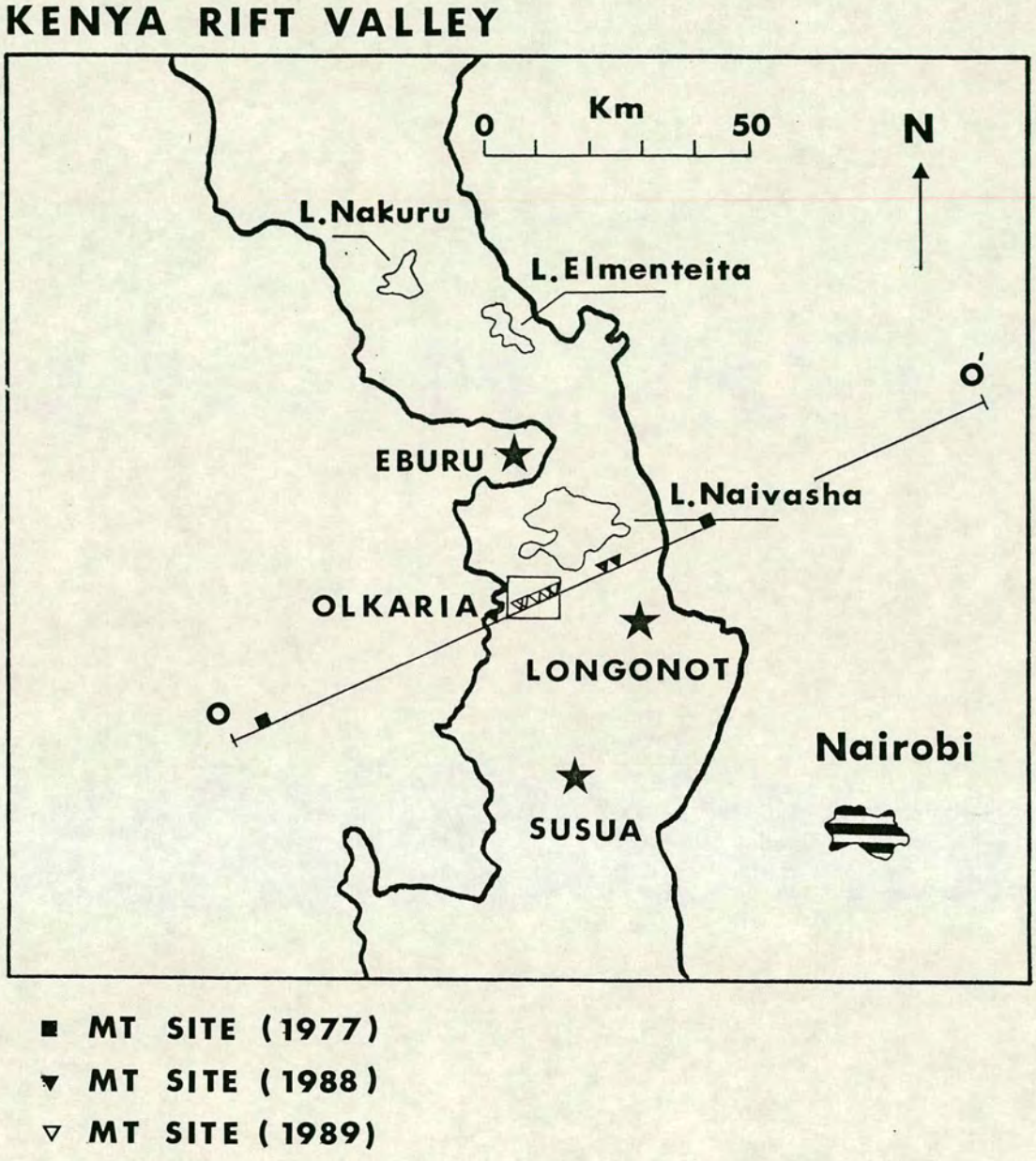

Fig.7.6. Two dimensional modelling along Profile OO'. Profile OO' crosses the Gregory rift approximately in a NW-SE (65°E) direction. Black stars indicate known volcanic centres in the region. The magnetotelluric stations are illustrated with solid squares - Rooney (1977) : solid triangles - Geotermica Italiana (Mwangi, personal communication) ; open triangles - present study.

bounded by two more resistive (300 Ohm.m) blocks. The 10 Ohm.m were assumed to represent the inner part of the Rift. Its boundaries were considered to extend about 5 km to the East and West, beyond the real topographic boundaries of the Rift. A thin layer (300 m) of 50 Ohm.m resistivity was included to represent the more resistive superficial structure.

Fig.7.7a (page 218) shows the starting model OO'-1. Figs.7.8c,e,i and 7.9c,e,i (pages 221-223) illustrate the resistivity and phase responses (dashed lines) of this model at three observation points, 961, 922 and JOR for the TE and TM modes respectively in comparison with the observed apparent resistivity and phase responses.

There is an obvious bad correlation between the computed and observed resistivity and phase curves at site locations 961 and 922 while the fit is acceptable at JOR.

The simple Model OO'-1 (Fig.7.7a) was modified as it is shown in Fig.7.7b in order to obtain a better fit between the model and observed responses at the nine observation points. A block with resistivity of 50 Ohm.m was included below the centre of Olkaria and West of Longonot extending from a depth of about 1 km down to a depth of 8-15 km. Two more conductive blocks of 3 and 6 Ohm.m about 3 and 5 km thick respectively and 13 km wide ware included below the western part of Olkaria. The whole crust and upper mantle below the eastern half of the rift were considered to have resistivity of 10 Ohm.m. The latter was constrained by the fact that the Parkinson arrows for periods 1500-2500 secs (see Appendix II, Fig.8c) seem to point towards a remote conductor probably located NE of Olkaria and the magnetotelluric sounding curves at JOR (Rooney, 1977).

Apparently Model OO'-2 displays a very good fit to the observed data at most of the nine stations of Fig.7.7b as this is illustrated in Figs.7.8a-i, 7.9a-i (solid thin lines) for the TE and the TM modes respectively. Figs.7.8g-h illustrate only the one dimensional magnetotelluric responses provided by Geotermica Italiana (Mwangi, personal communication) since the unrotated responses were not available in such form that they could be rotated.

7.6.(ii). Two dimensional modelling : results.

Model OO'-2 (Fig.7.7b) provides the following electrical structure :

(i). The inner part of the Rift is characterized by relatively low resistivities of about 10 Ohm.m.

(ii). The flanks of the Rift are more resistive, about 300 Ohm.m.

(iii). A more resistive block of 50 Ohm.m, about 20 km wide and 25 km thick with its top at a depth of 1 km extends from Central Olkaria to Longonot volcano.

(iv). A good conductor (3 Ohm.m), 3 km thick and about 13 km wide extends below the western part of Olkaria and overlies a second conductor (6 Ohm.m) about 5 km thick and 13 km wide.

(v). The uppermost 300 m below the inner part of the Rift have relatively higher resistivity of about 50 Ohm.m below the region west of Olkaria and 30 Ohm.m below Olkaria and Longonot in comparison with the deeper structure of 10 Ohm.m.

(vi). The presence of the 50 Ohm.m block below Central Olkaria and east of Olkaria seems to be necessary in order to satisfy the

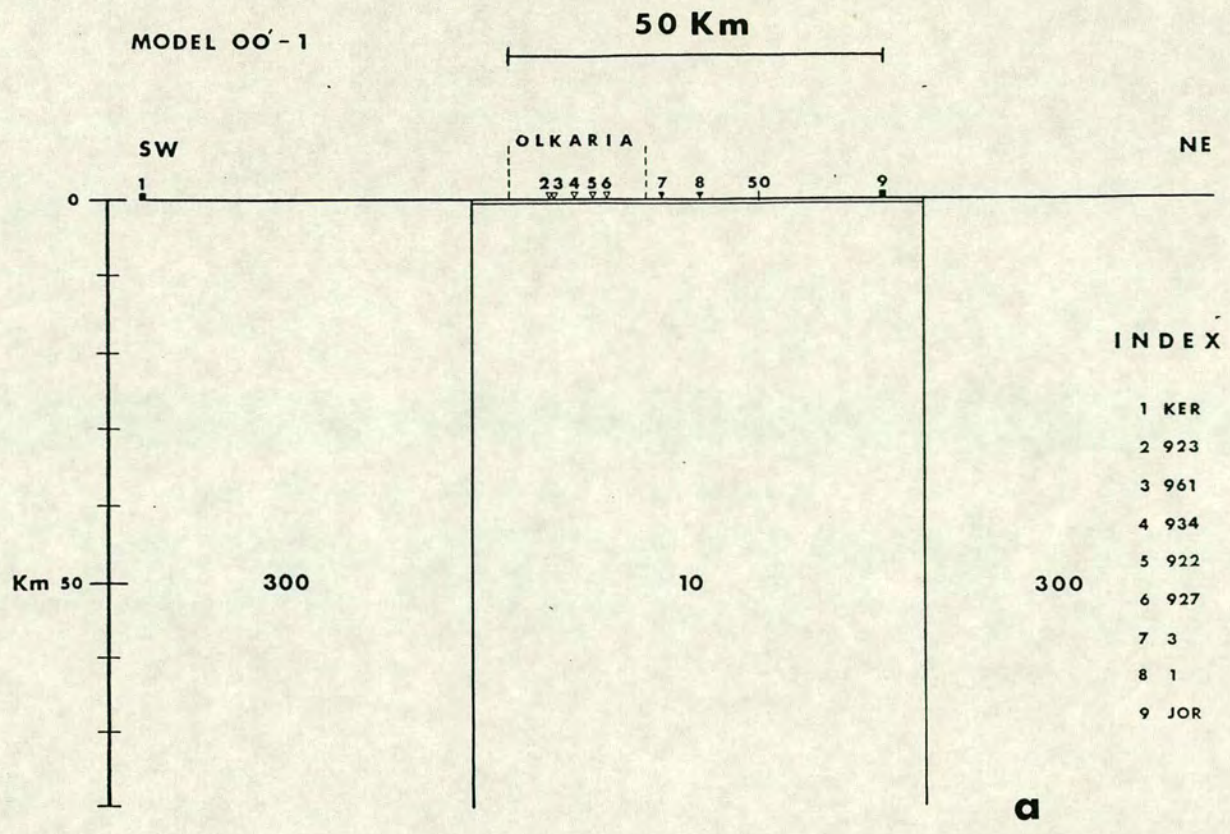

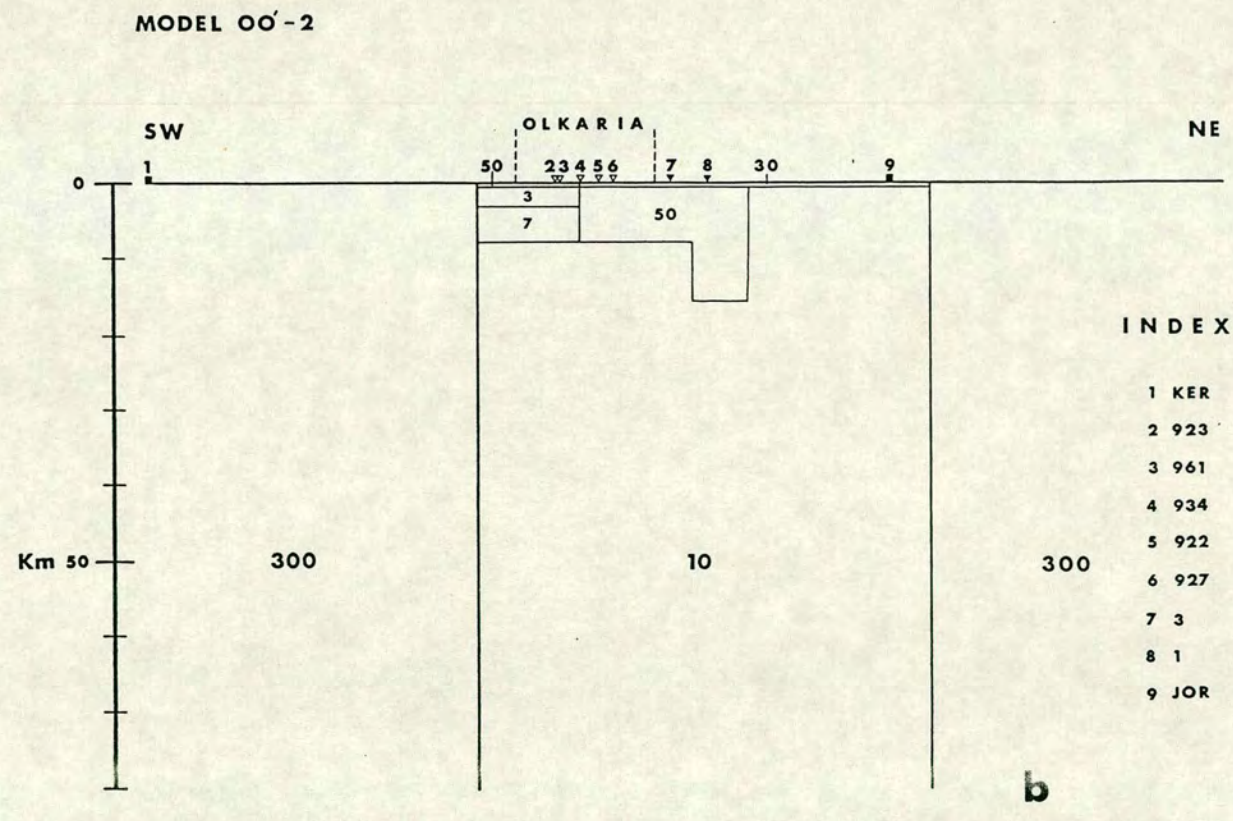

Fig.7.7. Two dimensional magnetotelluric models for the Gregory Rift Valley along Profile OO' of Fig.7.6. The given figures indicate resistivities in Ohm.m.

a. The starting Model OO'-1.
b. The best fit Model OO'-2.

Fig.7.8. Model resistivity and phase responses for the TE mode at nine sites along Profile OO'. The dashed (1) and thin solid (2) lines illustrate the computed responses of Models OO'-1 and -2. The experimental data are indicated with solid error bars. The dashed lines at sites 3 and 1 illustrate the one dimensional responses (1D) provided by Geotermica Italiana (Mwangi, personal communication).

a. Resistivity and phase responses at site KER (Rooney, 1997).

b. Resistivity and phase responses at site 923.

c. Resistivity and phase responses at site 961.

d. Resistivity and phase responses at site 934.

e. Resistivity and phase responses at site 922.

f. Resistivity and phase responses at site 927.

g. Resistivity and phase responses at site 3 (Geotermica Italiana).

h. Resistivity and phase responses at site 1 (Geotermica Italiana).

i. Resistivity and phase responses at site JOR (Rooney, 1977).

Fig.7.9. Model resistivity and phase responses for the TM mode at nine sites along Profile OO'. The dashed (1) and thin solid (2) lines illustrate the computed responses of Models OO'-1 and -2. The experimental data are indicated with solid error bars. The dashed lines at sites 3 and 1 illustrate the one dimensional responses (1D) provided by Geotermica Italiana (Mwangi, personal communication).

a. Resistivity and phase responses at site KER (Rooney, 1997).

b. Resistivity and phase responses at site 923.

c. Resistivity and phase responses at site 961.

d. Resistivity and phase responses at site 934.

e. Resistivity and phase responses at site 922.

f. Resistivity and phase responses at site 927.

g. Resistivity and phase responses at site 3 (Geotermica Italiana).

h. Resistivity and phase responses at site 1 (Geotermica Italiana).

i. Resistivity and phase responses at site JOR (Rooney, 1977).

Fig. 7.8

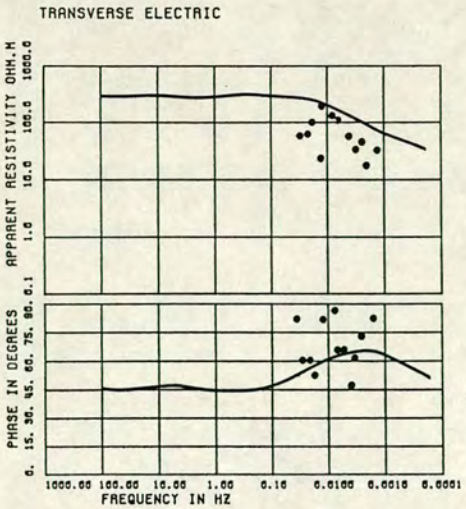

Fig. 7.9

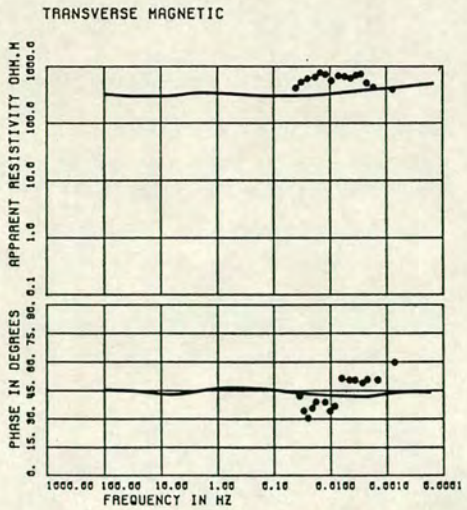

a

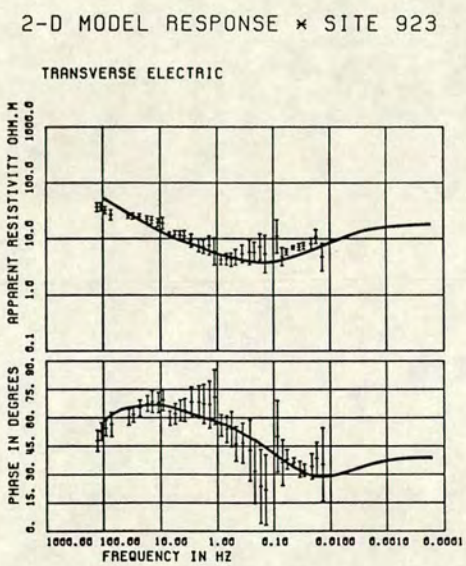

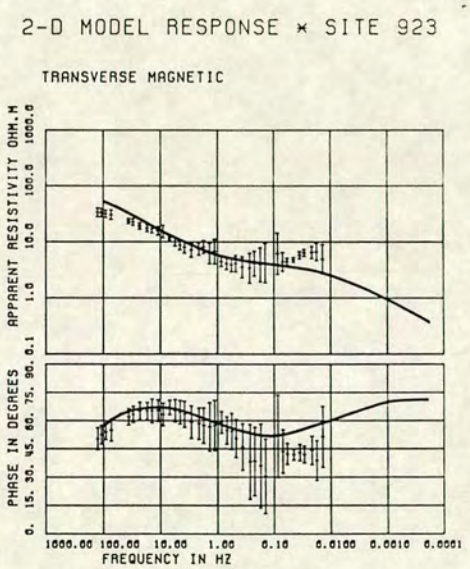

b

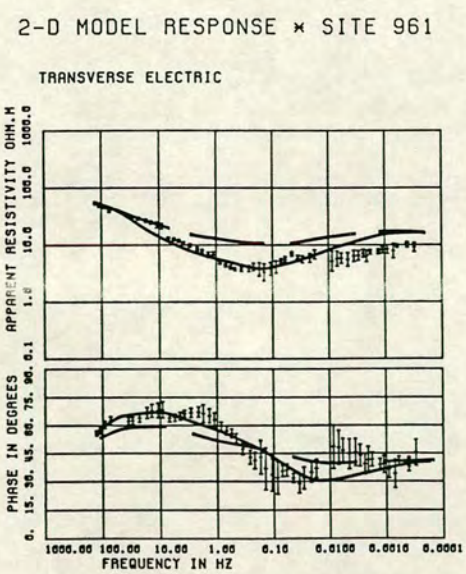

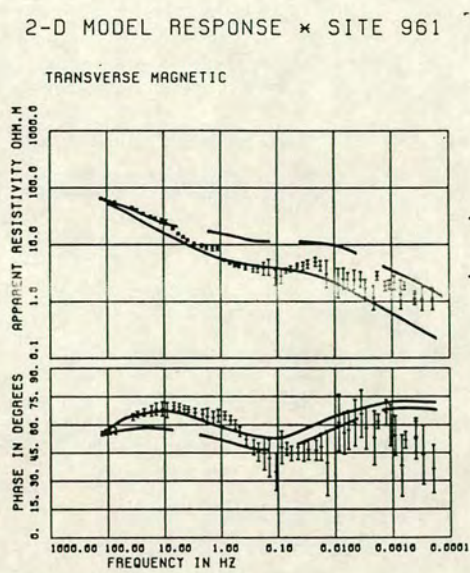

c

Fig.7.8

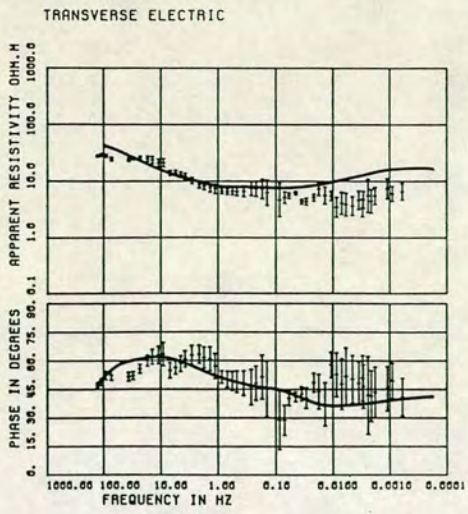

d

Fig.7.9

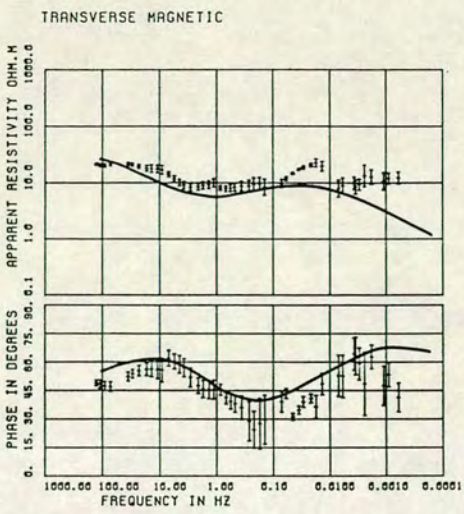

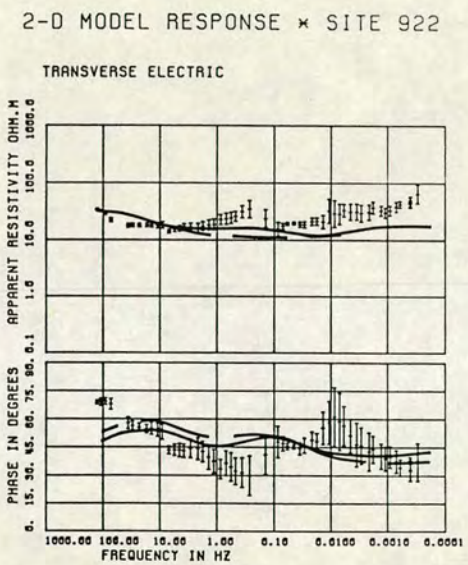

e

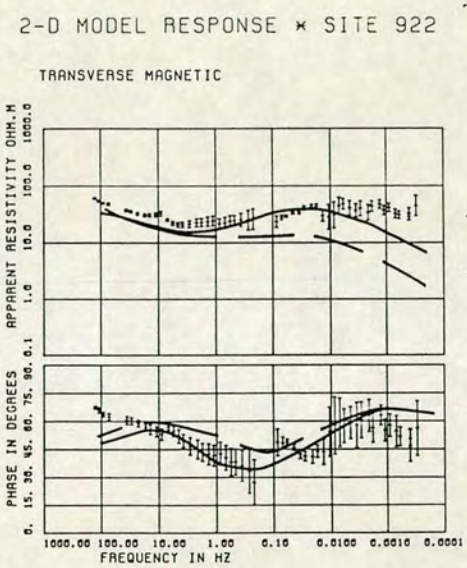

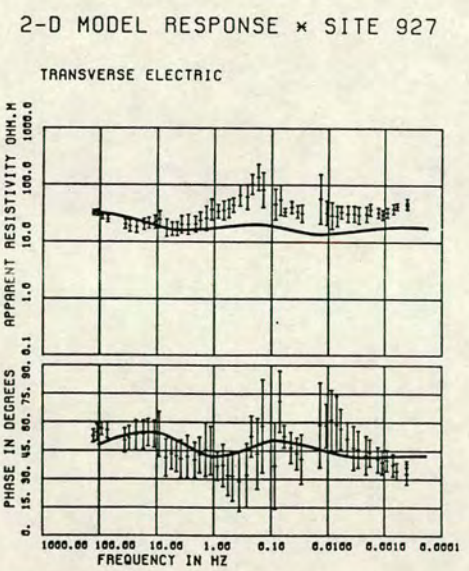

f

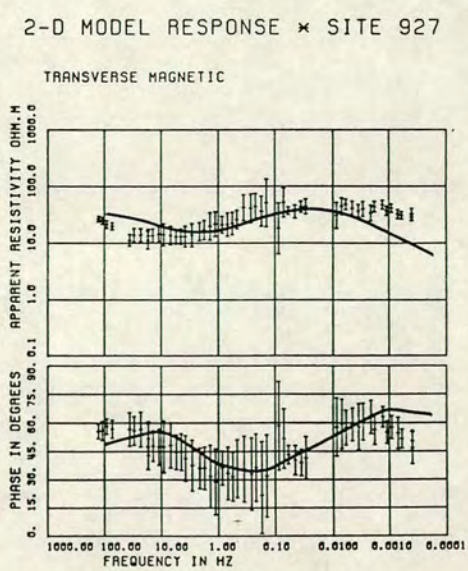

Fig.7.8

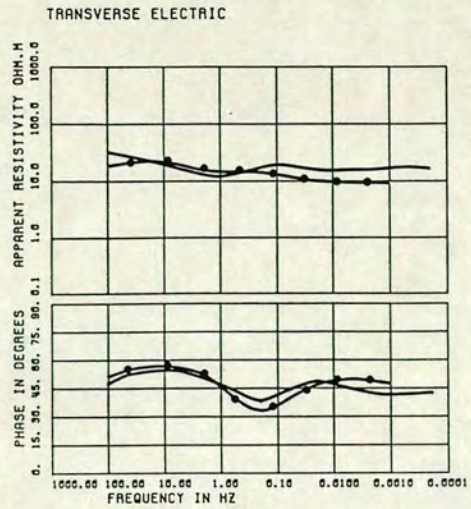

g

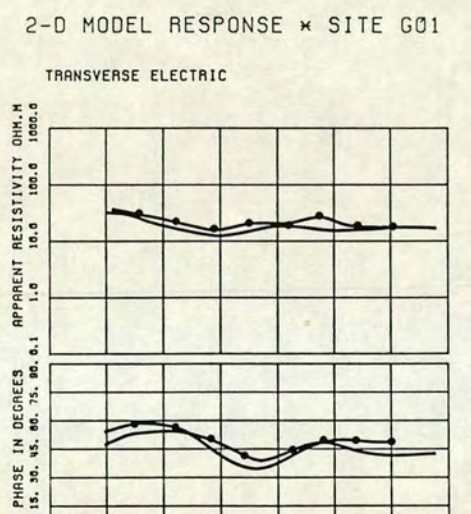

h

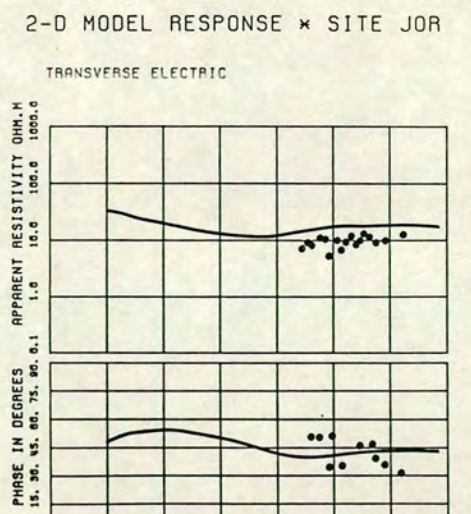

i

Fig.7.9

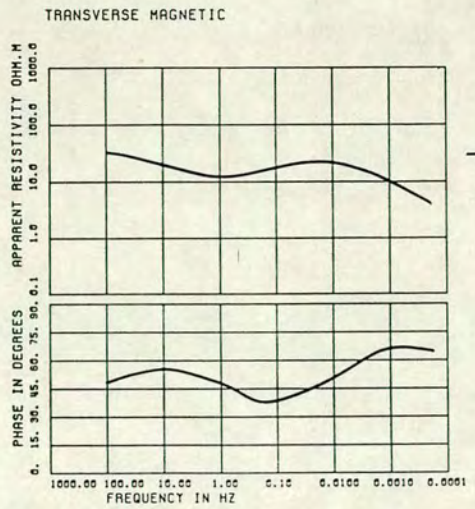

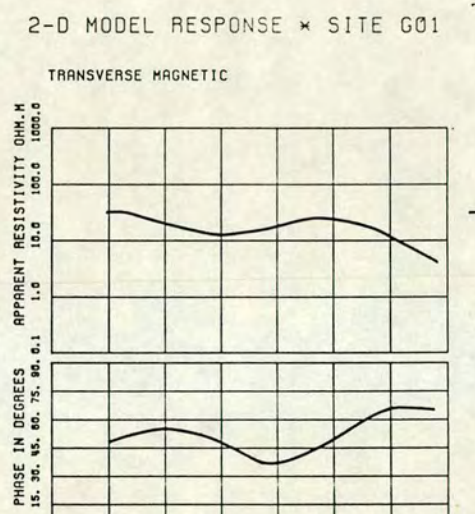

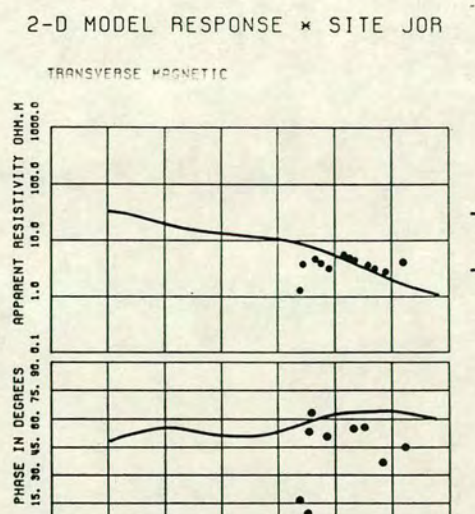

data at sites 922, 927, 3 and 1 as it is demonstrated in Figs.7.8e,f,g,h and 7.9e,f,g,h. However its two dimensional character is questionable since the Niblett-Bostick resistivity contours at various depths show that this is not necessarily an elongated feature along the NW-SE direction (Appendix II, Figs.9a-d) but it may terminate at a latitude of 0°52'S and this maybe a three dimensional body. Its dimensions and its electrical properties can only be determined more accurately with further soundings and three dimensional calculations.

7.7. Discussion and interpretation of the magnetotelluric results.

7.7.(i). Introduction.

The results of the one dimensional magnetotelluric modelling of the Olkaria geothermal field are discussed in Appendix II with respect to, the local geology, tectonics, existing temperature profiles and electrical models derived from D.C resistivity measurements.

The following discussion deals with the results of the limited two dimensional forward calculations undertaken so far. The best fit electrical model OO'-2 is discussed with respect to the local and regional geology the thermo-tectonic regime of Olkaria and the results of other geophysical methods.

7.7.(ii). Interpretation of the electrical resistivities with respect to geological and temperature gradient data.

A large number of geological and temperature data is available in Olkaria from several deep boreholes. Olkaria is characterized by extensive volcanism. The most recent volcanic eruptions were about 200 years ago and the volcanic products are such as pyroclastics, rhyolites, rhyolitic tuffs and trachytes with a maximum thickness of about 2000 m (KPLC, 1986). The one dimensional Parker-Whaler D^+ magnetotelluric models have been compared with these data and the following interpretation has been given to the electrical resistivities.

Two magnetotelluric sites, 927 and 934 have been selected for these comparisons as being very close ($\approx$ 1000 m) to boreholes OW701 and OW301 respectively. Figs.7.10a-b show the Parker-Whaler D^+ models for sites 927 and 934 respectively, in columnar form for comparison with the borehole stratigraphy and the temperature data from the nearby wells OW701 and OW301. Figures in the D^+ column are resistivities in Ohm.m. The delta function conductances are also provided on the right side of the column in Siemens.

The study of Figs.7.10a-b lead to the following conclusions.

(i). The geological stratigraphy at both the wells OW701 and OW301 is complex. The former consists of a sequence of interlayered rhyolites, rhyolitic tuffs and trachytes.

Fig.7.10. Parker-Whaler D^+ models for sites 927 and 934 in comparison with the geological and temperature data from the nearby (≈ 1000 m) wells OW701 and OW301. Models are illustrated in columnar form and figures on the columns are resistivities in Ohm.m. The delta function conductances are also provided in Siemens on the right side of each column.

a. Site 927.

b. Site 934.

Fig. 7.10

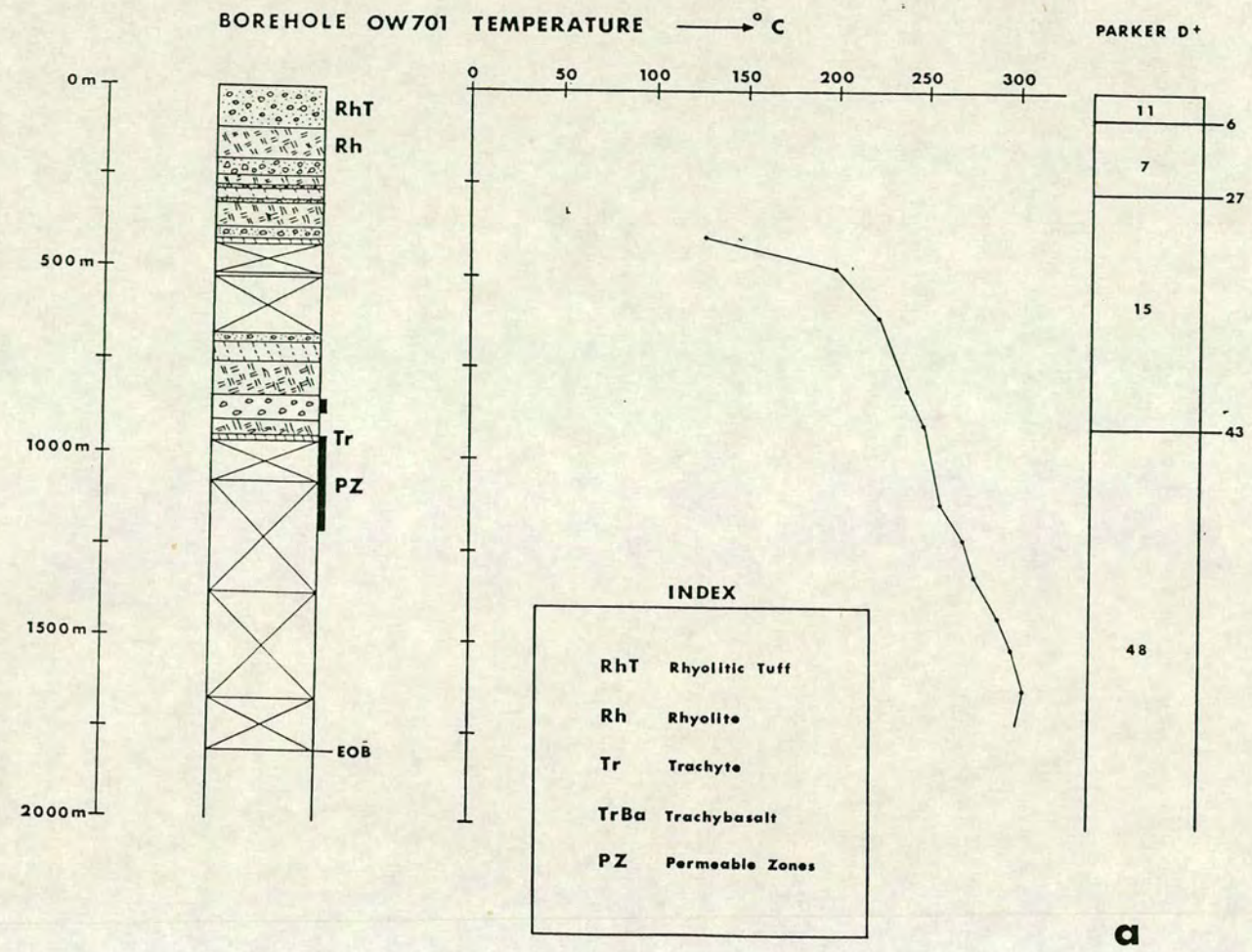
BOREHOLE OW701 TEMPERATURE → °C
PARKER D+
0 m
500 m
1000 m
1500 m
2000 m
RhT
Rh
Tr
PZ
EOB
0
50
100
150
200
250
300
11
6
7
27
15
43
48
INDEX
RhT Rhyolitic Tuff
Rh Rhyolite
Tr Trachyte
TrBa Trachybasalt
PZ Permeable Zones
a

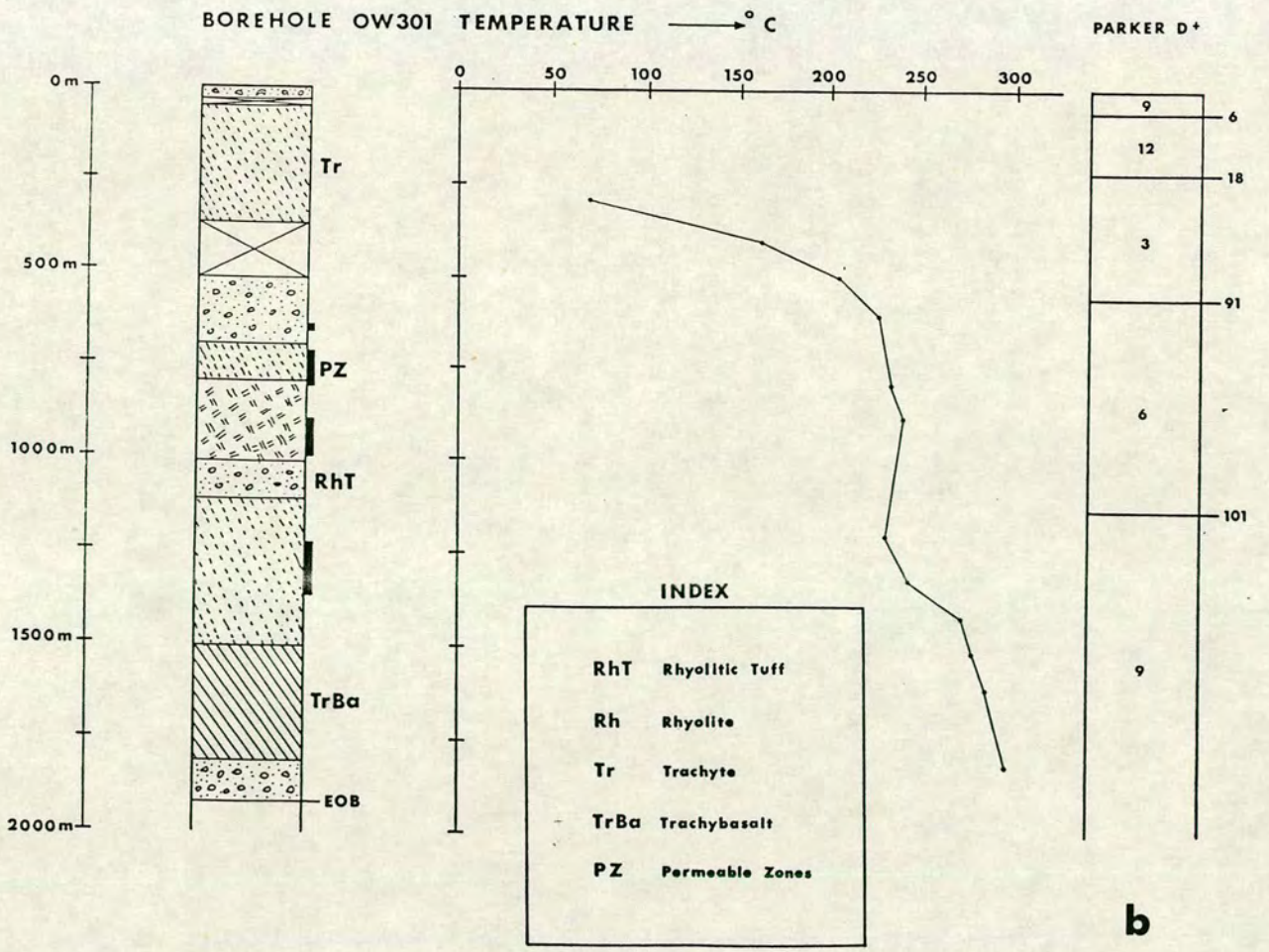
BOREHOLE OW301 TEMPERATURE → °C
PARKER D+
0 m
500 m
1000 m
1500 m
2000 m
Tr
PZ
RhT
TrBa
EOB
0
50
100
150
200
250
300
9
6
12
18
3
91
6
101
9
INDEX
RhT Rhyolitic Tuff
Rh Rhyolite
Tr Trachyte
TrBa Trachybasalt
PZ Permeable Zones
b

(ii). The permeable zones are encountered within the trachyte or rhyolite formations at depths of about 750-1250 m.

(iii). The proposed electrical boundaries do not correspond one by one with existing geological boundaries.

(iv). Figs.7.10a-b indicate that generally trachyte has higher resistivities (> 15 Ohm.m) than the rhyolites or rhyolitic tuffs (3-7 Ohm.m).

The following stand as interpretation to the conclusions above.

Rhyolites, rhyolitic tuffs, trachytes are igneous rocks and they are expected to have higher resistivities than sedimentary rocks (see section 1.2.(ii)). However it has been shown (Figs.1.4b, page 26) that the electrical resistivity of crystalline rocks can be decreased significantly with temperature and hydrothermal alteration (see section 5.4.(iii)). At depths of about 250-750 m various alteration clay minerals are present in both the boreholes. Illitic clays (interlayered illite-smectite and illite) are common in the western wells such as OW301 while chlorite is dominant in OW701 (KPLC, 1986). As discussed in section 5.4.(iii) these minerals are hydrous and good electrolytes and the electrical resistivity of the formations in which they are encountered decreases.

In addition presence of these clay minerals with their low permeability could provide the necessary " cap rock " (see section 5.4.(iii) and Mwangi, personal communication) for the Olkaria geothermal field.

7.7.(iii). Interpretation of the two dimensional magnetotelluric model.

Before going into any detail the results from the one dimensional modelling are reviewed to facilitate the discussions below.

The following stand as the main conclusions from the one dimensional magnetotelluric modelling of the Olkaria geothermal field (see Appendix II).

It was found that Olkaria has anomalously low resistivities of 1-100 Ohm.m to depths of 6-25 km. The region was subdivided into 3 distinct zones, each characterized by low resistivity ($\leq$ 15 Ohm.m).

The first zone lies northeast of the currently exploited geothermal field at the region of the Gorge Farm Fault and it was identified with the Olkaria NE potential field.

The second zone occupies the central part of the surveyed area. The uppermost 1-2 km are characterized by low resistivities ($\leq$ 15 Ohm.m) and overlie a more resistive region ($\geq$ 45 Ohm.m) which has a thickness of about 6 km. The Olkaria geothermal field is located within this zone.

The third zone is associated with the low resistivities ($\leq$ 15 Ohm.m) observed west of the cental Olkaria region and which seem to extend to upper mantle depths. The top few hundred meters in this region display higher resistivity ($\geq$ 15-20 Ohm.m).

It was found that the detected resistivity changes show remarkable correlation with the major fault zones and the temperature changes at the upper crustal depths and support the conceptual geothermal model of the area (see Appendix II, Fig.15).

Fig.7.7b shows the best fit two dimensional model which is proposed as a preliminary electrical model for Olkaria and the Kenya Rift Valley at the Olkaria latitude.

As illustrated in Fig.7.7b, the outer parts of the Kenya Rift Valley are characterized by relatively high resistivities of about 300 Ohm.m. A 10 Ohm.m conductor dominates in the inner part of the Rift and extends from upper crustal to upper mantle depths.

The following interpretation could be given for the upper 5 km of the crust. A large number of boreholes in Olkaria provides useful information for the local stratigraphy for the top 2.5 km. A series of interbedded pyroclastics, rhyolites, trachytes and basalts prevails at these depths and it would not be unreasonable for the latter to have resistivities of 10-50 Ohm.m. Similar resistivities for the same kind of formations were found at Yellowstone in USA by Stanley et al. (1977).

At greater depths (> 5 km) within the crust and even deeper (20-60 km) within the upper mantle depths, the 10 Ohm.m resistivity correlates with the 10 Ohm.m blob beneath the Rift floor at a depth of about 20 km, proposed by Banks and Ottey (1974). These authors have interpreted this low resistivity to be caused by partly melted peridotite in the upper mantle depths. In addition the low resistivity of the inner Rift part correlates with the low density and low velocity region of the Rift as it is illustated in Fig.6.2 (page 196).

Due to the localized field measurements, local electrical features are detected below the Olkaria region. These are the 3 Ohm.m conductor west of Olkaria Peak and the Ol Olbutot fault and the 50 Ohm.m block below Central Olkaria and west of Longonot.

The 3 Ohm.m conductor is about 3 km thick and about 13 km wide. The top of the conductor is located at 300 m depth. It correlates with the observed gravity low at this region (Searle, 1970 ; Mwangi, personal communication). D.C resistivity measurements at the same region display a 5 Ohm.m conductor at the same depth range, which seems to continue even below the Mau escarpment (Mwangi, personal communication).

The observed gravity low and the 5 Ohm.m conductor were interpreted by Mwangi (personal communication) with a possible graben infil mainly consisting of low density and low resistivity pyroclastics. The discussed electrical model implies that the proposed graben extends to the West about 5 km beyond the rift flank and to the East, towards the Olkaria Peak and the Ololbutot fault.

The upper 2 km of the 50 Ohm.m block below Olkaria could correlate with the cold water flow as indicated in the conceptual model of the Olkaria field (see Appendix II, Fig.15). The extent of this feature to greater crustal depths (> 2 km) would only correlate with the presence of a possible intrusive body. There is an indication of a gravity anomaly high in this region in Searle's (1970) residual gravity anomaly map which could relate the presence of high density material. However recent gravity modelling studies by Mwangi and Bromley (1986) do not suggest something like that. In addition from nearby boreholes there is no evidence for some dense intrusive body at the first 2 km but on the other hand the bottom of the nearby wells OW303, OW401, OW201 is not deeper than 2.5 km.

Conclusions

The following stand as general conclusions for the Olkaria geothermal region and the Kenya Rift Valley at the Olkaria latitude.

(i). The uppermost 300 m of the crust beneath the rift floor have resistivities of about 30-50 Ohm.m.

(ii). The rest of the crust and upper mantle beneath the rift are characterized by low resistivities (3-10 Ohm.m). These values correlate with those proposed by Banks and Ottey (1974), Rooney and Hutton (1977).

(ii). The above support the explanation for partial melting in the upper mantle and thinning of the crust beneath the Rift floor.

(iii). A 3 Ohm.m conductor is present beneath Olkaria West and its top is located at 300 m depth. The conductor correlates with the presence of low density material of pyroclastic origin. This region can be associated with the presence of a second geothermal field or the extension of the currently exploited field of Olkaria East.

(iv). The upper 2 km of the crust below Central Olkaria and the region west of Longonot have resistivity of about 50 Ohm.m and correlate with the zone of cold water flow but there is no geological evidence that this feature could extend to greater depths (> 2 km). However a small geophysical indication would be the observed gravity high in Searle's (1970) residual gravity anomaly map.

CHAPTER 8

FINAL CONCLUSIONS AND SUGGESTIONS FOR FURTHER WORK.

8.1. Introduction.

In chapters 3-7 of this thesis the contribution of the magnetotelluric method to geothermal exploration was discussed through the results of magnetotelluric surveys in Greece and Kenya respectively. The derived electrical resistivities were interpreted considering the factors of most significance in a geothermal context, namely ; temperature, pressure, salinity and water content, porosity, permeability, rock type and mineral composition. During the data analysis and modelling, special attention was paid to the resolving power of a particular one dimensional inversion algorithm, known as the Parker-Whaler D^+ method. A physical meaning was attempted to be given to the D^+ delta functions by considering other physical phenomena which involve energy propagation through various media.

8.2. The resolving power of the Parker-Whaler D^+ method.

In chapter 2 among various aspects of the background theory of magnetotellurics the Parker-Whaler D^+ method was studied. It was assumed that the D^+ models are not only a necessary and sufficient condition of a one dimensional solution but they can be interpreted physically with the delta function positions corresponding to electrical resistivity contrasts. The layered electrical

resistivities can be determined from the derived conductances. The electrical resistivity contrasts correspond to boundaries of different electromagnetic wave energy dissipation. The validity of these ideas was tested by applying this inversion technique on synthetic and real field magnetotelluric data. The method gave results which require further examination. Some drawbacks have been noticed when studying the synthetic examples. The difficulties are related to the fact that some delta functions do not correspond to input boundaries (section 2.9.1). Some explanation was given in section 2.9.2 when the problem of the beads on a vibrating string was considered. Computational improvements to overcome these difficulties have not been undertaken but it would be suggested as further work in the future. Since the electromagnetic induction in the Earth is usually a three dimensional problem, it would be interesting to apply these ideas for the study of three dimensional electrical structures.

8.3. Comparison of the magnetotelluric results from the Milos and Olkaria case studies.

The Milos and Olkaria volcanic centres are associated with regions of major tectonic interest such as the subduction of the African plate below the Aegean and the rifting in East Africa respectively.

The magnetotelluric surveys undertaken on Milos and Olkaria enabled electrical mapping and modelling of the two geothermal fields. The derived electrical models were described in chapters 4,5 and 7 respectively. They show differences but also similarities. The differences seem to be associated with the two distinctive tectonic

settings and the similarities with the mechanism of a geothermal system. The differences and similarities are the following.

Similarities

At both fields within the upper 1 km very low resistivities (Milos : 0.3-4 Ohm.m - Olkaria : 1-5 Ohm.m) are observed which have been interpreted as due to the presence of alteration minerals (Milos : mainly Kaolinite - Olkaria : illitic clays or chlorite) which are hydrous and impermeable and are expected to be a good " cap rock " for the geothermal reservoir.

At both studies, the geological formation where geothermal fluids circulate was detected by relative electrical boundaries. The former was found to have higher resistivity than its overlying formations and this was explained as due mainly to the absense of alteration minerals. At both the regions this geological formation was a crystalline rock (Milos : metamorphic basement - Olkaria : trachyte or rhyolite).

Among the objectives of this study was the detection of the heat source below the geothermal fields of Milos and Olkaria. The method was not successful on that. The inability to detect the kind of heat source was explained as due to the presence of shallow (uppermost 1 km) low resistivity (0.3-4 Ohm.m) zones which probably mask the existence of some deeper conductor (heat source). Fytikas et al. (1989) have assumed that below Milos the heat source could be a cooling magma chamber.

On Milos and in Olkaria the AMT magnetotelluric data were found to be nearly one dimensional. Most of the undertaken interpretation was based on the one dimensional results. Two dimensional models have

been proposed for both the geothermal regions. These models as shown were in agreement with the results of other geophysical methods and show a good fit to the observed magnetotelluric data. The proposed two dimensional models were constrained by the one dimensional results and it can be noticed that they have provided very similar electrical structure to that one derived by the one dimensional modelling. It is true that only very few hypotheses have been tested (especially Olkaria) and therefore further two or three dimensional modelling is suggested as further work, which may provide some alternative models.

Differences

On Milos island various geological boundaries were recognized electrically with a corresponding number of electrical resistivity contrasts. Correlation of electrical layers with geological layers is not so prominent in Olkaria.

Beneath Milos island and at depths $>$ 5 km the electrical resistivities are 30-150 Ohm.m. Below Olkaria and Longonot and at depths $>$ 8-10 Ohm.m, electrical resistivities are lower ($\approx$ 10 Ohm.m). In the first case, these relatively high resistivities were explained by the non-volcanic basement. In the second case, the lower resistivities were interpreted as due to the thinning of the crust and the partial melting in the upper mantle beneath the rift floor.

In order to improve the electrical model of the rift (at the Olkaria latitude), further magnetotelluric measurements are required at the flanks of the rift and the region east of Longonot volcano. In this case the model Parkinson induction arrows could be compared with the observed ones across the whole rift and would enable a better understanding of the induction problem in the Gregory Rift Valley.

REFERENCES

Angelier J., Lyberis N., Le Pichon X., Barrier E. and Huchon P., 1982. The tectonic development of the Hellenic arc and the sea of Crete : A synthesis. Tectonophysics., 86, 159-196.

Archie G.E., 1942. The electrical resistivity log as an aid in determining some reservoir characteristics. Trans.A.I.M.E., 146, 54-62.

Arfken G., 1985. Mathematical methods for Physicists. Academic Press.

Aubouin J., 1965. Geosynclines. Developments in Geotectonics. Vol. I. Elsevier ed. Amsterdam, 335 p.

Bahr K., 1983. Joint interpretation of magnetotelluric and geomagnetic data and local telluric distortion. J.Geomag.Geoelectr., 35, 555-566.

Baker B.H. and Wohlenberg, J., 1971. Structure and evolution of the Kenya Rift Valley. Nature, 229, 538-542.

Banks R.J and Ottey, P., 1974. Geomagnetic deep sounding in and around the Kenya Rift Valley. Geophys.J.R.astr.Soc., 36, 321-335.

Banks R.J. and Beamish D., 1979. Melting in the crust and upper mantle beneath the Kenya Rift : evidence from Geomagnetic Deep Sounding experiments. J.Geol.Soc., 136, 225-233.

Barcilon V., 1975. Well-possed eigenvalue problem. Geophys.J.R.astr.Soc., 42, 375-383.

Beauce A., Fabriol H., Le Masne D. and Decriaud J.P., 1989. Test of an integrated methodology for high enthalpy exploration on the island of Milos (Greece). Geothermics, 18, 547-563.

Beamish D., 1977. The mapping of induced currents around the kenya Rift : a comparison of techniques. Geophys.J.R.astr.Soc., 50, 311-332.

Beamish D., 1986. Geoelectric structural dimensions from magnetotelluric data : methods of estimation, old and new. Geophysics, 51(6), 1298-1309.

Bendat J.S and Piersol A.G., 1971. Random data : Analysis and measurement procedures. Willey-intersience. New York.

Berktold A., 1983. Electromagnetic studies in geothermal regions. Geophys.Surveys, 6, 173-200.

Bhogal P.S., 1980. Electrical resistivity investigations at the Olkaria Geothermal field, Kenya. GRC trans., 4.

Bostick F.X.Jr. and Smith H.W., 1962. Investigations of large scale inhomogeneities in the earth by the magnetotelluric method : Proc.IRE, 50, 2339-2346.

Brace W.F., 1971. Resistivity of saturated crustal rocks to 40 km based on laboratory measurements, In the Structure of physical properties of the earth's crust : AGU Geophysical Monograph 14, Washington D.C, 243-255.

Brewitt-Taylor C.R and Weaver, J.T., 1976. On the finite difference solution of two dimensional induction problems. Geophys.J.R. astr.Soc., 47, 375-396.

Brown G.C., Rymer H. and Thorpe R.S., 1987. The evolution of andesite volcano structures : new evidence from gravity studies in Costa-Rica. Earth and Planetary Science Letters., 82, 323-334.

Browne P.R.L., 1970. Hydrothermal alteration as an aid in investigating geothermal fields, Geothermics Spec.Issue, 2, 564-570.

Bullard E.C., 1936. Gravity measurements in East Africa, Phil.Trans.R.Soc.,A235, 445-531.

Cagniard L., 1953. Basic theory of the magnetotelluric method of geophysical prospecting. Geophysics, 18, 605-635.

Cevallos C., 1986. Magnetotelluric interpretation another approach. Ph.D thesis. MacQuarie University.

Chauveau J., 1967. Sur l'analogie des calculus d'un sismogramme et d'un sondage magnetotellurique. Ann.Geophys., 23, fasc.1, 49-60.

Dawes G.J.K., 1984. Short period automatic magnetotelluric (SPAM) system. In A broadband tensorial magnetotelluric study in the Travale-Randicondoli geothermal field. (Hutton et al.) Final report, EC Contract No. EG-A2-031-UK.

Dawes G.J.K., 1985. Magnetotelluric feasibility study. Island of Milos, Greece. Final Report EC Contract No.EN-3G-0026-UK(H), University of Edinburgh.

Dawes G.J.K., Galanopoulos D. and Hutton V.R.S., 1987. Magnetotelluric studies, Milos, Greece, 1986. Interim Report, EC Contract No. EN-3G-0026-UK(H)., University of Edinburgh.

Dawson T.W and Weaver J.T., 1979. Three dimensional induction in a non-uniform thin sheet at the surface of a uniformly conducting Earth. Geophys.J.R.astr.Soc., 59, 445-462.

Devlin T., 1984. A broadband electromagnetic induction study of the Travale geothermal field Italy. Ph.D. thesis, University of Edinburgh.

Dosso H.W., 1966. Analogue model measurements for electromagnetic variations near vertical faults and dykes. Can.J.Earth.Sci., 3, 287-303.

Dosso H.W., 1973. A review of analogue model studies of the coast effect. Phys.Earth.Planet.Int., 7, 294-302.

Dosso H.W., Nienaber W. and Hutton V.R.S., 1980. An analogue model study of electromagnetic induction in the British Isles Region. Phys.Earth.Planet.Int.,22,68-85.

Drakopoulos J.C. and Delibasis N.D., 1973. Volcanic type Microearthquake activity in Milos, Greece. Annali di Geofisica., XXVI, N.1., 131-151.

Drews C., Fürch, N., Maurer, H.M, Musmann, G and Weidelt, P., 1989. Active audiomagnetotellurics on Milos (Greece) for determination of electrical conductivity distribution and its correlation with geothermal anomalies. Geothermics 18, No.4., 507-520.

Duba A., 1976. Are laboratory electrical conductivity data relevant to the Earth ? Acta Geodat.,Geophys.et Montanist Acad.Sci.Hung., 11, 485-495.

Duprat A., Geoelectric survey on Milos island and Susaki area. C.C.G. Technical report., P.P.C of Greece, 14.

Economou E.N., 1979. Green's functions in quantum physics. Springer Verlag, Berlin.

Engelhard L., 1982. Eine skizze für eine aktive magnetotellurik nach dem reflexionsprinzip, GAMMA 40, 57 Seiten.

Everett J.E. and Hyndmann R.D., 1967. Geomagnetic variations and electrical conductivity structure in southwestern Australia. Phys.Earth Planet.Inter., 1, 24-34.

Fischer G., Scnegg P.A., Peguiron M.G and LeQuang B.V., 1981. An analytic one dimensional magnetotelluric inversion scheme.Geophys.J.R.astr.Soc., 67, 257-278.

Fitterman D.V., Stanley W.D and Bisdorf R.J., 1988. Electrical structure of Newburry Volcano, Oregon., J.Geophys.Res., 93(B9), 10119-10134.

Furgerson R.B., 1972. Schlumberger resistivity survey at Olkaria Prospect. UN Geothermal Exploration Project Report.

Fytikas M., 1977. Geological and Geothermal study of Milos island. IGMR Geological and Geophysical Research Vol. XVIII No.1.

Fytikas M., Innocenti F., Manetti P., Mazzuoli R., Peccerillo A. and Vilari L., 1984. Tertiary to Quaternary evolution of volcanism in the Aegean region. In Geol.Soc.London Spec.Publ., Dixon J.E

and Robertson A.H.F. (eds), 17, 687-699.

Fytikas M., 1989. Updating of the geological and geothermal research of Milos island. Geothermics 18, No.4, 485-496.

Fytikas M. and Kolios N., 1979. Preliminary heat flow map of Greece. In " Terrestrial heat flow in Europe ". Cermak V. and Rybach L., (editors), Springer-Verlag, 197-205.

Fytikas M., Garnish,J.D, Hutton,V.R.S, Staroste,E. and Wohlenberg, J., 1989. An integrated model for the geothermal field of Milos from geophysical experiments. Geothermics 18, No.4, 611-621.

Galanopoulos A., 1953. On the intermediate earthquakes in Greece. Bull.Seismol.Soc.Amer., 43(2).

Galanopoulos D., 1986. Audio-frequency magnetotelluric measurements in the Lochaber district, Northern Scotland. M.Sc thesis, University of Leeds.

Giese P. and Nicolich R., 1982. Explosion seismic crustal studies in the Alpine Mediterranean region and their implications to tectonic processes. In " Alpine-Mediterranean Geodynamics " Berckhemer H. and Hsu K., (eds). Geodynamic series (AGU)., 7, 39-73.

Girdler R.W., Fairhead J.D., Searle R.C. and W.T.C Sowerbutts., 1969. Evolution of rifting in Africa. Nature, 224, 1178-1182.

Goguel J., 1953. Le régime thermique de l'eau souterraine. Ann.de Mines, 10, 3-32.

Goldberg S. and Rotstein Y., 1982. A simple form of presentation of magnetotelluric data using the Bostick transform. Geophys.Prosp., 30, 211-216.

Goupillaud P.L., 1961. An approach to inverse filtering of near surface layer effects from seismic records. Geophysics, 26, 754-760.

Griffiths D.H., King R.F., Khan M.A. and Blundell D.J., 1971. Seismic refraction line in the Gregory rift. Nature Phys.Sci., 229, 69,-71.

Group 7 Inc., 1972. Electrical Resistivity Survey in the rift valley of Kenya. UN Geothermal Exploration Project Report.

Haak V., Ritter, O. and Ritter, P., 1989. Mapping the geothermal anomaly on the island of Milos by magnetotellurics. Geothermics 18, No.4, 533-546.

Harris F.J., 1978. On the use of windows for harmonic analysis with the discrete Fourier Transform. Proc.IEEE, 66, 51-83.

Harrison J.C., 1955. An interpretation of gravity anomalies in the

Eastern Mediterranean. Phil.Trans.R.Soc.London 248, 283-325.

Hermance J.F., 1973. An electrical model for the sub-Icelandic crust. Geophysics, 38(1), 3-13.

Hermance J.F., 1982. The asymptotic response of three-dimensional basin offsets to magnetotelluric fields at long periods : The effects of current channelling. Geophysics, 47, 1562-1573.

Hermance J.F. and Grillot L.R., 1974. Constraints on temperature beneath Iceland from magnetotelluric data. Phys.Earth planet.Int., 8, 1-12.

Hill R., 1987. A magnetotelluric study in the Moine thrust region of Northern Scotland. Ph.D thesis, University of Edinburgh.

Hirn A., Sachpazi, M. and Nercessian, A., 1989. Elements for a model of the geothermal field of Milos from seismological data. Geothermics 18, No.4, 779-596.

Horvath F. and Berckhemer H., 1982. Mediterranean backarc basins. In " Alpine-Mediterranean Geodynamics " Berckhemer H. and Hsu K., (editors). Geodynamic series (AGU)., 7, 141-173.

Hutton V.R.S., Galanopoulos, D., Dawes, G.J.K and Pickup, G.E., 1989. A high resolution magnetotelluric survey of the Milos geothermal prospect. Geothermics 18, No.4, 521-532.

Jady R.J. and Patterson G.A., 1983. Inversion methods applied to Dst data. J.Geomag.Geoelectr., 35, 733-746.

Jady R.J., Patterson G.A. and Whaler K.A., 1983. Inversion of the electromagnetic induction problem using Parker's algorithms with both precise and practical data. Geophys.J.R.astr.Soc., 75, 125-142.

Jones A.G., 1977. Geomagnetic induction studies in southern Scotland. Ph.D thesis, University of Edinburgh.

Jones A.G., 1983. On the equivalence of the 'Niblett' and 'Bostick' transformations in the magnetotelluric method. J.Geophys., 53, 72-73.

Jones A.G. and Hutton V.R.S., 1979. A multi-station magnetotelluric study in Southern Scotland - II. Geophys.J.R.astr.Soc., 56, 351-368.

Jones F.W and Pascoe L.J., 1971. A general computer programme to determine the perturbation of alternating electric currents in a two dimensional model of a region of uniform conductivity with an embedded inhomogeneity. Geophys.J.R.astr.Soc., 24, 3-30.

Jones F.W and Pascoe L.J., 1972. The perturbation of alternating geomagnetic fields by three dimensional conductivity

inhomogeneities. Geophys.J.R.astr.Soc., 24, 3-30.

Jones F.W and Vozoff K., 1978. The calculation of magnetotelluric quantities for three dimensional inhomogeneities. Geophysics, 43, 1167-1175.

Jones F.W and Price A.T., 1970. The perturbations of alternating geomagnetic fields by conductivity anomalies. Geophys.J.R.astr .Soc., 20, 317-334.

Jongsma D., Wissmann G., Hinz K. and Garde S., 1977. " Seismic studies in the Cretan Sea ". 2. The South Aegean Sea : An extensional marginal basin without sea-floor spreading ? Results of R.V." Meteor " and R.R.S " Shackleton " cruises. Meteor Forschungsergebnisse. Reihe C., Seite 3. 4-30.

Jupp D.L.B. and Vozoff K., 1975. Stable iterative methods for inversion of geophysical data. Geophys.J.R.astr.Soc., 42, 957-976.

Jupp D.L.B and Vozoff K., 1977. Two dimensional magnetotelluric inversion. Geophys.J.R.astr.Soc., 50, 333-352.

Kao D. and Orr D., 1982. Magnetotelluric studies in the Market Weighton area of eastern England. Geophys.J.R.astr.Soc., 70, 323-327.

Kao D. and Rankin D., 1977. Enhancement of signal to noise ratio in magnetotelluric data. Geophysics, 42, 103-110.

Keller G.V. and Frischknecht F.C., 1986. Electrical methods in geophysical prospecting. Pergamon.

Kissel C. and Laj.C., 1988. The Tertiary geodynamical evolution of the Aegean Arc : a paleomagnetic reconstruction. Tectonophysics., 146, 183-201.

KPLC, 1986. Olkaria scientific review.

Kong J.A., 1986. Electromagnetic wave theory. John Wiley & Sons.

Krauskopf K.B., 1979. Introduction to Geochemistry. McGraw Hill.

Kunetz G., 1972. Processing and interpretation of magnetotelluric soundings. Geophysics, 37, 1005-1021.

Lagios V. and Dawes G., 1989. Technical Report submitted to Public Power Corporation of Greece.

Lee K.H., Pridmore D.F. and Morrison H.F., 1981. A hybrid three dimensional electromagnetic modelling scheme. Geophysics, 46, 796-805.

Lee S., McMechan G. and Aiken C.L.V., 1987. Phase-field imaging. The electromagnetic equivalent of seismic migration. Geophysics,

52, 678-693.

Le Pichon X. and Angelier J., 1979. The Hellenic Arc and trench system : A key to the neotectonic evolution of the eastern Mediterranean area. Tectonophysics., 60, 1-42.

Levy S., Oldenburg D. and Wang J., 1988. Subsurface imaging using magnetotelluric data. Geophysics, 53, 104-117.

Long R.E., Backhouse R.W., Maguire P.K.H. and Sundaralingam K., 1972. The structure of East Africa using surface wave dispersion and Durham seismic array data. Tectonophysics, 15, 165-178.

Loewenthal D., 1975. Theoretical uniqueness of the magnetotelluric inverse problem for equal penetration discretizable models, Geophys.J.R.astr.Soc., 43, 897-903.

Madden T.R., 1980. Magnetotelluric interpretation in a crustal environment. DOE Contract No.OE-A502-77ET-28357, Cambridge, Massachusetts.

Madden T.R. and Nelson P., 1964. A defence of Gagniard's magnetotelluric method. ONR Rep.Proj.NR-371-401, Geophys.Lab.MIT.

Madden T.R. and Thompson W., 1965. Low frequency electromagnetic oscillations of the earth-ionosphere cavity. Rev.Geophys., 3(2), 211-254.

Madden T.R. and Park S.K., 1982. Magnetotelluric modelling for a crustal environment. Final report. USGS Contract No.14-08-0001-G-643.

Maguire P.K.H. and Long, R.E., 1976. The structure of the western flank of the Gregory rift. Part I. The crust. Geophys.J.R.astr.Soc., 44, 661-675.

Makris J., 1976. A dynamic model of the Hellenic Arc deduced from geophysical data. Tectonophysics., 36, 339-346.

Makris J., 1977. Geophysical investigations of the Hellenides. Hamburger Geophysikalische Einzelschriften. Technical report. reihe A : Wissenschaftlische Abhandlungen. Heft 34.

Makris J., 1978. The crust and upper mantle of the Aegean region from deep seismic soundings. Tectonophysics. 46., 269-284.

Makropoulos K.C and Burton P.W, 1984. Greek tectonics and seismicity. Tectonophysics, 106, 275-304.

Marinelli G., 1963. L'energie géothermique in Toscane. Ann.Soc.Geol.Belg., 85(10), 417-433.

McCall G.J.H., 1967. Geology of the Nakuru-Thomson's Falls-Lake Hannington area, Geol.Survey Kenya Report 78.

McKenzie D.P., Davies, D. and Molnar, P., 1970. Plate tectonics of the Red sea and east Africa. Nature, 224, 125-133.

McKenzie D.P., 1972. Active tectonics of the Mediterranean region. Geophys.J.R.Astr.Soc., 30, 109-185.

McKenzie D.P., 1978. Active tectonics of the Alpine-Himalayan belt : the Aegean Sea and the surrounding regions. Geophys.J.R.Astron.Soc., 55, 217-254.

Meju M.A., 1988. The deep electrical structure of the Great Glen Fault, Scotland. Ph.D. thesis, University of Edinburgh.

Morelli C., Pisani M. and Gantar C., 1975. Geophysical studies in the Aegean sea and in he Mediterranean. Boll.Geofis.Teor.Appl., 18, 127-167.

Mountrakis D., 1985. Geology of Greece. (In Greek) University Studio Press.

Mwangi M.N., 1983. Qualitative interpretation of head-on resistivity measurements in Olkaria. KPC Report GP/OW/005.

Mwangi M.N., 1986. Interpretation of additional sounding data of Olkaria. KPC Report GP/OW/010.

Mwangi M.N. and Bromley C.J., 1986. A review of geophysical model of Olkaria geothermal field. Kenya Power Company Ltd., Report No.GP/OW/012.

Naylor I., 1972. the geology of Eburru and Olkaria Prospects. A UNDP report.

O'Brien D.P and Morrison H.F., 1967. Electromagnetic fields in an n-layer anisotropic half-space. Geophysics, 32(4), 668-677.

Ochmann N., Hollnack, D., and Wohlenberg, J., 1989. Seismological exploration of the Milos geothermal reservoir, Greece. Geothermics 18, No.4, 563-578.

Oldenburg D., Whittal K.P. and Parker R.L., 1984. Inversion of ocean bottom magnetotelluric data revisited. J.Geophys.Res., 89, 1829-1833.

Oristaglio M.L and Worthington M.H., 1980. Inversion of surface and borehole electromagnetic data for two dimensional electrical conductivity models. Geophys.Prospect., 28, 633-657.

Orsinger A. and Van Nostrand R., 1954. A field evaluation of the electromagnetic reflection method. Geophysics, 19, 478-479.

Papanicolaou N., 1958. A geophysical survey of the Milos barite prospect. I.G.M.E, 725.

Papazachos B.C., 1977. A lithospheric model to interpret focal properties of intermediate and shallow shocks in Central Greece. Pure Appl.Geophys., 155, 655-666.

Papazachos B.C and Comninakis P.E., 1971. Geophysical and tectonic features of the Aegean Arc. J.Geophys.Res., 76, 8517-8533.

Park S.K., 1985. Distortion of magnetotelluric sounding curves by three dimensional structures. Geophysics, 50(5), 795-797.

Park S.K. and Torres-Verdin C., 1988. A systematic approach to the interpretation of magnetotelluric data in volcanic environments with applications to the quest for magma in Long Valley, California. J.Geophys.R., 93(B11), 13265-13283.

Park S.K., Orange A.S. and Madden T.R., 1983. Effects of three dimensional structure on magnetotelluric sounding curves. Geophysics, 48(10), 1402-1405.

Parker R.L., 1980. The inverse problem of electromagnetic induction : Existence and construction of solutions based on incomplete data. J.Geophys.Res., 85(B8), 4421-4428.

Parker R.L., 1983. The magnetotelluric inverse problem. Geophys.Surv., 6, 5-26.

Parker R.L. and Whaler K., 1981. Numerical methods for establishing solutions to the inverse problem of electromagnetic induction. J.Geophys.Res., 86, 9574-9584.

Parkinson W.D., 1962. The influence of continents and oceans on geomagnetic variations. Geophys.J.R.astr.Soc., 6, 441-449.

Patra H.P. and Mallick K., 1980. Geosounding principles, 2. Time varying geoelectric soundings. Elsevier.

Price A.T., 1962. The theory of magnetotelluric methods when the source field is considered. J.Geophys.Res., 67(5), 1907-1919.

Rai Ch.S. and Manghani M.H., 1981. The effects of saturant salinity and pressure on the electrical resistivity of Hawaiian Basalts. Geophys.J.R.astr.Soc., 65, 395-405.

Ranganayaki R.P., 1984. An interpretive analysis of magnetotelluric data. Geophysics, 49, 1730-1748.

Ranganayaki R.P. and Madden T.R., 1980. Generalized thin sheet analysis in magnetotellurics : an extension of Price's analysis. Geophys.J.R.astr.Soc., 60, 445-457.

Rankin D., Garland G.D. and Vozoff K., 1965. An analogue model for the magnetotelluric effect. J.Geophys.Res., 70(8), 1939-1945.

Reddy I.K., Rankin D. and Philipps R.J., 1977. Three dimensional modelling in magnetotelluric and magnetic variation sounding.

Geophys.J.R.astr.Soc., 51, 313-325.

Rokityanski I.I., 1982. Geoelectromagnetic investigation of the earth's crust and mantle. Springer-Verlag, Berlin.

Rooney D., 1977. Magnetotelluric measurements across the Kenyan Rift Valley. Ph.D. thesis, University of Edinburgh.

Rooney D. and Hutton V.R.S., 1977. A magnetotelluric and magnetovariational study of the Gregory Rift Valley, Kenya. Geophys.J.R.astr.Soc., 51, 91-119.

Savage J.E.G and Long R.E., 1985. Lithospheric Structure beneath the Kenya Dome. Geophys.J.R.astr.Soc., 82, 461-477.

Schellkunoff, S.A., 1943. Electromagnetic waves, D.Van Nostrand Co, New York.

Schmucker U., 1970. Anomalies of geomagnetic variations in the southwestern United States. Bull.Scripps Inst.Ocean.Univ.Calif., 13.

Schmucker U. and Weidelt P., 1975. Electromagnetic induction in the earth. Lecture notes. Aarchus University.

Searle R.C., 1970. Evidence from gravity anomalies for thinning of the lithosphere beneath the rift valley in Kenya. Geophys. J.R.astr.Soc., 21, 13-31.

Shankland T.J. and Waff H.S., 1974. Conductivity in fluid bearing rocks. J.Geophys.Res., 79, 4863-4868.

Sims W.E., Bostick F.X. and Smith R.W., 1971. The estimation of magnetotelluric impedance tensor elements from measured data. Geophysics, 36, 938-942.

Shoham Y. and Loewenthal D., 1975. Matrix polynomial representation of the anisotropic magnetotelluric impedance tensor. Phys.Earth Planet.Interiors., 11, 128-138.

Srivastava S.P., 1965. Method of interpretation of magnetotelluric data when the source field is considered. J.Geophys.Res., 70(4), 945-954.

Steiner A., 1968. Clay minerals in hydrothermally altered rocks at Weirakei, New Zewland, Clays Clay Miner., 16, 193-213.

Sule P.O., 1985. A broadband magnetotelluric investigation in southeast Scotland. Ph.D thesis, University of Edinburgh.

Swain C.J. and Khan M.A., 1977. Kenya, a catalogue of gravity measurements. Geology Dept. Leicester University.

Swift C.M., 1967. A magnetotelluric investigation of electrical conductivity anomaly in the southwestern United States : Ph.D

thesis, MIT.

Swift C.M., 1971. Theoretical magnetotelluric and Turam response from two dimensional inhomogeneities. Geophysics., 36, 38-52.

Szaraniec E., 1975. Fundamental functions for horizontally stratified earth, Geophys.Prosp., 24, 528-548.

Telford W.M., Geldart L.P., Sheriff R.E and Keys D.A., 1981. Applied Geophysics. Cambridge University Press.

Tichonov A.N. and Berdichevsky M.N., 1966. Experience in the use of the magnetotelluric methods to study the geologic structure of sedimentary basins. Bull.Izv.Acad.Sci.,U.S.S.R., Geophys.Ser., 2, 93-97.

Ting S.C. and Hohmann G.W., 1981. Integral equation modelling of three-dimensional magnetotelluric response. Geophysics, 46, 182-197.

Thanassoulas C.P., 1983. Technical report on the Gravity Measurements on Milos island. I.G.M.E, 3868, 19-?. (in Greek).

Thanassoulas C.P., 1989. Application of the self potential technique over the Milos geothermal test site. Geothermics 18, No.4, 497-506.

Tsapanos T., Galanopoulos D. and Burton P.W., 1989. A preliminary study of the distribution of the seismic parameters along the Hellenic Volcanic Arc. 1st Hellenic Geophysical Conference (Proceedings).

Tsokas G., 1985. Geophysical prospecting of Milos and Kimolos islands. (In Greek) Doctorate Thesis. University of Thessaloniki.

Tzanis A., 1987. Investigations on the properties and estimation of Earth Response Operators from EM sounding data. Ph.D Thesis. University of Edinburgh.

Valiant M., 1977. Geologger System Handbook. NERC publication.

Van Dijck M.F., 1986. Preliminary interpretation of Aeromagnetic data from the Olkaria Geothermal field (Kenya). Project Report GEOTHERM 86.23. Geothermal Institute, University of Auckland.

Vichos G., Vondikakis E. and Chlaboutakis M., 1986. Geothermal field of Milos. Technical report (In Greek). Public Power Company of Greece.

Virkir , 1985. Status report on steam production. KPC.

Vogt P.R. and Higgs R.H., 1969. An aeromagnetic survey of the Eastern Mediterranean Sea and its interpretation. Earth and Planetary Science Letters, 5, 439-448.

Volarovich M.P. and Parkhomenko E.I., 1976. Electrical properties of rocks at high temperatures and pressures. In Geoelectric and Geothermal studies (East Central Europe, Soviet Asia) KAPG Geophysical Monograph, editor-in-chief A.Adam, Akademiei Kiadó, Budapest.

Voutetakis S.K. Application of the D.C resistivity method for geothermal exploration on Milos. I.G.M.E., 1991, 617, 1973.

Vozoff K. and Swift C.M., 1968. Magnetotelluric measurements in the North German basin. Geophys.Prospect., 16(2), 454-473.

Wait J.R., 1954. On the relation between telluric currents and the earth's magnetic field. Geophysics, 19(2), 281-289.

Wall H.S., 1948. Analytic theory of continued fractions. Van Nostrand, New York.

Wannamaker P.E., 1986. Electrical conductivity of water undersaturated crustal melting, J.Geophys.Res., 91, 6321-6328.

Wannamaker P.E., Stodt J.A. and Rijo L., 1985. PW2D - finite element program for solution of two dimensional earth resistivity structure : User documentation. University of Utah Res.Inst.Rep.ESL - 158.

Wannamaker P.E., Hohmann G.W. and San Filipo W.A., 1984. Electromagnetic modelling of three dimensional bodies in layered earths using integral equations. Geophysics, 49, 6-74.

Wannamaker P.E, Stodt J.A. and Rijo L., 1986. Two dimensional topographic responses in magnetotellurics modelled using finite elements. Geophysics., 51(11), 2131-2144.

Weaver J.T. and Brewitt-Taylor C.R., 1978. Improved boundary conditions for the numerical solution of E-polarization problems in geomagnetic induction. Geophys.J.R.astr.Soc., 54, 309-317.

Weidelt P., 1972. The inverse problem of geomagnetic induction. J.Geophys. 38, 257-289.

Weidelt P., 1975a. Inversion of two dimensional conductivity structures. Phys.Earth Planet.Int., 10, 282-291.

Weidelt P., 1975b. Electromagnetic induction in three dimensional structures. J.Geophys., 41, 85-109.

Weidelt P., 1986. Discrete frequency inequalities for magnetotelluric impedances of one dimensional conductors. J.Geophys., 59, 171-176.

Woodhall D.G., 1987. The geology of Longonot volcano, the greater Olkaria volcanic complex and adjacent areas.

UK/KEN.Govt.Technical Cooperation project, Report no.BGSGENKEN/5.

Word D.R., Smith H.W. and Bostick F.X.Jr., 1970. An investigation of the magnetotelluric tensor impedance method. Tech.Rep.82, Elect.Geophys.Res.Lab., University of Texas.

Yee E. and Paulson K.V., 1988. Properties of the c-response function for conductivity distributions of class S^+. Geophys.J., 93, 265-278.

Yost J., 1952. The interpretation of electromagnetic reflection data in geophysical exploration-Part I, General theory, Geophysics, 17, 89-106.

Zhdanov M.S. and Frenkel M.A., 1983a. The solution of the inverse problems on the basis of the analytical continuation of the transient electromagnetic field in the reverse time. J.Geomagag.Geoelectr., 35, 747-765.

Zhdanov M.S. and Frenkel M.A., 1983b. Electromagnetic migration. In:S.E.Hjelt (Editor). The development of the deep geoelectric model of the Baltic Shield (Part 2), University of Oulu, 37-58.

Zhdanov M.S. and Frenkel M.A., 1984. Method of electromagnetic field migration Izv.AN.SSSR, Fizika Zemli, 4, 60-74.

APPENDIX I

Geothermics, Vol. 18, No. 4, pp. 521-532, 1989.
Printed in Great Britain.

0375-6505/89 $3.00 + 0.00
Pergamon Press plc

A HIGH RESOLUTION MAGNETOTELLURIC SURVEY OF THE MILOS GEOTHERMAL PROSPECT

V.R.S. HUTTON, D. GALANOPOULOS, G.J.K. DAWES, G.E. PICKUP

Department of Geology and Geophysics, University of Edinburgh, Mayfield Road, Edinburgh EH9 3YZ, UK.

ABSTRACT

A collaborative magnetotelluric survey involving 4 European institutions was undertaken in 1986 on the island of Milos, Greece, the geothermal resources of which are currently under development. To obtain a high resolution electrical resistivity model of the field, sites were located on a 500m by 500m grid over the field itself with a greater site spacing elsewhere. Soundings were made over 4 - 6 decades of period from 0.01s. In this paper, the results of the University of Edinburgh group, involving 37 soundings, are presented. Special care was taken over data acquisition in the so-called 'dead band' so that the resulting magnetotelluric responses were of good quality. The application of several dimensionality tests showed that the data were predominantly one dimensional except at the longest periods. Electrical resistivity models were derived from the application of several 1-D modelling procedures and for sites close to the boreholes M-1, M-2 and M-3 the resulting models were compared with the borehole data. The Dawes and Parker D+ algorithms were the most successful in revealing an interface at the reservoir depth at all three boreholes and, as a result, were used in the subsequent collation of 1-D models along a number of traverses. For interpretation of the longer period data, some 2-D modelling was also undertaken and is presented here in pseudo-3-D form. Maps of principal impedance azimuths and induction arrows were found to be in very good agreement with those described by Drews et al., (1988) in the 3-D modelling study - this took account of both the coast effect and lateral conductance variations on Milos itself. Contour maps of the depths to and conductances of certain layers showed good correlation with the temperature gradient contours and with the two directions of faulting. As in geothermal fields elsewhere, very low resistivities (<1 ohm.m) were detected at shallow depths at the centre of the field, with the underlying basement to depths of the order of 10 km being only of the order of 10's of ohm.m, a result indicative of the presence of fluid filled fractures.

INTRODUCTION

A study of the feasibility of the magnetotelluric technique for determining the electrical resistivity structure of the Milos geothermal field was undertaken in 1985 by Dawes (1985). This led in 1987 to an integrated and intensive magnetotelluric survey on the island by four European Institutions, the contribution from the University of Edinburgh group being the subject of this paper. It comprised 37 soundings in the period range 0.01 - 100 s (i.e. AMT/MT), and 12 in the range 30 - 10,000 s (i.e. LMT) at sites which were in general identical or close to the shorter period soundings. By agreement with colleagues the three groups - Edinburgh, Berlin and Orléans - undertaking comparable natural source field observations (the fourth group, Braunschweig used mainly the active AMT method) each occupied sites with approximately 500m spacing along 3 traverses across the region of the known high temperature gradient to the east of the island. The 9 traverses were also about 500m apart - the resultant being a network of sites over a 500m by 500m grid - with each group using a traverse spacing of approximately 1500m. The locations of the Edinburgh sites and traverses A,D,G and W are shown in Figure 1a together with other traverses W',D',G' and N discussed later in the text. Individual sites are subsequently specified by the traverse designation followed by a digit e.g. site An is the nth site from the most westerly on traverse A. For later reference also, a second map of Milos is

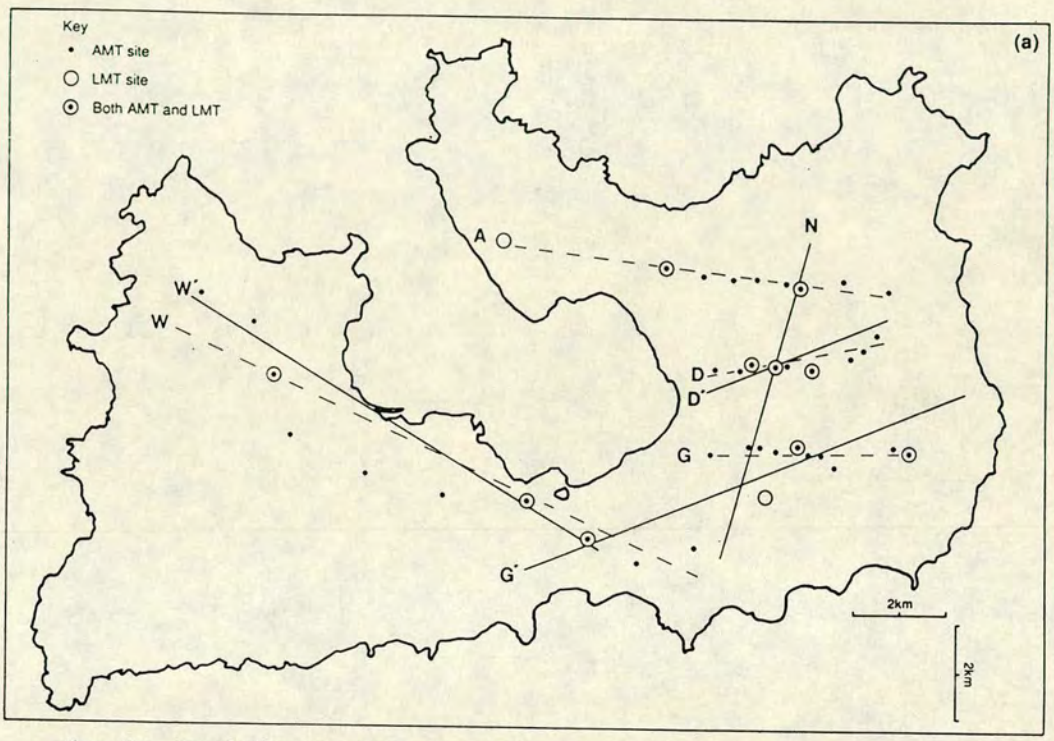

Figure 1(a). Map of Milos showing the locations of the magnetotelluric soundings. Measurements were made approximately along traverses A, D, G, and W. Stations are referred to by their number along a traverse, starting at the west. The traverses marked D', G', W', and N were used for modelling (see Figures 7 and 9).

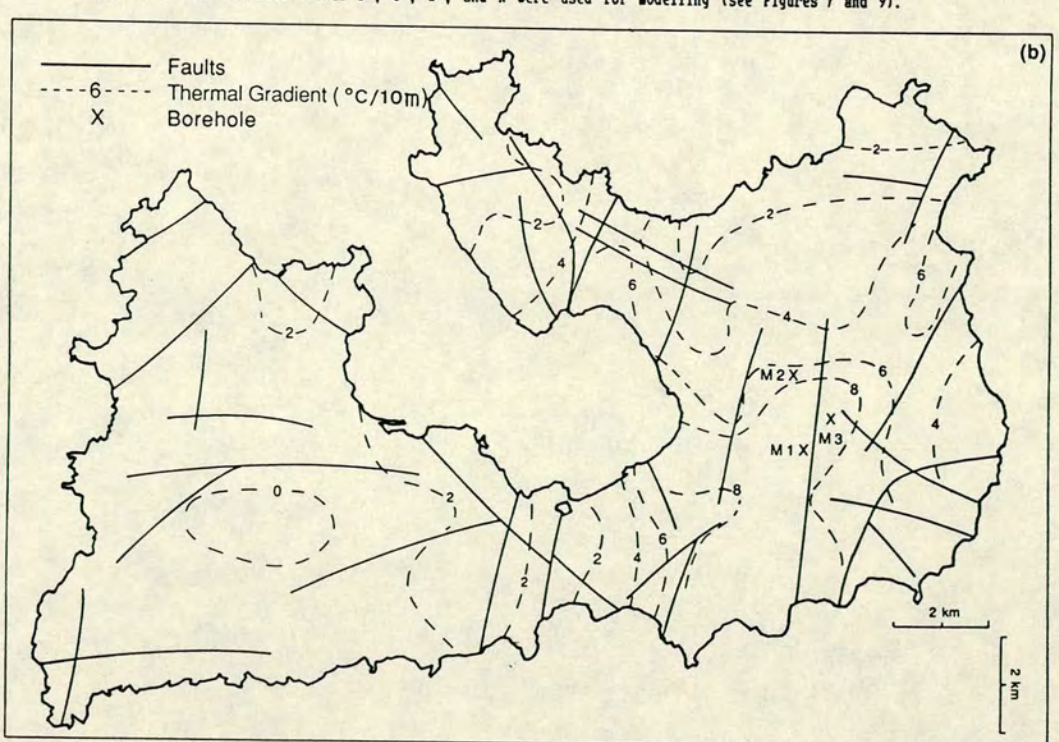

Figure 1(b). Map showing the main faults, the locations of boreholes and contours of thermal gradient (Fytikas, 1977).

provided as Figure 1b to show the major geological faults on the island, the locations of the boreholes M-1, M-2 and M-3, and the temperature gradient contours. It will be noted in Figure 1a that an additional traverse of soundings with approximately 3km spacing was undertaken to the west of the island. These logistics were compatible with the 'test of techniques' objective for the studies in the east of the island where borehole data and the results of previous surveys were available and in this respect complemented, in a different geological environment, the Travale, Italy, test site studies of the previous EC Programme (Barbier et al., 1985). The soundings to the west of the island, however, where previous work had been less intensive had a more exploratory objective.

THE FIELD STUDIES

The instrumentation used by the Edinburgh group comprised (a) an updated version (Mk II) of the 'real-time' S.P.A.M. system which was used in the Travale project (Dawes, 1984) for the period range 0.01 - 100s, the observations being made in four overlapping frequency bands and (b) five simultaneously operating long period (30 - 10 000s) systems incorporating E.D.A. Fluxgate magnetometers, telluric pre-amplifier-filter boxes (Dawes, 1985) and NERC Geologgers (Valiant, 1977). The Mk II version of S.P.A.M. has 7 channels, which provide a 'remote reference' capability in locations where cultural noise is significant and enable 2 station simultaneous observation. Its considerably enhanced computer memory provides the possibility of more thorough in-field data analysis and modelling than had been possible in the original design.

The same fieldwork procedure as used in the feasibility study (Dawes, 1984) was followed for the AMT/MT soundings and where appropriate for the LMT soundings also. At all sites, the horizontal magnetic field components were measured in the N-S and E-W directions (vertically also for the LMT observations) while the horizontal electric field components were measured in the N-S and E-W directions with either a cross shaped configuration of electrodes (in the AMT/MT range) or an L-shaped configuration (in the LMT range) and typical electrode spacing of 100m. Special care was taken - and frequently repeat measurements - to ensure that optimum quality of data was attained around 1Hz (the so-called MT 'dead band') as it was realised that this frequency range was crucial to the determination of the structure at the depths of prime interest in this study.

For the AMT/MT range, time series windows having 256 digitised values and satisfying preset criteria were recorded for the four horizontal field components and written to data cartridges. The sampling rates varied according to the S.P.A.M. Mk II sub-band frequency range. A pre-fixed sampling rate of 10s was used for the LMT observations for which the three orthogonal magnetic field and two horizontal electric field components were recorded digitally on magnetic tape cassettes.

DATA ANALYSIS

While the AMT/MT time series windows were selected automatically in the field, the LMT time series windows, also comprising 256 digitised values, were initially selected visually using a DEC LSI 11/73 computer system and preset criteria similar to those for selection of the AMT/MT windows. Subsequently, as described in Hutton et al. (1987) a program was written for automatic selection of acceptable windows, resulting both in a very considerable reduction in processing time and in improved quality of the resulting response functions.

In the reprocessing of all the data on the Edinburgh University Amdhal system, classical tensorial procedures were adopted with special attention being paid to the reduction of the effect of the biasing which results from random noise. Examples of reprocessed data are provided in full in earlier reports of this study (Dawes et al., 1987; Hutton et al., 1987) and the complete set in Hutton et al. (1988). For each site, frequency variations of apparent resistivity and phase - in both the measured and principal directions and also averaged - are presented in the latter, together with values of the frequency variations of the coherence function, the skew parameter (a measure of dimensionality) and the azimuth of the major impedance. In this report, further presentation of the magnetotelluric responses obtained from the Milos study is restricted to the apparent resistivities and phases in the principal directions for station A7 - Figure 2. These 'major' and 'minor' responses are typical in data quality and consistency of the sounding curves at all the sites. Such values of apparent resistivity and their associated azimuths can be mapped as shown in Figure 3 for all stations for a restricted period range by means of polarisation ellipse axes. These axes are illustrated in this figure for periods of (a) 5 - 10s and (b) 400 - 1000s, with the axes lengths being proportional to the square root of the apparent resistivity. For the shorter periods - Figure 3a - which are indicative of shallow structure, the apparent resistivities are all small, but particularly so in the region where the temperature gradient is greater than 6°/10m. They are also reasonably isotropic. On the other hand, for the longer periods - Figure 3b - which

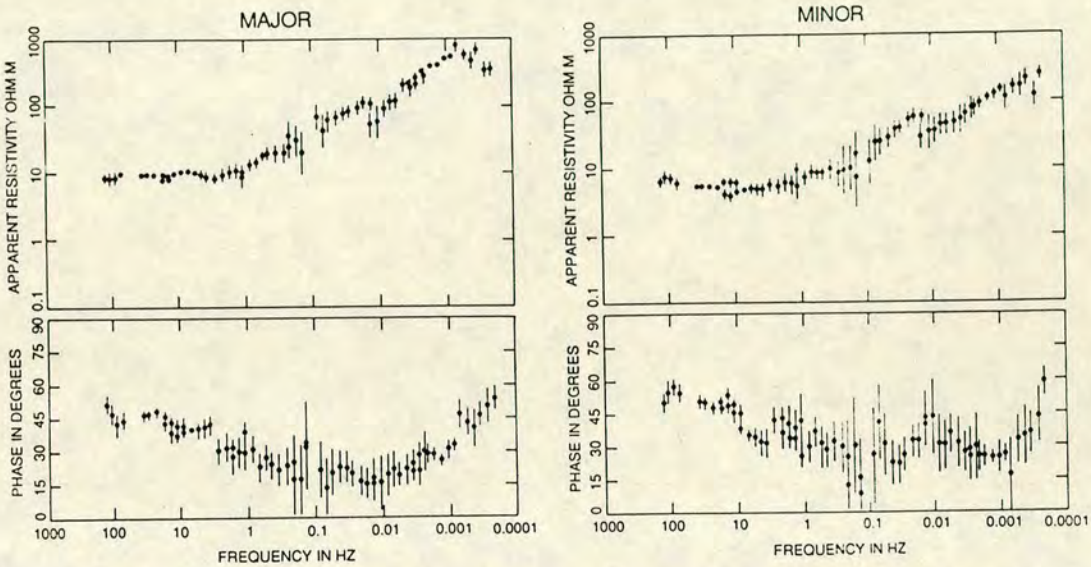

Figure 2. Frequency dependence of the apparent resistivity and phase in the major and minor directions for site A7. The points plotted are the mean of the upward and downward biased estimates.

penetrate to greater depths, there is considerable anisotropy and the major apparent resistivities are larger especially at the boundaries of the temperature gradient 'high'. In this latter case, it is significant for quantitative modelling to note also that the azimuths of the major impedances are predominantly in the NW-SE direction, i.e. the strike of the Aegean arc and the major faults on Milos, and also compatible with Weidelt's 3-D modelling study both of the coast effect and lateral conductance variations on the island of Milos itself as discussed in Drews et al. (1988). In this paper the computed E-field was mapped for 100s but a very similar pattern has been found for periods up to 10 000s (Weidelt, private communication,1988).

For the LMT data, since all three orthogonal components of the magnetic field were available, it was possible to obtain magnetic field transfer functions which for this study have been mapped in Figure 4 in the form of Parkinson arrows for two period ranges. Such arrows are helpful in delineating lateral variations in resistivity structure as they point in the direction of concentration of induced electric current flow and their amplitudes are functions of the distance from the resistivity contrast and of the contrast magnitude itself. In this case, Figure 4a shows arrows for the period range 100 - 300s and by the reversal of the arrows in the south of the island clearly indicates that this is a region of enhanced current flow and hence of lower than average resistivity for the island. For the longer period data set of 1000 - 3000s, mapped in Figure 4b, the amplitudes and azimuths are larger and much more uniform. These maps are also in good agreement with Weidelt's modelling study especially in the case of Figure 4a.

DIMENSIONALITY TESTS AND 1-D MODELLING

Prior to the inversion of the apparent resistivity and phase responses at each site to resistivity-depth models, several dimensionality indicators were computed. These were the skew factor (Word et al., 1970) and the D1, D2, D3 and D3' indices proposed by Kao and Orr (1982). Examples of the frequency variations of these indices have been presented for two sites in Dawes et al. (1987). These are typical variations for this study, with the skew increasing slowly and smoothly with increase in period in the range 0.0 - 0.2 between 0.01 and 100s. The complementary indices within this period range are 0.7 - 1.0 for D1, 0.0 - 0.5 for D2 and 0.0 - 0.1 for D3/D3'. Since the latter ratios are negligible within this period range, it is not surprising that the D1 and D2 indices show a reciprocal behaviour, with the contribution from 1-D effects dominating except at the longest periods when indications of two dimensionality begin. It is thus evident that useful and valid structural information can be obtained from 1-D inversion of the data, the invariant responses being used for this purpose as the best 'average' values (Ranganayaki, 1984 - the notation rho(det) and phi(det) is used by this author).

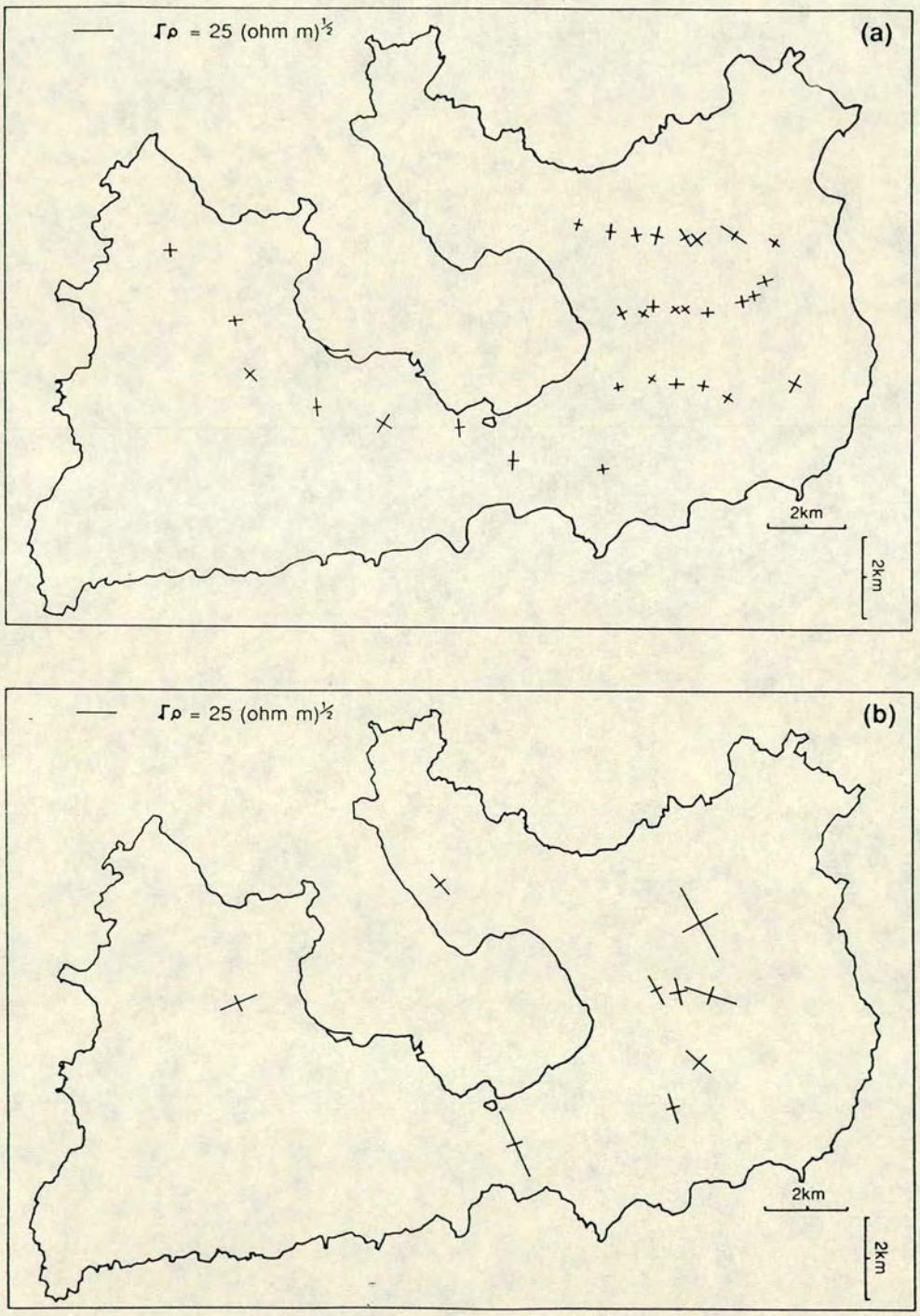

Figure 3. Axes of the impedance ellipses. (a) Averaged over 5-10 s. (b) Averaged over 400-1000 s.

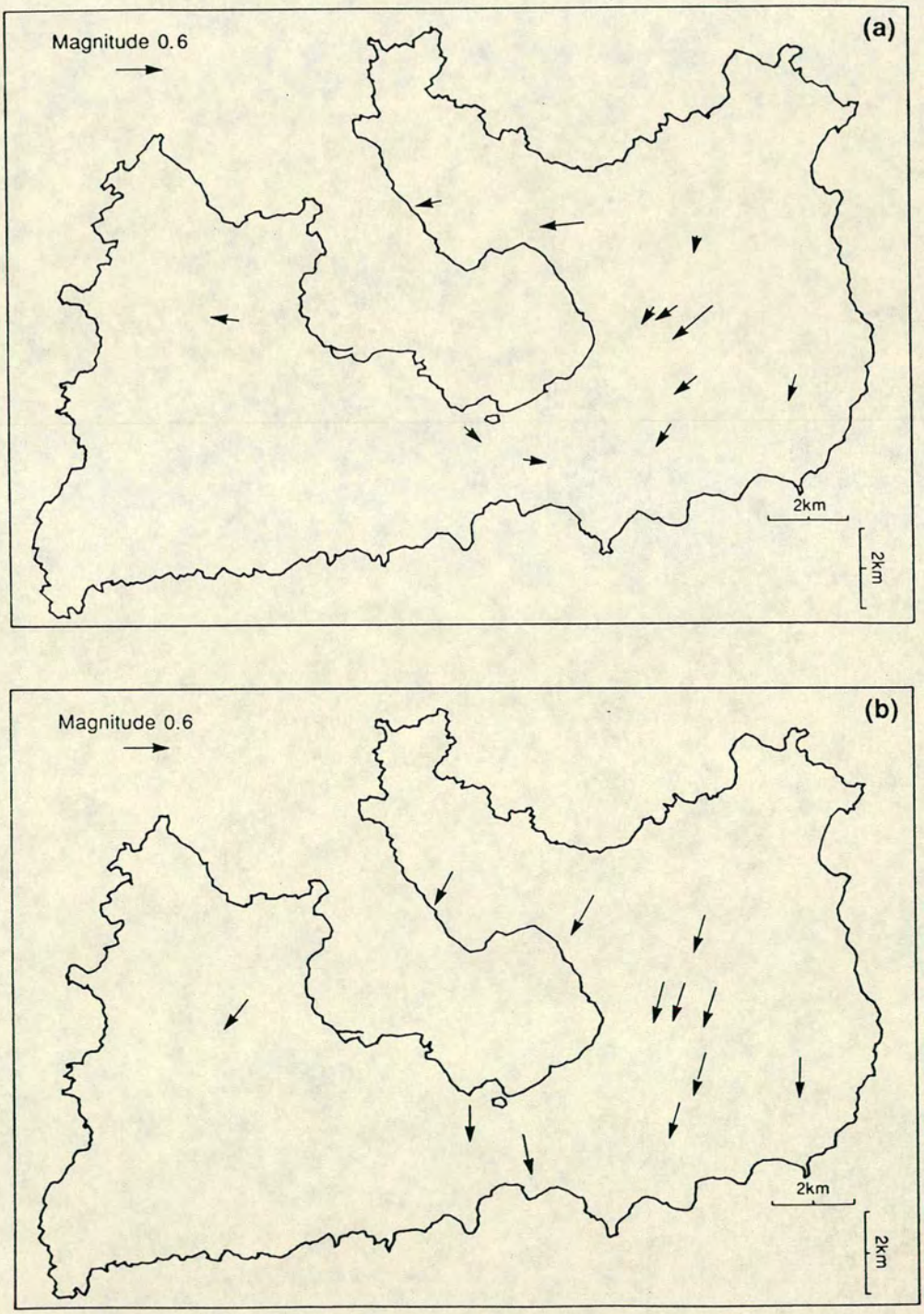

Figure 4. Parkinson induction arrows (real part). (a) Averaged over 100-300s. (b) Averaged over 1000-3000 s.

For each site, the invariant apparent resistivity and phase values were inverted using the following algorithms:-

(i) The Bostick transformation (1977).
(ii) The Dawes method - a hybrid Monte Carlo/Hedgehog procedure developed by Dawes, described by Sule (1985) and labelled MMC in Figure 6 of this paper.
(iii) The Fischer inversion (Fischer, 1981).
(iv) Parker's D+ and H+ methods (Parker, 1980; Parker and Whaler 1981; Parker, 1983).
(v) The Jupp and Vozoff method (Jupp and Vozoff, 1975).

In general there is very good agreement between the models derived by the application of these different methods, as has already been demonstrated in examples presented in previous reports (Dawes et al., 1987; Hutton et al., 1988). Results of the application of these algorithms for site G5, previously given in the latter report as site 701, are reproduced here in Figure 5 in a modified form. The invariant apparent resistivity and phase data are shown in Figure 5a together with the computed values - smooth curves - corresponding to the layered models of Figure 5b. Note that the Fischer, Dawes and Jupp and Vozoff models are given in terms of resistivity and depth while the Parker model is in terms of conductance and depth. The fit of the computed to the observational data is particularly good for the Dawes and the Jupp and Vozoff methods for the whole period range and for the Parker D+ also except for periods exceeding 100s. The main differences in the models themselves are the tendency for the Dawes model to require a smaller number of layers than any of the other methods and for the Parker D+ to require a larger number.

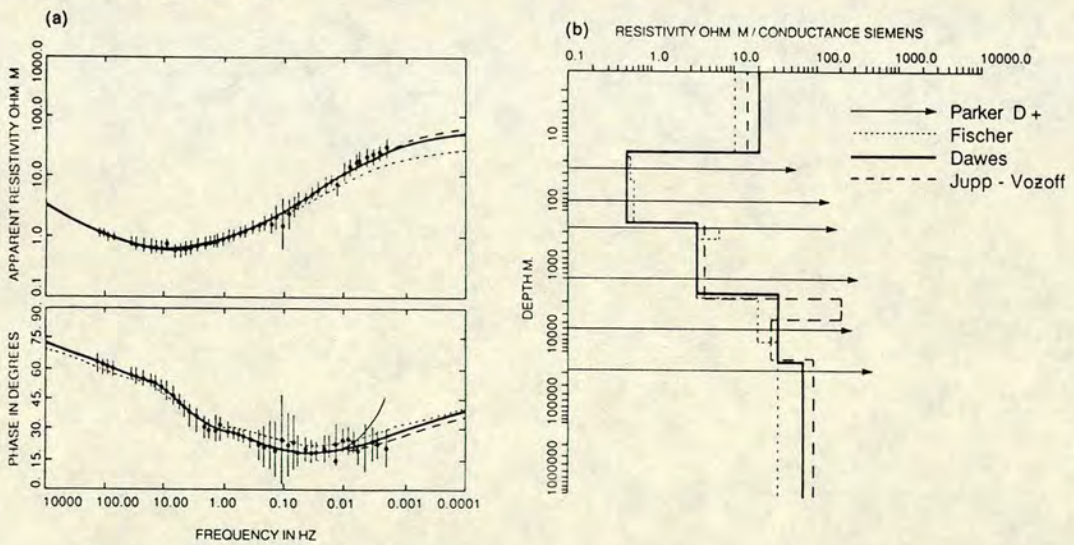

Figure 5. 1-D models for site G5. In (a) the frequency variations of the computed and observed responses are superimposed. In (b) are shown the electrical models on which the computed responses are based.

Comparison of the electrical models derived from the different algorithms with the stratigraphy and other borehole data from wells M-1, M-2 and M-3 has led to the preferential use of the Parker D+ and Dawes methods for subsequent mapping and preparation of sections. In Dawes et al. (1987) data from boreholes M-1 and M-2 were compared with the electrical models derived from CGG's Resistivity Survey (1973) and those from application of the Parker H+ and Dawes routines to data from adjacent Edinburgh sites, while in Hutton et al. (1988) additional electrical models for the same 2 sites were shown from Jupp-Vozoff, Fischer and Parker D+ inversions. One of the latter set of models - for M-2 - is presented here as Figure 6. Comparison of the data in this Figure and also the previously published CGG and Parker H+ models shows

(a) a good agreement between the green lahar layer and a layer of resistivity less than a few ohm.m;
(b) a crystalline basement of resistivity 30-50 ohm.m in the CGG model but of much lower resistivity in all the MT models.

The Parker H+, the Parker D+ and the Dawes models all indicate a resistivity boundary at a depth about 1000m - the depth at which the geothermal reservoir has been detected - and the total conductances of the uppermost basement although not necessarily the number of layers and resistivities are comparable. It has already been demonstrated in Dawes et al. (1987) that the 4-layer Dawes model shown here could have been replaced by a 5-layer model which would then been

in better agreement with the Parker H+ model. Following this comparison of modelling algorithms, two of them have been selected - the Dawes and Parker D+ - for use in the preparation of contour maps depicting the resistivity structure and of resistivity depth sections along certain traverses. The Parker D+ method has the advantage that it requires no 'starting model' and is faster than the H+ method in its implementation but the disadvantage that it presents an extreme structural model with a series of insulating layers separated by very thin highly conducting layers. The Dawes method requires a starting model and a specified number of layers - in number the minimum is normally preferred - but it can provide a very good fit to the data over the complete frequency range. It is considered that joint interpretation of the structure revealed by the two methods is the most meaningful approach on account of the inherent non-uniqueness of this, as with other, geophysical techniques.

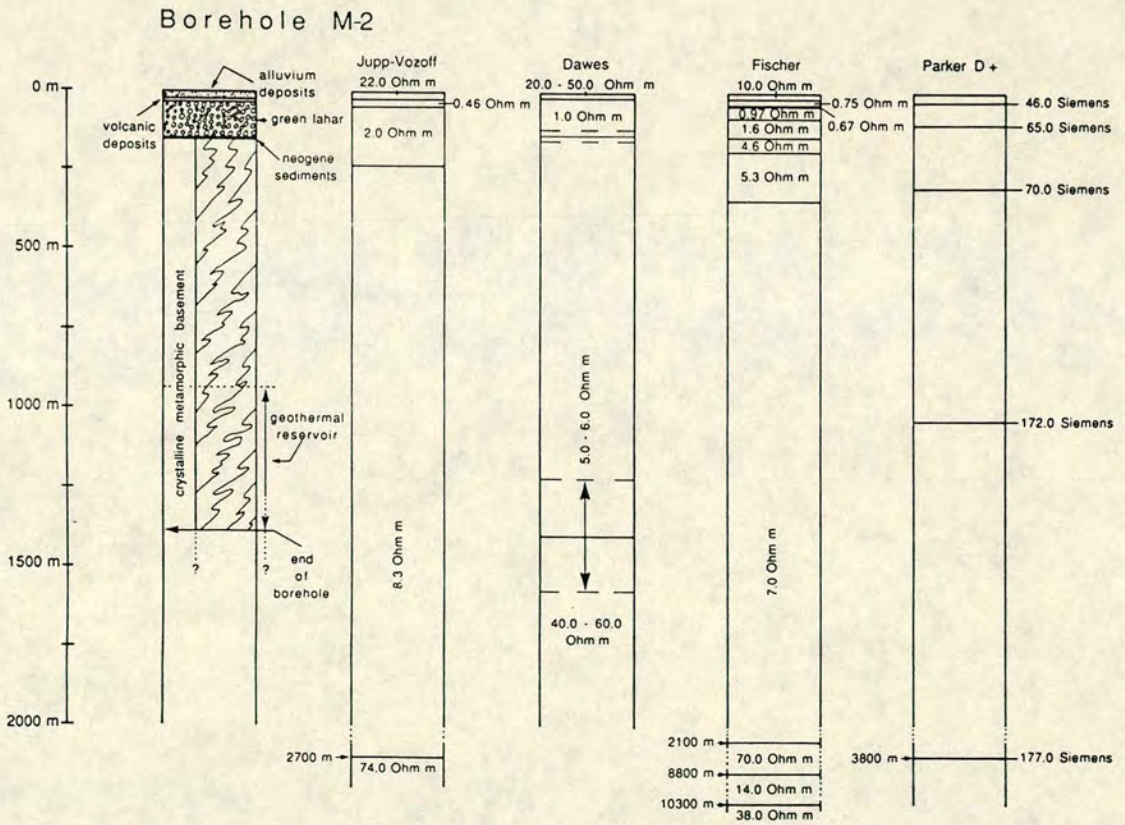

Figure 6. Comparison of 1-D models at site D6 with the stratigraphy from borehole M-2. Note that the model labelled 'MMC' in this figure is referred to in Figure 5 and the text as the Dawes method.

RESISTIVITY SECTIONS AND CONTOUR MAPS

The 1-D models at each site derived from the Dawes and Parker D+ methods have been collated as follows:-

(a) For the former method along traverses A,D,G and W - see Figure 1a.
(b) for the latter method along traverses A',D',G' and W' ; the exception of A' which is parallel to D' and G', these are also shown in Figure 1a.

These sections have already been presented in the interim reports with model parameters specified site by site as derived from the inversions. In Figure 7a of this paper sections W and G, which are based on Dawes' models, are presented as one section with resistivity values at neighbouring sites being averaged where appropriate. In Figure 7b sections W' and G', which are based on the Parker D+ models are shown with resistivity values estimated from the model conductances and interface separations (for direct comparison with the Dawes models), and with values at neighbouring sites averaged as before.

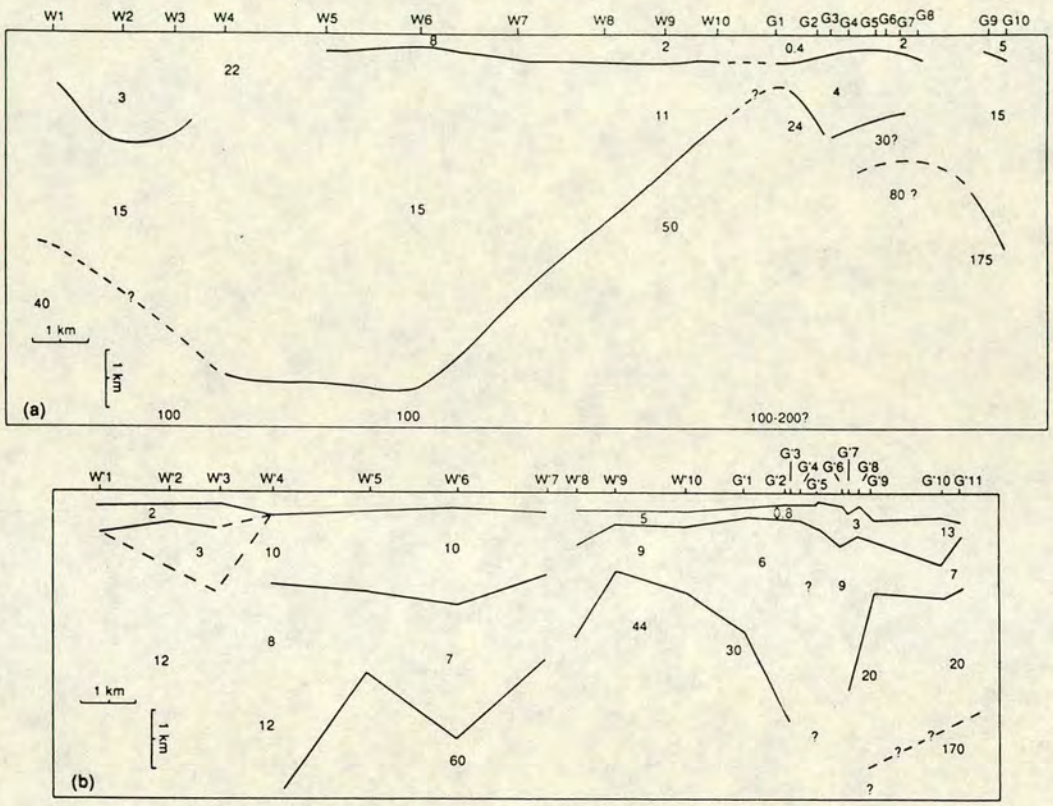

Figure 7. 1-D sections along traverses W and G (Dawes modelling procedure) and (b) along traverse W' and G' (Parker D+ modelling procedure).

Comparison of the two sections across the island shows that the general pattern of the structure is the same in the two cases but that both the number and locations of interfaces differ to some extent. Despite this there is clear evidence of very low resistivities (< 10 ohm.m) to a depth of several kilometres to the east of the section and also some evidence of low resistivities to the west, although here the station density is less. Using the borehole M-2 for calibration, the interface which can be associated at the borehole with the top of the reservoir - referred to later as the "R"-interface, is the second interface below the surface in both sections. The upper one corresponds at the borehole with the top of the crystalline basement. One further feature which should be noted is the indication of higher resistivities (> 100 ohm.m) in the bottom layer of Figure 7a and to the east of Figure 7b. Whether there is an increase of resistivity with depth or the values arise from the 1-D modelling of 2-D data - indication of two-dimensionality at the longer period end of the sounding has already been mentioned - will be discussed in the next section, as will the possible interpretation of the structure.

Contour maps have also been prepared of the interface depths and conductances derived from the Parker D+ models for sites on the east of the island. The two sets of contours presented in Figure 8 correspond to the depths to the top of the "R"-interface and the conductances of the "R"- layer. For comparison, the region of high thermal gradient is reproduced in the inset map.

It will be noted that the conductance high coincides approximately with the temperature gradient high and that the shape of the "R"-interface depth contours also corresponds roughly with the temperature gradient contours. For the depth contours, the dominant strike is approximately NW-SE which is the azimuth of the major impedance at most sites for the relevant sounding frequency and also the tectonic strike and main fault direction. As with the temperature gradient contours and the fault distribution (cf Figure 1b) the depth contours also show a distortion in the NE-SW direction in the central part of the region mapped. Similar maps drawn for the neighbouring interfaces and layers - to be published and discussed elsewhere - show some similarities and some differences.

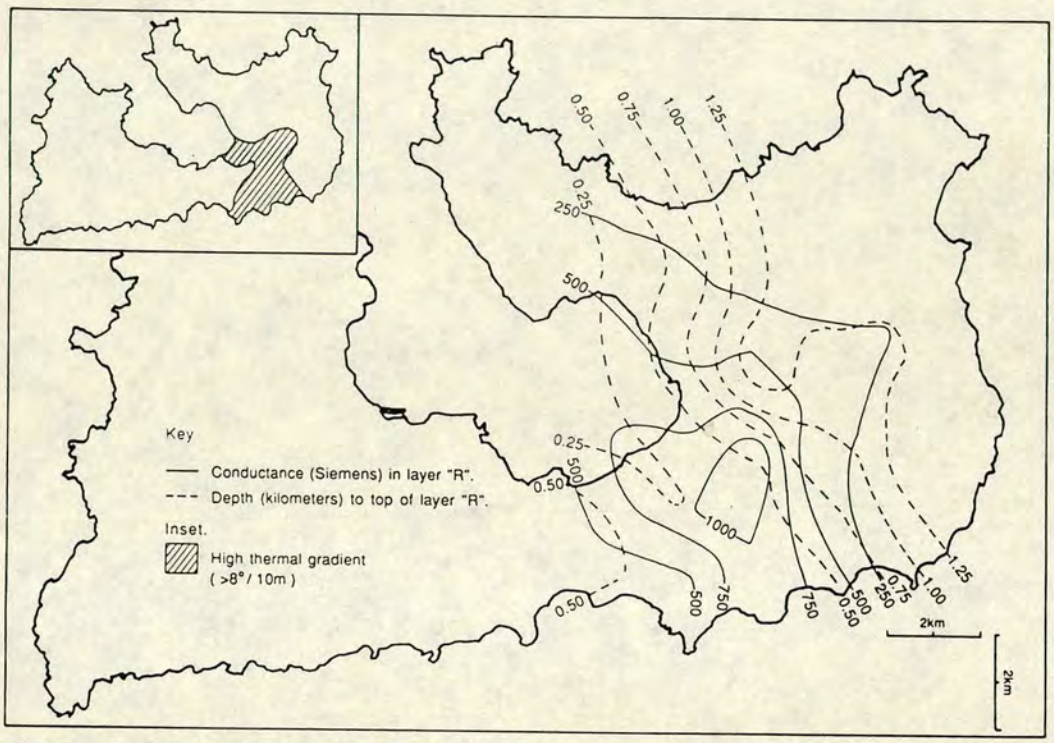

Figure 8. Contours of conductance in layer "R" - solid lines - and depth to the top of layer "R" - dashed lines - as derived from the Parker D+ modelling procedure. The shaded area (inset) shows the region of high thermal gradient.

2-D MODELLING

It has already been noted in the discussion of the dimensionality indicators that the data begin to show two dimensional behaviour at periods greater than about 100s at some sites. At the same time, the mapping of the parameters and the island location of the study region clearly indicate that the problem is in fact a three dimensional one. To provide some qualitative 3-D information, 2-D modelling has been undertaken along traverses D' and N - see Figure 1a. Different procedures have been used for the two directions. For traverse N, a 2-D inversion algorithm developed in the Edinburgh department by Zhang (1988) was used while forward modelling using Brewitt-Taylor and John's finite difference program (1980) was undertaken for traverse D'. For both traverses, satisfactory fit of the computed to the observed MT responses was obtained for the longer period E and H polarisation. Although further 2-D model studies are likely to improve the fit, it was felt that this was probably less worthwhile than attempting at a later stage to apply 3-D techniques. The best 2-D models at present are presented in Figure 9 with the sections as viewed in the direction indicated in the diagram at the top left hand corner. In this figure, traverse N of Figure 1a is labelled YY' and traverse D' is labelled XX'. As the sections extend to a depth of more than 10km, the small scale features of the surface layers are not included in this figure. The main points of interest in these sections are (a) the confirmation of the features observed in the presentations of the 1-D models for the uppermost few kilometres, and (b) indications of more resistive zones in the upper crust either at a few kilometres depth outside the main study region, as shown along traverse YY', or at depths greater than about 10 km under the study region as shown in the model XX'. It is also probable that satisfactory models could be found with the resistivity increasing laterally outside the 'resistivity low' and also with depth.

DISCUSSION AND CONCLUSIONS

The resistivity models resulting from this study have features consistent with those observed in previous studies of geothermal fields in that in the region of known field values, very low resistivities (< 1 ohm.m) have been detected in the surface layers - values which, in this study area, are consistent with the presence of sea water in the rock fabric. At greater depth, the

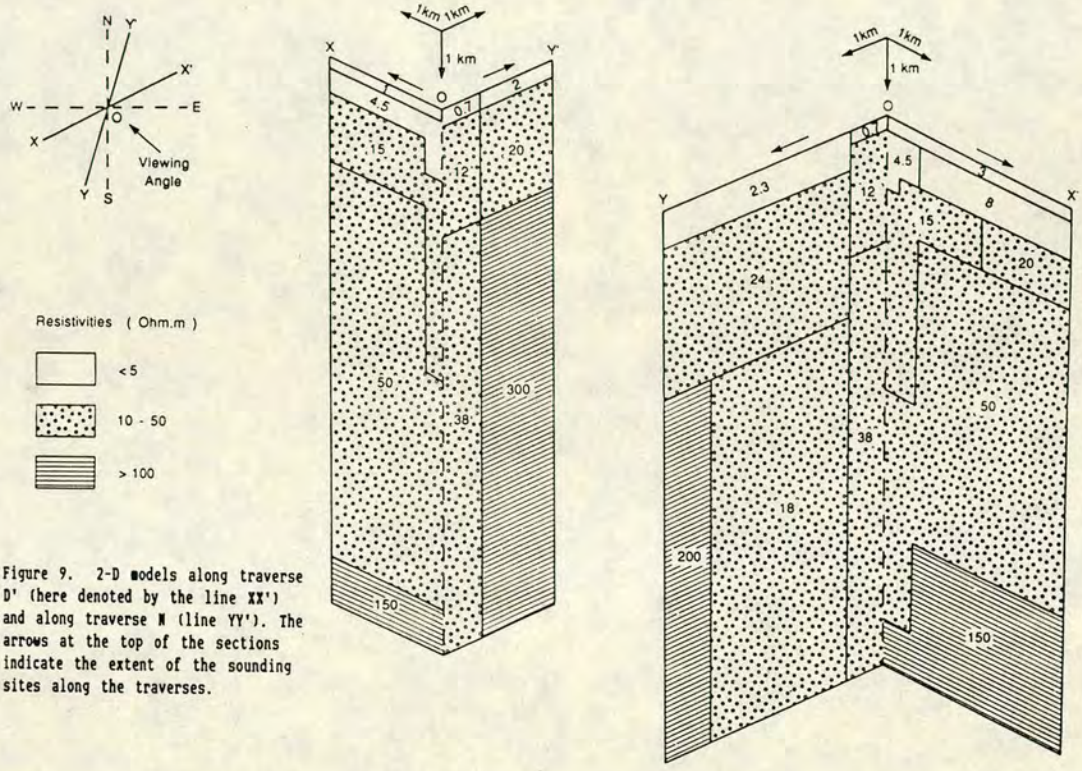

Figure 9. 2-D models along traverse D' (here denoted by the line XX') and along traverse N (line YY'). The arrows at the top of the sections indicate the extent of the sounding sites along the traverses.

resistivity of the crystalline basement below the geothermal is anomalously low (< 10 ohm.m) in the uppermost part of the basement and with values remaining less than 50 ohm.m to at least a depth of 10 km. As in previous studies (e.g. the Travale study in 1985) the most plausible interpretation of these basement resistivity values is in terms of fluid filled cracks, and it is suggested that small variations in the resistivity of the zone may well be associated with the fracture density and regions where there is evidence of faulting in crossed directions. There is also some evidence that in this region, as in Travale, the geothermal field is bounded by more resistive and thus more 'normal' crustal rocks.

From the results presented in this paper, it is considered that the use of a dense array of soundings and the efforts taken to obtain high quality responses have been fully justified. The success of the collaboration of the different groups undertaking electrical studies is discussed elsewhere in this volume. Further discussion of the contribution to geothermal studies from the application of electrical methods on Milos and other potential and productive fields e.g. Kos, Greece and Olkaria, Kenya, will be presented at a later stage.

ACKNOWLEDGEMENTS

We thank Nancy Butterworth, Alex Jackson, Maxwell Meju, Ronnie Parr and Andrew Tzanis for their assistance with the field work and Dr C. Thanassoulas of IGME for much help with Customs formalities. We acknowledge the financial and logistic support of the C.E.C. and the loan of some equipment from the U.K. Natural Environment Research Council Equipment Pool, whose Officer-in-Charge, Val Valiant, provided valuable help. We enjoyed many fruitful discussions with and much hospitality from other EC institutions.

REFERENCES

Barbier, E., Wohlenberg, J., Ungemach, P., (eds.) (1985) - Testing geophysical methods in the Travale geothermal field. Special Issue, *Geothermics*, 14, 609-775.

Bostick, F.X. (1977) - A simple almost exact method of MT analysis. Workshop on Electrical Methods in Geothermal Exploration, U.S. Geol. Survey, Contract No. 14080001-8-359.

Brewitt-Taylor, C.R., Johns, P.B. (1980) - Diakoptic solution of induction problems. *J.Geomagn.Geoelectr.*, **32** Suppl.I SI73-SI78.

Dawes, G.J.K. (1984) - Short period automatic magnetotelluric (S.P.A.M.) system. In A broadband tensorial magnetotelluric study in the Travale-Radicondoli geothermal field. (Hutton et al.) Final Report, EC Contract No. EG-A2-031-UK.

Dawes, G.J.K. (1985) - Magnetotelluric feasibility study, Island of Milos - Greece. Final Report EC Contract No. EN-3G-0008-UK (H).

Dawes, G.J.K., Galanopoulos, D., Hutton, V.R.S. (1987) - Magnetotelluric studies, Milos, Greece, 1986. Interim Report, EC Contract No. EN-3G-0026-UK (H), University of Edinburgh.

Drews, C., Furch, N., Maurer, H.M., Musman, G., Weidelt, P. (1988) - Active Audiomagnetotellurics on Milos (Greece) for determination of electrical conductivity distribution and their correlation to geothermal anomalies. Final Report, EC Contract No. EN-3G-0024-D, Technische Universität Braunschweig.

Fischer, G., Schnegg, P.A., Peguiron, M., Le Quang, B.V. (1981) - An analytic one dimensional magnetotelluric inversion scheme, *Geophys.J.R.Astr.Soc.*, 67, 257-278.

Fytikas, M.D., (1977) - Geological and geothermal study of Milos island, Ph.D Thesis, (in Greek with summary in English), Geological and Geophysical Research I.G.M.E, 18, No.1.

Hutton, V.R.S., Dawes, G.J.K., Galanopoulos, D. (1987) - Magnetotelluric Studies, Milos, Greece. Interim Report, EC Contract No. EN-3G-0026-UK (H), University of Edinburgh.

Hutton, V.R.S., Dawes, G.J.K., Galanopoulos, D. (1988) - Magnetotelluric studies, Milos, Greece. Interim Report, EC Contract No. EN-3G-0026-UK (H), University of Edinburgh.

Jupp, D.L., Vozoff, K. (1975) - Stable iterative methods for inversion of geophysical data. *Geophys.J.R.Astr.Soc.*, 42, 957-976.

Kao, D., Orr, D. (1982) - Magnetotelluric studies in the Market Weighton area of eastern England. *Geophys.J.R.Astr.Soc.*, 60, 323,327.

Parker, R.L. (1980) - The inverse problem of electromagnetic induction: Existence and construction of solutions based on incomplete data. *J.Geophys.Res.*, 85, 4421-4428.

Parker, R.L., Whaler, K.A. (1981) - Numerical methods for establishing solutions to the inverse problem of electromagnetic induction. *J.Geophys.Res.*, 86, 9754-9584.

Parker, R.L. (1983) - The magnetotelluric inverse problem. *Geophysical Surveys*, 6, 5-25.

Ranganayaki, R.P. (1984) - An interpretive analysis of magnetotelluric data. *Geophysics*, 49, 1730-1748.

Sule, P.O. (1985) - A broadband magnetotelluric investigation in southeast Scotland. Ph.D. Thesis, University of Edinburgh.

Valiant, M. (1977) - Geologger System Handbook. NERC Publication.

Word, D.R., Smith, H.W., Bostick F.X. (1970) - An investigation of the magnetotelluric tensor impedance method. Tech.Rep.No. 82, Elec. Geophys. Lab., University of Texas at Austin.

Zhang, A.J. (1988) - Modelling and inversion of two-dimensional magnetotelluric data. Ph.D. Thesis, University of Edinburgh.

APPENDIX II

THE KENYA POWER COMPANY LTD.

OLKARIA GEOTHERMAL PROJECT

A Broadband Magnetotelluric Survey

A report prepared by

V.R.S. Hutton, D. Galanopoulos and G.E. Pickup

June 1989

University of Edinburgh

Department of Geophysics

Contents

Figures

Plates

1. Introduction

The Working Documents for the Scientific Review Meetings (G.E.N.Z.L. 1986 and K.P.C. Ltd. 1988) and Mwangi and Bromley (1986) summarise the extensive studies already undertaken for the assessment of the resources of the Olkaria geothermal field. As in geothermal regions elsewhere, these have understandably concentrated on direct observations, eg temperature, made at the Earth's surface or in boreholes, and on application of exploration techniques eg magnetic, gravity and electrical resistivity from which the physical parameters of the crust's upper few kilometres can be inferred. Information about the deeper crust under the Olkaria field, in particular the detection and nature of the source or sources of the high heat flow have not yet been provided by the procedures previously adopted. With this as the main objective in mind the University of Edinburgh in collaboration with the Kenya Power Company Ltd. has undertaken a broadband magnetotelluric survey in the region of the Olkaria geothermal field. A useful introduction to the magnetotelluric method and some case studies can be found in the S.E.G.'s Geophysics reprint series No. 5 (ed. Vozoff 1985). The procedures adopted followed closely those which contributed to a successful integrated model of the Milos, Greece geothermal field as described in the special issue of Geothermics (Garnish et al. 1989).

2. Fieldwork

Between 1 February and 15 March, 1989, magnetotelluric soundings were undertaken at 30 locations in the region of the Olkaria geothermal field. Participants in the fieldwork included G. Dawes, as team leader, D. Galanopoulos and P. Jones of the University of Edinburgh and M. Mwangi and S. Onacha of KPLC. The location of the soundings are shown in Fig. 1(a) which overlays a map, Fig. 1(b), showing the major faults and wells. The site identification numbers and the 4 profiles P1, P2, P3 and P4 for which resistivity sections are included in this

Fig.1 b

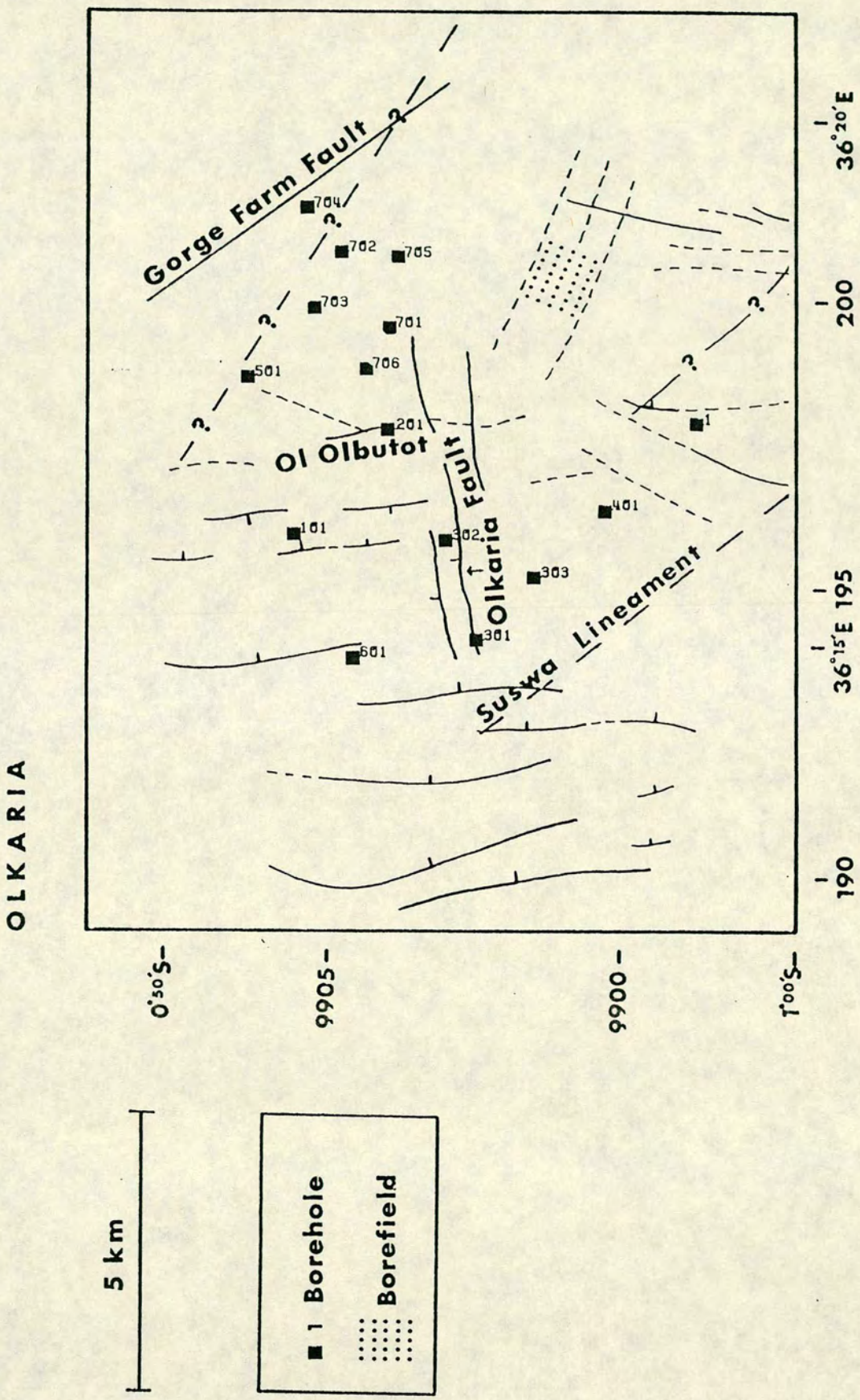
OLKARIA
Gorge Farm Fault
Ol Olbutot
Olkaria Fault
Suswa Lineament
704
702
705
703
701
706
501
201
1
401
101
302
303
301
601
0°30'S
9905
9900
1°00'S
36°20'E
200
36°15'E
195
190
5 km
1 Borehole
Borefield

272 A.

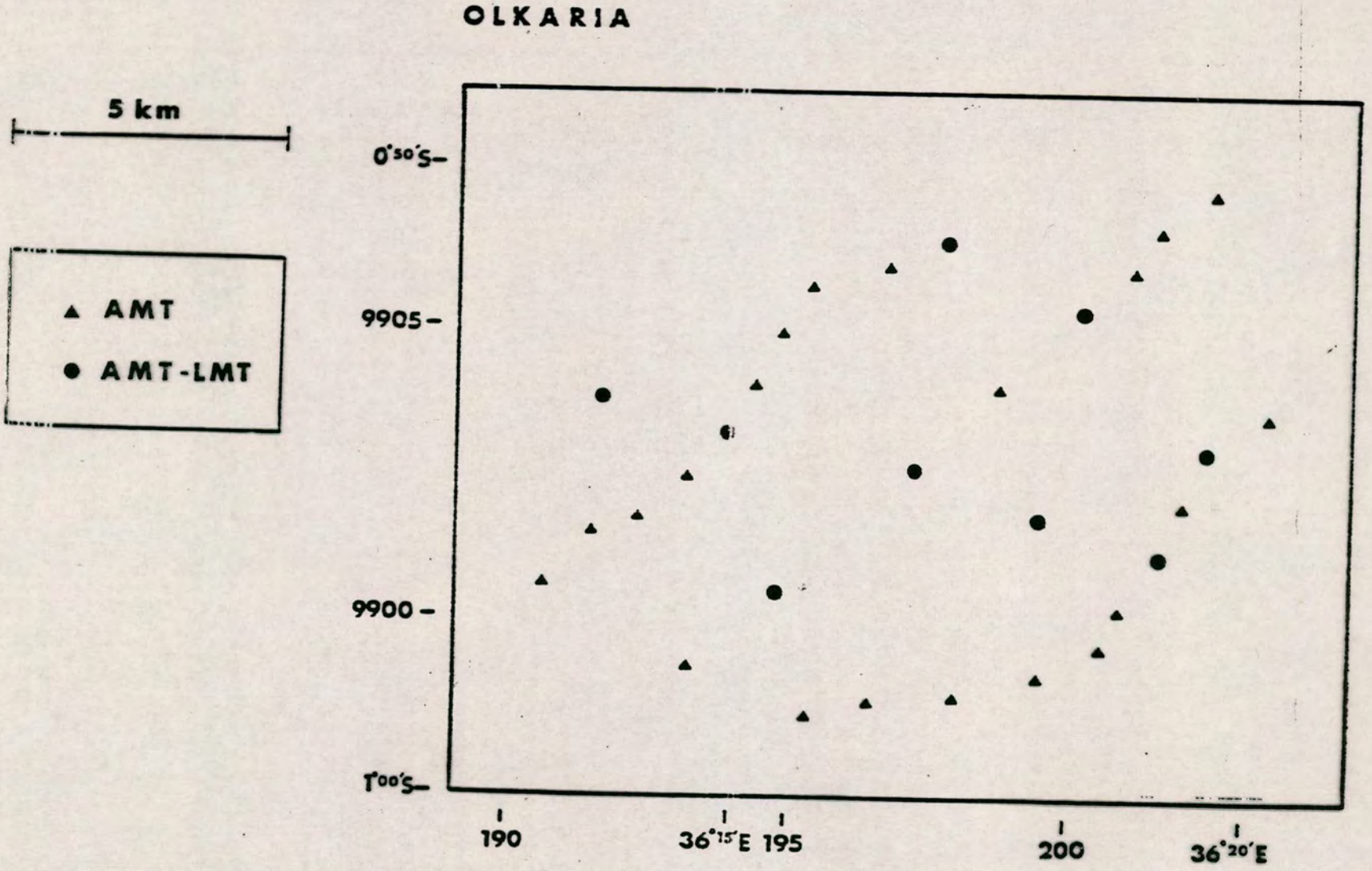
OLKARIA
5 km
AMT
AMT-LMT
0°50'S
9905
9900
1°00'S
190
36°15'E
195
200
36°20'E

Fig. 1 a

Fig.1 c

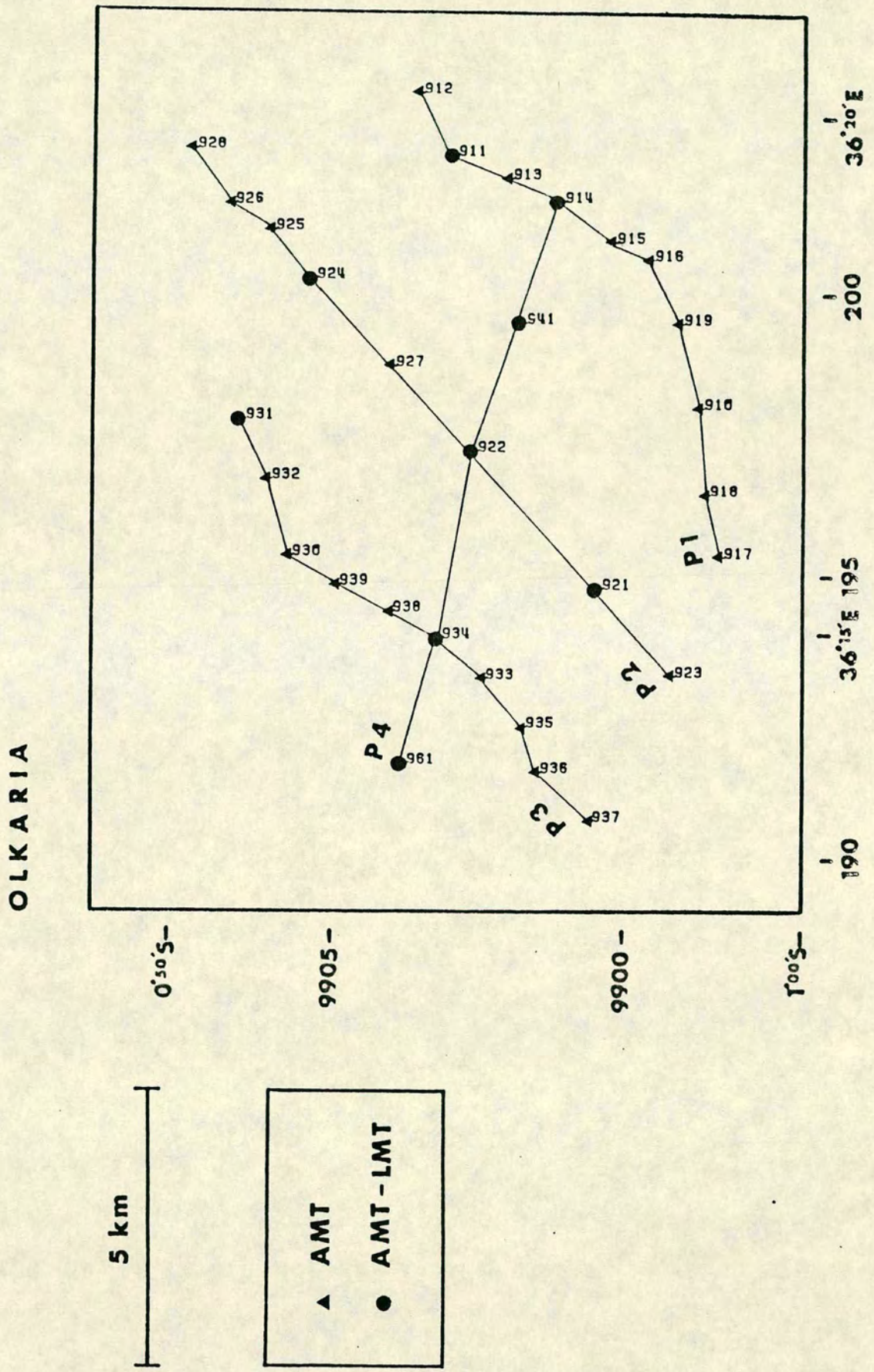
OLKARIA
0°30'S
9905
9900
1°00'S
190
195
200
36°15'E
36°20'E
912
911
913
914
915
916
919
918
917
928
926
925
924
927
S41
931
932
930
939
938
934
933
935
936
937
961
922
921
923
P1
P2
P3
P4
5 km
AMT
AMT-LMT

report are shown in Fig. 1(c). At 21 of the sites - indicated by small triangles on Figs. 1(a) and (c) - the sounding range was 128-0.016 Hz, and at 9 sites - indicated by dots on the same figures - was 128-0.0003 Hz. The Edinburgh S.P.A.M. Mk IIb system, developed by Dawes from the original system described by him in 1984 - see Plates 1 and 2, was used for the former range and the NERC/LMT system provided the data for the additional deeper sounding range.

Plates 3-5 show the installation of the magnetic and telluric sensors for the S.P.A.M. system which took about one hour for each site. The setting up of the LMT system - Plate 7 - was accomplished in about 2 hours per site. The S.P.A.M. data were selected and analysed automatically - see Plate 6 - with adequate good quality results being acquired in a period of 8 hours at most sites. As natural long period activity is intermittent, the LMT data were recorded digitally on magnetic tape cassettes for approximately 10 days at each LMT site. To ensure satisfactory data acquisition and to monitor the level of magnetic activity these magnetic tapes were read in the evening on to floppy discs and visually examined on an LSI computer screen. The only difficulty encountered during the field program was the malfunctioning of the S.P.A.M. printer unit. This developed progressively after the first few soundings and was eventually abandoned. Figure 2 of a 'Broadband Magnetotelluric Survey - a Preliminary Report' (Hutton 1989) shows an example of a successful in-field output. The normal automatic data acquisition and analysis of the S.P.A.M. system was unaffected by this fault and the data quality was monitored on the S.P.A.M. terminal by visual observation of various parameters. Other computer programs enabled the output on the terminal of apparent resistivity and phase data and preliminary 1-dimensional models (Bostick and Fischer). The latter formed the basis of the resistivity sections presented in that preliminary report.

For both data acquisition systems 3 orthogonal components of the Earth's magnetic field - Hx, Hy, and Hz and the 2 horizontal components - Ex and Ey of

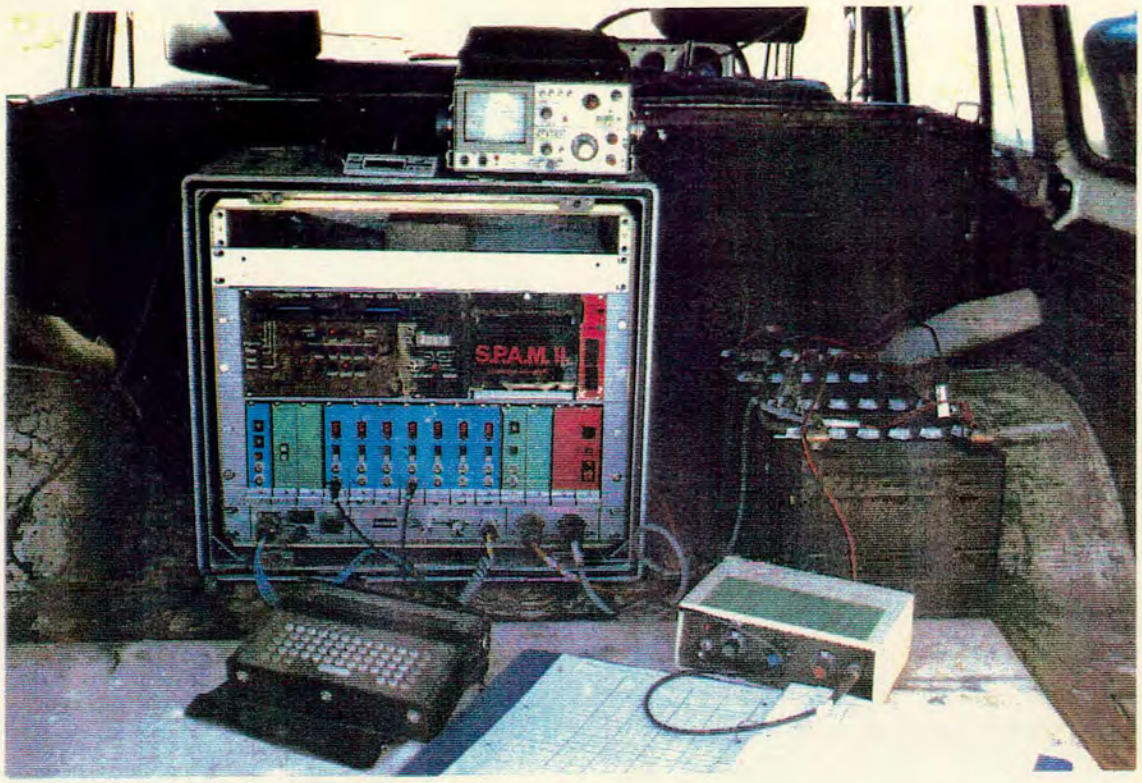

PLATE 1

PLATE 2

PLATE 3

PLATE 4

PLATE 5

PLATE 6

PLATE 7

the telluric field were monitored. Data were thus available not only for application of the tensorial magnetotelluric (MT) techniques but additionally for the determination of the magnetovariational (MV) parameters such as tipper. The MT procedures provide information about resistivity anisotropy in addition to resistivity-depth profiles and the MV procedures help locate lateral variations in structure.

3. Data Processing and Modelling Procedures

All data were re-processed on the Edinburgh mainframe computer to provide the frequency variations of

(i) apparent resistivity and phase in each of the N-S and E-W directions

(ii) apparent resistivity and phase rotated to the principal directions

(iii) the average coherency, number of estimates averaged, the skew (a dimensionality indicator) and the azimuth of the major impedance

(iv) the invariant average apparent resistivity and phase

(v) the real and imaginary vertical magnetic field response functions and their azimuths.

An example of the above computer output for one site (961) is given in Fig. 2(a) for (i), and Fig. 2(b) for (ii) - (iv). The frequency variations (v) for site 961 are given in Fig. 3. It should be noted that before modelling was carried out, the computer files were edited to remove poor quality data near the limits of the filter pass bands. Although the modelling presented in this report is restricted to the assumption of one dimensional structures (i.e. resistivity as a function of depth only) and is derived from variations (iv), it is useful to examine all the plots of the type produced in Fig. 2(b) for indication of the extent to which the observations reflect one dimensionality. Site 961 is typical of the majority of sites in that the skew factor is small, less than 0.2, for frequencies greater than 0.001 Hz. This suggests one dimensionality if the major and minor apparent resistivities are

Fig. 2a

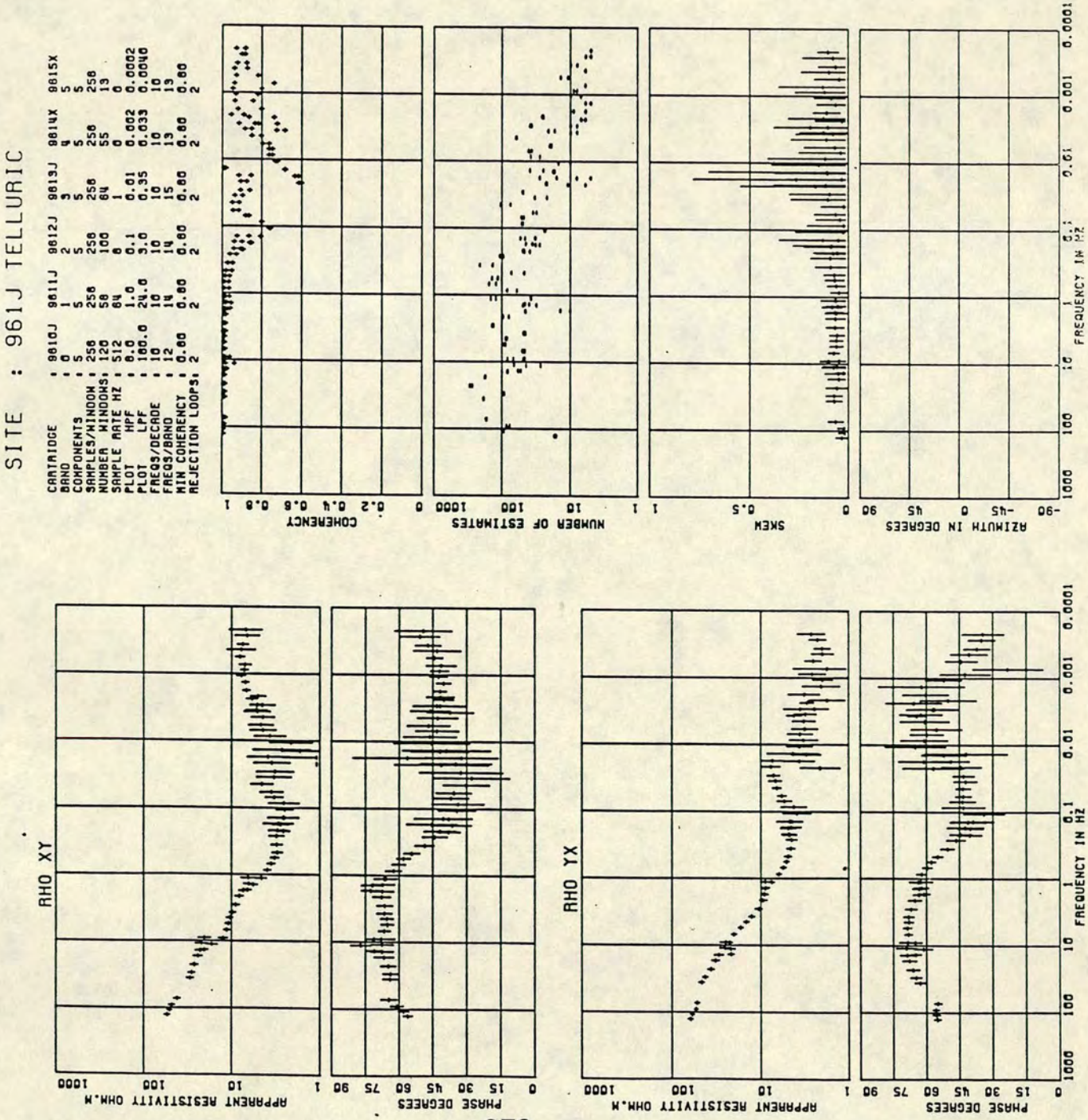
SITE : 961J TELLURIC
CARTRIDGE : 961J 961J 961J 961J 961X 961X
BAND : 0 1 2 3 4 5
COMPONENTS : 5 5 5 5 5 5
SAMPLES/WINDOW : 256 256 256 256 256 256
NUMBER WINDOWS: 120 50 100 64 55 13
SAMPLE RATE HZ : 512 64 8 1 8 8
PLOT HPF : 8.8 1.0 0.1 0.01 0.002 0.0002
PLOT LPF : 160.0 24.0 3.0 0.35 0.033 0.0046
FREQS/DECADE : 10 10 10 10 10 10
FREQS/BAND : 12 14 14 15 13 13
MIN COHERENCY : 0.60 0.60 0.60 0.60 0.60 0.60
REJECTION LOOPS: 2 2 2 2 2 2
COHERENCY
NUMBER OF ESTIMATES
SKEW
AZIMUTH IN DEGREES
FREQUENCY IN HZ
RHO XY
APPARENT RESISTIVITY OHM.M
PHASE DEGREES
RHO YX
APPARENT RESISTIVITY OHM.M
PHASE DEGREES
FREQUENCY IN HZ

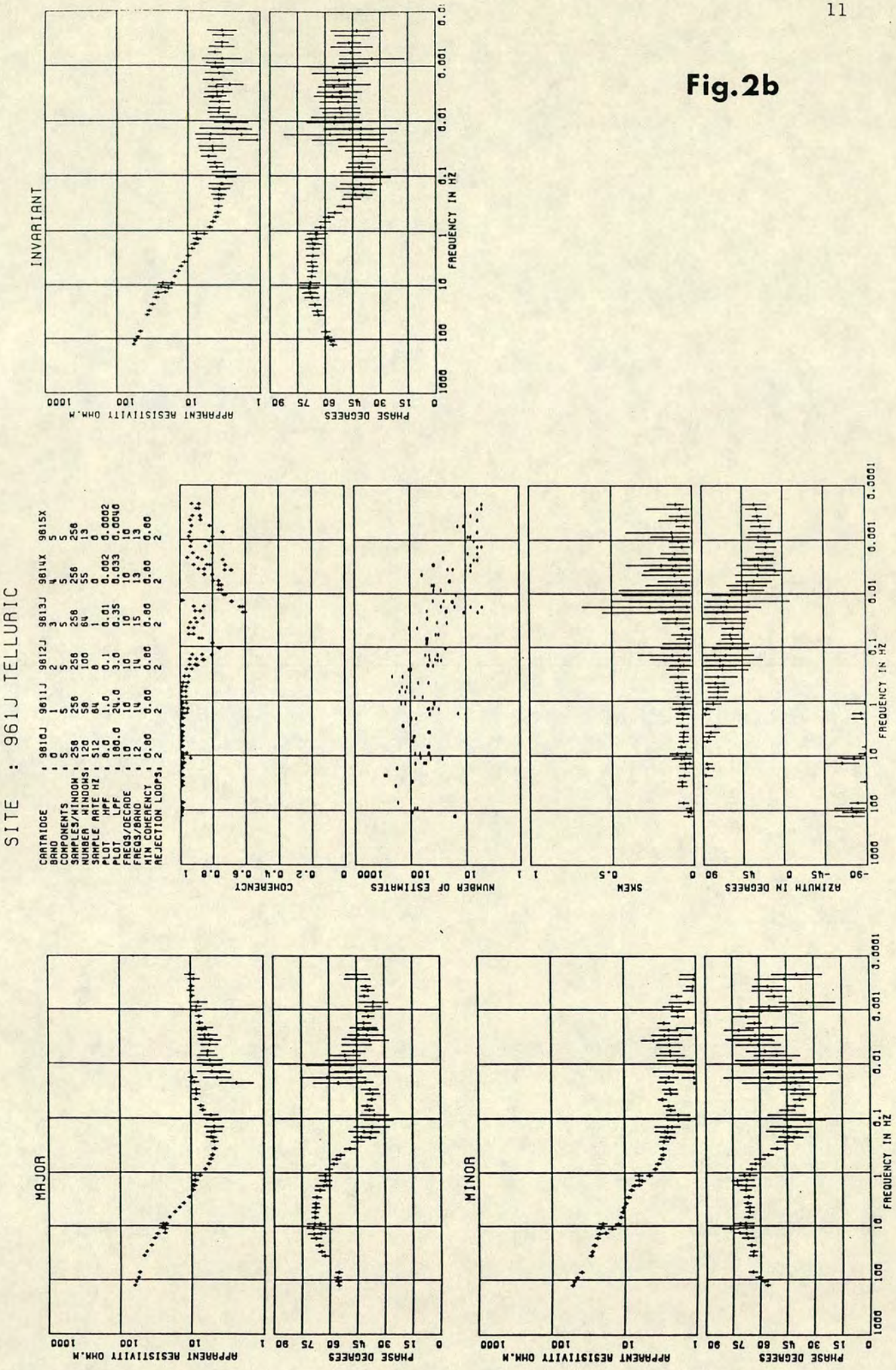
INVARIANT
APPARENT RESISTIVITY OHM.M
PHASE DEGREES
FREQUENCY IN HZ
SITE : 961J TELLURIC
CARTRIDGE : 9810J 9811J 9812J 9813J 9814X 9815X
BAND : 0 1 2 3 4 5
COMPONENTS : S S S S S S
SAMPLES/WINDOW : 256 256 256 256 256 256
NUMBER WINDOWS : 120 50 100 64 55 13
SAMPLE RATE HZ : 512 64 8 1 0 0
PLOT HPF : 8.0 1.0 0.1 0.01 0.002 0.0002
PLOT LPF : 100.0 24.0 3.0 0.35 0.033 0.0040
FREQS/DECADE : 10 10 10 10 10 10
FREQS/BAND : 12 14 15 13 13
MIN COHERENCY : 0.80 0.80 0.80 0.80 0.80 0.80
REJECTION LOOPS: 2 2 2 2 2 2
COHERENCY
NUMBER OF ESTIMATES
SKEW
AZIMUTH IN DEGREES
MAJOR
MINOR

Fig.2b

Fig.3

SITE : 961J MAGNETIC

CARTRIDGE	9610J	9611J	9612J	9613J	9614X	9615X
BAND	0	1	2	3	4	5
COMPONENTS	5	5	5	5	5	5
SAMPLES/WINDOW	256	256	256	256	256	256
NUMBER WINDOWS	120	50	100	64	55	13
SAMPLE RATE HZ	512	64	8	1	0	0
PLOT HPF	8.0	1.0	0.1	0.01	0.002	0.0002
PLOT LPF	160.0	24.0	3.0	0.33	0.033	0.0040
FREQS/DECADE	10	10	10	10	10	10
FREQS/BAND	12	14	14	15	13	13
MIN COHERENCY	0.70	0.70	0.70	0.70	0.70	0.70
REJECTION LOOPS	2	2	2	2	2	2

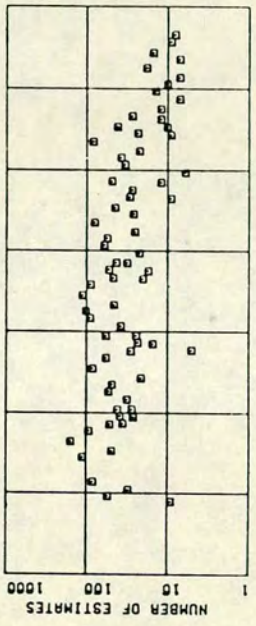

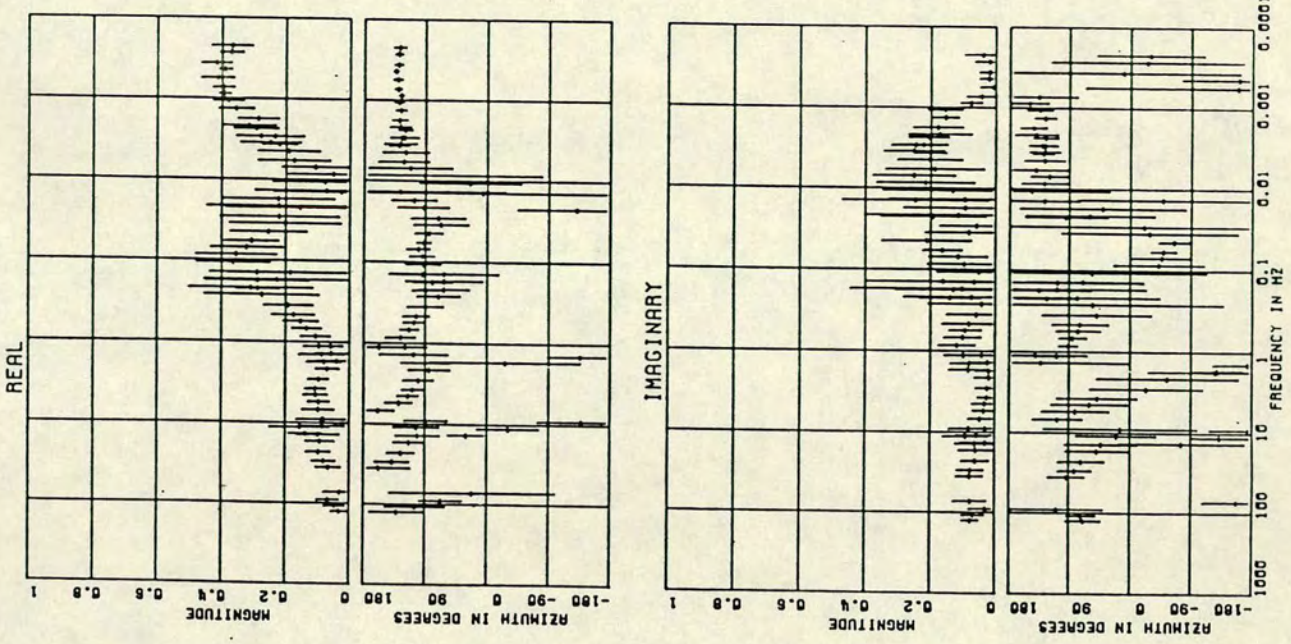

approximately equal and 2 dimensionality if they differ. Comparison of the plots ρmaj and ρmin versus frequency - re-drawn without error bars as Fig. 4 - suggests approximately 1D structure for site 961 at higher frequencies i.e. shallow depths, tending to 2D structure at greater depth. The degree of anisotropy over the study area as a whole can be seen from an examimation of all six examples of Fig. 4. They indicate 1D structure at site 931 while at other sites there is a tendency towards two dimensionality normally at lower frequencies i.e. at greater depths. It must be noted, however, that by comparison with the results of many regional MT surveys, the maximum difference between ρmaj and ρmin of about 1 decade is relatively small - differences of 2 or 3 decades can be found (eg Rooney and Hutton's (1977) study of the Gregory Rift in Kenya). It follows as a result that, for the upper few kilometers at least, one dimensional modelling procedures should provide a close approximation to the actual resistivity structures of the Olkaria region.

Three different modelling procedures were adopted in this study - the Fischer(1981) and Dawes (see Sule, 1985 for description) methods providing layered Earth models and the Bostick method (1977) a continuous resistivity versus depth profile. Fischer and Bostick models only are presented in this report but all three algorithms resulted in comparable models when a large number of layers was assumed in the Dawes algorithm - the layer number is not constrained in the Fischer routine. An example of the compatability of the Fischer and Bostick models is shown in Fig. 5 for site 934 - in the former case the top layer resistivity was constrained by the surface resistivity as provided by a previous DC resistivity model for that site (Mwangi and Bromley, 1986).

While the modelling routines were equally satisfactory for single site inversions, the Bostick method was adopted for preparation of resistivity maps and sections in view of the ease with which the parameters of neighbouring sites could be collated. As an illustration of the effect of anisotropy, the Bostick models

Fig.4

931

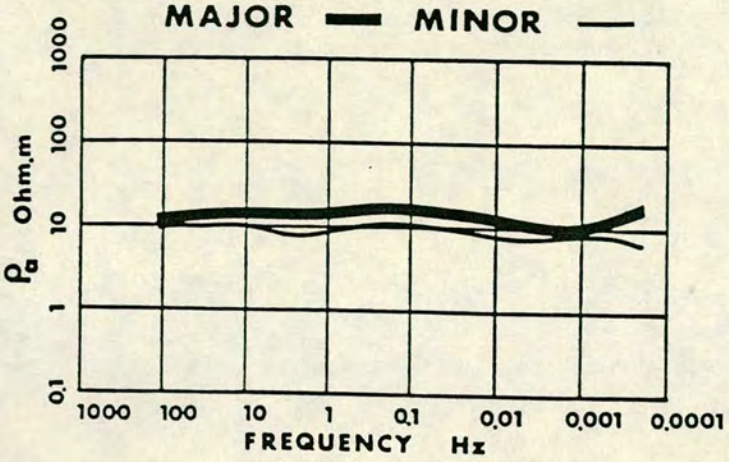

921

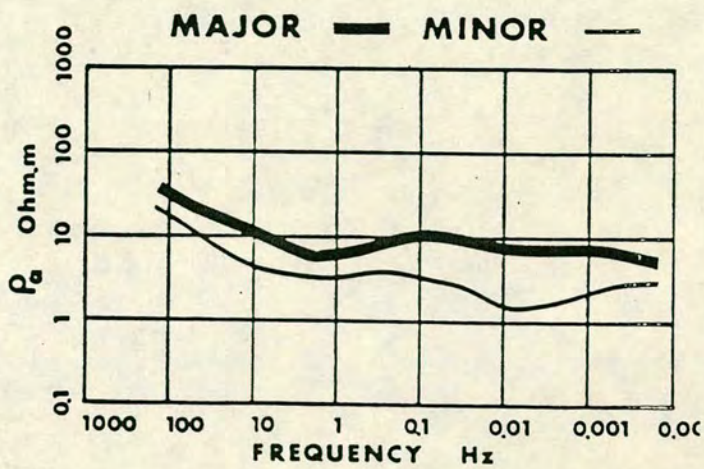

961

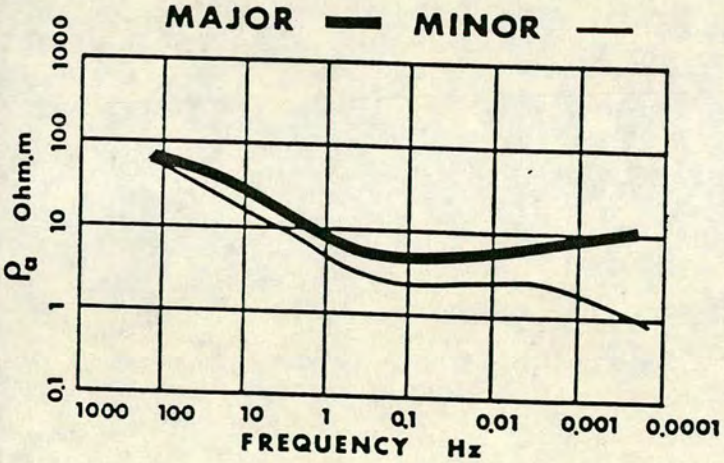

922

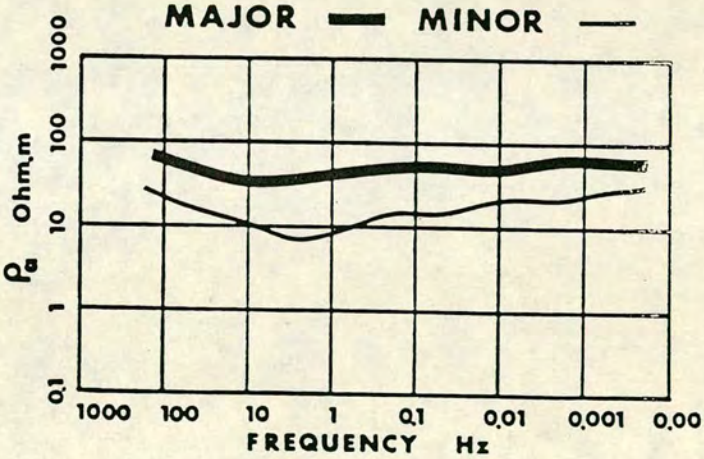

914

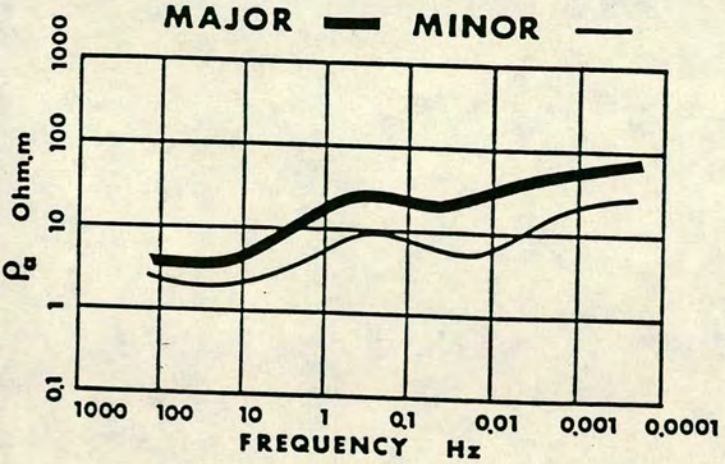

911

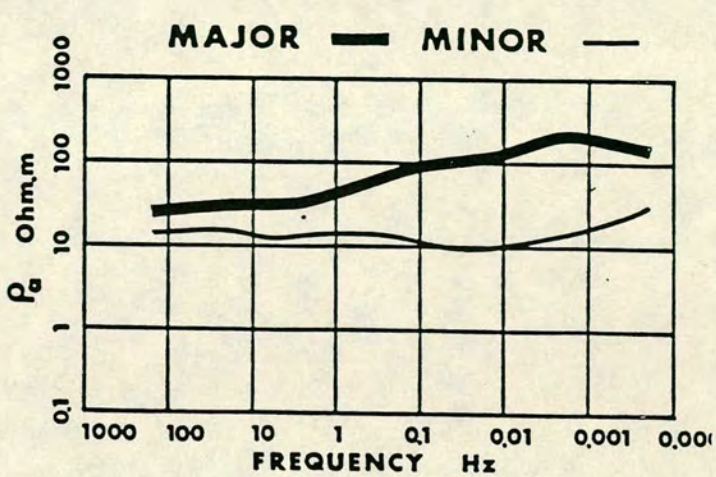

Fig.5

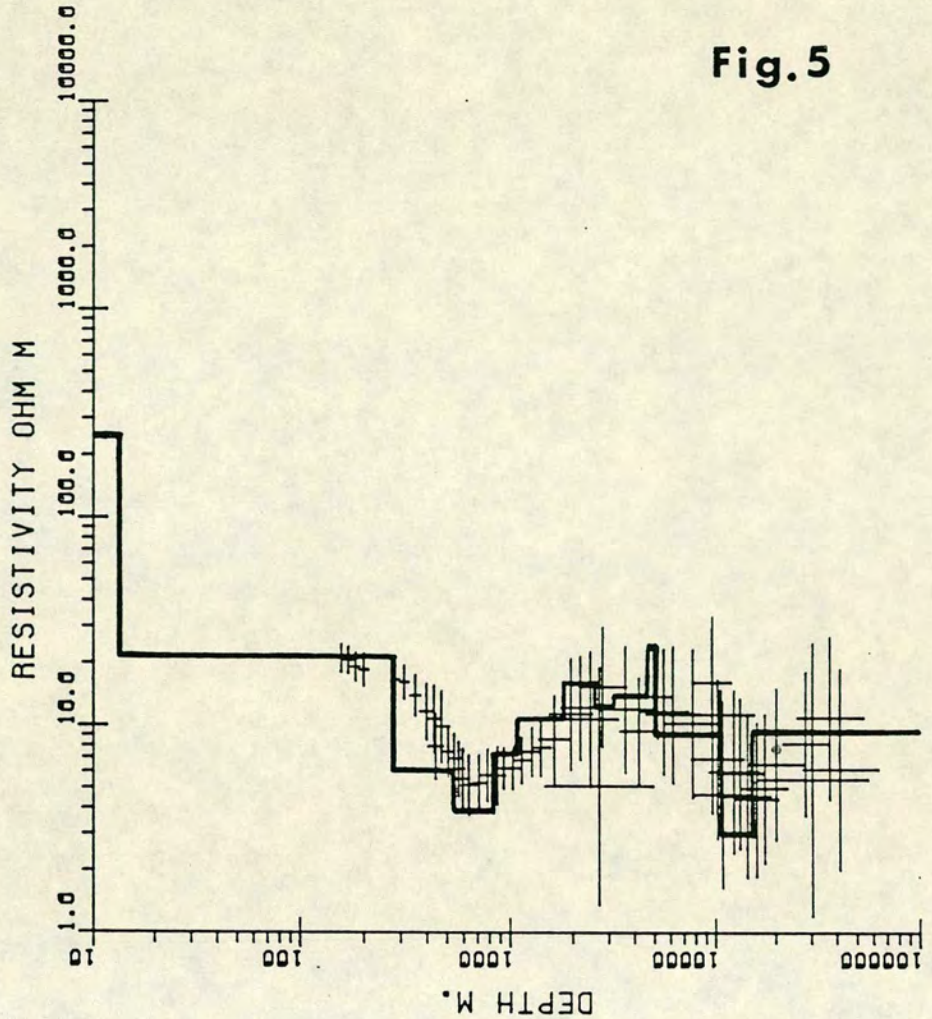
RESISTIVITY OHM M
10000.0
1000.0
100.0
10.0
1.0
10
100
1000
10000
100000
DEPTH M.

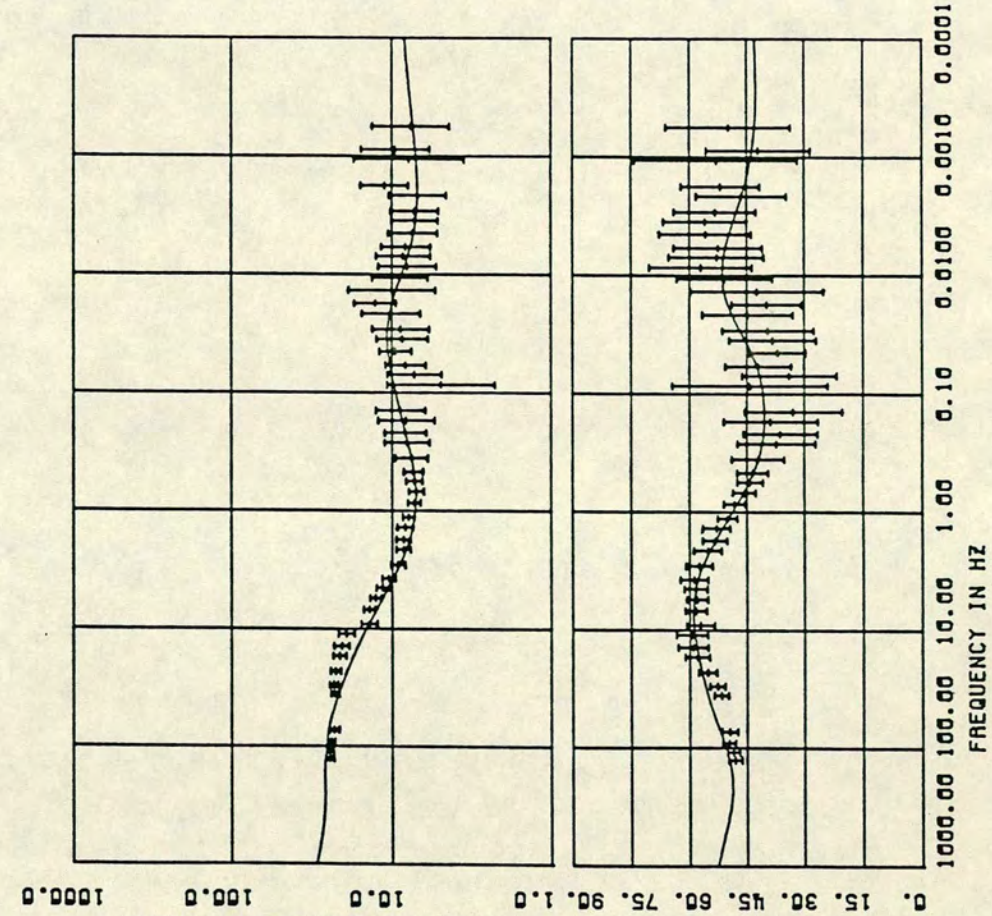
1-D MODEL 934
APPARENT RESISTIVITY OHM.M
1000.0
100.0
10.0
1.0
PHASE DEGREES
0.
15.
30.
45.
60.
75.
90.
1000.00 100.00 10.00 1.00 0.10 0.0100 0.0010 0.0001
FREQUENCY IN HZ

derived from the major, minor and invariant average resistivities and phases at site 911 are presented in Fig. 6. There is considerable discrepancy between the resistivities at depths between 3 and 30 km. It has already been noted, however, that this is the most anisotropic site of the present survey.

4. The Results of Data Processing

For a qualitative overview of all the apparent resistivity data, it is first useful to map the axes of the MT polarisation ellipses (ie ρmaj and ρmin amplitudes and azimuths) for a set of period ranges. In Figs. 7(a)-(c) these are presented for 3 different frequency bands - (a) 0.01-0.02s, (b) 5-25s and (c) 25-50s. The main features of these maps are as follows:

(a) In the lowest period band - 7(a) - which corresponds to shallow depths, the resistivities are relatively isotropic at most sites with the lowest resistivities occurring along profile 1.

(b) In the longest period band - 7(c) - the resistivities are anisotropic at most sites with the azimuth of the major resistivities being approximately E-W in general. The significance of this trend is relevant to the 2D modelling which is now being initiated. In contrast to Fig. 7(a), the resistivities at the longer periods of Fig. 7(c) which refer to several km depth are lowest in the western part of the survey area. These facts together suggest an electrical strike in the N-S direction with an interface separating a low from a higher resistivity area to the west of Olkaria Peak.

(c) The intermediate map shows many of the features of map 7(c) but additionally it shows local changes with period at the most southerly 3 sites.

The complementary magnetovariational response functions (tippers) have been mapped and the real parts are presented in figs. 8(a) - (c) for three period bands - (a) 0.02-0.05s, (b) 25-50s and (c) 1,500-2,500s. Normally such maps are

Fig. 6

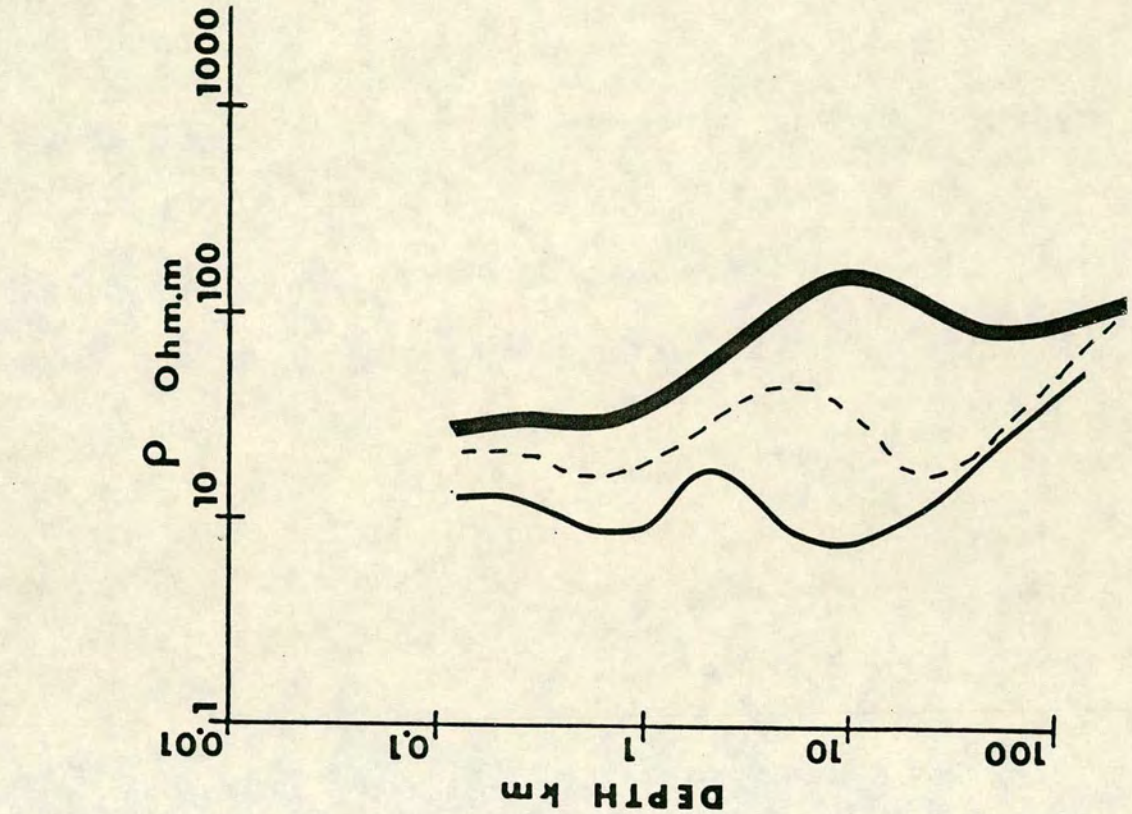
ρ Ohm.m
1000
100
10
1
0.1
0.01
DEPTH km
0.1
1
10
100

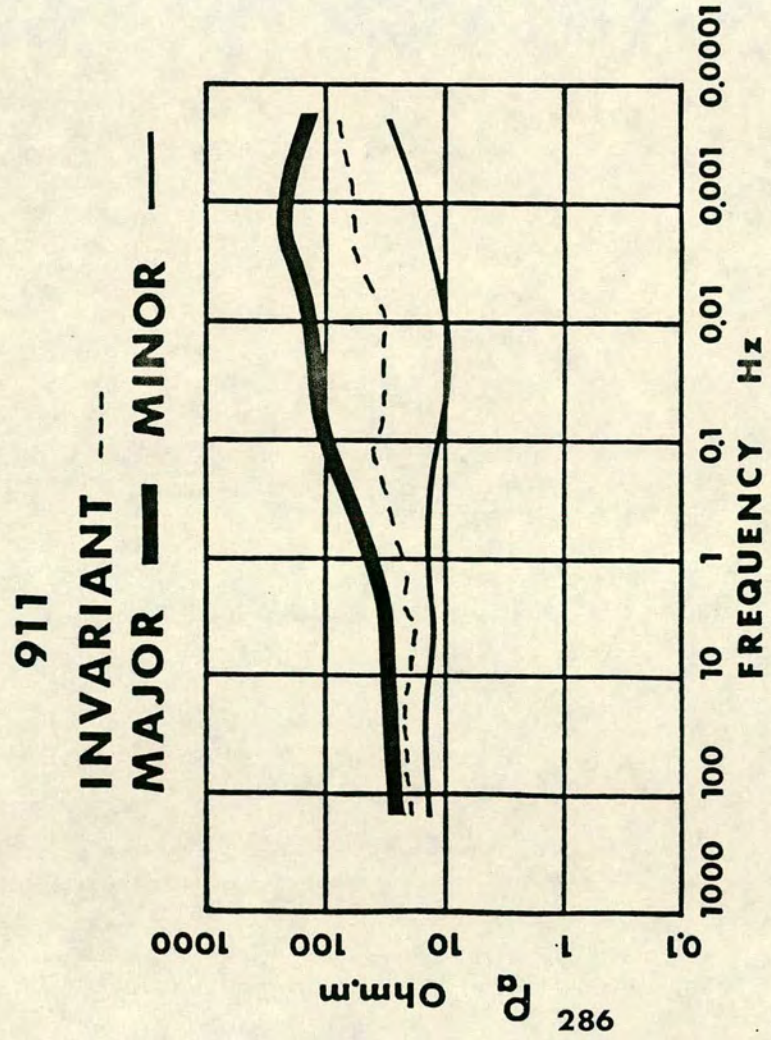
911
INVARIANT ---
MAJOR ▬ MINOR —
ρ_a Ohm.m
0.1
1
10
100
1000
FREQUENCY Hz
1000
100
10
1
0.1
0.01
0.001
0.0001

Fig.7

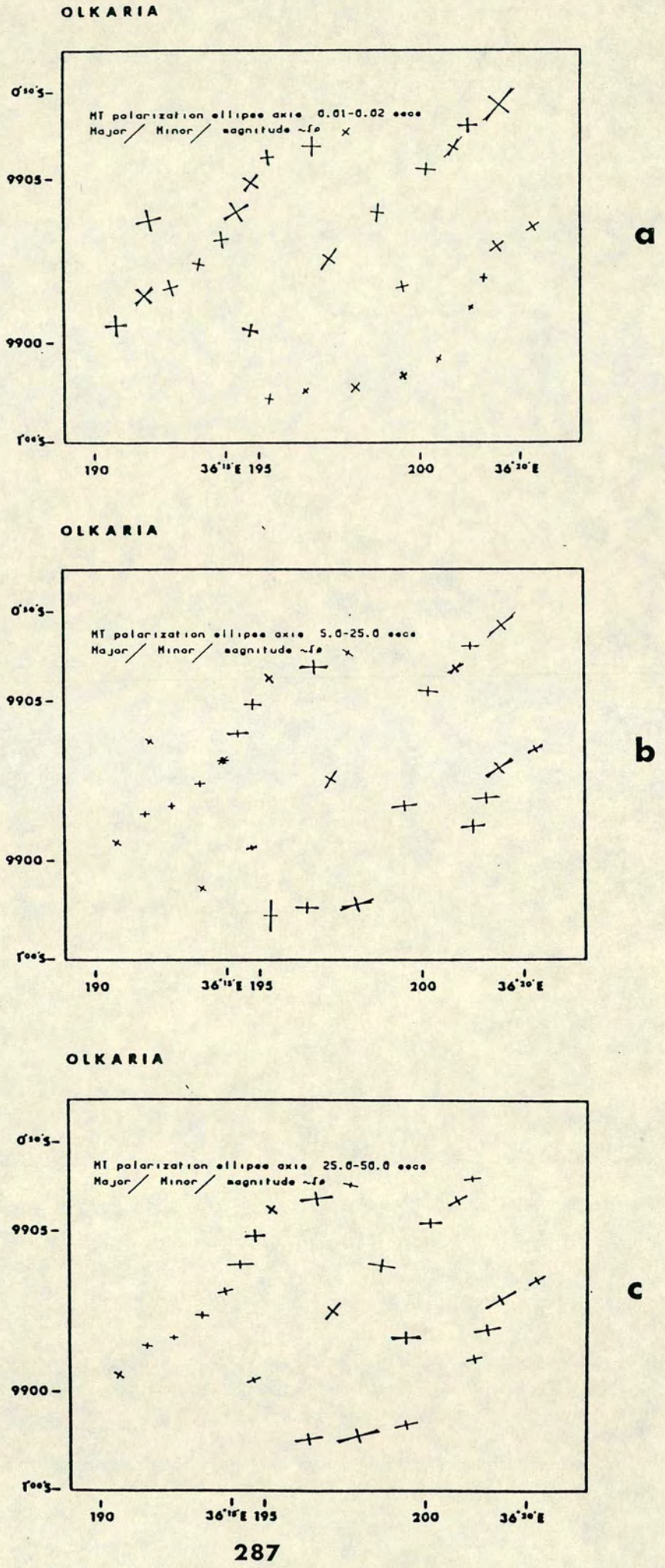
OLKARIA
MT polarization ellipse axis 0.01-0.02 secs
Major / Minor / magnitude ~fs
9905
9900
190
36°15'E 195
200
36°20'E
a
OLKARIA
MT polarization ellipse axis 5.0-25.0 secs
Major / Minor / magnitude ~fs
9905
9900
190
36°15'E 195
200
36°20'E
b
OLKARIA
MT polarization ellipse axis 25.0-50.0 secs
Major / Minor / magnitude ~fs
9905
9900
190
36°15'E 195
200
36°20'E
c

Fig.8

OLKARIA

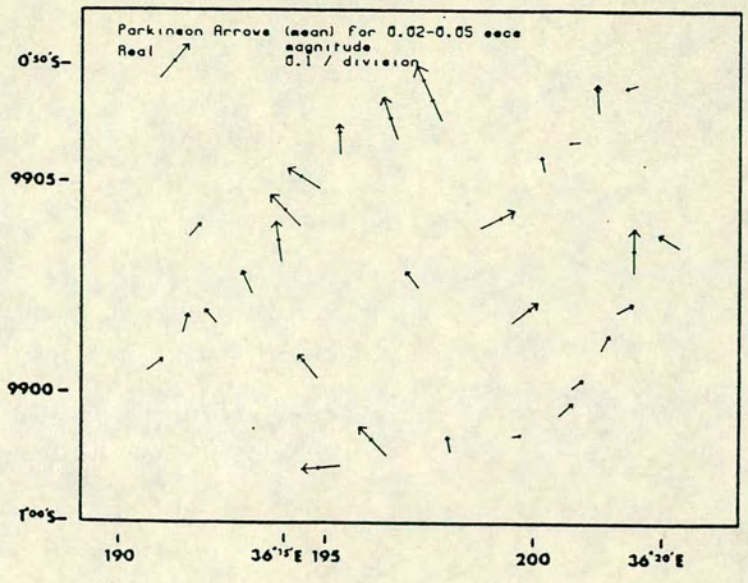

a

OLKARIA

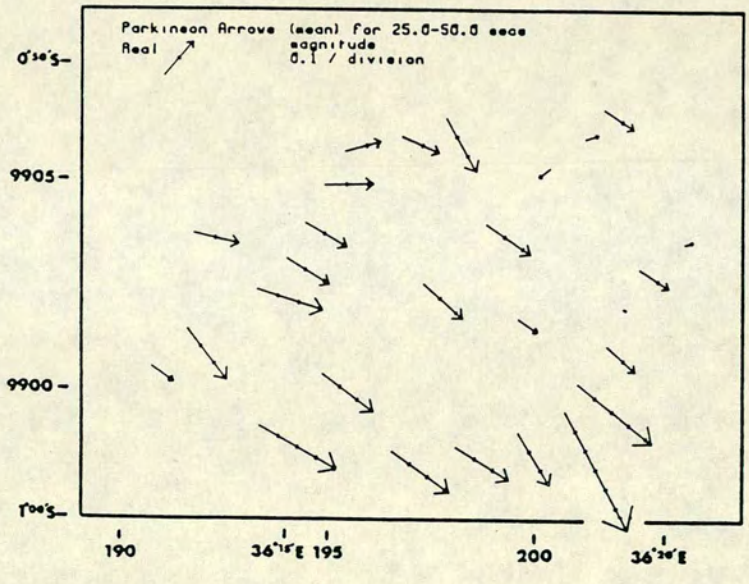

b

OLKARIA

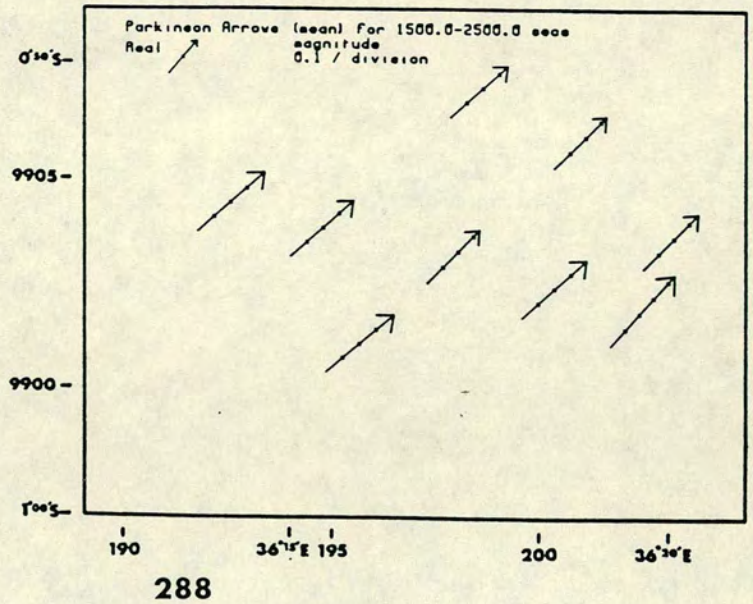

c

helpful in locating zones of low resistivity since, with the convention (Parkinson) used in these figures, the arrow heads point towards them. In this study, it is only for the lowest period band i.e. Fig. 8(a) that lateral variations in resistivity can be inferred for the study region. In that map, the Parkinson arrows point towards a more conducting region in the north and west sections - in a subsequent section of this report it will be shown that this deduction is compatible with the maps of resistivity at depths of 0.5–10 km. It is also compatible with the comments made on Fig. 7(c) above. For the longer periods considered in Figs. 8(b) and 8(c) interpretation is only possible in a more regional setting. For example, Fig. 8(b) shows arrows with a more or less uniform SE azimuth but with amplitudes increasing in that direction. This pattern together with increased amplitude relative to Fig. 8(a) implies that a major conductivity contrast exists to the S.E. of the present study area. This interesting feature certainly merits further study to determine if it is associated with the Longonot or Suswa volcanoes or perhaps with Onacha's (1989) Tandamara anomaly.

The uniformity in amplitude and direction of the arrows of the longest period map, Fig. 8(c), is directly compatible with the results of Rooney and Hutton (1977) and Banks and Beamish (1979) and reflects the low resistivity of the Gregory Rift Valley as a whole relative to the resistive zones on its flanks. Further study of these and other such maps has been deferred to a later date so that the Olkaria data can be collated with the results from the adjacent U.N.D.P. survey and with previously published data. The magnetotelluric results can however lead to an electrical model for the Olkaria field with less need for consideration of the regional setting. They are discussed in the next section.

5. The 1D Resistivity Modelling Results

(a) Maps

The results of the modelling of the average resistivity and phase data at each site are first presented in this report as contoured maps at depths of 0.5, 1, 5 and 10 km, the latter two being in colour - Figs. 9(a)-(d). These have been derived from Bostick resistivities and depths. As in all such contour maps, great care must be taken to avoid over-interpretation of the sections of the maps which lie outside the observational area or at depths greater than those penetrated by the longest period signals. Within the study area, however, these maps show some striking features as fóllows:-

(a) at 0.5 and 1 km depths - Figs. 9(a) and (b) the lowest resistivities (<10 Ωm) lie to the West and North, thus supporting the inferences made from the induction arrows of Fig. 8(a).

(b) The resistivity variations are greatest, ranging from less than 10 to more than 75 Ωm at a depth of 5 km - Fig. 9(c). The pattern here retains the N-S and E-W striking resistivity boundaries of the shallower maps.

(c) The high resistivity 'tongue' striking northwards in the direction of the Ol Olbutot Fault persists to 10 km - Fig. 9(d) - but with a reduced resistivity contrast across the whole zone.

(b) Sections

The complete data set (the maps discussed above represent a sub-set) are now presented as vertical sections in Figs. 10(a)-(d). The profile locations have already been presented in Fig 1. Bearing in mind the colour code indicated on the left of each section, the main features of these sections are as follows

(a) For profile 1 a relatively resistive block exists between 1 and 5 km near the centre of the traverse while a low resistivity zone (<= 15 Ωm) is apparent between 5 and 10 km between sites 914 and 916, with low resistivities also

Fig.9

BOSTICK ρ_{det} 0.5 Km

OLKARIA

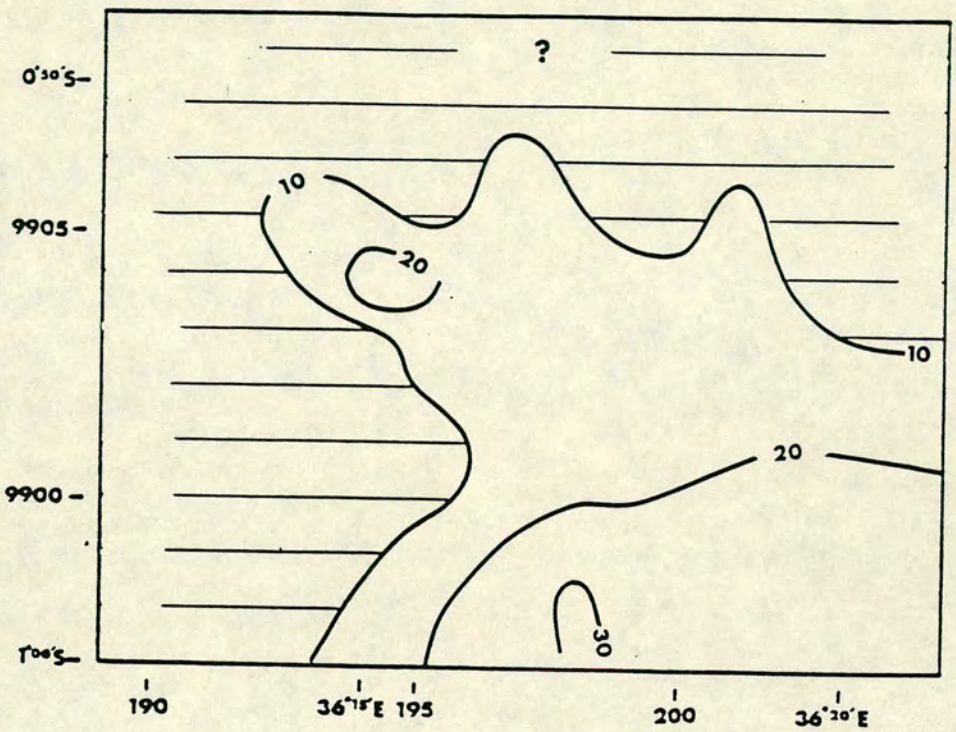

a

BOSTICK ρ_{det} 1 Km

OLKARIA

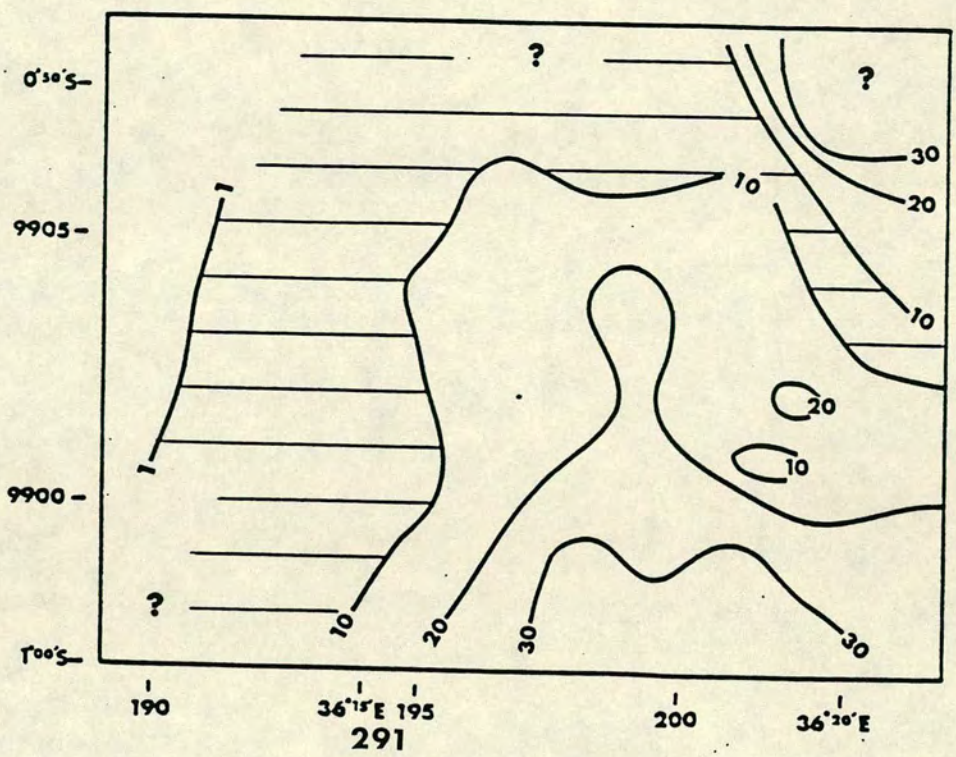

b

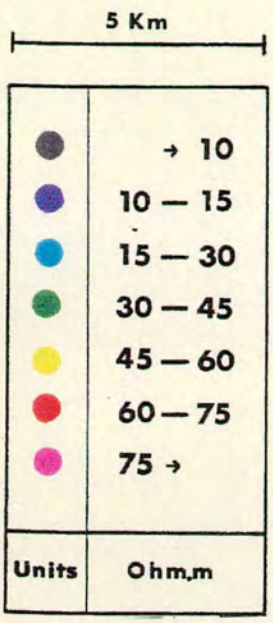

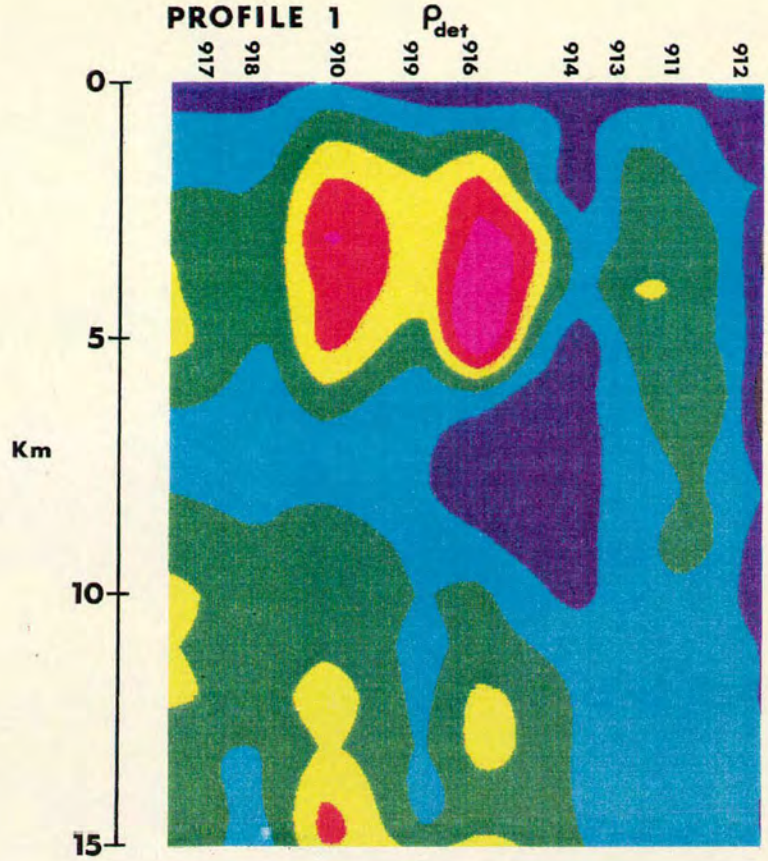

FIG.10(a)

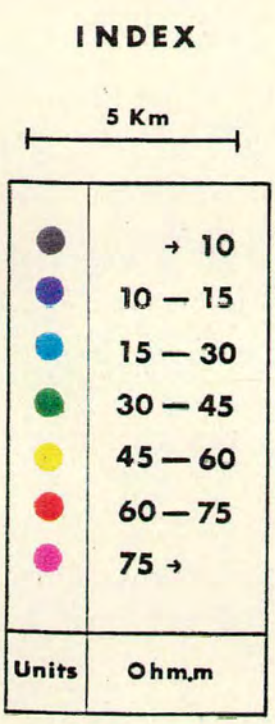

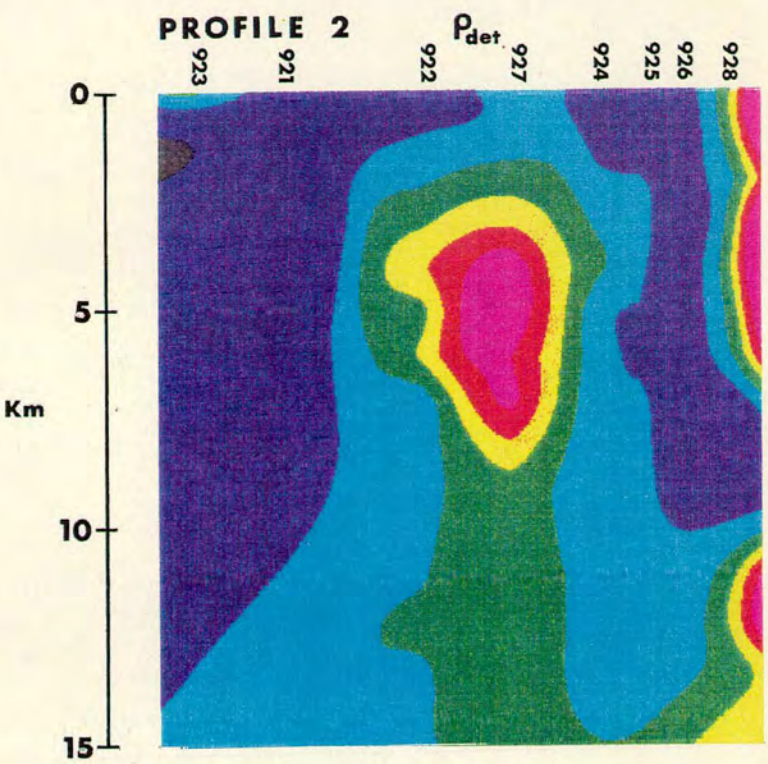

FIG.10(b)

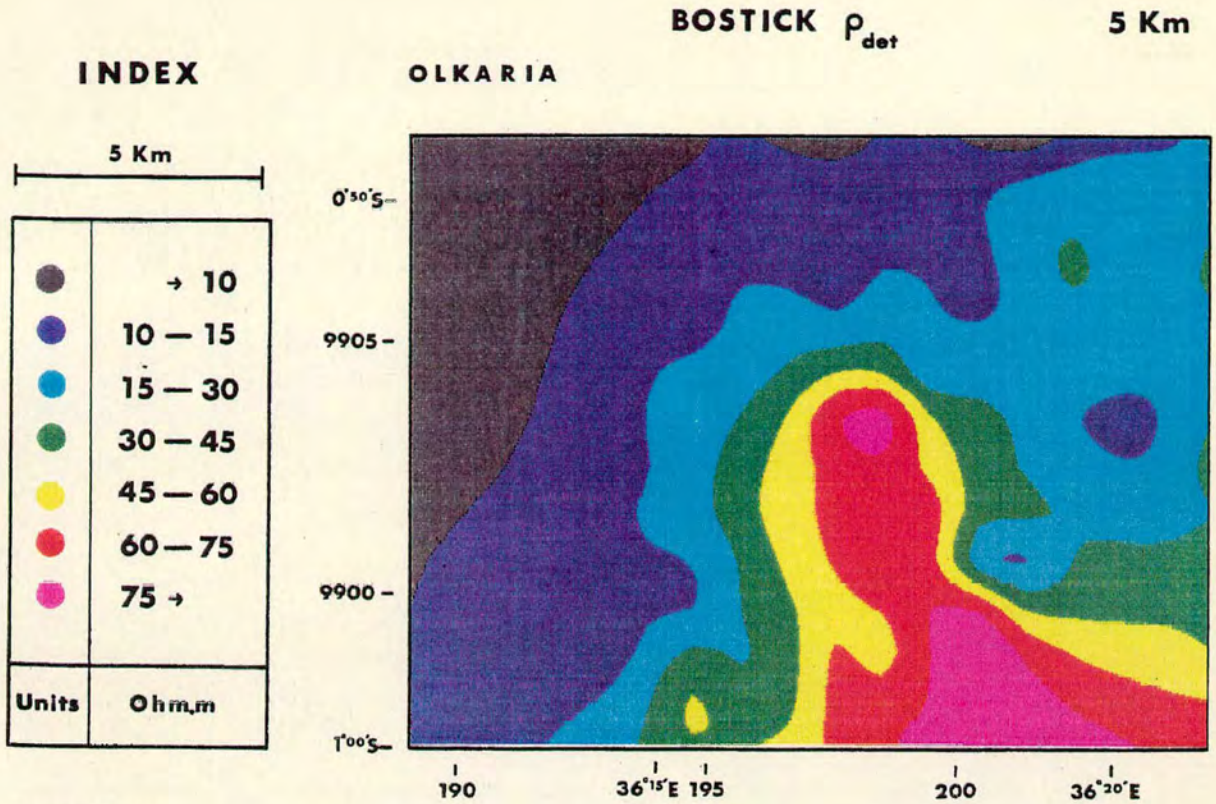
BOSTICK ρ_{det} 5 Km
INDEX
OLKARIA
5 Km
→ 10
10 — 15
15 — 30
30 — 45
45 — 60
60 — 75
75 →
Units
Ohm.m
0°30'S
9905
9900
1°00'S
190
36°15'E
195
200
36°20'E

FIG. 9(c)

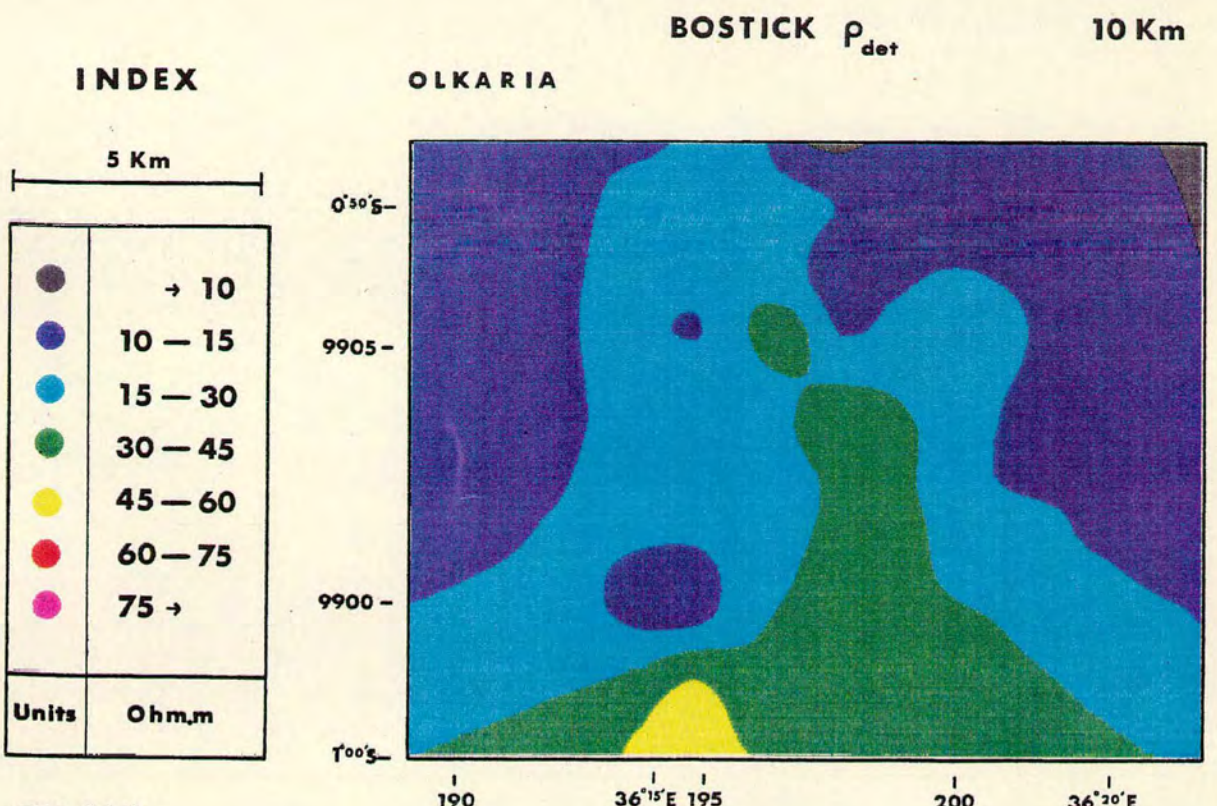
BOSTICK ρ_{det} 10 Km
INDEX
OLKARIA
5 Km
→ 10
10 — 15
15 — 30
30 — 45
45 — 60
60 — 75
75 →
Units
Ohm.m
0°30'S
9905
9900
1°00'S
190
36°15'E
195
200
36°20'E

FIG. 9(d)

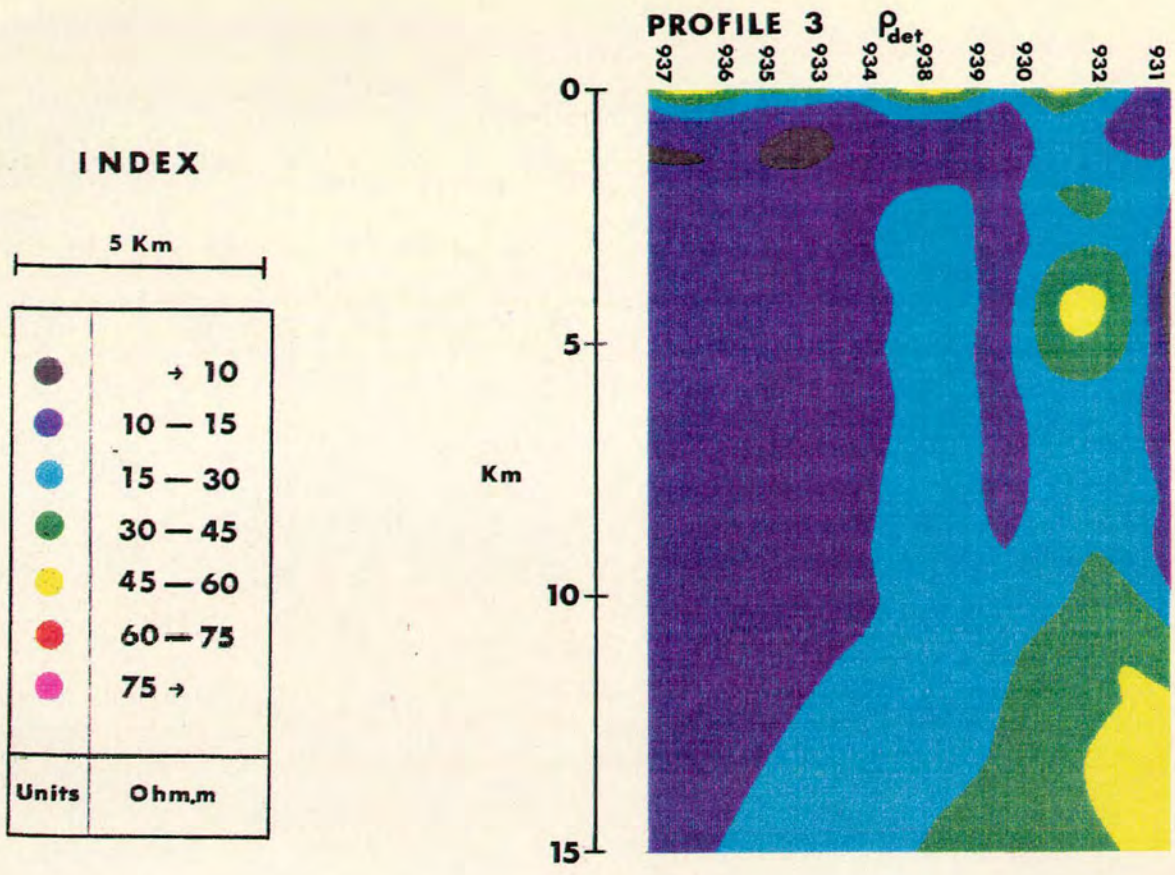

FIG. 10(c)

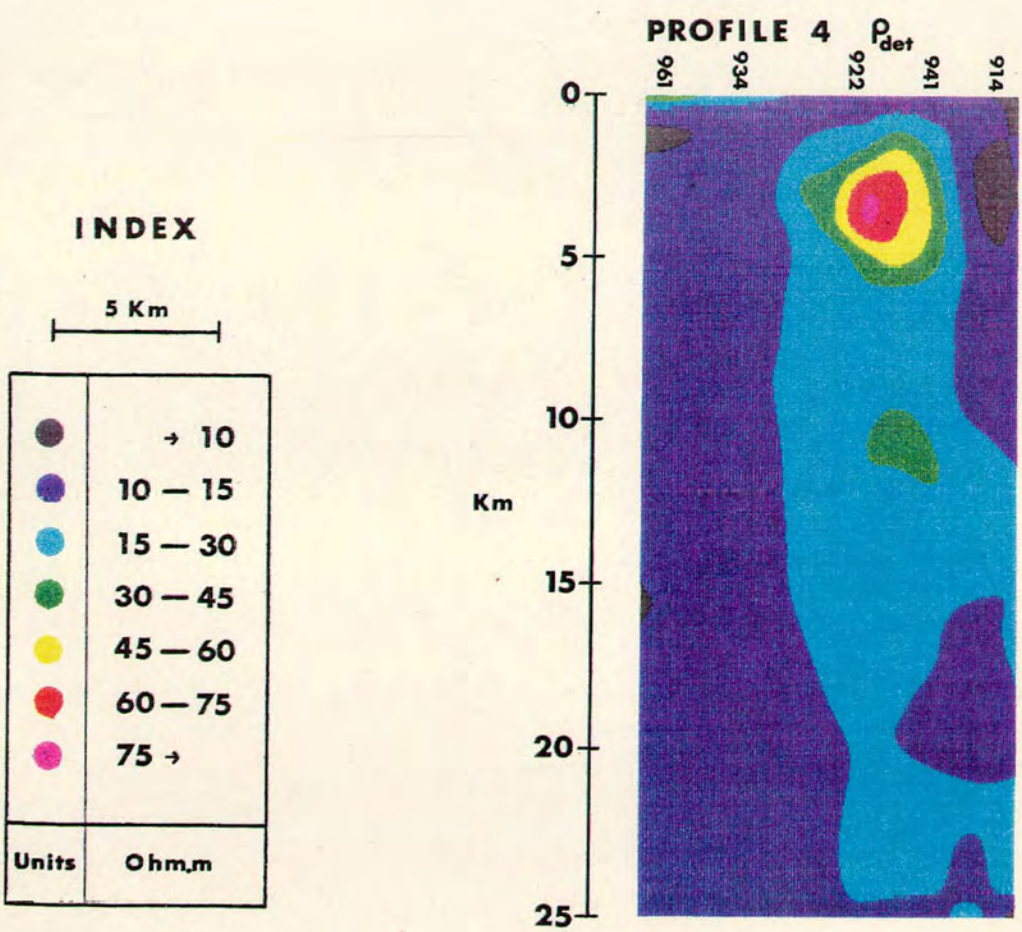

FIG. 10(d)

extending to shallow depths at the latter sites. It is interesting to note here that these are the sites closest to the Olkaria field.

(b) For Profile 2, two low resistivity zones (<= 15 Ωm) are present, extending from shallow depths to at least 10 km. These lie on either side of a resistive block.

(c) The resistivities of profile 3 are in general lower with none exceeding 60 Ωm. There is a broad zone of <= 15 Ωm extending to at least 6 km under the western half of the profile. It should be noted that the depth of penetration of the soundings in this region did not exceed 8 km - the contours presented at greater depth in this part of the profile result only from extrapolation.

(d) In contrast, along profile 4, LMT data were acquired at all sites and thus the depth of all the P4 soundings exceeded 25 km. Resistivities of <= 15 Ωm extend from near the surface under 961 and 934 to >= 25 km and are <= 30 Ωm for a similar depth range under 914. The apparent differences in pattern between profile 4 and the other profiles under 914, 922 and 934 can be explained in terms of smoothing in the contouring program.

6. Discussion of Results

(a) Comparison of resistivity sections

Profile 3 has been chosen for examination of compatibility between the layered resistivity section derived from the Fischer algorithm and the model derived from the Schlumberger soundings. Both models are presented to the same scale in Figs. 11(a) and (b). Bearing in mind the scalar nature of the Schlumberger soundings and the non-uniqueness of the electrical models, the agreement is reasonable over the depth ranges which are common. The advantage of the MT method for deep sounding over conventional resistivity soundings is illustrated by comparison of Figs. 11(b) and 10(c). The more recent

Fig.11

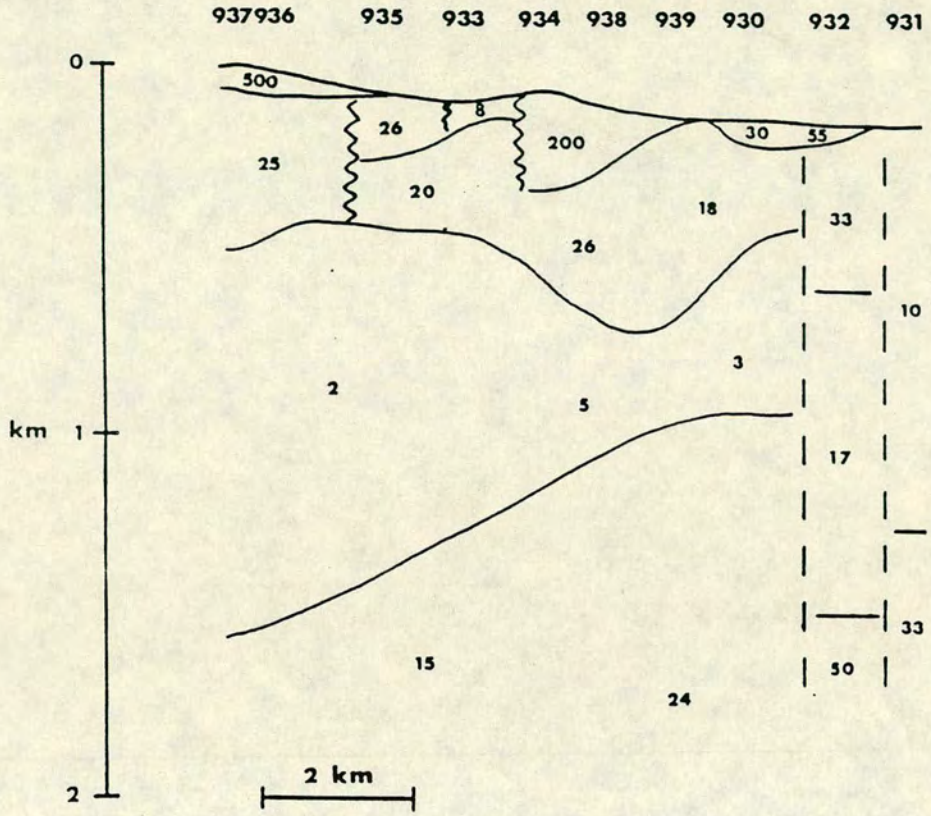
937936
935
933
934
938
939
930
932
931
0
km 1
2
500
26
8
200
30
55
25
20
18
33
26
10
3
2
5
17
33
15
50
24
2 km

a

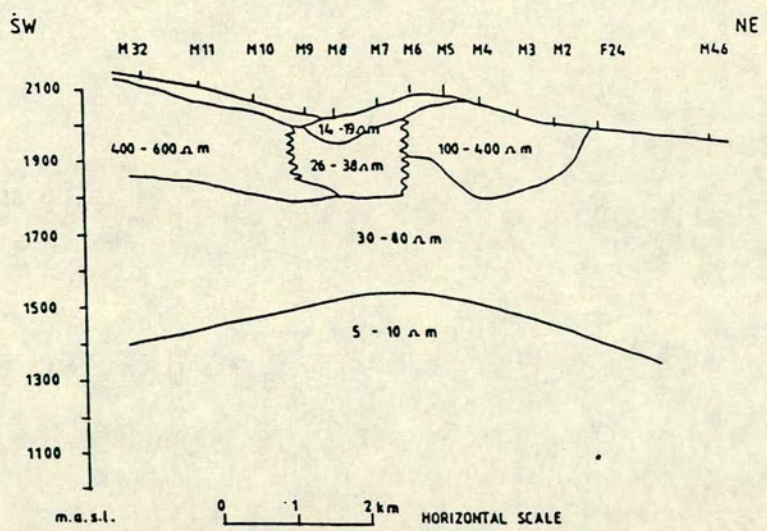
SW
NE
M32
M11
M10
M9
M8
M7
M6
M5
M4
M3
M2
F24
M46
2100
1900
1700
1500
1300
1100
14 -19 Ω m
400 - 600 Ω m
26 - 38 Ω m
100 - 400 Ω m
30 - 80 Ω m
5 - 10 Ω m
m.a.s.l.
0
1
2 km
HORIZONTAL SCALE

b

extensive resistivity soundings with electrode spreads up to 8 km (Onacha, 1989) have yielded interesting contour maps for 1/2 electrode spacings of 2000 and 4000m. An E-W profile across these maps at the location of this MT survey compares favourably with the MT results, although the actual resistivity values appear to be greater.

(b) Comparison with local tectonic features

Several features of the resistivity maps and sections presented in section 5 of this report can be correlated with the local tectonics. To illustrate the association, the resistivity map of Fig. 9(b) for a depth of 1 km is reproduced as Fig. 12 with the faults and lineaments superimposed. Good agreement is apparent between the N-S strike of the faults and thrusts associated with the Gregory Rift and the boundary separating the more resistive central zone from the conducting zone to the west. It can also be noted that this conducting zone appears to trend approximately E-W in the north of the study region, ie parallel to the Olkaria Fault. For confirmation of this E-W striking feature of the resistivity model, additional MT data are required to the north of profile 3.

The resistive block is most prominent at 5 km depth, ie Fig. 9(c). Superposition of the tectonic map on the 5 km resistivity map shows that the most resisitive area is coincident with the Ol Olbutot Fault. It is also close to the Olkaria Peak.

Although only a few MT soundings were undertaken in the NE corner of Fig. 9(b), there is some indication of an association between a NW-SE trending conducting zone and the Gorge Farm Fault. Additionally, in Fig. 11(a) a discontinuity in resistive structure around site 932 may also be associated with the Ol Olbutot Fault.

(c) Comparison with temperature data

In the interpretation of the electrical resistivity models in general, one has to take account of the dependence of resistivity on parameters such as fluid

Fig.12

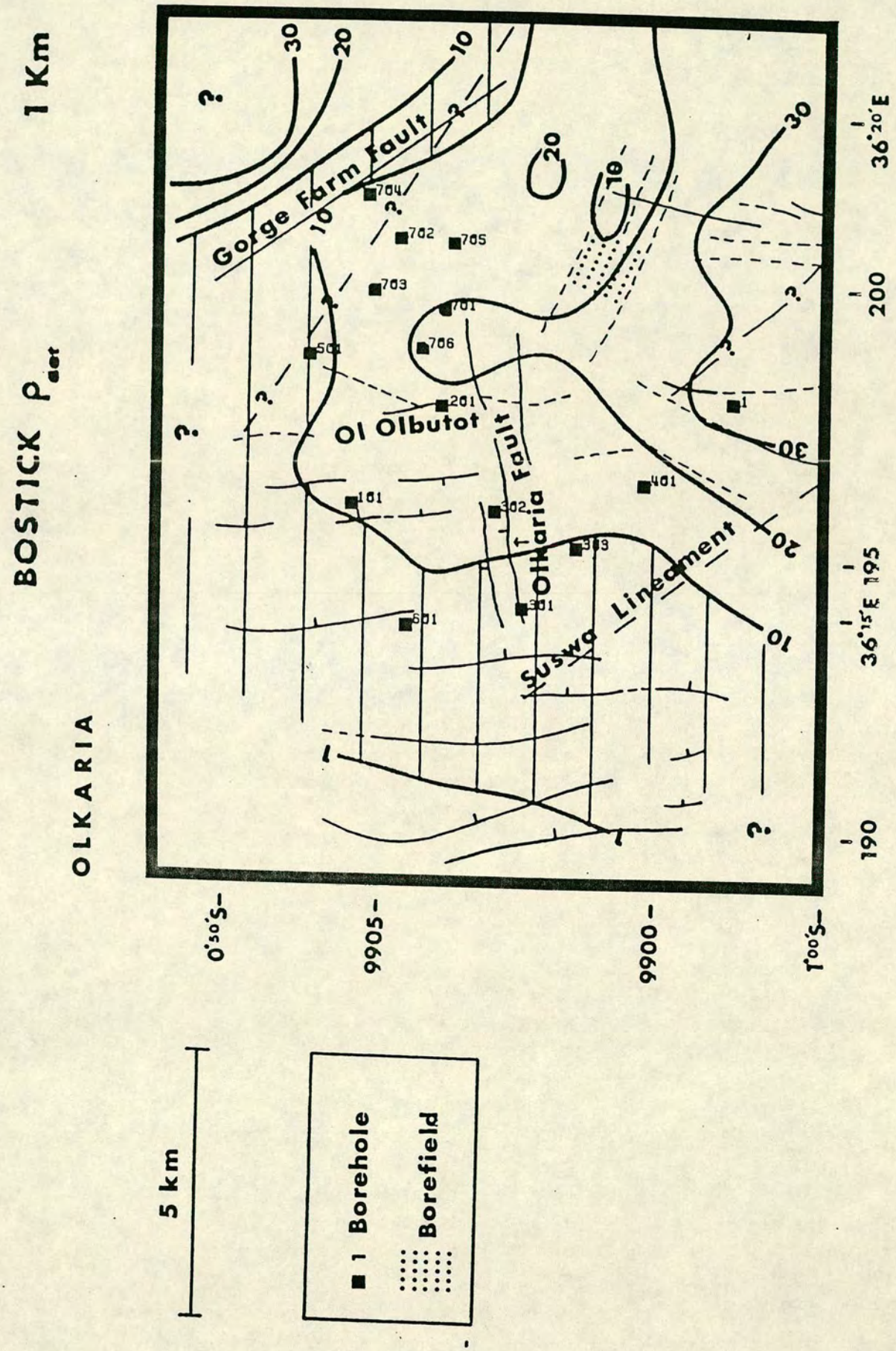
BOSTICK ρ_{app}
1 Km
OLKARIA
Gorge Farm Fault
Ol Olbutot
Olkaria Fault
Susuwa Lineament
C20
30
20
10
?
704
702
705
703
701
706
501
201
1
401
101
302
303
301
601
0°30'S
9905
9900
T°00'S
36°20'E
200
36°15'E
195
190
5 km
1 Borehole
Borefield

content and salinity, temperature and partial melt fraction. In this study the apparent correlation between resistivity and temperature suggests that temperature may be the dominating factor controlling the resistivity of a fluid saturated upper crust. This correlation is illustrated by Fig. 13 which shows that the general form of the temperature contours at about 1km reflects that of the resistivity contours at 5 km. In fact it reflects the general form of the resistivity contours at all depths from 0.5 to at least 10 km, the greatest resistivity contrasts being at 5 km.

Fig. 14(a) shows the isotherms deduced from boreholes adjacent to profile 2 superimposed on the resistivity section for that profile. In general, in Figs. 13 and 14, regions of lower resistivity correspond to higher temperatures. It is tempting to consider extrapolation to depth of the near surface temperature data and to interpret directly the resistivity data at depth in terms of projected isotherms. A more cautions approach to the interpretation of the Kenyan MT study has however been adopted in view of the probable changes in the resistivity model which are anticipated following 2D modelling studies. These changes are expected to occur at depths of the order of a few km or more and are likely to affect the resistivity values themselves rather than the overall structure. The general procedure which should lead to the eventual interpretation is given in the appendix.

(d) Further Comments

For the reasons given above regarding the anticipated changes in the electrical model following 2D modelling studies no attempt has yet been made to find an integrated geophysical model. As indicated in the appendix this will be attempted at a later date. It is, however, realised that the resitricted area of coverage of the MT survey – all sites are within the region of the magnetic high – may inhibit the integration to some extent. With regard to a conceptual model of the Olkaria region, the MT results to date appear to give considerable support to the general ideas expressed in Fig. 1.3 of the 1986 Olkaria Scientific Review. This is reproduced as Fig. 15 and should be compared with Fig. 10(d) for profile 4.

FIG. 13(b)

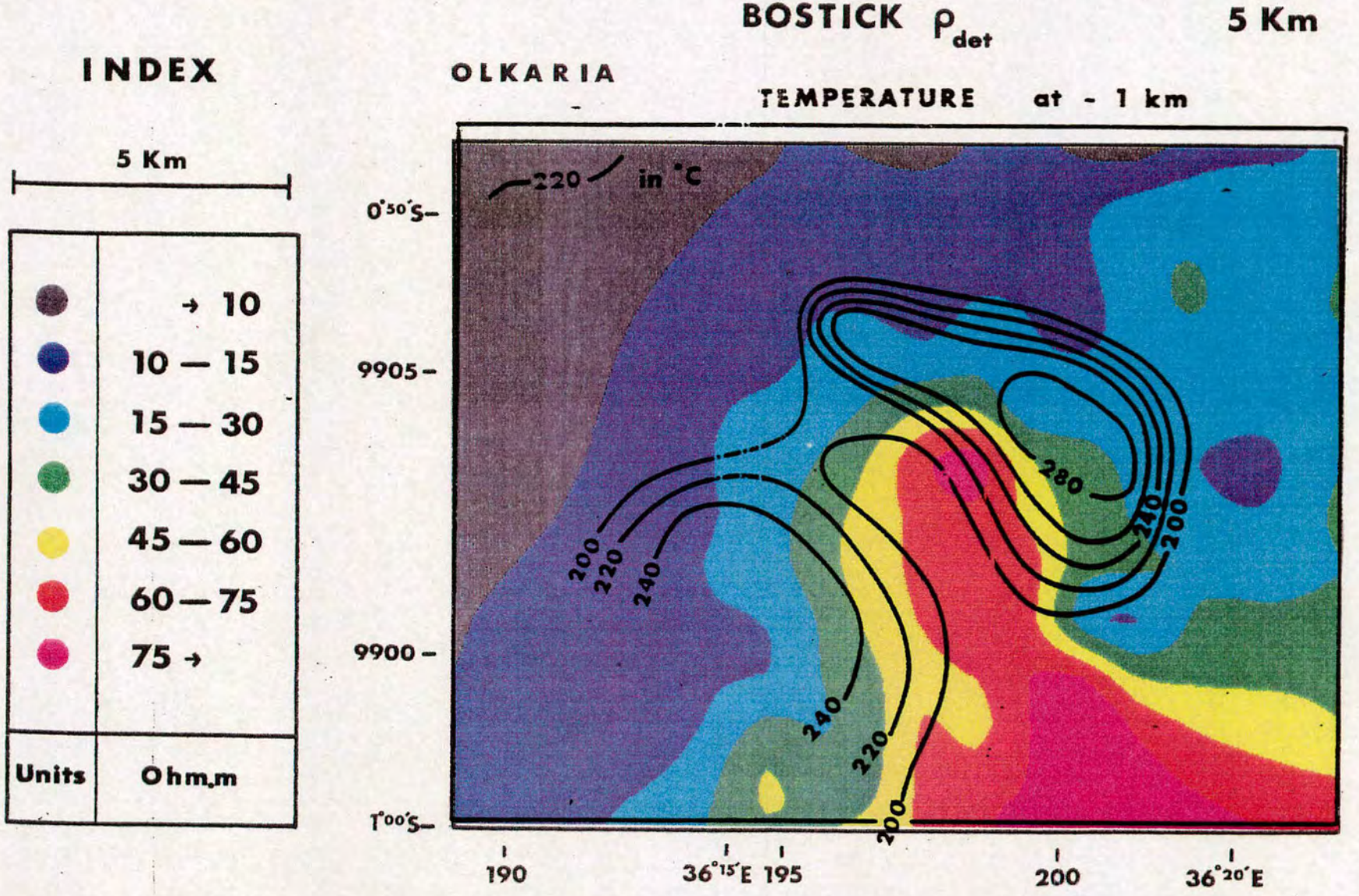

Fig. 13 a

FIG. 13(b)

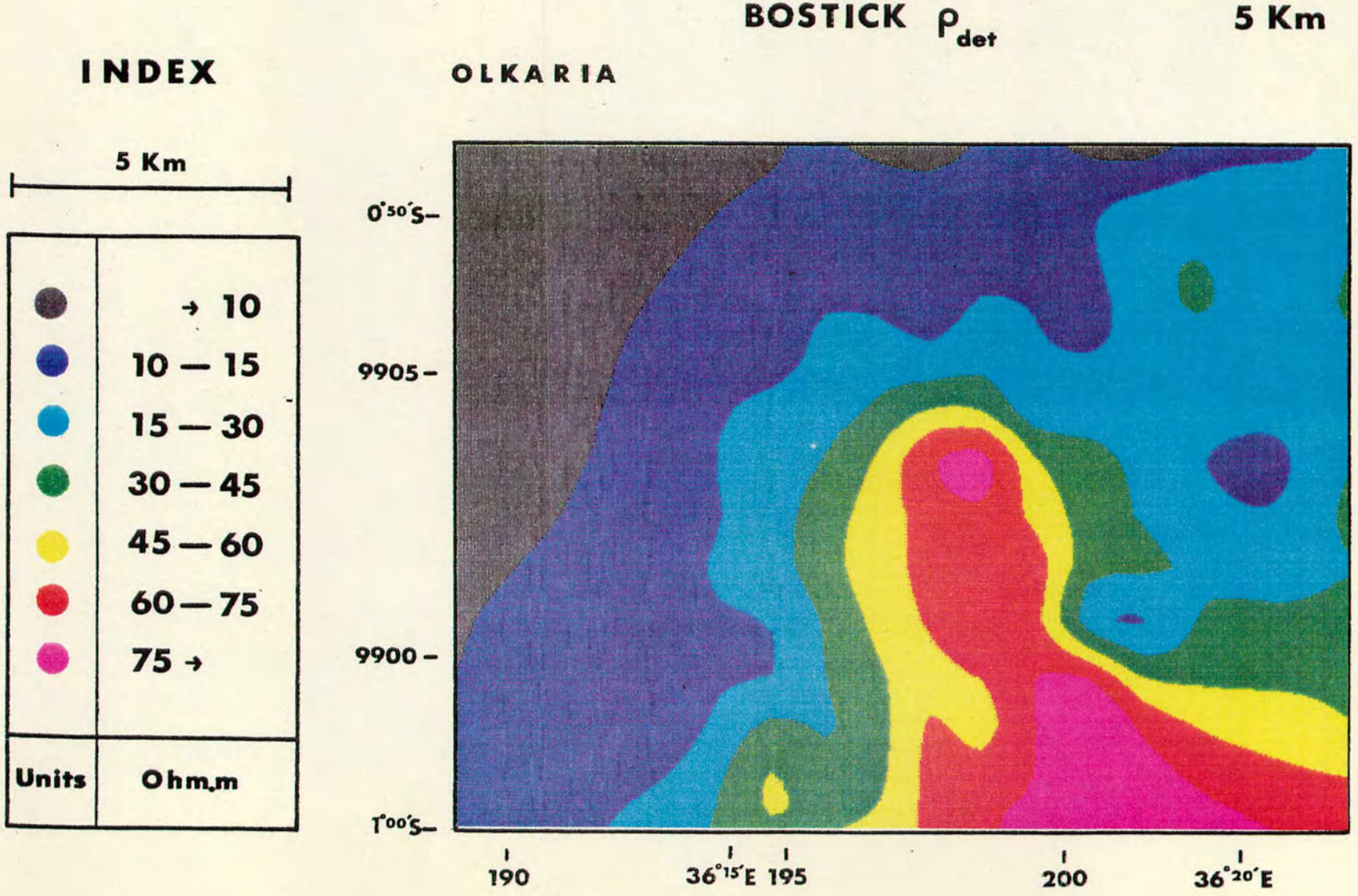
BOSTICK ρ_{det}
5 Km
OLKARIA
INDEX
5 Km
→ 10
10 — 15
15 — 30
30 — 45
45 — 60
60 — 75
75 →
Units
Ohm.m
0°50'S
9905
9900
1°00'S
190
36°15'E
195
200
36°20'E

Fig.14 a

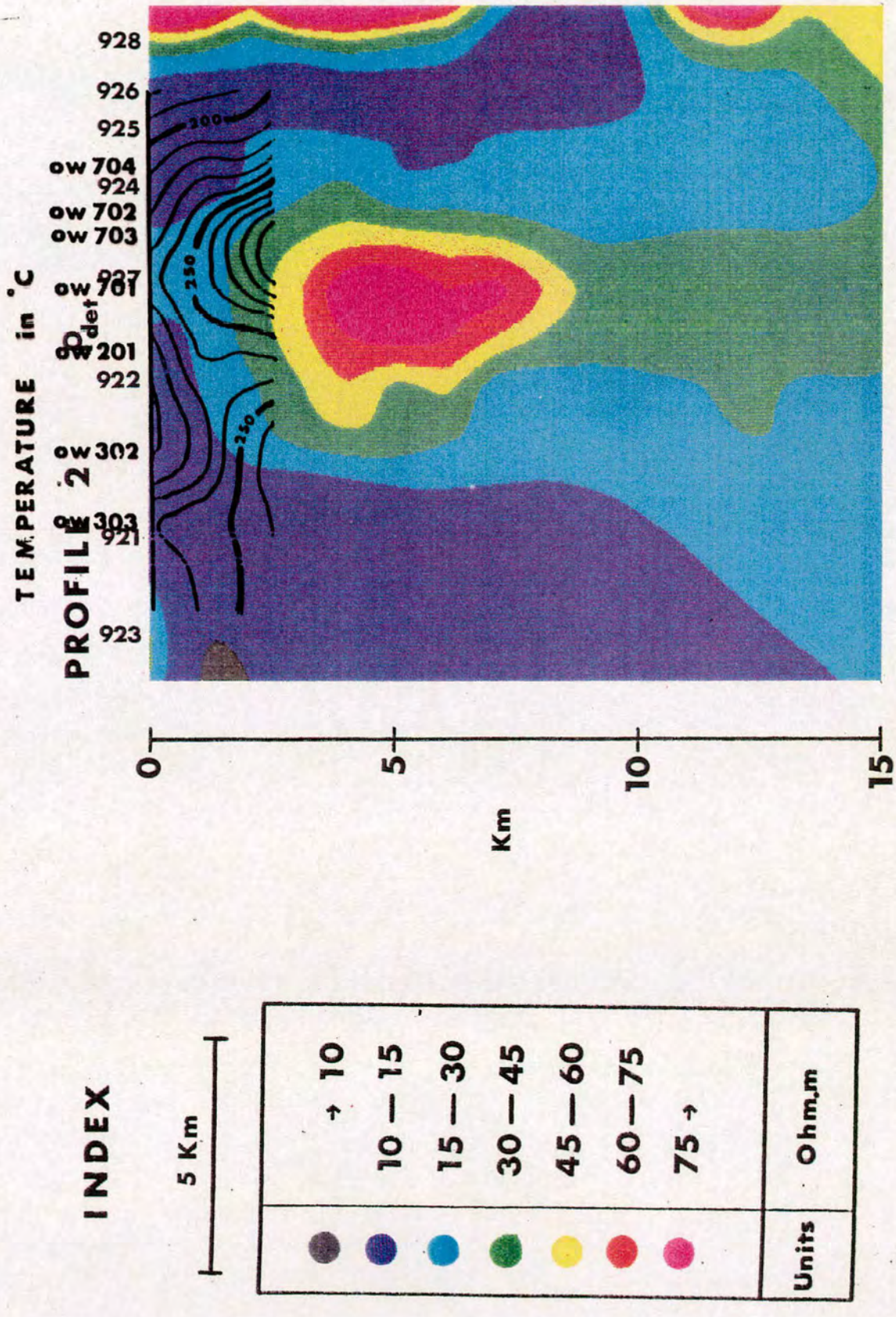

FIG. 14(b)

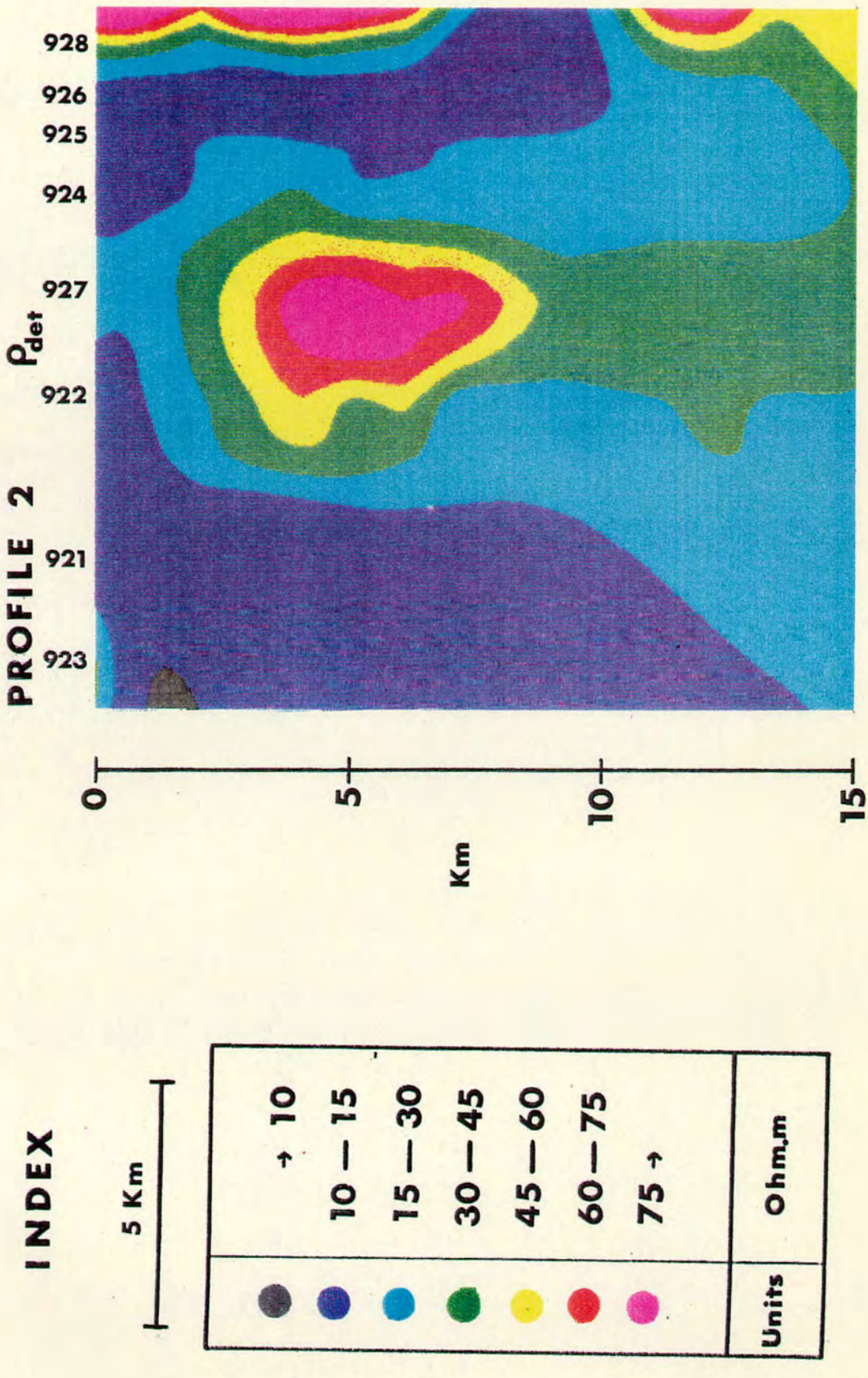
PROFILE 2
ρ_{det}
928
926
925
924
927
922
921
923
0
5
10
15
Km
INDEX
5 Km
→ 10
10 — 15
15 — 30
30 — 45
45 — 60
60 — 75
75 →
Units
Ohm.m

FIG. 14(b)

Fig.15

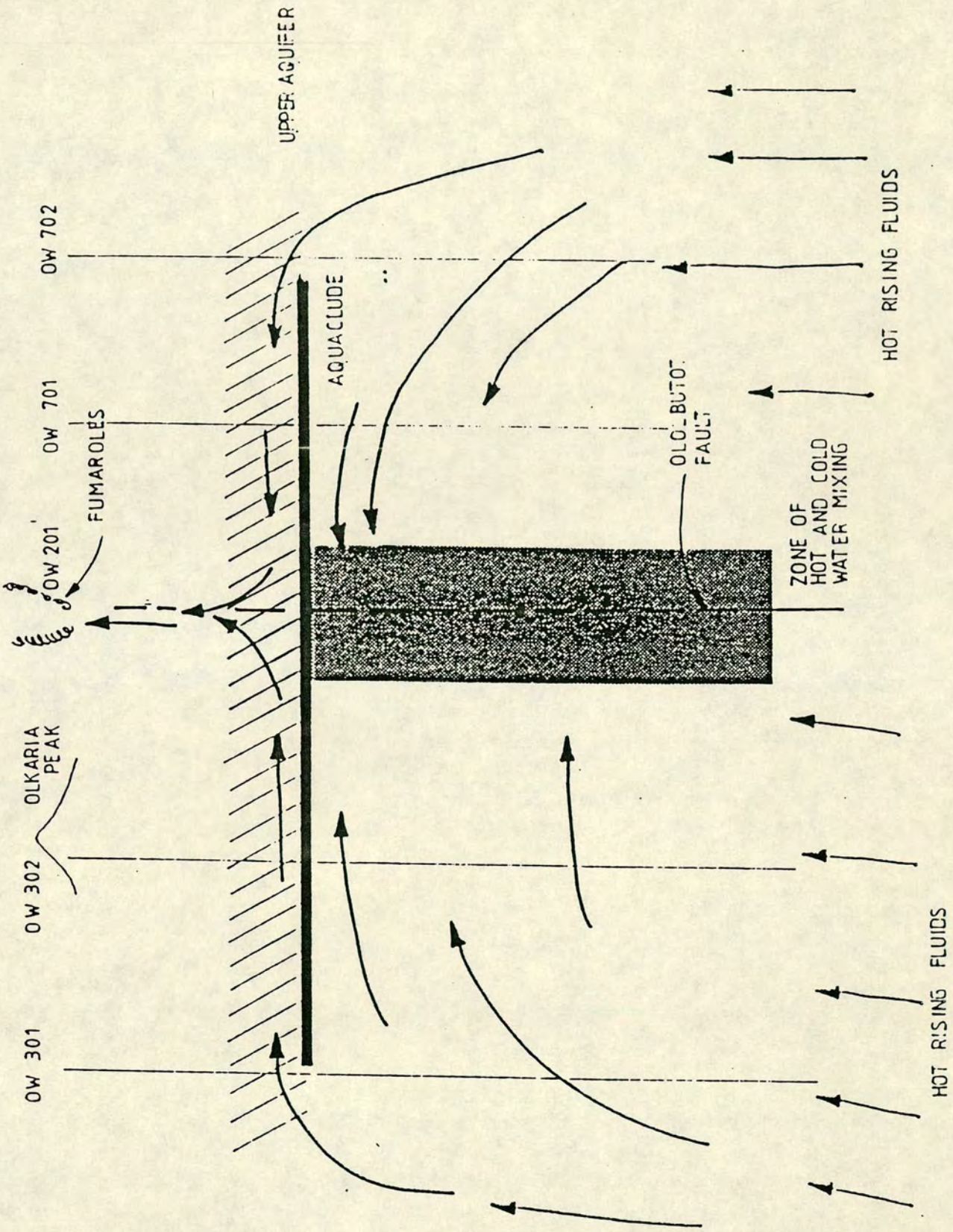
UPPER AQUIFER
AQUACLUDE
OW 702
OW 701
OW 201
FUMAROLES
OLKARIA PEAK
OW 302
OW 301
OLO_BUTOT FAULT
ZONE OF HOT AND COLD WATER MIXING
HOT RISING FLUIDS
HOT RISING FLUIDS

7. Main Conclusions

1) At all sites surveyed and to depths of 6 - > 25 km, the electric resistivities fell within the range 1 to 100 Ωm. Thus in general, the whole of the Olkaria region has anomalously low resistivity.

2) The region can, however, be subdivided into 3 distinct zones, each of which has its own electrical character.

(a) In the region of the Gorge Farm Fault there is a narrow zone of low resistivity ($\rho <= 15$ Ωm) which appears to extend to at least 10 km. There is a rapid increase in ρ within a few km NE of the fault - see Fig 10(b). This zone can be identified with the Olkaria NE potential field.

(b) The central part of the survey is characterised by very low resistivies ($\rho <= 15$ Ωm) within the uppermost 1-2 km, overlying a more resitive block which has a thickness of approximately 6 km. The Olkaria geothermal field is located within this region.

(c) The western part of the survey comprises an extensive zone of low resistivity ($\rho <= 15$ Ωm) which probably extends to upper mantle depths, at least under sites 934 and 961, and perhaps also under sites 932, 936 and 937. It may be significant that, unlike the zone described in (a) above, relatively high resistivies are observed in this western zone in the uppermost few hundred meters. This zone can be identified as the Olkaria West potential field.

3) The above 3 zones are less well defined around the perimeter of the survey area. Thus further observations are required to confirm the terminations to the north of the Olkaria Fault of the central resistive block. It may be that it continues northwards in the region of the Ol Olbutot Fault.

4) Maps of the electrical resistivity at upper crustal depths correlate well with the major faults and the strike of the Gregory Rift Valley.

5) There is a remarkable agreement between the resistivity contours at the upper crustal depths and the temperature contours at 1 km.

6) The MT study to date supports the conceptual model as described in the 1986 reports.

7) There is surprisingly good agreement between the electrical models at many of the Olkaria sites and those obtained at the Rift Valley sites of Rooney and Hutton (1977). This may support the hypothesis of extensive geothermal resources in other parts of the Rift Valley.

8. Acknowledgements

The collaboration between the University group and K.P.C. Ltd. staff was most fruitful. In particular, the authors of this report would like to acknowledge the significant contribution of their colleagues Graham Dawes, whose dedicated leardership of the field study enabled the acquisition of a valuable data set, and Phil Jones for his conscientious and enthusiastic contribution to the Ph.D. project of his fellow student (D.G.). They would also like to record their appreciation to the K.P.L.C. staff at Olkaria for their substantial support, hospitality and kindness. They are too numerous to acknowledge individually other than M.N. Mwangi, especially for the stimulating discussions about the Olkaria field and the interpretation of the existing data, and S.A. Onacha for both scientific discussions and valuable field assistance. The interest of E.D. Wasunna and S.B. Ojiambo in the MT study itself and the manner in which the collaboration was evolving was most rewarding. Substantial support for the field study was provided by the loan of LMT systems from the NERC Geophysical Equipment Pool and of a field vehicle from U.N.D.P., Nairobi, whose Geothermal Project Manager, G. Gislason demonstrated, by this loan and by his references to the adjacent U.N.D.P. MT survey, his interest in the future integration of the results of the two studies.

9. Appendix

Further Study of the Present Data

The programme of work now being initiated is as follows:-

(a) 2D modelling of the MT data will be undertaken. It is hoped that data from the U.N.D.P. project can be made available for incorporation in this exercise.

(b) The gravity and magnetic data will then be re-modelled and account taken of seismic data in an attempt to find an integrated geophysical model for the region. It is hoped that this will be undertaken with the collaboration of Kenyan geophysicists.

(c) Finally consideration will be given to the geothermal significance of the integrated geophysical model. It is expected that the interpretations of Rooney and Hutton (1977) and Mwangi and Bromley (1986), and the detailed discussions in the report concerning the Snake River Plain MT survey by Stanley et al. (1977) will be relevant for this purpose.

Recommendations for Further Work

1) Additional LMT observations in the Olkaria West would help confirm the deeper structure at sites where the data from the S.P.A.M. system penetrate to about 6 km only. With some additional LMT sites further north west, more information would be provided regarding the overall extent of this low resistivity zone. A loan from Edinburgh of the necessary equipment would be considered.

2) If the U.N.D.P. data support the hypothesis that the SE directed tippers at periods of 25-50s are associated with the Longonot and/or Suswa caldera, additional LMT observations at a series of locations around the

caldera(s) could be very diagnostic. This was the basis of the topic proposed recently for a University of Nairobi M.Sc. student. The same equipment as for (1) could probably be made available for this purpose.

3) Many suggestions for further MT work beyond the Olkaria region could be made.

References

Banks, R.J. and Beamish, D. (1979) Melting in the crust and upper mantle beneath the Kenya Rift: evidence from Geomagnetic Deep Sounding experiments, *J.Geol.Soc.* **136,** 225–233.

Bostick, F.X. (1977) A simple almost exact method of MT analysis. Workshop on Electrical Methods in Geothermal Exploration, U.S. Geol. Survey, *Contract No. 14080001–8–359.*

Dawes, G.J.K. (1984) Short period automatic magnetotelluric (S.P.A.M.) system, in A broadband tensorial magnetotelluric study in the Travale–Radicondoli geothermal field. (Hutton et al.) *EEC Final Report. Contract No. EG–A2–031–UK.*

Fischer, G., Schnegg, P.A., Peguiron, M. and Le Quang, B.V. (1981) An analytic one dimensional magnetotelluric inversion scheme, *Geophys.J.R.Astr.Soc,* **67,** 257–278.

Garnish, J., Staroste, E. and Wohlenberg, J. (eds) (1989) Testing geophysical techniques on the island of Milos (Greece), *Geothermics,* **18,** No. 4, 481–621.

G.E.N.Z.L. (1986) Olkaria Scientific Review.

K.P.C. Ltd. (1988) Working document for scientific review meeting.

Mwangi, M.N. and Bromley, C.J. (1986), A review of geophysical model of Olkaria geothermal field, Kenya Power Company Ltd, *Report No. GP/OW/012.*

Onacha, S.A. (1989) Private communication.

Rooney, D. and Hutton, V.R.S. (1977) A magnetotelluric and magnetovariational study of the Gregory Rift Valley, Kenya, *Geophys.J.R.Astr.Soc.,* **51,** 91–119.

Stanely, W.D., Boehl, J.E., Bostick, F.X. and Smith, H.W. (1977) Geothermal significance of magnetotelluric sounding in the eastern Snake River Plain – Yellowstone Region, *J. of Geophys. Research,* **82,** 2501–2514.

Sule, P.O. (1985) A broadband magnetotelluric investigation in southeast Scotland. Ph.D. Thesis, University of Edinburgh.

Vozoff, K. (ed) (1985) 'Magetotelluric Methods', *S.E.G. Geophysics reprint series No. 5,* pp763.